Charles University
Faculty of Medicine in Hradec Králové

Doctoral degree programme

Medical chemistry and biochemistry

Proteomic analysis of gamma-irradiated human leukemic cells
(Phosphoproteomic analysis of radiosensitized MOLT-4 cells)

Proteomická analýza leukemických buněčných linií po ozáření
(Fosfoproteomická analýza radiosensibilizovaných buněk MOLT-4)

Barbora Šalovská, M.Sc.

Supervisor: Prof. Martina Řezáčová, M.D., Ph.D.
Consultant supervisor: Assoc. Prof. Aleš Tichý, PharmD., Ph.D.

Hradec Králové, 2017 Defence on: .....

Declaration

I declare hereby that this dissertation thesis is my own original work, and that I indicated by references all used information sources. I also agree with depositing my dissertation in the Medical Library of the Charles University, Faculty of Medicine in Hradec Králové and with making use of it for study and educational purpose provided that anyone who will use it for his/her publication or lectures is obliged to refer to or cite my work properly.

I give my consent to availability of my dissertation´s electronic version in the information system of the Charles University.

Hradec Králové, 13.2.2017

Signature of the author

Acknowledgements

I would like to express my sincere gratitude to my consultant supervisor Assoc. Prof. Aleš Tichý, PharmD., Ph.D. and my supervisor Prof. Martina Řezáčová, M.D., Ph.D. for their support of my Ph.D. study and related research. In particular, I am grateful to Assoc. Prof. Aleš Tichý, PharmD., Ph.D. for helping me with preparing my oral presentations and writing my grant applications, papers, and this thesis. I really appreciate his help with the application for the SCIEX NMSch fellowship, which enabled me to work for ten inspiring months in the lab of Prof. Dr. Ruedi Aebersold. Besides my supervisors, I would like to thank the heads of the Department of Radiobiology and the Department of Molecular Pathology and Biology of the Faculty of Military Health Sciences in Hradec Králové, Prof. RNDr. Jiřina Vávrová, Ph.D. and Prof. Jiří Stulík, M.D., Ph.D., respectively, for enabling me to work in their laboratories and using their laboratory equipment for my experiments. Furthermore, I would like to thank my colleagues from the above mentioned departments and Faculty of Military Health Sciences in Hradec Králové: Ivo Fabrik, M.Sc., Lenka Mervartová, B.Sc., Klára Kubelková, Ph.D., Eva Novotná, M.Sc., Kamila Ďurišová, M.Sc., Monika Schmidt, Ph.D., Petr Jošt, M.Sc., David Herman, M.Sc., Alena Fučíková Ph.D., Nela Váňová, M.Sc., Adéla Kmochová, M.Sc., Lucie Čecháková, M.Sc., Martin Ondrej, M.Sc., Marie Vajrychová, M.Sc., Iva Šenitková, Ph.D., Lenka Plzáková, M.Sc., Daniela Putzová, M.Sc., Lucie Balonova, Ph.D., Marek Link, Ph.D., Pavel Řehulka, Ph.D., Helena Řehulková, Ph.D., Jaroslav Pejchal, M.D., Ph.D., Lenka Zárybnická, Ph.D., and Assoc. Prof. Zuzana Šinkorová, D.V.M, Ph.D. for all their professional and personal support during my study. I would like to acknowledge Ivo Fabrik, M.Sc. and Marek Link, Ph.D., who performed the LC-MS/MS analyses presented in this thesis. I am very grateful to Ivo Fabrik, M.Sc. for his advice and the fruitful discussions we had about my work. I also would like to acknowledge Hana Janečková, Ph.D. and RNDr. David Friedecký, Ph.D. for conducting the metabolomic analysis of irradiated MOLT-4 cells, which is a part of this thesis. Finally, I would like to express my sincere gratitude to my family, friends, and boyfriend for their support of my Ph.D. study and their patience, especially during the last months of writing this dissertation thesis.

This work was supported by the Grant Agency of the Charles University in Prague (GAUK 1220313), the Grant Agency of the Czech Republic (P206/12/P338), by the grant of the "Internal competition of the Faculty of Medicine in Hradec Králové, by the programme PRVOUK (P37/01), by "Specific research" (MŠMT, SVV-2014-260058; SVV-2013-266901), and by the Ministry of Defence of the Czech Republic (A long-term organization development plan no. 1011).

Table of Contents

Summary (CZE)

V této dizertační práci jsme se zaměřili na objasnění molekulárních mechanismů radiosensibilizace leukemické buněčné linie MOLT-4 specifickou inhibicí kináz z rodiny fosfatidylinositol-3-kináza příbuzných kináz (PIKKs). Byly testovány dva vysoce účinné a selektivní inhibitory VE-821 (inhibitor ATR) a KU55933 (inhibitor ATM) pro jejich účinky na proliferaci, viabilitu a buněčný cyklus neozářených a ozářených buněk MOLT-4. Aplikace obou inhibitorů způsobila radiosensibilizaci MOLT-4 buněk a 10 μM VE-821 navíc působil jako silné antiproliferativní agens i v neozářených MOLT-4 buňkách.

K dalšímu popisu mechanismů, které jsou zodpovědné za radiosensibilizaci MOLT-4 buněk VE-821 inhibitorem, byly použity metody využívající hmotnostní spektrometrii. Pomocí metod kvantitativní proteomiky jsme identifikovali a kvantifikovali změny v proteomu a fosfoproteomu (tj. změny na úrovni fosforylace proteinů) buněk, které byly způsobeny účinkem inhibitoru v ozářených buňkách. Protože detekce a kvantifikace fosforylovaných peptidů v komplexních vzorcích je komplikována mimo jiné jejich relativně nízkým zastoupením, zaměřili jsme se nejprve na výběr optimální metody pro jejich selektivní izolaci ze směsi s nemodifikovanými peptidy. Optimalizovaný protokol byl pak dále využit ke studiu změn v buňkách radiosensibilizovaných VE-821. Dle očekávání inhibitor hodinu po ozáření nevyvolal žádné změny na úrovni proteomu. Při studiu fosfoproteomu jsme ale nalezli 623 signifikantně změněných fosforylačních míst, z nichž většina (431) byla zvýšeně fosforylována. Pomocí bioinformatických nástrojů jsme identifikovali změny v signálních drahách a aktivitách kináz přímo odpovídajících na poškození DNA, ale také v signálních drahách a kinázách primárně souvisejících s regulací buněčného metabolismu. Detekovali jsme snížení v aktivitě mTOR kinázy, které bylo nejspíše způsobené nespecifickým působením inhibitoru v 10 μM koncentraci. Tato snížená aktivita může pravděpodobně přispívat k zástavě proliferace buněk po podání vysoké dávky inhibitoru. Vliv VE-821 na metabolismus ozářených buněk byl dále zkoumán pomocí cílené metabolomické analýzy. V této analýze bylo kvantifikováno 206 intermediárních metabolitů. Při následné analýze dat bylo zjištěno, že VE-821 potencuje rozvrat energetického metabolismu a může ovlivňovat odpověď na oxidační stres způsobený ozářením. Dále jsme ukázali, že obnova poškozených deoxynukleotidů by mohla být negativně regulována VE-821.

V této práci jsme tedy komplexně popsali, jaké signální a metabolické dráhy by mohly být závislé na ATR nebo spuštěny ATR inhibicí VE-821 v ozářených MOLT-4 buňkách. Výsledky této práce mohou být dále použity jako zdroj informací pro další navazující studie.

Summary (ENG)

In the presented doctoral thesis, we aimed to elucidate molecular mechanisms underlying radiosensitization of MOLT-4 cell line (T-ALL) by specific inhibition of kinases from the phosphatidylinositol-3 kinase-related kinases (PIKKs) family. We tested two highly potent inhibitors of ATR and ATM, VE-821 and KU55933, respectively, for their effects on proliferation, viability, and cell cycle of sham-irradiated and irradiated MOLT-4 cells. Both inhibitors proved to radiosensitize MOLT-4 cells and furthermore, 10 μM VE-821 was shown to act as a strong antiproliferative agent in sham-irradiated MOLT-4 cells.

To further describe cellular mechanisms underlying the VE-821-mediated radiosensitization of MOLT-4 cells, we employed high-resolution mass spectrometry to identify and quantify changes in proteome and phosphoproteome of irradiated VE-821-treated cells. As the detection and quantification of phosphorylated peptides in complex biological samples is challenging due to their low stoichiometry, we first compiled and optimized protocol for their enrichment. The protocol was then applied to study changes in radiosensitized MOLT-4 cells. In concordance with our expectations, VE-821 did not cause any significant changes on the proteome level one hour after irradiation. However, we detected 623 differentially regulated phosphorylation sites; most of them (431) were upregulated in response to VE-821 treatment. Using bioinformatic tools, we revealed changes in DDR related pathways and kinases, but also pathways and kinases involved in maintaining cellular metabolism. Notably, we found downregulation of mTOR, the main regulator of cellular metabolism, which was most likely caused by an off-target effect of the inhibitor, and we proposed that mTOR inhibition could be one of the factors contributing to the phenotype observed after treating MOLT-4 cells with 10 μM VE-821. To investigate the potential modulation of cellular metabolism, we performed a targeted metabolomic analysis of irradiated MOLT-4 cells pre-treated by 10 μM VE-821. In this analysis, 206 intermediary metabolites were quantified. Subsequent data analysis showed that VE-821 potentiated metabolic disruption induced by IR and affected response to IR-induced oxidative stress. Our data indicated that upon IR, recovery of damaged deoxynucleotides might be affected by VE-821, hampering DNA repair by their insufficiency.

Thus, in this thesis we described a complex scenario of cellular events that might be dependent on ATR or triggered by ATR inhibition by VE-821 in irradiated MOLT-4 cells. Importantly, data presented in this work might serve as a resource for follow-up studies and provide a platform for future work with other kinase inhibitors.

List of Abbreviations

AA - amino acid

ABC - ammonium bicarbonate

Acn - acetonitrile

A-T - ataxia-telangiectasia

BP - biological process

BSA – bovine serum albumin

CC - cellular compartment

CDKs - cyclin-dependent kinases

CHCA - α-cyano-4-hydroxycinnamic acid

CID - collision-induced dissociation

CV - coefficient of variation

DDR - DNA damage response

DHB - 2,5-dihydroxybenzoic acid

DMEM - Dulbecco's modified eagle medium

DMSO - dimethyl sulfoxide

dNDPs - deoxynucleoside diphosphates

dNTPs - deoxynucleoside triphosphates

DSBs - double-strand breaks

DTT - dithiothreitol

ECD - electron capture dissociation

EGF - epidermal growth factor

EGFR - epidermal growth factor receptor

ERLIC - electrostatic repulsion hydrophilic interaction chromatography

ESI – electrospray ionization

ETD - electron transfer dissociation

FA - formic acid

FBS - foetal bovine serum

FDR - false discovery rate

Glu - glutamic acid

GO - gene ontology

GRT - global rank test

GSH - reduced glutathione

GSH/GSSG - reduced/oxidized glutathione ratio

HCD - high-energy CID

HDR – homology-directed recombination

HILIC - hydrophilic interaction chromatography

IAA - iodoacetamide

IMAC - immobilized metal affinity chromatography

IMDM - Iscove's modified Dulbecco's media

IP - immunoprecipitation

IR – ionizing radiation

iTRAQ - isobaric tag for relative and absolute quantitation

K0 - L-lysine

K6 - L-$^{13}C_6$-lysine

LA - lactic acid

LC – liquid chromatography

LC-MS/MS - liquid chromatography-tandem mass spectrometry

MALDI – matrix-assisted laser desorption/ionization

MDLC−MS/MS - multidimensional liquid chromatography-tandem mass spectrometry

MF - molecular function

MOAC - metal oxide affinity chromatography

MRN - Mre11/Rad50/Nbs1 complex

MS – mass spectrometry

MS/MS - tandem mass spectrometry

NDPs - nucleotide diphosphates

NHEJ - non-homologous end joining

NSCLC - non-small cell lung cancer

NTPs - nucleotide triphosphates

OPLS-DA - orthogonal PLS discriminant analysis

PBS - phosphate buffer saline

PCA - principal component analysis

PI - propidium iodide

PIKKs - phosphatidylinositol-3 kinase-related kinases

PLS-DA - PLS discriminant analysis

pS - phosphoserine

pT – phosphothreonine

PTMs - post-translational modifications

pY – phosphotyrosine

QC - quality control

R0 - L-arginine

R6 - L-$^{13}C_6$-arginine

ROS – reactive oxygen species

ROS/RNS - reactive oxygen and nitrogen species

RPA - replication protein A

RPLC – reversed phase liquid chromatography

RPLC-MS/MS - reversed phase liquid chromatography-tandem mass spectrometry

SAX - strong anion-exchange chromatography

SCX - strong cation-exchange chromatography

SDS - sodium dodecylsulfate

Ser - serine

SILAC - stable isotope labelling with amino acids in cell culture

SIMAC - sequential elution from IMAC

SSBs - single-strand breaks

ssDNA - single stranded DNA

T-ALL - T-cell acute lymphoblastic leukaemia

TFA - trifluoroacetic acid

Thr - threonine

TMT - tandem mass tag

TOF – time of flight

Tris-HCl - tris hydrochloride

Preface

DNA damage induction by either radio- or chemo-therapy has been the most widely used approach in oncology exploiting one of the hallmarks of cancer: genomic instability. However, these therapies are very unspecific and often accompanied by collateral damage to healthy tissues. In recent years, much effort has been put on discovery and development of tumour specific treatment, which would specifically target cancer cells and not affect the normal tissues. A promising approach that has been developed recently is to take advantage of tumour specific abnormalities in DDR. Most of the cancer cells possess defects in one or more DDR pathways and suffer from elevated levels of replication stress due to dysregulated oncogenic signalling and increased levels of endogenous DNA damage. Importantly, given the vast number of the DDR genes mutated in cancers, it has been emphasized that to effectively exploit the DDR targets in cancer treatment, the therapy should be individually tailored to patients lacking specific DDR functions based on the synthetic lethality principle.

Two promising examples of such treatment strategies are targeting the S and G2/M DNA damage checkpoints in G1/S DNA damage checkpoint-deficient cells and specific targeting of proteins and protein kinases involved in replication stress response. Inhibition of the ATR/Chk1 pathway has been shown to be synthetically lethal in both above mentioned scenarios. In several studies, it has been shown that inhibiting this pathway is selectively toxic in cells with high levels of oncogene-induced replication stress (1–7). On the other hand, there have been several papers published, in which the authors emphasized the efficiency of ATR inhibition in combination with genotoxic therapy in p53- or ATM-deficient cells (8–12). Therefore, selective targeting of the ATR/Chk1 pathway offers a promising therapeutic approach for cancer treatment in a broad range of tumours in both monotherapy and for selectively sensitizing cancer cells towards current genotoxic treatment.

In order to reveal molecular mechanisms involved in such therapeutic approach, we decided to describe changes in phosphoproteome in a given cellular model. Our efforts were driven by the fact that protein phosphorylation is a transient, reversible PTM with dynamic nature enabling it to be the major steering force of most of the cellular processes which require rapid and tightly regulated signalling. These processes include cellular signalling and communication, proliferation, differentiation, metabolism, transcriptional and translational regulation, degradation of proteins, and cell survival (13).

The presence of phosphorylation in specific regions of a protein molecule is believed to induce conformational changes in the target protein, which influence its behaviour within a cell. Such conformational changes can modulate activity of an enzyme (such as phosphorylation in an activation loop in a protein kinase), subcellular localization of a protein, or its stability (14). Phosphorylation is mediated by protein kinases, which compose one of the largest enzyme superfamilies in higher eukaryotes. The reverse reaction, dephosphorylation, is mediated by protein phosphatases. Tight cooperation of protein kinases and protein phosphatases is essential for regulation of biological processes in a cell, and dysregulation of these processes has been described to contribute to multiple diseases including cancer (15). Technological advances in the recent past led to development of phosphoproteomic approaches that allow researchers to identify aberrantly activated signalling pathways in a particular disease state, and establish appropriate therapeutic targets that can be exploited as specific targets for small molecule inhibitors (16).

In this thesis, we aimed to elucidate molecular mechanisms underlying radiosensitization of MOLT-4 cell line (T-ALL) by specific inhibition of kinases from the phosphatidylinositol-3 kinase-related kinases (PIKKs) family using two highly potent and selective inhibitors of ATR and ATM, VE-821 and KU55933, respectively. To do so, we decided to combine multiple approaches: cell biology techniques to investigate the inhibitor-induced phenotypes, phosphoproteomics to study protein phosphorylation triggered by irradiation and its modulation by kinase inhibitors, and metabolomics to reveal drug-induced changes in metabolome of irradiated cells. Since the detection and quantification of phosphorylated peptides in complex biological samples is challenging due to their low stoichiometry, we also dedicated a part of this doctoral thesis to selection of an optimal method for phosphopeptide enrichment.

That said, we present here different data of various nature, and thus the Results and Discussion sections are organized into several blocks. Furthermore, the nature of “omic” data implies a complicated data analysis and implementation of multiple bioinformatic tools and database searches in order to interpret the data. Therefore, the Results section differs from the theses based on the approach of “classical” biochemistry or biology and it comprises of a brief overview of the acquired results, and their detailed description is given in the Discussion section where they are discussed in context of all data presented in this thesis and recent literature.

1. Introduction

1.1. Characterization of DNA damage induced by ionizing radiation

The term **ionizing radiation (IR)** describes a radiation that has enough energy to liberate an atomic particle from an originally electrically neutral atom or molecule, ionizing it. The ionization can occur either directly or indirectly. The **direct ionization** is mediated by any charged massive particle that carries sufficient kinetic energy (e.g. alpha and beta particles) to ionize atoms or molecules. On the other side, gamma rays, X-rays, and neutrons are referred to as the **indirectly ionizing radiation**. Since they have no charge, their effects are induced secondary by liberation of directly ionizing particles.

When cells are exposed to IR, cellular structures can be damaged by ionization directly by deposition of energy (this mechanism dominates in cells with a low water content), but also indirectly by ionization of water molecules in cells with a high water content – by a mechanism called **water radiolysis**. Such ionization leads to generation of highly **reactive oxygen species (ROS)**, which secondary attack DNA and other biomolecules (reviewed in (17,18)).

There is a wide range of DNA lesions typically occurring in response to IR. It has been previously estimated that the irradiation of a mammalian cell by a dose of 1 Gy results in approximately **1000-2000 damaged bases**, **800-1600 damaged deoxyriboses**, **500-1000 single-strand breaks (SSBs)**, and most importantly, **20-40 double-strand breaks (DSBs)**, which are the most deleterious damage to the mammalian DNA, and thus they represent the biggest threat to genomic integrity amongst all types of DNA lesions (19).

DSBs are assumed to be the most lethal class of DNA damage since a failure to repair just a single DSB can result in cell death (20) implying the importance of DSB repair for cell viability. Moreover, both repair and misrepair of DSBs can lead to mutations and chromosomal rearrangements, potentially resulting in cancer development. Since genetic alterations have such a significant impact on cell survival and viability, cells have evolved robust, but finely regulated molecular mechanisms that include detection of DNA lesions, signalling of their presence, promoting their repair, and activation of cell cycle

checkpoints. Altogether, these mechanisms are summarized under the term **DNA damage response (DDR).**

The key components of DDR, which trigger cellular response to detected DNA lesions, are protein kinases that belong to **phosphatidylinositol 3-kinase (PI3K) family class IV**, better known as **phosphatidylinositol-3 kinase-related kinases** (**PIKKs**; reviewed in (21)).

1.2. Phosphatidylinositol-3 kinase-related kinase family

The PIKK family comprises 6 proteins with most of the members possessing serine/threonine kinase activity: ataxia telangiectasia mutated kinase (**ATM**), ataxia telangiectasia and Rad3 related kinase (**ATR**), DNA-dependent protein kinase catalytic subunit (**DNA-PKcs**), mammalian target of rapamycin (**mTOR**), suppressor with morphological effect on genitalia family member (**SMG-1**), and transactivation/transformation-domain-associated protein (**TRRAP**). All 6 members of the PIKKs family show considerable similarities in their domain architecture and extensive sequence homology, particularly in their C-terminal kinase domains FAT (FRAP-ATM-TRAP) and FATC (FAT- C-terminal), both of them particularly important for their kinase activity and its regulation (22,23). On the contrary, the N-terminal region is poorly conserved and thus believed to be responsible for regulation of interactions with differential substrates and adaptor proteins (24).

Among the PIKKs, **ATM, ATR, and DNA-PK** act as the main regulators of cellular response to DNA damage and DNA replication stress. They share the same phosphorylation motif (as shown in **figure 1**, they predominantly phosphorylate their targets on serine and threonine residues followed by Gln (25)) and many substrates such as the histone variant H2AX (26–28); however, they are activated by different types of DNA lesions and act in distinct pathways, which are partially overlapping, but non-redundant - the crosstalk between the pathways often occurs as a consequence of the inter-conversion of the activating lesions. A large scale proteomic study investigating proteins that are inducibly phosphorylated on a consensus site recognized by ATM and ATR after exposure to IR identified 900 phosphorylation sites in 700 proteins, demonstrating for the first time how extraordinarily broad is the landscape of ATM/ATR substrates phosphorylated

in response to DNA damage (29). The distinct roles of each of ATM and ATR will be further discussed.

The importance of **DNA-PK** mainly derives from its essential role in non-homologous end joining (NHEJ), which is considered to be the major DSB repair pathway. A detailed description of DNA-PK, its role in NHEJ, and its potential as a drug target for the support of radiotherapy is beyond the extent of this dissertation thesis; more details are given in our publication (30).

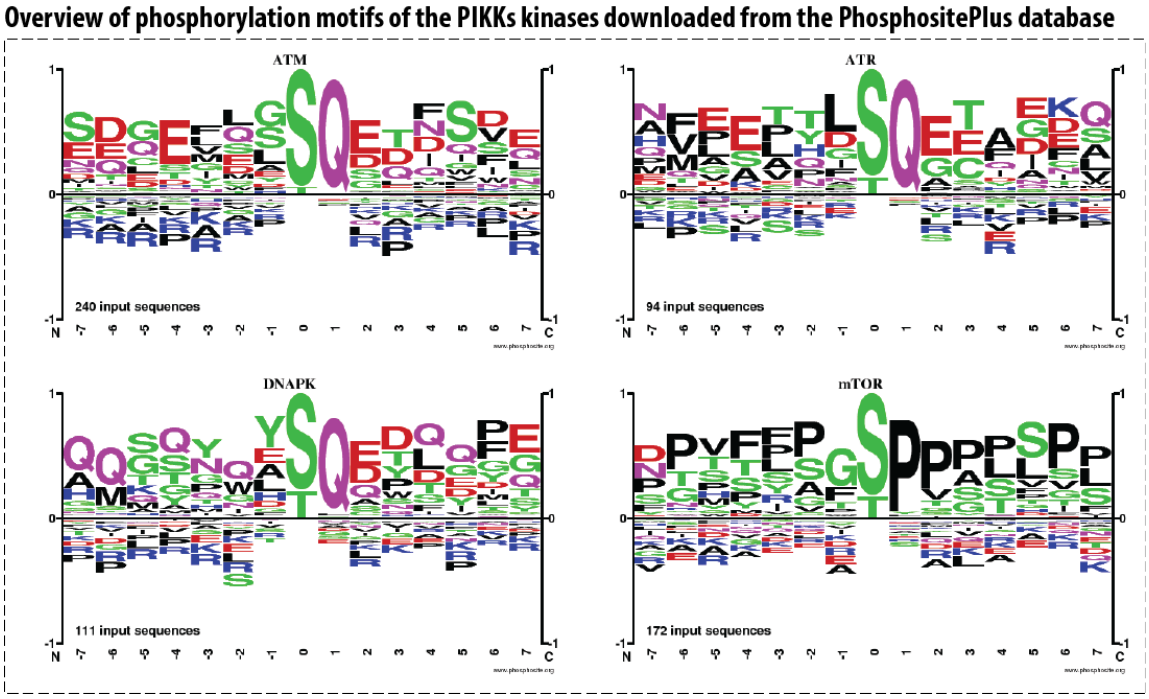

Figure 1: Overview of the visualised phosphorylation motifs of the PIKKs members. *Sequence logo for each one of the PIKKs was generated using manually curated phosphorylation sites from the PhosphoSitePlus database (June 2016) with known experimentally assessed kinase responsible for their phosphorylation. The sequence motifs (STY ± 7 AA) for ATM, ATR, DNA-PK, and mTOR are depicted together with the number of their substrates annotated in the database.*

The protein kinase **mTOR** is the principle regulator of cellular metabolism promoting anabolic processes and inhibiting catabolic processes such as autophagy. It integrates signals from different upstream pathways triggered by a wide variety of signals including nutrients, hormones, growth factors, and also cellular stresses to regulate cell growth, metabolism, cell survival, protein synthesis, and transcription (reviewed in (31)). Although mostly known for its metabolism-regulating functions, mTOR is also an integral member of DDR playing an important role in the determination of cell faith after DNA damage induction (reviewed in (32)). A direct link has been shown between DNA damage induced ATM activation and mTOR inhibition – the crosstalk between these two kinases

is mediated by ATM-activated AMP-activated protein kinase (**AMPK)**, which in turn both directly and indirectly inhibits mTOR (reviewed in (33)). Indeed, mTOR inhibition has been also shown to affect radiosensitivity and DDR in irradiated cells (34,35).

TRRAP has been shown to have an important role in embryonic development, cell-cycle progression, and mitotic control (36). Interestingly, it is the only member of this family that lacks serine/threonine kinase activity. **SMG-1** is the newest member of the PIKKs family. It plays a critical role in the mRNA quality control system, termed nonsense-mediated mRNA decay, which protects cells from an accumulation of aberrant mRNAs (37).

1.2.1. Ataxia-telangiectasia mutated kinase (ATM)

ATM is the best known as the chief mobilizer of the vigorous cellular response to DSBs; however, recent studies have indicated that ATM is also involved in signalling pathways maintaining cellular homeostasis in response to hypoxia, oxidative stress, and regulation of cellular metabolism (reviewed in (38)).

The *ATM* gene was originally identified in **ataxia-telangiectasia (A-T)**, a human genome instability disorder inherited in an autosomal recessive manner. All A-T patients carry mutations in the *ATM* gene which encodes the ATM protein (39). The hallmarks of this disease include progressive cerebellar degeneration that develops into severe neuromotor dysfunction (ataxia), telangiectasia (dilation of blood vessels observed primarily in the eyes), immunodeficiency, hypersensitivity to ionizing radiation, and increased incidence of malignancies, mostly lymphoreticular (40). On the cellular level, A-T is characterized by increased chromosomal instability, premature senescence of cultured primary fibroblasts, and hypersensitivity to DNA damaging agents. The disease phenotype can be attributed to the abrogation of the cellular response to DSBs.

Activation of ATM is one of the first steps in response to DSBs caused by the exposure to ionizing radiation (40). In undamaged cells, inactive ATM exists in a form of a homodimer, which dissociates into active monomers after activation. The activation is associated with **autophosphorylation at Ser1981** (41), which is a marker of activated ATM. However, there are more post-translational modifications (PTMs) accompanied with ATM in its catalytically active state; to date, three additional autophosphorylation sites (42–44) and one acetylation site (Lysine 3016; (45,46)) have been identified in fully activated ATM.

The full and timely activation of ATM is dependent on the **Mre11/Rad50/Nbs1** (**MRN) complex**, an evolutionary conserved protein complex composed of **Mre11**, **Rad50**, and **Nbs1** proteins (47). Mutations of each one of the genes coding these three proteins result in genetic disorders characterized by symptoms similar to A-T (48–50). The indispensability of this complex to cells is affirmed by the fact that null mutation of either one of the three genes causes embryonic lethality in mice (51). MRN is one of the first complexes recruited to DNA DSBs, where it functions as a damage sensor and a physical bridge spanning the DSB ends (52). In addition to ATM recruitment and retention at the DSB sites, it is also required for both NHEJ and homology-directed recombination (HDR) repair of DSBs - the DSB-end resection mediated by MRE11 nuclease activity is one of the first steps in HDR. Moreover, MRN is also phosphorylated by ATM, which is important for activation of different DDR pathways and may create a positive feedback loop that maintains ATM activity (reviewed in (38)). In addition to MRN complex, there are other proteins important for timely ATM activation, such as mediator of DNA damage checkpoint protein 1 (MDC1), which interacts with both ATM and phosphorylated H2AX (**γH2AX**) and facilitates the phosphorylation of additional H2AX by ATM, creating another positive feedback loop (53).

A vast functional network of proteins is precisely orchestrated by ATM-mediated phosphorylation. In this network, the proteins often undergo direct phosphorylation mediated by ATM as well as phosphorylation by other kinases whose activity is ATM-dependent. Frequently, these proteins phosphorylated by ATM are targeted by other PTMs, such as ubiquitylation or sumoylation, and together, these PTMs contribute to the regulation of ATM-dependent DDR signalling pathways (54). Nowadays, the map of ATM targets contains hundreds of proteins, some of them have been extensively studied and validated in multiple studies; however, many of them were discovered by proteomic and phosphoproteomic screenings and need further evaluation (29,42,55–57). In June 2016, the largest phosphorylation sites database PhosphoSitePlus® (58) contained 240 manually curated substrates of ATM (as can be also seen in **figure 1** as a number of input sequences for sequence motif visualization). **Figure 2A** depicts a map of ATM interactors downloaded from STRING *v10.0* database (June 2016; STRING interaction score > 0.9); selected statistically overrepresented KEGG pathways in which the proteins from are involved are also given (**figure 2B**). Predictably, many of the interactors are proteins involved in DDR pathways (such as HDR, NHEJ, or p53 signalling pathway); however,

there are also pathways usually more referred in the context with cellular metabolism (such as PI3K-Akt, AMPK, or mTOR signalling pathways), demonstrating the aforementioned overlap between the DDR- and cellular metabolism- regulating functions of ATM.

One of the most important examples of ATM phosphorylated and regulated proteins involved in DDR is the tumour suppressor protein **p53**. Under normal conditions, **p53** is present in a latent form with low affinity to specific sequences of DNA; however, following DSBs formation, its transcriptional activity increases substantially, and this increase is to a great extent ATM-dependent. p53 is regulated by ATM in a multi-layered manner – both direct phosphorylation by ATM and indirect, but ATM-dependent phosphorylation, contribute to the rapid activation and stabilization of p53 in response to DNA damage (59). ATM directly phosphorylates p53 on **serine (Ser) 15** (60), but the **Ser 20** located on the same (transactivation) domain is phosphorylated by activated checkpoint kinase 2 (**Chk2 ;** (61,62)), a key downstream target of ATM (63). This phosphorylation events stabilize p53 by preventing its murine double minute protein-2 (**Mdm2)**-mediated ubiquitylation and degradation (64,65). Moreover, ATM also phosphorylates **Mdm2 on Ser 166** and **Ser 395** (66,67), which further contribute to the accumulation of p53.

The ATM-dependent activation and stabilization of p53 are central to the modulation of the cellular transcriptome following IR-induced DSBs formation. The activated p53 directly drives the expression of many genes, including the cell cycle regulating cyclin dependent kinases (CDKs) inhibitor **p21** (68,69) and pro-apoptotic proteins **BAX**, **PUMA**, and **NOXA** (70). Additionally, p53 also indirectly negatively regulates transcription of a number of genes, including those encoding anti-apoptotic proteins **BCL-2** and **MCL-1** (71). Thus, p53 is a crucial ATM target, regulating cell cycle progression (mostly the G1/S checkpoint) and cell death after genotoxic stress.

Besides p53, ATM also regulates other ***transcription factors*** such as **NF-κB** (72)), ***protein kinases*** (e.g. **Chk2** (73), **DNA-PK** (74), protein kinase B (**AKT** ; (75))), and a large number of ***other proteins and members of protein complexes involved in DSBs repair*** (e.g. **H2AX** , **Artemis** (76), CtBP-interacting protein (**CtIP** ; (77)), or the members the MRN complex (78–81)).

Chk2 is a serine/threonine protein kinase, which is a downstream effector of ATM orchestrating the cell cycle arrest after DSBs induction (63). It regulates the cell cycle through phosphorylation of **CDC25A**, **CDC25B**, and **CDC25C** phosphatases, inhibiting

their activity and promoting their degradation (82). Consequently, these phosphatases cannot remove inhibitory phosphorylation on **CDK-cyclin complexes** and thus promote the cell cycle arrest (reviewed in (83)).

A Map of ATM interactors downloaded from STRING database (highest confidence level interactions - STRING score > 0.9)

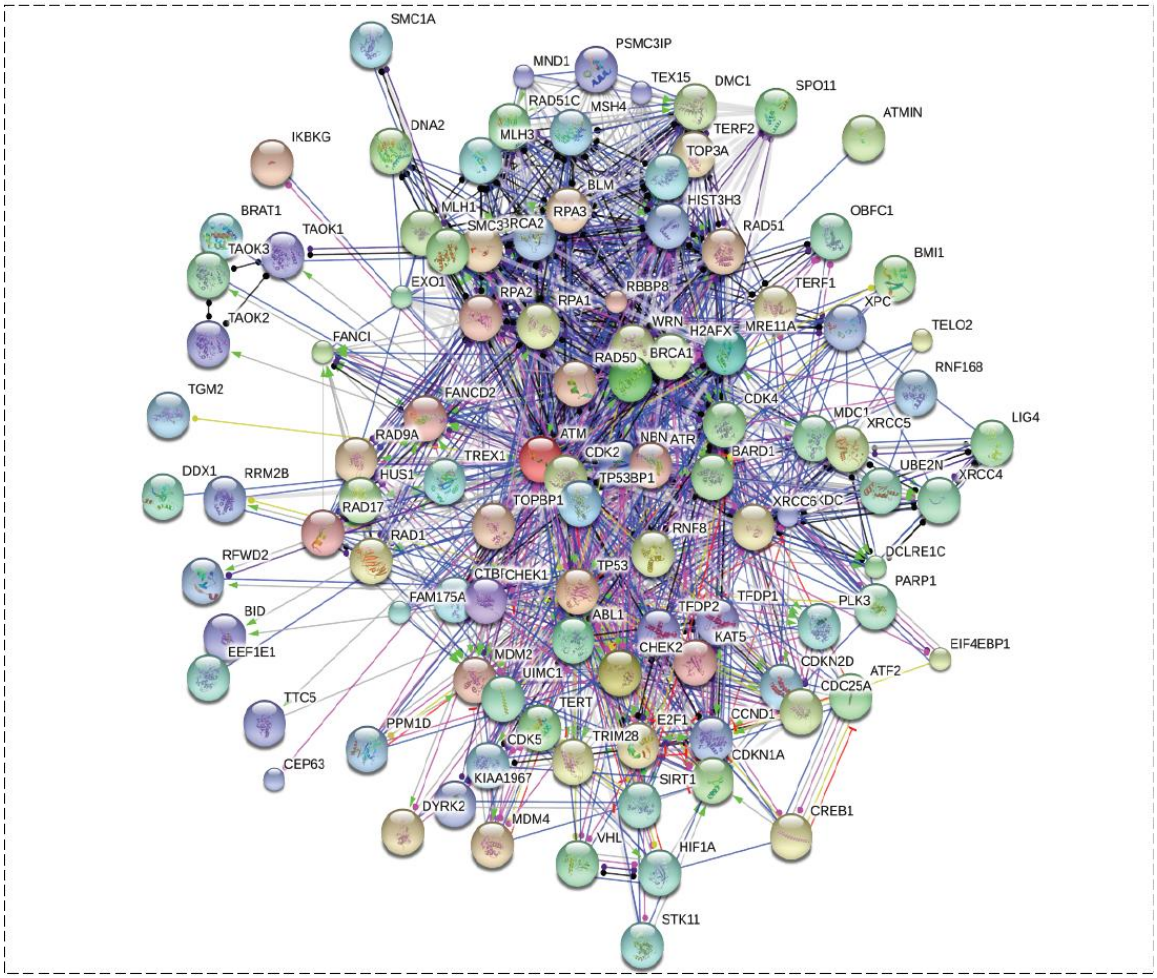

B Enriched KEGG pathways

pathway ID	pathway description	gene count	fdr	matching proteins in the network (gene names)
4110	Cell cycle	18	2.64E-19	ABL1,ATM,ATR,CCND1,CDC25A,CDK4,CDKN1A,CDKN2D,CHEK1,CHEK2,E2F1,MDM2,PRKDC,SMC1A,SMC3,TFDP1,TFDP2,TP53
3460	Fanconi anemia pathway	14	4.93E-19	ATR,BLM,BRCA1,BRCA2,FANCD2,FANCI,MLH1,RAD51,RAD51C,RPA1,RPA2,RPA3,TELO2,TOP3A
4115	p53 signaling pathway	14	1.85E-17	ATM,ATR,BID,CCND1,CDK4,CDKN1A,CHEK1,CHEK2,MDM2,MDM4,PPM1D,RFWD2,RRM2B,TP53
3440	Homologous recombination	11	2.97E-17	BLM,BRCA2,MRE11A,NBN,RAD50,RAD51,RAD51C,RPA1,RPA2,RPA3,TOP3A
3450	Non-homologous end-joining	8	2.45E-14	DCLRE1C,LIG4,MRE11A,PRKDC,RAD50,XRCC4,XRCC5,XRCC6
3430	Mismatch repair	6	4.03E-08	EXO1,MLH1,MLH3,RPA1,RPA2,RPA3
4068	FoxO signaling pathway	8	3.94E-06	ATM,CCND1,CDKN1A,CDKN2D,MDM2,PLK3,SIRT1,STK11
4151	PI3K-Akt signaling pathway	11	1.82E-05	ATF2,BRCA1,CCND1,CDK4,CDKN1A,CREB1,EIF4EBP1,IKBKG,MDM2,STK11,TP53
3030	DNA replication	4	0.00042	DNA2,RPA1,RPA2,RPA3
3420	Nucleotide excision repair	4	0.00114	RPA1,RPA2,RPA3,XPC
5202	Transcriptional misregulation in cancer	6	0.0023	ATM,BMI1,CDKN1A,HIST3H3,MDM2,TP53
4152	AMPK signaling pathway	5	0.00408	CCND1,CREB1,EIF4EBP1,SIRT1,STK11
4120	Ubiquitin mediated proteolysis	5	0.00676	BRCA1,MDM2,RFWD2,UBE2N,VHL
4210	Apoptosis	4	0.00946	ATM,BID,IKBKG,TP53
4010	MAPK signaling pathway	6	0.0184	ATF2,IKBKG,TAOK1,TAOK2,TAOK3,TP53
4150	mTOR signaling pathway	3	0.0262	EIF4EBP1,HIF1A,STK11

Figure 2: ATM-interacting network. *Proteins interacting with ATM were downloaded from the STRING database v10.0 (June 2016). Only those interactions with STRING score > 0.9 (i.e. high confident interactions) are depicted* ***(A)****. Proteins depicted in the network were subjected to functional annotation over-representation analysis. Selected over-represented KEGG pathways are depicted* ***(B)****.*

1.2.2. **ATM-Rad3 related kinase (ATR)**

While activation of ATM is triggered by DSBs and is active throughout the cell cycle, ATR responds to **single stranded DNA (ssDNA)** structures and acts primarily in S and G2 phases. It is the central kinase responding to replication stress, which cells undergo during DNA replication as well as after exposure to genotoxic events. DNA damage induced by IR, UV, chemotherapeutic drugs, or inhibitors of DNA replication causes the DNA-polymerases to stall at DNA lesions while the replicative helicases continue to unwind the DNA helix ahead of the replication fork leading to generation of long ssDNA stretches. Additionally, ssDNA structures can be formed at DSB sites after 5' to 3' nucleolytic degradation of one of the chains, a step required for DSBs repair by homologous recombination (reviewed in (9,84)). ATR is an essential protein; homozygous mutation of ATR caused peri-implantation embryonic lethality in mice (85,86), and no living human completely lacking ATR has been identified. Nevertheless, a hypomorphic ATR mutation is responsible for the **Seckel syndrome** – a recessive autosomal hereditary disorder characterized by microcephaly and mental- and growth-retardation (87).

Similar to ATM, which is recruited to DSB indirectly via MRN complex, ATR requires specific protein complexes for its localization to ssDNA and subsequent activation. Cortez et al. identified **ATR-interacting protein** (**ATRIP**; (88)), which interacts with the N-terminus of ATR to form a protein complex. ATRIP is responsible for localization of the ATR/ATRIP complex at ssDNA sites via its interaction with a heterotrimeric protein complex - **Replication protein A** (**RPA**), which coats most forms of ssDNA in cells including the ssDNA that is formed during DNA replication and damage (89). After the recruitment of ATR/ATRIP to ssDNA stretches, ATR needs to be activated, and this activation is dependent on co-localization of the ATR/ATRIP complex with the **9-1-1 complex (RAD9/RAD1/HUS1)**, a heterotrimeric ring-shaped molecule that serves as a docking site of **DNA topoisomerase II-binding protein-1 (TOPBP1)**. The co-localization of these two complexes is mediated by **Rad17**-containing, **RFC-like** 'clamp loader' that recognizes the RPA-ssDNA and dsDNA junctions and loads the 9-1-1 complex to DNA (90,91). TOPBP1 contains an **ATR activation domain**, which has been confirmed to be the actual activator of ATR kinase (90,92–94). As in other the case of other PIKKs, ATR is transformed into a hyperphosphorylated state upon activation; however, only Thr 1989 has been identified to be essential for robust ATR activation. The **Threonine (Thr)**

1989 autophosphorylation is the crucial step in ATR activation; it enables the binding to the ATR activation domain of TOPBP1 and ATR activation (95).

As in the case of other PIKKs, ATR phosphorylates many substrates bearing the typical S/TQ motif (**figure 1**). As visualized in the network in **figure 3A**, the list of direct ATR-interacting proteins downloaded from STRING database *v10.0* (June 2016, STRING score > 0.9) contained 105 proteins. The structure of the network is in concordance with known biological roles of ATR; many of the interactors are organized into densely interconnected clusters as they form ATR-regulated protein complexes essential for DNA replication and response to DNA replication stress (*i.e.* Replication factor A, Replication factor C, Minichromosome maintenance complex, Origin recognition complex). Besides these complexes, there are also proteins involved in DDR pathways such Fanconi anaemia pathway, Homologous recombination, Mismatch repair, and other KEGG pathways listed in **figure 3B**.

Checkpoint kinase 1 (Chk1) is often described as the primary target and main downstream effector of activated ATR. However, it has been repeatedly reported that ATR- and Chk1- inhibition provided different outcomes when combined with genotoxic stress in cancer cells (96,97) suggesting that despite being the main effector, Chk1 is not responsible for all downstream signalling of activated ATR.

To fully activate Chk1, several ATR-driven steps are necessary. First, **Rad17** is phosphorylated by ATR, which promotes its association with **Claspin** (98). Claspin is subsequently also phosphorylated by ATR, which enables its interaction with Chk1. Finally, Chk1 brought to the proximity of the activated ATR is phosphorylated in its kinase activation loop region, which in turn leads to its activation (99). Two Chk1 sites have been described to be ATR-phosphorylated during this activation step – **Ser 345** and **Ser 317**; however, only Ser 345 is considered and often monitored as a specific marker of ATR activation, and it is also the essential phosphorylation site required for Chk1 function while the latter is considered to be rather contributory (10,100,101). Chk1 is then **autophosphorylated** at **Ser 296** and released from chromatin to trigger cell cycle checkpoints signalling, which is of a great importance for damaged cells as it allows time for repair to occur.

Two downstream protein phosphatases **cdc25a** and **cdc25c** are the two main Chk1 targets responsible for S and G2/M arrests, which occur after their inactivation by Chk1 (102). Under unperturbed conditions, these phosphatases remove inactivating phosphates

from CDKs/cyclin complexes to maintain normal cell cycle progression. When inactivated, the activity of CDKs decreases to slow down cell cycle progression. Another Chk1 target that contributes to CDKs inhibition, and thus cell cycle arrest after ATR activation, is the **Wee1** protein kinase, which is stabilized by Chk1-mediated phosphorylation.

A Map of ATR interactors downloaded from STRING database (highest confidence level interactions - STRING score > 0.9)

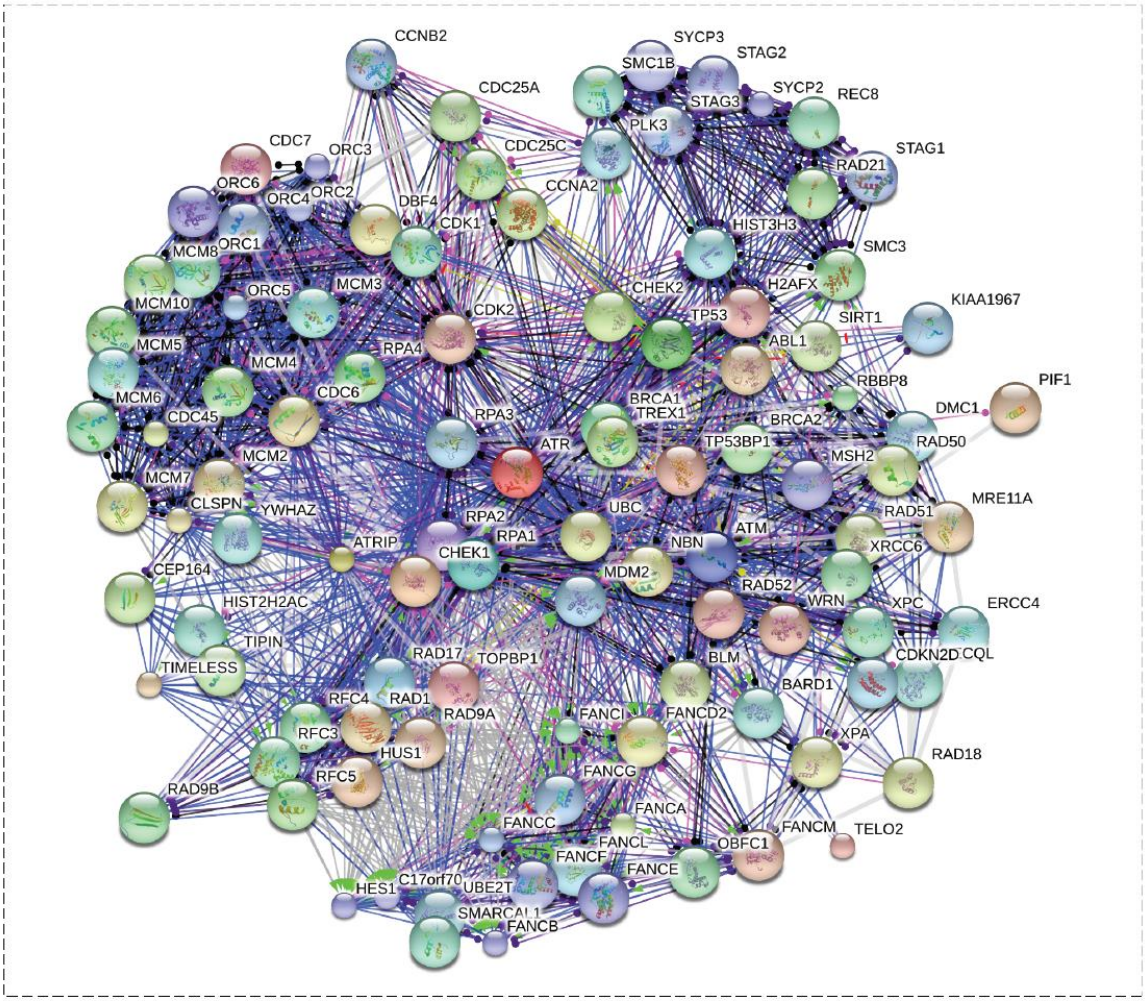

B Enriched KEGG pathways

pathway ID	pathway description	gene count	fdr	matching proteins in the network (gene names)
4110	Cell cycle	34	9.81E-49	ABL1,ATM,ATR,CCNA2,CCNB2,CDC25A,CDC25C,CDC45,CDC6,CDC7,CDKN2D,CHEK1,CHEK2,DBF4,MCM2,MCM3,MCM4, MCM5,MCM6,MCM7,MDM2,ORC1,ORC2,ORC3,ORC4,ORC5,ORC6,RAD21,SMC1B,SMC3,STAG1,STAG2,TP53,YWHAZ
3460	Fanconi anemia pathway	25	8.38E-43	ATR,ATRIP,BLM,BRCA1,BRCA2,C17orf70,ERCC4,FANCA,FANCB,FANCC,FANCD2,FANCE,FANCF,FANCG,FANCI,FANCL,FANCM, HES1,RAD51,RPA1,RPA2,RPA3,RPA4,TELO2,UBE2T
3030	DNA replication	13	1.02E-19	MCM2,MCM3,MCM4,MCM5,MCM6,MCM7,RFC3,RFC4,RFC5,RPA1,RPA2,RPA3,RPA4
3440	Homologous recombination	11	3.32E-17	BLM,BRCA2,MRE11A,NBN,RAD50,RAD51,RAD52,RPA1,RPA2,RPA3,RPA4
3420	Nucleotide excision repair	10	1.64E-12	ERCC4,RFC3,RFC4,RFC5,RPA1,RPA2,RPA3,RPA4,XPA,XPC
3430	Mismatch repair	8	8.08E-12	MSH2,RFC3,RFC4,RFC5,RPA1,RPA2,RPA3,RPA4
4115	p53 signaling pathway	7	1.91E-06	ATM,ATR,CCNB2,CHEK1,CHEK2,MDM2,TP53
3450	Non-homologous end-joining	3	0.000944	MRE11A,RAD50,XRCC6
4068	FoxO signaling pathway	6	0.000944	ATM,CCNB2,CDKN2D,MDM2,PLK3,SIRT1

Figure 3: ***ATR-interacting network.*** *Proteins interacting with ATR were downloaded from the STRING database v10.0 (June 2016). Only those interactions with STRING score > 0.9 (i.e. high confident interactions) are depicted* ***(A)****. Proteins depicted in the network were subjected to over-representation analysis of functional annotation. Selected over-represented KEGG pathways are depicted* ***(B)****.*

As in the case of its upstream kinase, the list of known Chk1 targets is relatively long, comprising 192 manually curated substrates (as listed in the PhosphoSitePlus® database, June 2016). In addition to its DNA damage checkpoint functions mentioned above, Chk1 has been shown to regulate the mitotic spindle checkpoint, contribute to several DNA damage repair pathways (HDR, Fanconi anaemia pathway), and repression of transcription after DNA damage induction (reviewed in (103)).

1.3. **Targeting DDR as a promising strategy in oncology**

DNA damage induction by either radio- or chemo- therapy has been the most widely used approach in oncology exploiting one of the hallmarks of cancer: genomic instability. However, such treatment is very unspecific and often accompanied by collateral damage to healthy tissues. In recent years, much effort has been put on discovery and development of tumour specific treatment, which would only specifically target cancer cells and not affect the normal tissues. A promising approach that has been developed recently is to take advantage of the tumour specific abnormalities in DDR.

In a current study (104), manually curated data stored in signalling pathways and protein-protein interactions databases were analysed to compile a list of **450 human DDR genes**, which were further examined in terms of their association with individual cancer types to identify deregulated components of the DDR, discover novel therapeutic targets within the DDR network, and predict their druggability. Given the vast number of the DDR genes mutated in cancers, the authors of the study emphasized that to effectively exploit the DDR targets in cancer treatment, the therapy should be individually tailored to patients lacking specific DDR functions based on the **synthetic lethality** principle. This principle was originally presented in *Drosophila*, and it describes two genetic loss-of-function events - each one of them still compatible with cell viability; however, they are lethal when both of them occur in the same cell (105). In the context of cancer treatment using DDR proteins inhibitors, one of the two events is cancer-specific and cannot be found in normal cells; the second one is achieved pharmacologically by the targeted inhibitor treatment. A clinically validated example of a successful use of this approach is the application of poly(ADP-ribose) polymerase (PARP) inhibitors (olaparib) in BRCA-deficient cancer cells (106,107).

Moreover, the synthetic lethality term can be also used more loosely to describe strategies in which the tumour-specific defects only causes increased sensitivity to a

combination of therapeutic agent (such as chemo- or radio- therapy) and DDR-targeting compound – *i.e.* the DDR inhibitor can be used for a **specific radio- or chemo-sensitisation** of the cancer cells. The key differences in DDR between cancer cells and normal cells that can be exploited to develop a specific therapy comprise following aspects: most of the cancer cells have **defects in one or more DDR pathways**, suffer from **elevated levels of replication stress** due to dysregulated oncogenic signalling and **increased levels of endogenous DNA damage** (caused for instance by increased intrinsic ROS generation (108); reviewed in (109)) .

A promising example of such a strategy is **targeting the S and G2/M DNA damage checkpoints in G1/S DNA damage checkpoint deficient cells** (110). A recent study investigated mutational profiles in 3,281 tumours across 12 tumour types, identified 127 significantly mutated genes, and categorized them based on cellular processes they are involved in (111). The *TP53* tumour suppressor gene was affected by mutations in 42.0 % of cancer cells sequenced in this study, and thus it was the most frequently mutated gene in cancer genome. The list of the 127 significantly mutated genes in cancer also contained other members of the ATM/Chk2/p53 pathway - ATM and Chk2 kinases were found to be targeted by mutations in 3.3 % and 0.9 % of cancer cells analysed, respectively. As this pathway is essential for maintaining the G1/S DNA damage checkpoint after IR, the results of this study suggested that targeting the remaining DNA damage checkpoints might be a promising strategy in a considerable portion of solid tumours conventionally treated using radiotherapy (111).

Another promising strategy is to **target proteins and protein kinases involved in replication stress response** (7). Elevated level of DNA replication stress has been recently proposed as a hallmark of cancer because it is present in almost all cancers from the earliest stages (112). The mutations in genes controlling cellular growth and proliferation are responsible for this phenomenon – cancer cells deficient in G1/S checkpoint or with mutations deregulating replication origin firing suffer from premature entry into S-phase, and thus DNA replication can start before the necessary resources have been generated, which leads to triggering the replication stress response. Examples of such mutations that are common in cancers are *RB1* deficiency, *CDKN2A* deletion, Cyclin D1 or Cyclin E amplifications, *KRAS* mutations, or *MYC* amplifications (111,112).

Inhibition of the ATR/Chk1 pathway has been shown to be synthetically lethal in both above mentioned scenarios. In several studies, it has been shown that inhibiting this

pathway is selectively toxic in cells with high levels of oncogene-induced replication stress (1–7). On the other hand, there have been several papers published, in which the authors emphasized the efficiency of ATR inhibition in combination with genotoxic therapy in p53- or ATM- deficient cells (8–12). Taken together, selective targeting of the ATR/Chk1 pathway offers a promising therapeutic approach for cancer treatment in a broad range of tumours in both monotherapy and for the purpose of selectively sensitizing cancer cells to current genotoxic treatment.

1.3.1. The preclinical and clinical development of ATR inhibitors

Given their importance in DDR, small molecule kinase inhibitors have been synthesised for each one of the kinases from the PIKKs family to investigate their potential for development of a cancer-specific treatment. The preclinical and clinical development of current inhibitors of DNA-PK, ATM, and ATR has been extensively reviewed in two papers we published recently (30,113); therefore, for the purpose of this dissertation thesis, we will only discuss the development and use of ATR inhibitors.

The first ATR inhibitor identified proven to radiosensitize cancer cells was **caffeine** (1,3,7-trimethylxanthin) (114,115). However, caffeine is a low potent and unspecific inhibitor of ATM, ATR (IC50 (ATM): 0.2 mM; IC50 (ATR): 1.1 mM), and the rest of the PIKKs family. Moreover, the concentration that is required to radiosensitize human cancer cells is toxic. Another natural compound that has been identified as an ATR inhibitor is **schisandrin B** (1,2,3,13-tetramethoxy-6,7-dimethyl-5,6,7,8-tetrahydrobenzo[3',4']cyclo-octa[1',2':4,5]benzo[1,2-d][1,3]dioxole), which was isolated from the mature fruits of *Schisandra Chinensis*, a herb used in Chinese medicine (116,117). Although schisandrin B is more ATR-specific than caffeine (IC50 (ATR): 7.25 μM), it is weaker than the newly synthesised chemical inhibitors, so its use has been only evaluated in two preclinical studies.

NU6027 (2,6-diamino-4-cyklohexyl-methyloxy-5-nitroso-pyrimidine) was originally identified as a CDK2 inhibitor (IC50(CDK2): 10 μM); however, Harrison et al. noticed that this inhibitor sensitised cancer cells to cisplatin independently on its CDK2 inhibitory activity (118). Further study revealed that NU6027 is a more potent inhibitor of ATR than of CDK2 (IC50(ATR): 6.7 μM), and it was the ATR inhibition that was responsible for radio- and chemo- sensitization of NU6027-treated breast cancer cells (10).

Importantly, the results of this breast cancer study indicated that ATR-inhibitor treatment could be efficient in cancer cells with XRCC1 polymorphism and thus showing for the first time a synthetic lethality of ATR inhibition and a loss of a specific DNA repair protein. This XRCC1-ATR inhibition relationship has been further confirmed in another study (119); however, further evaluation of NU6027 in *in vivo* experiments is hampered by its poor solubility in water.

In a cell-based screening of 623 compounds previously reported to have some activity towards PI3K (120), Toledo at el. identified two compounds with a marked potency against ATR – **ETP-46464** (IC50(ATR): 25 nM) and **NVP-BEZ235** (IC50(ATR): 100 nM) (6), but these compounds also presented substantial activity towards ATM, PI3K, mTOR, and DNA-PKcs and thus lacked selectivity against ATR. Prior to this screening, **NVP-BEZ235** had been proposed as a PI3K and mTOR inhibitor (121) and shown to radiosensitize Ras-overexpressing tumours (122). However, considering another study that had reported cytotoxicity of ATR suppression in cells overexpressing Ras (2), the radiosensitization of cells in the aforementioned study was more likely to be dependent on the ATR inhibitory activity of NVP-BET235 rather than on PI3K/mTOR inhibition. Altogether, these reports confirmed the potential of chemical ATR inhibition in cells suffering from elevated levels of replication stress caused by dysregulated oncogenic signalling. The more selective compound – **ETP-46464** – has been further proven to sensitize cancer cells to IR and platinum drugs (123,124). Unfortunately, it has been shown to have poor pharmacological properties in mice and thus is not suitable for further in *vivo* evaluation.

The first potent and selective inhibitors of ATR that may offer a great promise in cancer treatment were presented by Vertex Pharmaceuticals in 2011. Charrier et al. reported the discovery of selective ATR inhibitors from the series of **3-amino-6-arylpyrazines** (125). In the following studies, two compounds from this series were further evaluated – **VE-821** and **VE-822 (**or **VX-970)**.

VE-821 (3-amino-6-(4-(methyl-sulfonyl)phenyl)-N-phenylpyrazine-2-carboxamide; IC50(ATR): 26 nM, Ki(ATR): 13 nM, Ki(mTOR) > 1 μM, Ki(DNA-PK): 2.2 μM, Ki(ATM): 16 μM) has been shown to be able to selectively induce irreversible growth arrest in several cancer cell lines that were either p53-deficient or p53-wt, but with dysfunctional ATM/Chk2/p53 pathway, while inducing only reversible growth arrest in normal cells. Moreover, VE-821 showed synergy with different genotoxic agents

including cross-linking drugs, antimetabolites, topoisomerase I and II poisons, and ionizing radiation. The dependence on the functionality of ATM signalling for the sensitivity to ATR inhibition was confirmed in experiments with A-T primary skin fibroblasts, in normal cells treated with ATM inhibitor KU-55933 or with knockdown of p53 expression (11). These results were confirmed in 2012 by Pires et al., who mostly focused on the radiosensitizing effect of ATR inhibition. In this study, the radiosensitization using VE-821 was proven in a variety of cell lines from a number of different tumour types suggesting that this effect is independent of tumour type. Moreover, VE-821 was shown to increase radiation-induced DNA damage and loss of viability of cancer cells under hypoxic conditions (126), which is of particular interest, as hypoxic tumours have been reported to be more resistant to radiotherapy (127). The ability of VE-821 to sensitize pancreatic cancer cell lines to radiotherapy or antimetabolites-based chemotherapy under both normoxic and hypoxic conditions was further confirmed by Prevo et al. (128). Since then, VE-821 has been consistently shown in several studies to sensitize a variety of different tumour types to different genotoxic events (97,129–135). Interestingly, Huntoon et al. compared the sensitization of ovarian cancer cells using VE-821 and a Chk1 inhibitor (MK-8776). Unexpectedly, even though these two kinases are reported as members of one ATR/Chk1 signalling pathway, where Chk1 serves as a downstream effector of ATR, the inhibition of each one of these kinases provided differential sensitization of the cancer cells to commonly used chemotherapy agents.

In 2012, Fokas et al. presented **VE-822,** which is a close analogue of VE-821 with increased potency against the ATR kinase (IC50 (ATR): 19 nM), excellent ATR selectivity, and most importantly, good pharmacokinetic properties. In their study, VE-822 was tested for in *vitro* and in *vivo* radiosensitization of pancreatic ductal adenocarcinoma cell lines. As in the case of VE-821, VE-822 did not affect the chemo- and radio- sensitivity of normal cells. *In vivo* experiments performed in mice bearing PDAC xenografts proved the efficiency of combination of VE-822 and chemo/radiotherapy without affecting normal tissue homeostasis (8). Furthermore, VE-822 has been tested in combination with cisplatin drugs in a panel of lung cancer cell lines and a panel of xenografts models derived from primary human non-small cell lung cancer (NSCLC) samples. Notably, VE-822 in combination with cisplatin caused tumour growth inhibition even in tumours that were originally non-responsive to cisplatin. Experiments performed in the NSCLC cell line models also confirmed the previously reported differences between the outcome of ATR

and Chk1 inhibition (136). Based on the consistently promising data from the preclinical in *vitro* and in *vivo* testing and its favourable pharmacokinetic properties, which allow intravenous administration of the drug to humans, VE-822 (as **VX-970**) is currently tested in phase I clinical trials to assess its safety and tolerability in combination with cytotoxic drugs (ClinicalTrials.gov Identifier: NCT02157792). Several expansion phase I and phase II trials are planned and currently recruiting patients to evaluate applications of VX-970 in different carcinomas and combination with genotoxic treatment (ClinicalTrials.gov Identifiers: NCT02595931, NCT02567422, NCT02589522, NCT02595892, NCT02627443, NCT02723864, NCT02487095).

The second series of highly potent and selective ATR inhibitors was developed by AstraZeneca. The first compound from the series of **sulfonyl-morpholino-pyrimidines** reported and shown to suppress tumour growth in mice xenografts after oral administration of the drug was **AZ20** (IC50(ATR): 50 nM, IC50(mTOR): 2.4 μM, IC50(other PIKKs)> 30 μM; (137).

An analogue of AZ20, **AZD6738** has a significantly improved ATR selectivity (IC50 (ATR): 74 nM, IC50 (mTOR): 23 μM, IC50 (ATM, DNA-PK) > 30 μM), solubility, and pharmacokinetic properties and thus is more suitable for oral dosing. It has been shown to be efficient in monotherapy as well in combination with chemotherapy in NSCLC cell lines and xenografts, especially in ATM-deficient cell lines (12) and also proven to be synthetically lethal in p53- or ATM- defective chronic lymphocytic leukaemia cells in *vitro* and in *vivo* (138,139). Due to its oral bioavailability and tolerability proven in *in vivo* xenografts models, AZD6738 is the second ATR inhibitor that has been subjected to clinical trials. The initial study testing the safety and tolerability in patients with leukaemia has been completed (ClinicalTrials.gov Identifier: NCT01955668), and three phase I trials are currently ongoing focused on the combination of AZD6738 with radio- and chemo- therapy in patients with advanced malignancies (ClinicalTrials.gov Identifier: NCT02264678, NCT02630199, NCT02223923).

1.4. Protein phosphorylation and its role in eukaryotic cells

Several hundred of PTMs of proteins have been described so far; among them, protein phosphorylation is one of the most studied as it is one of the most important PTMs in nature. Protein phosphorylation is a transient, reversible PTM, and this dynamic nature

of phosphorylation enables being the major driving force of most of the cellular processes which require rapid and tightly regulated signalling. These processes include cellular signalling and communication, proliferation, differentiation, metabolism, transcriptional and translational regulation, degradation of proteins, and cell survival (13). It is one of the most widespread regulatory mechanisms; it has been originally estimated that more than 50 % of proteins in mammalian cells are phosphorylated at some point during their life time (140). However, in a recent study conducted by Sharma et al., more than 75 % of cellular proteins were found to be phosphorylated (141). Cellular protein phosphorylation events are site-specific, often occur at multiple sites within a phosphoprotein, and more than 100 000 phosphorylation sites may exist in the human proteome (142). Some of them are always quantitatively phosphorylated whereas the occupancy of many phosphosites is very low.

There are four distinct types of phosphorylation known: O- phosphorylation, which occurs on serine, threonine, and tyrosine residues, N- (143), S- (144), and acyl- (145) phosphorylation, which are far less common and occur on histidine, lysine, cysteine, aspartic, and glutamic residues. In eukaryotic cells, it is the O- phosphorylation on serine, threonine, and tyrosine residues, which is considered to be predominant (146). Phosphorylation of histidine residues has been also described; it has been estimated that 6 % of the total phosphorylation in eukaryotes occurs on histidine residues (147). However, phosphohistidines are usually not observed in proteins due to rapid hydrolysis of the phosphoryl group under acidic conditions (148). The proportions of phosphoserine (pS), phosphothreonine (pT), and phosphotyrosine (pY) sites in a phosphoproteome were reported for the first time by Hunter and Sefton (1980), who determined them in chicken cells as 92.19 %, 7.77 %, and 0.03 %, respectively (149). Since then, several studies have been performed reporting similar trends: about 85-90 % of pS, 10-15 % of pT, and 0.5-5 % of pY. Substantial differences in the phospho-amino acids proportions are introduced by different model organism studied, degree of perturbation of a phosphoproteome by treatment conditions used in a particular study, and various methodological approaches used for a phosphopeptide enrichment and detection. In a recent label-free phosphoproteomic study, an intriguing trend was reported showing that the proportion of pY drastically decreases as coverage of the studied phosphoproteome increases, while pS and pT saturate only for technical reasons. Moreover, in comparison to pS and pT, phosphorylation stoichiometry of pY was maintained at a very low level in the absence

of any specific stimuli. Based on these observations, the authors proposed that pY should be considered a functionally separate PTM (141).

The presence of phosphorylation in specific regions of a protein molecule is believed to induce conformational changes in the target protein, which influence its behaviour within the cell. Such conformational changes can modulate activity of an enzyme (such as phosphorylation in an activation loop in a protein kinase), subcellular localization of a protein, or its stability (14). Phosphorylation is mediated by protein kinases, which compose one of the largest enzyme superfamilies in higher eukaryotes; it has been estimated that 2-3 % of all eukaryotic genes are coding protein kinases (150). The reverse reaction, dephosphorylation, is mediated by protein phosphatases. Tight cooperation of protein kinases and protein phosphatases is essential for regulation of biological processes in a cell, and dysregulation of these processes has been described to contribute to multiple diseases including cancer (15). Technological advances in the recent past led to development of phosphoproteomic approaches that allow researchers to identify aberrantly activated signalling pathways in a particular disease state, and establish appropriate therapeutic targets that can be exploited as specific targets for small molecule inhibitors (16).

Despite being such a widespread regulatory mechanism, the analysis of protein phosphorylation is hampered by several facts: (1) phosphorylated peptides are relatively low abundant in comparison to the non-phosphorylated peptides pool in cells; thus, it is not feasible to study phosphoproteome from an unfractionated peptide sample; (2) due to its dynamic nature, only a subfraction of cellular phosphoproteome is phosphorylated in a particular time; (3) techniques used to study protein phosphorylation have a limited dynamic range; therefore, it might be difficult to detect phosphopeptides from low abundant phosphoproteins; (4) the presence of the modification on the peptide alters its behaviour during liquid chromatography-tandem mass spectrometry (LC-MS/MS) analysis, which can affect phosphopeptide identification and phosphorylation site localization; (5) quantification of phosphorylation might be difficult as it relies only on one modified peptide and a phosphopeptide might contain several phosphorylation sites, which can be differentially phosphorylated in response to a specific treatment. However, in the last decade, numerous techniques have been developed to overcome the aforementioned difficulties. To address the low stoichiometric nature and limited dynamic range of the detection methods, many one or multi- dimensional fractionation techniques for the

enrichment and fractionation of phosphopeptides have been established. New fragmentation methods for mass spectrometry analysis have been established to improve the phosphopeptide identification and site localization. Quantification techniques have been optimized to be suitable for phosphopeptide quantification. Moreover, the improvements in identification and quantification software for the interpretation of mass spectrometry data and development of specific programs and algorithms for phosphorylation site localization and further data interpretation enabled the use of phosphoproteomic methods in wide range of biological applications.

In following chapters, the methods for enrichment of phosphorylated proteins and peptides will be discussed as well as the techniques for their detection and quantification.

1.5. Strategies for the enrichment of phosphorylated proteins

Although in bottom-up proteomics, the enrichment of phosphorylated peptides is far more common than the enrichment on the protein level, enrichment of phosphoproteins is still adequate in some specific applications. As it was mentioned above, the amount of tyrosine phosphorylated peptides in a phosphoproteome is relatively very low in comparison to pS and pT. Therefore, in studies specifically focusing on tyrosine phosphorylation driven signalling in cells, there is a need to use a method that would specifically enrich for phosphorylated tyrosine residues. The current method of choice is the immunoprecipitation of tyrosine-phosphorylated proteins using phospho-tyrosine specific antibodies (151–154). Although antibodies against specific phosphorylated motifs in phospho-threonine and phosphoserine have been also used in some studies (155,156), immunoprecipitation is not applicable to a high-throughput enrichment of pS and pT containing proteins as there are no pan-pS or pan-pT antibodies available. For such studies, the method of choice is the enrichment on peptide level.

In addition to the antibody based approaches, phospho-proteins can be also precipitated using lanthanum ions (157,158) or enriched with affinity chromatography using metal oxides as the affinity media. Commercial kits for the enrichment of phosphoproteins e.g. Phosphoprotein Purification Kit (QIAGEN, Hilden, Germany;(159)) or Thermo Scientific Pierce Phosphoprotein Enrichment Kit (Thermo Fischer Scientific, Rockford, IL; (160)) are also available and used for phosphoprotein enrichment.

There are also methods available to specifically capture protein kinases using immobilized low-molecular weight inhibitors, e.g. bisindolylmaleimide compounds (161), or to immunopurify their substrates using an antibody raised against their substrate motif (162).

1.6. Overview of fractionation and enrichments methods used for the phospho-enrichment on peptide level

Multiple methods for the bottom-up phosphoproteomics have been developed so far. Broadly speaking, these methods either exploit the presence of a phosphate group in a peptide to chemically introduce an affinity tag (*i.e.* ***chemical derivatization methods***), the affinity of a phosphate group for Lewis' acids such as metal ions and their compounds (*i.e.* ***affinity enrichment methods***), or physicochemical properties of phosphorylated peptides that can be used to more or less specifically fractionate their mixture with unmodified peptides (*i.e.* ***chromatographic fractionation methods***). Nevertheless, none of them capable of yielding comprehensive information about the phosphoproteome of a complex biological sample. Therefore, the approaches described thereinafter are often combined to obtain complete information about the phosphopeptide pool in analysed samples.

The affinity enrichment and separation methods include **IMAC** (Immobilized metal affinity chromatography), **MOAC** (Metal oxide affinity chromatography), **HAP** (Hydroxyapatite chromatography), **SCX** (Strong cation-exchange chromatography) and **SAX** (Strong anion-exchange chromatography), **HILIC** (Hydrophilic interaction chromatography) and **ERLIC** (Electrostatic repulsion hydrophilic interaction chromatography).

1.6.1. Chemical derivatization methods

In chemical derivatization techniques, phosphorylated amino acids residues are chemically modified by adding a tag that is selectively captured by affinity chromatography. Most of the methods take advantage of the lability of phosphate groups on serine and threonine residues under alkaline conditions. In the presence of a strong base (e.g. NaOH or $Ba(OH)_2$), phosphoserines and phosphothreonines undergo a β-elimination reaction to form dehydroalanine or dehydrobutyric acid, respectively, which serve as

Michael acceptors. **β-elimination is followed by Michael addition** reaction with different nucleophiles such as ethanedithiol (163–166), dimethylaminoethanethiol (167), or mercaptoethylpyridine (168), which can be linked to an affinity tag (e.g. biotin; (165)) or immobilizing agent (e.g. dithiopyridine resin; (169)). The major drawbacks of methods based on the β-elimination reaction are associated with nonspecific labelling of cysteines and O-glycosylated peptides and inability of phosphotyrosines to undergo the β-elimination. The nonspecific labelling can, however, be reduced by blocking the sulfhydryl group of cysteines by alkylation or oxidation or by performing enzymatic deglycosylation in case of O-glycosylated peptides.

Another covalent chemical derivatization technique is a carbodiimide catalysed condensation reaction with excess amine to form phosphoramidate (*i.e.* phosphate with the hydroxyl group replaced by NR_2). In comparison with the β-elimination chemistry, **phosphoramidate chemistry**-based approach is also capable of enrichment of tyrosine-phosphorylated peptides. Zhou et al. (170) for the first time presented this method in a multistep approach (six steps), where cystamines attached to phosphate groups by a condensation reaction were further reduced to form free sulfhydryl groups, which provided the attachment of phosphopeptides to a solid phase by reacting with iodoacetyl groups immobilized on glass beads. Although the final yield was only about 20 % due to considerable sample loss, this approach was very selective providing contaminant-free phosphopeptides. The complicated multistep procedure was further simplified in the Aebersold's lab; the simplified method included the methylation of the carboxyl groups, a condensation reaction with a dendrimer (synthetic polyamine) in the presence of carbodiimide and imidazole, and finally an acidic hydrolysis of the phosphoramidate bonds between phosphopeptides and the dendrimer (171). This method provided higher recovery of phosphopeptides than the previous approach, however, wider utilization of it was hampered by extremely slow conversion during the carbodiimide catalysed condensation step.

Another approach suitable for phosphorylated serine, threonine, and tyrosine peptides that included chemical derivatization was presented in 2004. Carboxylic groups were protected by methylation and the peptide mixture was subjected to the reaction with αdiazo functionalized resin, which resulted in the formation of a covalent phosphopeptide--resin bond, which was cleaved afterwards with an acid hydrolysis (172).

1.6.2. Chromatographic fractionation methods used in phosphoproteomics - SCX, SAX, HILIC, and ERLIC

1.6.2.1. Strong Cation Exchange Chromatography (SCX)

In **SCX** chromatography, the interaction between positively charged peptides and negatively charged column resin is responsible for the retention of the analytes. Under acidic conditions, with pH typically lower than three, tryptic peptides become positively charged by protonation at the peptide N-termini and side chains of arginine, lysine, and histidine residues whereas carboxyl groups and the C-termini become neutrally charged. Phosphoryl group stay negatively charged at such pH conditions, and thus peptides containing phosphoryl groups exhibit a lower affinity for the negatively charged SCX resin. Hence, phosphopeptides are eluted in the early fractions during SCX fractionation (173).

SCX was originally presented as a component of a multidimensional protein identification technology for shotgun proteomics (174,175). In 2004, SCX was for the first time described for phosphopeptide enrichment of HeLa cell nuclear phosphoproteins as a standalone method resulting in identification of 2002 phosphorylation sites from 967 proteins (176). Since then, SCX has been frequently used as a fractionation method in combination with other phosphopeptide enrichment methods: IMAC (177–181) or titanium dioxide enrichment (182–186), but also as a single method for phosphopeptide enrichment after combined cleavage with Lys-N and trypsin (187,188).

1.6.2.2. Strong Anion Exchange Chromatography (SAX)

SAX chromatography is the second ion exchange method used for peptide fractionation, and as opposed to SCX, the negatively charged peptides are more likely to retain on the chromatographic resin during the separation. Dependent on pH of the solvents used for the separation, acidic and phosphorylated peptides are retained on the chromatographic resin and elute in later fractions, and thus the use of SAX for phosphopeptide fractionation typically results in lower loss of phosphopeptides than SCX. Another significant advantage of using SAX over SCX for phosphoproteome analysis is that SAX has a better ability to fractionate phosphopeptides in multiple fractions (189).

In 2003, Nühse et al. successfully used SAX chromatography with salt gradient elution as a prefractionation step prior to IMAC for the identification of plasma membrane

phosphoproteins (190). More recently, SCX and SAX fractionation were combined for sequential fractionation of samples (flow-through fractions from SCX were further subjected to SAX) and the collected fractions were analysed by RPLC-MS/MS. Such approach was named yin-yang multidimensional liquid chromatography tandem mass spectrometry method (Yin-yang MDLC−MS/MS; (191)), and led to improved identification of phosphopeptides than it is common in a proteomic experiment (13 256 unmodified peptides and 849 phosphopeptides were identified). The yin-yang MDLC-MS/MS approach in combination with quantification using stable isotope labelling with amino acids in cell culture was further successfully used for the quantification of phosphoproteome changes during adipocyte differentiation (192).

SAX has been shown to be complementary with Fe^{3+}-IMAC. However, when comparing these two techniques, more peptides, especially monophosphorylated, were identified by SAX approach than by Fe^{3+}-IMAC as the monophosphorylated peptides were probably lost because of the weaker interaction with Fe^{3+} IMAC. Enrichment and fractionation of phosphopeptides by SAX itself was then applied to phosphoproteomic analysis of human liver tissue (189). SAX chromatography has been also compared with a method combining SCX and titanium dioxide (TiO_2) enrichment. The SAX system preferred to identify more acidic and multiphosphorylated peptides than SCX/TiO_2, and it also covered a more complete series of phosphorylation states of peptides (193). AFET (Anion exchange followed by flow-through enrichment with TiO_2) is a phosphopeptide enrichment and identification strategy, where SAX is used as the first step for the pre-separation of peptides that are further subjected to TiO_2 chromatography and RPLC-MS/MS detection of the enriched phosphopeptides (194).

1.6.2.3. Hydrophilic Interaction Chromatography (HILIC)

HILIC has been more commonly used for small polar solutes (e.g. pharmaceuticals, saponins, urea, aminoglycoside antibiotics, glucosinolates, sugars and glycans, folic acid and its metabolites, nicotine and its metabolites, and glycoalkaloids) than for peptides fractionation. The retention of an analyte is believed to be based on partitioning between a water- enriched layer of stagnant eluent which hydrates the polar stationary phase and a relatively hydrophobic bulk eluent, with mobile phase usually being 10-40% water in acetonitrile. In this settings, the retention of an analyte increases with the increasing polarity of the peptide (Alpert, 1990), and thus phosphorylated peptides are retained by the polar stationary phase usually more than unmodified peptides (195,196). Additionally, it

has been demonstrated that HILIC has the highest degree of orthogonality to the reversed phase liquid chromatography (RPLC) among all commonly used peptides fractionation techniques (197).

McNulty and Annan (2008) used HILIC in 2D separation approach with IMAC being the second dimension. Applying this approach, they identified more than 700 novel phosphorylation sites in HeLa cells phosphoproteome. Additionally, they revealed that HILIC performed prior to the IMAC enrichment (HILIC-IMAC) improved dramatically the selectivity of IMAC while HILIC performed after IMAC enrichment (IMAC-HILIC) was found to be a less beneficial approach (198). Contrary to this finding, Albuquerque et al. (2008) performed IMAC enrichment before HILIC prefractionation followed by RPLC-MS/MS with acceptable results; thousands of phosphopeptides (8764) from yeast phosphoproteome were identified using this settings (199).

1.6.2.4. Electrostatic Repulsion- Hydrophilic Interaction Chromatography (ERLIC)

The most novel chromatographic approach that was developed specifically for the enrichment and fractionation of phosphopeptides is the **electrostatic repulsion-hydrophilic interaction chromatography**. This approach combines the electrostatic attraction with hydrophilic interactions to selectively capture phosphopeptides. At low pH (pH < 2) phosphate groups still retain their negative charge whereas carboxyl groups of acidic amino acids become neutrally charged and basic amino groups are charged positively. Phosphate groups are electrostatically bound to the column; nevertheless, their affinity would not be sufficient to overcome electrostatic repulsion from the positively charged amino groups from the N-terminus and basic amino acids. Therefore, hydrophilic interactions of the phosphate group are to be enhanced by using high concentrations of an organic solvent increasing the hydrophobicity of mobile phase (e. g. 70% acetonitrile; (200)).

In a study performed on HeLa cells, SCX, HILIC, and ERLIC based fractionation methods were combined for phosphopeptides separation prior to sequencing by RPLC-MS/MS. A total of 9069 unique phosphopeptides were identified with only 1697 phosphopeptides (18.7 %) overlap between the phosphopeptides identified by each one of the three fractionation methods, which indicated that these three techniques are complementary to each other and can be combined for more comprehensive phosphoproteome analysis (201). In a phosphoproteomic study investigating Marek's disease virus-infected chicken embryonic fibroblasts, ERLIC was used as a first

fractionation step followed by IMAC enrichment of phosphopeptides in the ERLIC separated fractions and RPLC-MS/MS identification of enriched peptides (202).

1.6.3. Immobilized Metal Affinity Chromatography

IMAC is the oldest affinity chromatography method for phosphopeptide enrichment that was originally used for affinity purification of His-tagged proteins (203). However, in 1986, the binding of phosphoproteins and phosphorylated amino acids to ferric ions immobilized on a iminodiacetate-agarose gel was demonstrated for the first time (204), and since then, IMAC technique has been further optimized and widely used for enrichment of phosphopeptides prior to MS analysis.

IMAC takes advantage of a high affinity of positively charged metal cations (Fe^{3+}, Al^{3+}, Ga^{3+}, Zr^{4+}, or Co^{2+}) to negatively charged phosphopeptides. Metal ions are typically chelated by nitriloacetic acid or imidoacetic acid coated matrix to form the IMAC material. Several kinds of matrices including polymer beads (205), the inner wall of capillaries (206), and monoliths (207) have been successfully used for metal ion immobilization. Despite being a relatively old method, IMAC is still widely used presumably due to its ease of use and availability of well optimized and robust protocols. Nowadays, the most common variant is Fe^{3+}-IMAC used for both single step purification or in combination with a prefractionation method.

The most significant drawback of IMAC is a high level of nonspecific binding of nonphosphorylated proteins containing multiple acidic amino acid residues, which co-elute with phosphopeptides during the enrichment of highly complex peptide samples. However, this problem can be overcome by extensive optimization as the phospho-selectivity seems to be dependent on multiple parameters including on the type of metal ions, pH value, ionic strength, and organic phase which can be adjusted to develop a robust protocol (reviewed in (208)). Another approach to increase the efficiency of IMAC is the prefractionation of the peptide samples by various chromatographic methods (described therein before). In addition to the low specifity, IMAC has some other disadvantages. It has been reported that IMAC favours multiphosphorylated peptides over monophosphorylated ones since multiply phosphorylated peptides are more strongly retained on the IMAC resin (209). However, this disadvantage can be also taken as an advantage when the enrichment of multiply phosphorylated peptides is desired (210). The technique can be also affected by various buffers, detergents, and other reagents that are used in biochemical and

molecular biology procedures. Therefore, pre-purification steps are necessary prior to IMAC enrichment, which might lead to an increased sample loss (208).

Sequential elution from IMAC (SIMAC) strategy was designed to separate monophosphorylated and multiply phosphorylated peptides from complex biological samples. Monophosphorylated peptides were eluted from the IMAC resin using acidic solution (1% trifluoroacetic acid, 20% acetonitrile) while multiphosphorylated peptides were subsequently eluted under basic conditions (NH_4OH solution, pH 11.3). The first acidic eluent was further enriched using TiO_2 chromatography to sequester the pool of monophosphorylated peptides from acidic nonphosphorylated peptides (210).

A similar procedure including TiO_2 enrichment of the flow-through fractions from IMAC was used for the characterization of human T lymphocytes phosphoproteome (211). Other study used a combination of IMAC and TiO_2 enrichment to produce a large data set with only small degree of overlap between these two methods suggesting the complementary nature of these methods (212). Some of the recent phosphoproteomic studies employing IMAC for phosphopeptide enrichment were mentioned above since they applied two dimensional enrichment settings using pre- or post-fractionation with one of the chromatographic methods (177–181,198). Other studies used IMAC enrichment without any prefractionation only followed by LC-MS/MS for identification of the enriched peptides. For instance, Chen L. et al. studied phosphoproteome of human prostate cancer specimens obtained from tissue depository to evaluate feasibility of phosphoproteomics for biomarker discovery from archived tumour specimens (201).

Recent promising innovation to IMAC technique has been the introduction of **immobilized titanium ion affinity chromatography (Ti^{4+}-IMAC)**. A phosphate polymer was applied to immobilize Ti^{4+} through the chelating interaction between phosphate groups on the polymer and Ti^{4+}. The resulting Ti^{4+}-IMAC resin was compared to other enrichment methods including Fe^{3+}-IMAC, Zr^{4+}-IMAC, TiO_2, and ZrO_2, and demonstrated superior selectivity and efficiency of Ti^{4+}-IMAC for the isolation and enrichment of phosphopeptides (213,214). Matheron at al. recently compared performance and biases of TiO_2 enrichment and Ti^{4+} IMAC using a very large synthetic library and a tryptic digest of a cellular lysate (HeLa cells). Their data revealed that there are no clear differences between the two enrichment methods considering biochemical and biophysical parameters such as peptide length, sequence surrounding the site, hydrophobicity, and nature of the amino acid phosphorylated. Also the abundance of the enriched

phosphopeptides was rather similar except for the preferential enrichment of multiply phosphorylated peptides by Ti^{4+}-IMAC (215), which was in concordance with previously reported tendencies of IMAC resins to efficiently enrich multiply phosphorylated peptides. Ti^{4+}-IMAC has been successfully applied for phosphopeptide enrichment in phosphoproteomic studies: for instance, in a label-free quantitative phosphoproteomic study of Jurkat T-cells stimulated by prostaglandin E_2 (216) or a targeted quantitative proteomics study of phosphorylation dynamics of the PI3K-mTOR and MAPK signalling pathways (217).

1.6.4. Metal Oxide/hydroxide Affinity Chromatography

MOAC is one of the most powerful and promising approaches for phosphopeptide enrichment. Metal oxides have been shown to have affinity for phosphate ions at acidic pH; the mechanism of phosphate-metal oxide interaction is described as ion-exchange, where metal oxide acts as a Lewis acid, and the phosphate group behaves as a Lewis base (218–220).

The mechanism of this interaction implicates that phosphopeptides are most effectively enriched under low pH conditions. It has been established that especially nonphosphorylated- peptides containing greater proportions of aspartic and glutamic acid bind non-specifically (221). Therefore, various additives have been tested to increase binding specifity to selectively capture phosphorylated peptides. Namely, trifluoroacetic acid (TFA) or formic acid (FA) have been used to establish low pH (typically in a range of 2-3); relatively high acetonitrile concentrations (50-70%) have been used in the "buffers" to prevent hydrophobic interactions with the sorbent, and different monocarboxylic or dicarboxylic acids have been tested as "buffer" additives to compete for binding sites with non-phosphorylated peptides but to not decrease the binding affinity of phosphopeptides. The first one presented was 2,5-dihydroxybenzoic acid (DHB; (222)); nevertheless, lactic acid (LA; (223)), glutamic acid (Glu; (192)), or ammonium glutamate (224) have also been reported to increase the selectivity of MOAC. Naturally, the concentration of these additives might have a strong influence on the nature of phosphopeptides that are enriched. Using high concentration during the binding step may improve specifity, but more weakly bound mono-phosphorylated phosphopeptides could be lost. A variety of pH conditions during the binding or the elution step have been also employed to optimize the protocol (225,226). An alternative approach described

to minimize the level of nonspecifically bound peptides is chemical derivatization before the enrichment, e. g. methyl esterification of peptides (209,226).

Two different settings have been used to enrich phosphopeptides using MOAC. The most common experimental approach is the use of MOAC beads in an off-line strategy. Metal oxide particles can be embedded in pipette tips or mixed and incubated with peptides in a microtube, and the enrichment protocol proceeds through multiple steps performed manually. The second is an on-line strategy, which does not allow so much flexibility in the protocol in comparison with the off-line strategy, but it has other undeniable advantages such as automation, higher sensitivity, and repeatability. In the on-line strategy, the metal oxides are integrated into the LC-MS/MS system in the form of pre-columns prior to the RPLC-MS/MS (e.g. (227,228)).

A variety of metal oxides have been used for phosphopeptide enrichment so far comprising aluminium hydroxide (229), gallium oxide (230), iron oxide (183), niobium pentoxide (231), tin dioxide (232,233), hafnium oxide (234), tantalum oxide (235), zirconium dioxide (236), and titanium dioxide (227); among them the last two have been the most commonly used in phosphoproteomic studies.

1.6.4.1. Titanium dioxide enrichment

Titanium dioxide enrichment (in text referred as TiO_2 enrichment) was the first MOAC method discovered (227), and even though there were many other metal oxides in different forms proven to have affinity for phosphopeptides, it became the most popular metal oxide resin used for phosphopeptide enrichment presumably due to its favourable enrichment behaviour, chemical stability, and commercial availability. TiO_2 is highly selective to preferentially bind phosphopeptides under optimal conditions during sample loading, washing, and peptide elution steps. One of the advantages of TiO_2 enrichment is that TiO_2 is more robust and tolerant towards many reagents normally used in biochemistry and cellular biology than conventional IMAC, which is sensitive to common buffers or detergents - various detergents have been actually demonstrated to enhance the efficiency of TiO_2 enrichment (237).

TiO_2 enrichment was introduced already more than a decade ago, in 2004, as a novel promising strategy for selective phosphopeptide enrichment prior to RPLC-ESI-MS/MS (227). In this setup, TiO_2 was used in a form of an on-line TiO_2 pre-column coupled to a reversed phase capillary column; loading solution contained 0.1 M acetic acid, and the elution was performed with ammonium bicarbonate (pH 9.0). Phosphorylated peptides

were successfully enriched; nevertheless, the selectivity of the enrichment was not sufficient and needed further optimization.

Larsen et al. examined the effect of different loading "buffer" composition on phospho-selectivity of TiO_2 packed in home-made microcolumns. Different aromatic and aliphatic carboxylic acids were added to the loading buffer and the selectivity of the enrichment was evaluated using MALDI-TOF MS (matrix-assisted laser desorption/ionization-time of flight mass spectrometry). DHB and other substituted aromatic carboxylic acids (salicylic acid, phthalic acid) showed the best efficacy in inhibition of adsorption of nonphosphorylated peptides followed by monofunctional carboxylic aromatic and aliphatic acids (benzoic acid, cyclohexanecarboxylic acid, phosphoric acid, trifluoroacetic, and acetic acid) (222). DHB was also found to be the most potent additive in a study performed by Yu et al. minimizing the inference from nonphosphorylated peptides. (238). These results indicated the importance of a hydroxyl group in ortho- position of a benzene ring that is probably more relevant for reducing the nonspecific peptide binding than a hydroxyl group in meta- position; presumably because the interactions between substituted aromatic carboxylic acid and TiO_2 surface are based on a coordination bond that forms a chelating bidentate (239).

On the other hand, DHB has been shown to cause problems when analysing the samples using an RPLC-ESI-MS/MS system, reducing the number of identified phosphopeptides and affecting the performance of the LC-MS/MS system. When comparing the effect of hydroxy acids (DHB, glycolic acid, lactic acid, malic acid, tartaric acid, and hydroxypropanoic acid) on the phosphopeptide enrichment with various MOAC tips, lactic acid and hydroxypropanoic acid were the most effective for both TiO_2 and ZrO_2 enrichment. Furthermore, aliphatic hydroxy acids are hydrophilic enough to be removed during the desalting step, and thus they did not appear to affect the LC-MS/MS system as it was described in the case of DHB (223).

Jensen and Larsen also compared the effect of hydroxy acids, namely phthalic, glycolic, oxalic, lactic, gallic, and citric acid. In their comparison, 1 M glycolic acid was shown to be the most beneficial for the minimization of nonspecific absorption of acidic nonphosphorylated peptides without any effect on the binding of phosphopeptides to TiO_2 (237). Contrary to their report, Aryal and Ross revealed that the addition of glycolic acid to the loading solution reduced the specifity towards phosphopeptides (240). A possible explanation of this discordance is variability in properties of TiO_2 used in different studies.

There are many commercial products available provided by different companies, which might vary because of different technology used for their production. For instance, it has been shown that structure and retention properties of titania are strongly dependent on the calcination temperature of the beads (241).

The optimized protocol for the TiO_2 enrichment presented by Wu et al. included the addition of glutamic acid in the sample loading buffer as an effective nonphosphopeptide excluding agent (186). Other investigations showed that loading buffer consisting of a combination of high concentrations of 1-octanesulfonic acid and low concentrations of DHB also improved the selectivity for phosphopeptides without affecting the LC-MS system as it was observed also when DHB was used as nonphosphopeptide excluding additive alone in a high concentration (242). This protocol was further optimized with the addition of heptafluorobutyric acid (243).

Peptide-to-TiO_2 ratio has been also investigated as a substantial factor for the selectivity of the phosphopeptide enrichment. The optimum ratio for HeLa cell lysate was from 1:2 to 1:8 (mass/mass); less or more TiO_2 beads used for the enrichment decreased the selectivity. Interestingly, multiple phosphorylated peptides were identified by deficient TiO_2 beads while with the increasing beads dosage, the monophosphorylated peptides became dominant (244). Similar findings were obtained for acute myeloid leukaemia cell line P31 in a quantitative label-free phosphoproteomic study (245).

The TiO_2 enrichment method has been further improved by developing various nanoparticles, nanocomposites, and microspheres. For instance, nano-titanium dioxide composites were synthesized from TiO_2 nanoparticles via photopolymerization in the presence of a diacrylate cross-linker. The enrichment efficacy of these nanocomposites was evaluated to be up to five times larger compared to 5μm TiO_2 particles. Moreover, the cross-linking of the TiO_2 nanoparticles helps to prevent loss of the particles from the packed cartridges during washing procedures (246). Lin and co-workers deposited a thin TiO_2 layer onto the inner surface of capillary column by liquid phase deposition technique. This TiO_2 nanoparticle-deposited capillary column was then used in an off-line setup with MALDI-TOF MS or on-line with ESI-QTOF MS and nano-LC-ESI-MS/MS, and a good capability for enriching of phosphopeptides was demonstrated, *i.e.* phosphopeptides from α-casein were detected in a mixture of tryptic peptides from α-casein and BSA at the femtomole level (247). Mesoporous nanostructured TiO_2 clusters were also employed for selective separation of phosphopeptides. TiO_2 nanocrystals were first self-assembled

and then further modified to form submicrometer clusters with relatively uniform mesoscale pores and hydrophilic and negatively charged surface that enhanced the water dispersibility of the clusters. The incorporation of various components that further facilitated the separation of phosphopeptides, e. g. superparamagnetic nanocrystals, was demonstrated to be feasible because of the self-assembly process (248). The affinity material particles can also be immobilized on MALDI plates. The on-plate enrichment for subsequent MALDI-MS analysis has been shown to have some advantages in comparison with the conventional resin-based techniques such as minimal sample handling and thus lower sample loss (e.g. (249–251)).

1.6.4.2. Zirconium dioxide enrichment

The application of zirconium dioxide (ZrO_2) enrichment for phosphopeptide isolation prior to MS analysis was first demonstrated by Kweon and Håkansson in 2006. Phosphoselectivities of ZrO_2 and TiO_2 were compared; both materials were highly specific for phosphopeptides. Nonetheless, ZrO_2 provided more selective enrichment for monophosphorylated peptides whereas TiO_2 was more selective for multiphosphorylated peptides (236). The observed difference in binding selectivity between ZrO_2 and TiO_2 was explained by the fact that under acidic conditions, ZrO_2 is a stronger Lewis acid than TiO_2, together with different coordination numbers of zirconia and TiO_2 in crystalline forms (7 and 6, respectively; (236)).

As in the case of TiO_2, the ZrO_2 enrichment method has been further improved by using various loading, washing, and elution conditions in the enrichment protocols, and by preparing different ZrO_2 containing microspheres, nanoparticles, or nanocomposites. For instance, in the study published by Sugiyama and his co-workers, previously mentioned in context with TiO_2 enrichment, β-hydroxypropanoic acid was shown to be the most effective non-phosphopeptide excluder for zirconium dioxide chromatography among all the hydroxy acids tested (223). Lo et al. presented iron oxide nanocomposites of magnetic particles coated with zirconia with high surface-to-volume ratio improving the trapping capacity and reducing the time required for enrichment; phosphopeptides could be enriched by pipetting the sample with the particles for only 30 seconds. Moreover, magnetic property enabled easy isolation by application of an external magnetic field (252). Li et al. prepared Fe_3O_4/ ZrO_2 core-shell microspheres with well-defined core-shell structure and higher selectivity than ZrO_2 coated magnetic particles (with no core-shell structure) described before. Furthermore, Fe_3O_4/ZrO_2 core-shell microspheres were more

selective in comparison with commercially available IMAC material (PHOSselect- iron affinity beads, Sigma; (253)). In 2009, mesoporous ZrO_2 nanomaterial with very large surface areas and many surface sites that provide higher loading capacity for binding of phosphate groups than micro- and nano- particles was first applied for phosphopeptide enrichment (254). However, mesoporous ZrO_2 had some disadvantages including its thermal instability and hence mesoporous silica microspheres coated with zirconia layer were synthesized with improved thermal stability. Due to the interactions of metal oxide and silica support, the physicochemical properties of metal oxide differed greatly to the bulk crystalline metal oxides and enabled high phosphopeptide recovery, especially for multi-phosphorylated peptides, which was shown to be even higher than that of the widely used commercial TiO_2 microparticles (GL Sciences, Tokyo, Japan; (255)).

1.7. **Detection of phosphorylation**

Mass spectrometry is a current method of choice to detect dynamic changes in protein phosphorylation. However, a direct MS analysis of phosphorylation from unfractionated peptide samples is still not feasible because of relatively low abundance of phosphorylated proteins in eukaryotic cells. Also, the ionization efficiency used to be frequently reported as a reason for difficulties in phosphopeptide identification. It was suggested that ionization efficiencies and thence, signals of phosphopeptides in MS, are lower compared with their nonphosphorylated analogues (256,257). Contrary to these reports, in a more recent study, Steen et al. tested the ionization/detection efficiencies of the synthetic peptide/phosphopeptide pairs by using online LC-ESI-MS/MS. In this study, it was shown that the statement about lower ionization efficiency is not valid in general, and it is highly dependent on the MS instrumentation used in the particular study. Based on their results, the authors concluded that phosphopeptides are difficult to identify in protein digests because of the substoichiometric nature of phosphorylation, not because of their low ionization efficiencies (258). Nonetheless, it is of a great importance to choose an appropriate “phosphate-friendly” fragmentation method to preserve phosphorylation during peptide fragmentation. It has been shown that during that the most common fragmentation method used in proteomics, collision-induced dissociation (**CID**) operated in positive-ion mode, the phospho-amino acid containing peptides will typically undergo β-elimination of phosphoester bond resulting in a loss of the phosphate group and limited fragmentation across the peptide backbone. Application of an alternative fragmentation

method such as high-energy CID (**HCD**; (259)), electron capture dissociation (**ECD**; (260)), or electron transfer dissociation (**ETD**; (261)) leads to more efficient fragmentation without the cleavage of the phosphoester bond and thus allows more confident peptide identification and localization of the modification. More details on the appropriate selection of fragmentation method for a phosphoproteomic analysis are given in our publication (262).

1.8. Quantification techniques for phosphoproteomics

Quantitation in proteomics has become very robust in recent years; there are multiple well established quantitation techniques that provide very precise and accurate quantification of proteins in samples and allow comparison of samples coming from different origin. Quantification of PTMs has also become relatively feasible – but it is important to consider that the quantification of modifications is more difficult than and not as straightforward as quantification of whole proteins. The quantification of PTMs usually rely on one modified peptide, contrary to proteins with more peptides available (and usually required). Additionally, a modified peptide can bear multiple modifications with different degree of regulation, further complicating the analysis. In this chapter, a brief overview of the most popular quantification techniques for phosphoproteomics is provided.

1.8.1. Label-free quantification

As the name of the quantification approach implies, label-free quantification is the "simplest" quantification method that does not require any labelling step in the experimental workflow and only relies on spectral counting or MS^1 intensity of the quantified feature. The unnecessity to use any isotopic label provides this method several attractive benefits: the implementation costs are low; there are no additional steps in the workflow that may introduce undesirable biases into the analysis, and the number of treatment conditions and replicates is basically unrestrained allowing relative flexibility in the experimental designs. On the other hand, the absence of multiplexing increases the total number of samples to be measured, and thus longer acquisition time costs must be considered when choosing this strategy.

The most of the challenges occur within the post-acquisition analysis of the recorded data. A common problem in shotgun proteomics are missing values. The data-dependent acquisition method, which is used in shotgun proteomics, is based on scanning

peptide ions and choosing the most intense peptides for subsequent fragmentation. This stochastic sampling approach then leads to a high number of missing values, which might hamper subsequent data analysis. In fact, missing values can be imputed using various imputation methods (reviewed in (263)). However, label-free quantitation software has been improved in recent years, for instance MaxQuant (MaxLFQ algorithm (264,265)); these developments increased the robustness of label-free quantitation workflows and provided tools that can salvage many quantitative values from the unidentified spectral features, so the imputation is usually still used, but it is required for a lower number of missing values.

Although labelling-dependent quantitation approaches provide more confident quantification and multiplexing, label-free approaches have become popular too and have been used in several phosphoproteomic studies. Especially, the largest phosphoproteomic studies identifying up to 50,000 of phosphorylation sites were conducted using this quantitation technique. However, it is important to point out that quantification of label free phosphoproteomics data is still challenging as the quantification of a phosphorylation site is usually dependent on one peptide (common issue in phosphoproteome quantification) and the normalization of acquired data is not as straightforward as in the case of label-based proteomics. Furthermore, to conduct a label-free phosphoproteomic experiment, it is essential to have a robust and reproducible phospho-enrichment protocol to avoid possible biases introduced in the sample preparation step.

In 2010, Huttlin et al. published a large phosphoproteomic study of difference between 9 mouse tissues to identify common and tissue-specific phosphorylation. In this study, 6296 phosphoproteins harbouring nearly 36,000 phosphorylation sites were identified (266). In the largest phosphoproteomic study conducted so far, more than 50,000 distinct phosphorylation sites were detected in HeLa cell line with more than 75 % of cellular proteins revealed to be phosphorylated. Importantly, this study provided an intriguing insight into differences between pS/pT and pY signalling, and presented a large-scale quantification of site occupancies using label-free data in MaxQuant (141). The unnecessity of additional steps within the workflow makes label-free quantitation very attractive to use in high-throughput automated sample preparation workflows. EasyPhos was designed to allow rapid quantification of phosphoproteomes in cells and tissues at a depth of more than 10,000 phosphorylation sites per analysis without the need of any pre-fractionation prior to phospho-enrichment, analysing the samples in one LC-MS/MS run

(267). In a recent study, a multi-protease based approach was presented for protein digestion markedly increasing the coverage of the studied phosphoproteome. The authors pointed out that there is a bias in phosphopeptides detected in phosphoproteomic studies caused by the fact that trypsin is usually used for sample digestion providing the same set of tryptic peptides (268).

1.8.2. Metabolic labelling

In metabolic labelling, the labels are incorporated into every protein during cell growth and division. Consequently, the isotopic label is introduced in the earliest possible step of the experiment, thereby eliminating systematic errors that could arise from sample handling. The most widely used metabolic labelling method in both proteomics and phosphoproteomics – **stable isotope labelling with amino acids in cell culture (SILAC)** was introduced in 2002 (269).

In classical SILAC, isotopically labelled lysine and arginine (containing ^{13}C or ^{15}N) are typically used as a component of cell culture media, in which the cell are cultivated for at least six cell doublings to ensure a complete incorporation of labels into the proteins of growing cells (270). As the most common protease in proteomics is trypsin alone or in combination with Lys-C, the digestion of cellular proteins in the ideal case leads to generation of peptides that contain one lysine or arginine and thus contain one isotopic label. Relative quantification is then achieved on MS^1 level by comparing the intensities of two co-eluting isotopic clusters (*i.e.* labelling pair) which are distinguished by their m/z value. The disadvantages of SILAC are limited multiplexing (only 2 or 3 samples are maximally combined in a typical SILAC experiment) and the increase of complexity of MS^1 spectra, which can in turn limit sampling depth. Another problem might be caused by metabolic turnover of labelled amino acids – typically arginine, which can be converted to proline – but this issue can be avoided by careful optimization of the arginine and lysine concentration in cell culture media, choosing an appropriate experimental design and arginine isotope (271), or adding high amounts of proline to limit the metabolic conversion of arginine by a negative feedback loop (272).

The first phosphoproteomic studies that employed SILAC as a quantification technique were conducted in Mann's lab. Blagoev et al. studied phosphotyrosine-mediated signalling events in epidermal growth factor (EGF) stimulated cells using an antibody-based approach to enrich for phosphotyrosine containing proteins. When combining two

triple-labelling states experiments (*i.e.* double-triple SILAC), an activation profile of 81 signalling proteins early after EGF receptor (EGFR) stimulation was obtained, and thus it was for the first time demonstrated that SILAC can be employed to study cellular signalling in a high-throughput phosphoproteomic study (151). In a complementary study using the same labelling approach (*i.e.* double-triple SILAC) to generate five-time-points profiles for the detected phosphorylation sites and the same stimulation using EGF, Olsen et al. for the first time demonstrated that SILAC could be used to study pS and pT mediated signalling pathways. Using a two dimensional chromatographic approach including SCX as a prefractionation technique prior to TiO_2 enrichment, 6,600 phosphorylation sites on 2,244 proteins were detected (273). In these initial studies, stringency criteria for only accepting 1.5 fold changed sites as regulated were set (151) and classification of phosphorylation sites based on their localization probability calculated by MaxQuant was developed with only accepting class I sites (i.e. localization probability > 0.75) for downstream bioinformatic analysis (273); both of these criteria are still widely used in current phosphoproteomic studies. Since then, classical SILAC has been used for quantification in many phosphoproteomic studies mainly because of the high precision and accuracy of quantification achieved by this technique as well as the early introduction of the labelling into the experiment.

Furthermore, Mann's lab has developed new techniques based on the classical SILAC labelling that further expanded experimental designs that are applicable to quantitative proteomics and phosphoproteomics using SILAC. In a so-called **pulsed SILAC**, all experimental groups are cultivated in a SILAC "light" cell culture medium (i.e. a medium that contains non-labelled versions of amino acids) and the "heavy" isotopes are only added for a certain period of time to pulse-label the newly synthesized proteins. As a consequence, protein turnover can be estimated from the obtained SILAC rations (274). To be able to analyse primary tissues and compare a higher number of samples than in the classical SILAC approach, **spike-in SILAC** (sometimes referred as **super-SILAC**) was developed. The idea of spike-in SILAC is to produce a representative super-SILAC mixture of different SILAC-labelled cell lines to develop an internal standard for a subsequent comparison of multiple samples (275,276). Further development also enabled the use of SILAC for the purpose of in *vivo* studies by introducing SILAC labelled model organisms such as **SILAC mouse** (277,278).

These modifications of the classical SILAC approach have been also used in quantitative phosphoproteomics. Phosphoproteomes of insulin treated and untreated mice liver were compared using the spike-in method. In this study, the super-SILAC mix was composed of a mixture of peptides prepared by tryptic digestion of six mouse liver cell lines treated or untreated with insulin. Using this mixture as an internal standard, 10,000 of phosphorylation sites were compared in response to insulin treatment, which provided a considerable deep insight into cellular signalling in an in *vivo* system (279). In addition to in *vivo* phosphoproteomic studies, spike-in SILAC also enabled a quantitative comparison of tumour samples obtained from different donors. Schweppe et al. established a super-SILAC internal standard derived from NSCLC cell lines, which was further used to relatively quantify phosphopeptides from two tumours to determine pathways that differ between the two tumours (280). The SILAC mouse technology was used to investigate cancer progression through distinct stages of skin cancer providing a detailed insight into molecular pathways altered during skin carcinogenesis obtained in an in *vivo* system (281).

1.8.3. **Chemical labelling**

In chemical labelling approach, the isotopic labels are incorporated into the proteins later in the experimental workflow – either on the protein level (possible, but not widely used), or much more often on the peptide level. In principle, any reactive group within the amino acid residues might be used to chemically attach a label to a peptide; however, most of the current labelling techniques take advantage of the reactivity of primary amines and target either peptide N-terminus or ε-amino group of lysine. The later incorporation of the label might introduce a systematic bias into the experiment; on the other hand, chemical labelling is feasible also in cases when the labelling on the growing culture level is not possible (e.g. in primary cells, human, animal, or plant tissues, and biological fluids) or not applicable to a desired experimental design (e.g. when a higher level of multiplexing is desired). The relative (or absolute) quantification using the chemical labelling approach can be conducted either on the MS^1 level by comparing intensities of the differentially labelled peptides or on the MS^2 level via comparing differentially isotope encoded reporter ions in the peptide fragmentation spectra.

1.8.3.1. MS^2 quantitation

The MS^2 quantitation methods are based on chemical labelling using isobaric tags. That means that peptides labelled with different labels have the same mass, and thus they co-elute from the LC system, cannot be distinguished based on their m/z on the MS^1 level, and co-fragment during MS/MS. The quantification of the peptides in samples is then achieved by comparing the intensities of reporter ions that are recorded in the lower mass range of the MS/MS spectra. The fact that including multiple labelling states does not increase complexity of the samples provides a considerable advantage of this approach – it enables parallel quantification of more than two or three samples that are usually combined in MS^1 labelling based experiments (up to ten samples). Furthermore, the quantification using chemical labelling and MS/MS detection of the tags is usually very precise; nonetheless, there is a possible bias in accuracy that has to be considered when using these approaches – the fold changes measured in highly complex samples are often smaller than the "real" fold changes. This phenomenon, called as **ratio compression** effect, happens due to the co-isolation of peptide ions during the MS^2 precursor selection. As most of the proteome/phosphoproteome usually remains unperturbed by applied treatment, the ratios of co-isolated reporter ions are most likely to be close to 1, and thus they might "dilute" the real differences between the regulated peptides. However, there are already methods available that have been designed to overcome this issue enabling more confident use of these techniques for proteome quantification (282,283).

The most common isobaric labelling techniques used in quantitative proteomics and phosphoproteomics are tandem mass tags (TMT; (284)) and isobaric tag for relative and absolute quantitation (iTRAQ; (285,286)). In phosphoproteomics, prefractionation and enrichment steps are typically included into the experimental design as additional steps that might potentially introduce systematic errors into the analysis; therefore, including the labelling in the earliest possible step of the experiment is desired, ideally immediately after the cells are harvested (or samples collected - in case of samples of different than cell culture origin). On the other hand, the low abundance of phosphorylated peptides implicates the necessity of higher amount of starting material ranging from hundreds of micrograms to several milligrams, which might be costly, especially when replicate experiments are conducted. Therefore, labelling of isolated phosphopeptides might be an alternative; however, the enrichment and fractionation steps must be highly efficient and reproducible.

Zhang et al. used **pre-enrichment iTRAQ labelling** as a relative quantification method in a time-course study using the EGFR model system. Tryptic peptides from four different EGFR stimulation time points were labelled with four isoforms of the iTRAQ reagent, and after mixing of the samples, tyrosine-phosphorylated peptides were immunoprecipitated with an anti-phosphotyrosine antibody and further enriched by IMAC before LC-MS/MS analysis. The analysis led to the identification of 78 tyrosine phosphorylation sites on 58 proteins from a single analysis (287). Another instance of a study that also used iTRAQ labelling of peptides prior to application of phospho-enrichment (TiO_2) was a phosphoproteomic analysis of porcine hearth mitochondria to study pyruvatdehydrogenase (PDH) phosphorylation (288). In 2010, Wu et al. demonstrated that **post-enrichment iTRAQ labelling** of phosphopeptides was possible to achieve confident identification and quantification of phosphopeptides in HeLa-S3 cells tryptic digest. In their workflow, phosphopeptides were reproducibly enriched using a chromatographic column packed with TiO_2 beads (289).

Another application of iTRAQ to phosphoproteome investigation developed recently is the use of isobaric labelling to study phosphorylation stoichiometry and absolute quantification of phosphopeptides. In **Phospho-iTRAQ**, peptide samples are split in two identical parts and differentially labelled prior to phosphatase treatment of one of the parts. After de-phosphorylation, the samples are pooled together and analysed by LC-MS/MS. The reporter ions intensities are then used to calculate phosphorylation stoichiometries of detected phosphopeptides, and due multiplexing, this method also allows multiple samples comparison and relative quantification of unmodified peptides in the same run. However, additional confirmation of the identified phosphopeptides with complementary techniques remains necessary, since using this approach, it is not possible to exactly localize the phosphorylation site when there are multiple STYs in a peptide available (in a non-phospho-enriched mixture, only the non-phosphorylated counterparts are usually fragmented providing no information about the site localization; (290,291)). **Multiplex Absolute Regressed Quantification with Internal Standards (MARQUIS)** is a different method employing iTRAQ for absolute quantification of phosphorylated peptides. In this approach, isobaric tags are combined with synthetic heavy-labelled standard peptides to construct internal standard curves for phospho-peptides of interest. The standard labelled heavy peptides are added to biological samples – cell lysates – in a different concentration per sample and after iTRAQ labelling, the samples are pooled together and analysed using

MS/MS. The fragmentation of the heavy-labelled peptides then provides an internal standard curve, which serves as a reference for the reporter ions produced by fragmentation of the endogenous (non-labelled) counterpart of the heavy peptide and thus enables absolute quantification of a particular phospho-peptide across different conditions (292).

TMT has been also used for both absolute quantification of phosphorylation stoichiometries (293) and in studies that required a higher level of multiplexing such as a phosphoproteomic study of genistein treated triple-negative breast cancer cell line MDA-MB-231 (294), a study investigating changes in brain-phosphoproteome of VX (neurotoxic agent) treated rats (295), or a study that provided an insight into molecular pathways triggered by nicotinic acetylcholine receptor ligands in pancreatic cells (296).

1.8.3.2. MS^1 quantitation

MS^1 quantitation using chemical labelling is an alternative to SILAC labelling in cases when SILAC is not applicable (as listed above), or it is too expensive. The most widely used MS^1 chemical labelling quantitation methods in proteomics are mTRAQ and stable-isotope dimethyl labelling.

mTRAQ is basically a non-isobaric variant of iTRAQ. Thus, it uses the same chemistry, but the differentially labelled peptides are already distinguishable in MS^1 spectra as in the case of SILAC labelling. Initially, mTRAQ was used to label standard peptides for multiple reaction monitoring to quantify potential markers for endometrial cancer (297); however, studies applying mTRAQ to study phosphorylation dynamics also emerged more recently. Mertins et al. compared iTRAQ- and mTRAQ-based quantification and revealed that iTRAQ quantified almost threefold more phosphopeptides than mTRAQ (12,129 *versus* 4,448, respectively). Furthermore, iTRAQ was shown to be less variable and had an additive effect on precursor intensities. The loss of accuracy caused by co-fragmentation of peptides in the same isolation window and ratio compression was observed in iTRAQ; however, the authors suggested that since logarithmic iTRAQ and mTRAQ ratios were linearly correlated, the iTRAQ ratios could be corrected by an average compression factor to achieve more accurate results (298). Oppermann et al. compared two MS^1 quantification methods – metabolic labelling by SILAC and chemical labelling by mTRAQ. They reported that mTRAQ was a comparable alternative to SILAC that enabled quantification of almost as many significant changes in phosphorylation after a kinase inhibitor treatment, although mTRAQ was shown to be slightly less precise than SILAC (299).

Stable isotope labelling of primary amino-groups using deuterium-labelled-formaldehyde in combination with reduction of the initially formed Schiff base with deuterium-labelled-cyanoborohydride – **stable-isotope dimethyl labelling** - is another labelling technique attractive enough to be widely used in many studies (300–302); the method is relatively cheap, fast, and robust. The main limitation of this technique is the use of deuterium as a heavy part of the label, which can lead to retention time shifts of the heavy labelled peptides in LC-MS/MS, and thus the labelling pair might not co-elute precisely. Since 2006, when it was for the first time used in combination with IMAC to study uteri of pregnant rats (303), **reductive dimethylation** has been used in multiple phosphoproteomic studies. Dimethyl labelling has been used in combination with immunoaffinity purification of tyrosine-phosphorylated peptides to study tyrosine phosphorylation in EGF treated HeLa cells (304). In **TiSH**, three different phospho-fractionation methods were employed to maximally increase the coverage of a studied phosphoproteome: TiO_2, SIMAC, and HILIC. In this three dimensional fractionation, dimethyl labelling was applied after the first TiO_2 enrichment step (305). Wilson-Grady at al. presented a modified **lower-pH dimethylation** protocol as a quantification technique that can be used for quantitative proteomics and phosphoproteomics in animal tissues (306). Dimethyl labelling has been also employed, as well as other approaches, for calculation of phosphorylation stoichiometries. Combined with kinase reaction, the published protocol has been also designed to enrich for specific substrates of particular kinases (307).

2. Aims

2.1. **Optimization of experimental workflow for the enrichment, detection, and quantification of phosphorylated peptides using mass spectrometry:**

- Selection of MOAC resin and protocol for enrichment of phosphorylated peptides using standard peptide mixtures
- Application of the best performing protocols to the enrichment of phosphorylated peptides from a real complex sample and to the analysis of the selected model system (irradiated SILAC-labelled MOLT-4 cells)

2.2. **Characterization of cellular mechanisms underlying the VE-821-mediated radiosensitization of MOLT-4 cells on three levels:**

- Characterization of the response of MOLT-4 cells to VE-821 and its combination with IR using cell biology methods
- Application of the optimized phospho-enrichment workflow to analyse phosphorylation response of irradiated MOLT-4 cells and its modulation by VE-821
  - Detection of phosphorylation sites responsive to VE-821 treatment
  - Functional annotation of regulated phosphorylation sites and identification of potentially perturbed signalling pathways and biological processes
  - Analysis of phosphorylation motifs surrounding detected phosphorylation sites and identification of activated/inhibited protein kinases
- Description of VE-821-induced metabolome alterations in irradiated MOLT-4 cells using targeted metabolome analysis
  - Identification of metabolites with abundance changes induced by VE-821 treatment in irradiated MOLT-4 cells
  - Functional characterization of regulated metabolites, detection of modulated metabolic pathways
- Integration of the acquired data and validation using database and literature search

3. Materials and Methods

3.1. Materials and Instrumentation

3.1.1. Cell lines

HeLa (American Type Culture Collection (University Blvd., Manassas, USA))

MOLT-4 (European Collection of Animal Cells Cultures (Porton Down, Salisbury, UK))

3.1.2. Kinase inhibitors

VE-821 – ATR inhibitor, 3-amino-6-(4-(methylsulfonyl)phenyl)-*N*-phenylpyrazine-2-carboxamide (APIs Chemical Co., Ltd., Shanghai, China)

KU55933 – ATM inhibitor, 2morpholin4yl6thianthrene1ylpyran4-one (Merck KGaA, Darmstadt, Germany)

3.1.3. Cell culture media, chemicals and solvents

Acetic acid (no. 49199, Sigma-Aldrich, St. Louis, MO, USA)

Acetone for HPLC (no. 270725, Sigma-Aldrich, St. Louis, MO, USA)

Acetonitrile LiChrosolv® hypergrade for LC-MS (no. 100029, Merck KGaA, Darmstadt, Germany)

Acetonitrile CHROMASOLV® Plus (Acn; no. 34998, Sigma-Aldrich, St. Louis, MO, USA)

Acetonitrile CHROMASOLV® gradient grade for HPLC (no. 34851, Sigma-Aldrich, St. Louis, MO, USA)

Acrylamide, minimum 99 % (no. A5667, Sigma- Aldrich, St. Louis, MO, USA)

Albumin, from bovine serum (BSA; no. A2153, Sigma-Aldrich, St. Louis, MO, USA)

Albumin, from bovine serum (BSA; no. A8022, Sigma-Aldrich, St. Louis, MO, USA)

Ammonium bicarbonate (ABC; no. 09830, Sigma-Aldrich, St. Louis, MO, USA)

Ammonium hydroxide solution ≥99.99% (no. 338818, Sigma-Aldrich, St. Louis, MO, USA)

L-Arginine (R0; no. A8094, Sigma-Aldrich, St. Louis, MO, USA)

L-$^{13}C_6$-arginine (R6; no. 643440, Sigma-Aldrich, St. Louis, MO, USA)

Asialofetuin, from foetal calf serum (no. A4781, Sigma-Aldrich, St. Louis, MO, USA)

Bensonase® Nuclease (no. E1014, Sigma-Aldrich, St. Louis, MO, USA)

Blotting-Grade Blocker (no. 170-6404, BIO-RAD)

α-Casein, from bovine milk (no. C6780, Sigma-Aldrich, St. Louis, MO, USA)

CHCA Matrix (CHCA; α-cyano-4-hydroxycinnamic acid recrystallized, no. M101, Laserbio Labs)

Complete™ Mini, EDTA-free Protease inhibitor cocktail (no. 11836170001, Roche, Manheim, Germany)

DHB Matrix (2,5-dihydroxybenzoic acid recrystallized, no. M103, Laserbio Labs)

2,5-dihydroxybenzoic acid (DHB; no. 149357, Sigma-Aldrich, St. Louis, MO, USA)

Dimethyl sulfoxide ≥ 99.5% (DMSO; no. D5879, Sigma-Aldrich, St. Louis, MO, USA)

DL-Dithiothreitol BioXtra ≥99.0% (DTT; no. 5545, Sigma-Aldrich, St. Louis, MO, USA)

Dodecylsulfate. Na-salt (SDS; no. 20760, SERVA)

Dulbecco's modified eagle medium, high glucose, L-glutamine (DMEM; no. 11965-092, Gibco® by Life technologies™, Thermo Fisher Scientific)

Ethanol absolute p.a. (no. 603-002-00-5, PENTA s.r.o., Prague, Czech Republic)

Ethyl acetate for HPLC (no. 439169, Sigma-Aldrich, St. Louis, MO, USA)

Foetal bovine serum (FBS; no. 10270-106, Gibco® by Life technologies™, Thermo Fisher Scientific)

Foetal bovine serum, dialyzed by ultrafiltration (no. F0392, Sigma-Aldrich, St. Louis, MO, USA)

Formic acid, eluent additive for LC-MS (FA; no. 56302 FLUKA, Sigma-Aldrich, St. Louis, MO, USA)

L-Glutamic acid (Glu; no. 49449, Sigma-Aldrich, St. Louis, MO, USA)

L-Glutamine solution, 200 mM (no. G7513, Sigma-Aldrich, St. Louis, MO, USA)

Glycerol Ultrapure, MB grade (no.16374, USB Corporation, Cleveland, OH, USA)

Iodoacetamide (IAA; no. I6125, Sigma-Aldrich, St. Louis, MO, USA)

Iscove's modified Dulbecco's media without L-glutamine (no. E15-018, PAA Laboratories GmbH, Pashing, Austria)

Iscove's modified Dulbecco's media (IMDM; no. 12440-053, Gibco® by Life technologies™, Thermo Fisher Scientific)

Iscove's modified Dulbecco's media for SILAC (no. 88423, Thermo Fisher Scientific)

Lactic acid solution (LA; no. L1875, Sigma-Aldrich, St. Louis, MO, USA)

L-Lysine (K0; no. L5501, Sigma-Aldrich, St. Louis, MO, USA)

L-$^{13}C_6$-Lysine (K6; no. 608041, Sigma-Aldrich, St. Louis, MO, USA)

Magnesium chloride anhydrous ≥ 98 % (no. M8266, Sigma-Aldrich, St. Louis, MO, USA)

Methanol LC-MS CHROMASOLV® (no. 34966, Sigma-Aldrich, St. Louis, MO, USA)

Methanol LiChrosolv® hypergrade for LC-MS (no. 106035, Merck KGaA, Darmstadt, Germany)

N, N'-Methylenebisacrylamide (no. 66667, Sigma-Aldrich, St. Louis, MO, USA)

Myoglobin from equine heart (no. M1882, Sigma-Aldrich, St. Louis, MO, USA)

N-Octyl-β-D-glucopyranoside, BioXtra, ≥ 98% (no. O9882, Sigma-Aldrich, St. Louis, MO, USA)

Orthophosphoric acid solution, 85 wt % in H_2O (no. W290017, Sigma-Aldrich, St. Louis, MO, USA)

Penicillin-Streptomycin for cell culture (no. P0781, Sigma-Aldrich, St. Louis, MO, USA)

Phosphatase inhibitor cocktail 2 (no. P726, Sigma-Aldrich, St. Louis, MO, USA)

Phosphatase inhibitor cocktail 3 (no. P044, Sigma-Aldrich, St. Louis, MO, USA)

Phosphate buffer saline, pH 7.4 (no. 10010015, Gibco™, Thermo Fisher Scientific)

Precision Plus Protein™ Standards Kaleidoscope (no. 161-0375, BIO-RAD)

L-proline (no. P5607, Sigma-Aldrich, St. Louis, MO, USA)

Propidium iodide (PI; no. 81845, Sigma-Aldrich, St. Louis, MO, USA)

Ribonuclease A, from bovine pancreas (no. R6513, Sigma-Aldrich, St. Louis, MO, USA)

Sequencing grade modified trypsin, frozen (no. V5113, Promega Corporation, Madison, WI, USA)

Sequencing grade modified trypsin, lyophilized (no. V5111, Promega Corporation, Madison, WI, USA)

Sodium chloride, for molecular biology (NaCl; no. S3014, Sigma-Aldrich, St. Louis, MO, USA)

Sodium deoxycholate (no. 30970, Sigma-Aldrich, St. Louis, MO, USA)

Sodium fluoride, BioXtra, ≥ 99% (NaF; no. S7920, Sigma-Aldrich, St. Louis, MO, USA)

Sodium orthovanadate, 99.98%, trace metal basis (Na_3VO_4; no. 450243, Sigma-Aldrich, St. Louis, MO, USA)

Trifluoroacetic acid LC-MS grade (TFA; no. 85183, Thermo Scientific)

Trifluoroacetic acid ≥99% (TFA; no. 299537, Sigma-Aldrich, St. Louis, MO, USA)

Trizma® base (no. T6066, Sigma-Aldrich, St. Louis, MO, USA)

Trizma® hydrochloride (Tris-HCl; no. T5941, Sigma-Aldrich, St. Louis, MO, USA)

Triton® X-100 for molecular biology (no. T8787, Sigma-Aldrich, St. Louis, MO, USA)

Trypan blue (no. T6146, Sigma-Aldrich, St. Louis, MO, USA)

Trypsin-EDTA 0.25% (no. 25200-072, Gibco® by Life technologies™)

Tween® 20 (no. P1379, Sigma-Aldrich, St. Louis, MO, USA)

Water LiChrosolv® LC-MS Grade (no. 115333, Merck KGaA, Darmstadt, Germany)

Westran® S (no. 10413096, GE Healthcare Life Sciences Whatman™)

3.1.4. Antibodies

3.1.4.1. Primary antibodies:

Monoclonal Mouse Anti-β-actin Antibody (no. A5316, Sigma-Aldrich, St. Louis, MO, USA)

Monoclonal Mouse Anti-Chk1 Antibody (no. 2360, Cell signalling Technology®)

Monoclonal Rabbit Anti-Phospho-Chk1 (Ser245) Antibody (no. 2348, Cell signalling Technology®)

Polyclonal Rabbit Anti-Chk2 Antibody (no. 2662, Cell signalling Technology®)

Monoclonal Rabbit Anti-Phospho-Chk2 (Thr68) Antibody (no. 2197, Cell signalling Technology®)

Monoclonal Rabbit Anti-p70 S6 Kinase Antibody (no. 2708, Cell signalling Technology®)

Monoclonal Rabbit Anti-p70 S6 Kinase Antibody (no. 9234, Cell signalling Technology®)

3.1.4.2. Secondary antibodies:

P**olyclonal Goat Anti-Mouse Immunoglobulins/HRP** (no. P0447, Dako, Glostrup, Denmark)

Polyclonal Swine Anti-Rabbit Immunoglobulins/HRP (no. P039901, Dako, Glostrup, Denmark)

3.1.5. **Commercial kits and assays**

Apoptest™-FITC kit (no. K2350, DakoCytomation, Copenhagen, Denmark)

QuantiPro™ BCA Assay Kit (no. QPBCA, Sigma-Aldrich, St. Louis, MO, USA)

BM Chemiluminescence Western Blotting Kit (no. 11500708001, BM Chemiluminescence-POD, Roche)

Cell Proliferation Reagent WST-1 (no. 11644807001, Roche Diagnostics, Mannheim, Germany)

3.1.6. **Chromatographic material**

3M Empore™ C18 Extraction disk (no. 66883, Supelco®, Bellefonte, PA, USA)

3M Empore™ C18-SD 4 mm/1 ml Extraction disk cartridge (no. 66871-U, Supelco®, Bellefonte, PA, USA)

3M Empore™ C18-SD 7 mm/3 ml Extraction disk cartridge (no. 66872-U, Supelco®, Bellefonte, PA, USA)

C18 PepMap100, 3 µm, 100 A, 0.075 × 20 mm capillary trap column (Dionex, Thermo Scientific™, Bremen, Germany)

C18 PepMap RSLC, 2 µm, 100 A, 0.075 × 150 mm capillary separation column (Dionex, Thermo Scientific™, Bremen, Germany)

NuTip® (TiO_2/ZrO_2 1:1) (no. NT2TIZR, Glygen, Columbia, MD, USA)

Oasis® HLB SPE cartridges (Waters, Manchester, UK)

Oligo™ R3 reversed-phase material (no. 1133903, Applied Biosystems™, Foster City, CA)

Supelco C18 SPE cartridges 500 mg (Supelco Analyticals, Bellefonte, PA, USA)

Titansphere® 5 µm particles (no. 5020-75000, GL Sciences, Japan)

TopTip® (TiO_2, TiO_2/ZrO_2 1:1, and ZrO_2) (Glygen, Columbia, MD, USA)

TSKgel® Amide-80 HR 5 µm 4.6 × 25 cm separation column (Tosoh Biosciences, Stuttgart, Germany)

TSKgel® Amide-80 HR 5 µm 4.6 × 1 cm guard column (Tosoh Biosciences, Stuttgart, Germany)

3.1.7. **Instrumentation**

^{60}Co gamma-ray source (VF, Černá Hora, Czech Republic)

ABI 4800 mass spectrometer (Applied Biosystems, USA)

FACS analyser CyAn DakoCytomation (Beckman Coulter, USA)

PARADIGM™ Detection Platform (Beckman Coulter, Brea, CA, USA)

Q Exactive™ Hybrid Quadrupole-Orbitrap™ Mass Spectrometer (Thermo Scientific™, Bremen, Germany)

Thermo Scientific™ Dionex Ultimate™ 3000 RSLCnano system (Thermo Scientific™, Bremen, Germany)

Waters® Alliance Separations Module e2695 (Waters, Milford, MA, USA)

3.1.8. Commercial software

Summit v4.3 software (Beckman Coulter, Miami, FL, USA)

GPS Explorer TM Software vision *v3.6* (Applied Biosystems, USA)

3.2. Optimization of Metal Oxide Affinity Enrichment of Phosphorylated Peptides from Standard Peptide Mixtures

3.2.1. Model proteins and peptide mixtures

α-casein, asialofetuin, BSA, and myoglobin were dissolved in 50 mM ABC buffer (pH 7.8), reduced with 10 mM DTT, alkylated with 20 mM IAA, and subjected to trypsin digestion at an enzyme to protein ratio 1:50 at 37 °C overnight. Digested samples were desalted using Oasis® HLB SPE cartridges.

Peptide mixture A contained tryptic peptides originating from α-casein, asialofetuin, BSA, myoglobin in a molar ratio of 1:1:5:5 (*i.e.* 40 pmol of each phosphorylated protein α-casein and asialofetuin and 200 pmol of each non-phosphorylated protein BSA and myoglobin)

Peptide mixture B contained tryptic peptides originating from α-casein, asialofetuin, BSA, myoglobin in a molar ratio of 1:1:50:50 (*i.e.* 40 pmol of each phosphorylated protein α-casein and asialofetuin and 2 nmol of each non-phosphorylated protein BSA and myoglobin).

3.2.2. **Standard HeLa sample preparation**

HeLa cells were cultured in DMEM supplemented with 10% FCS, 100 UI/ml penicillin, and 0.1 mg/ml streptomycin at 37 °C under controlled 5% CO_2 and humidified atmosphere. The cells were harvested at about 80 % density. Whole cell extracts were prepared using an ice-cold lysis buffer containing 137 mM NaCl, 10% glycerol, 1% n-octyl-β-glucopyranoside, 50 mM NaF, 20 mM Tris-HCl, (pH=8), and 1 mM Na_3VO_4, followed by centrifugation at 14 000 g for 30 min at 4 °C. 0.5 mg of extracted proteins were diluted with 50 mM NH_4HCO_3 to a final concentration of 2 mg/ml, reduced with 10 mM DTT, alkylated with 20 mM IAA, and subjected to trypsin digestion at an enzyme to protein ratio 1:50 at 37 °C overnight. Peptides were desalted using Oasis HLB SPE cartridges (30 mg sorbent per cartridge). Enriched phosphopeptides were desalted using 3M Empore^{TM} C18-SD 4 mm/1 ml Extraction disk cartridges.

3.2.3. **MOLT-4 sample preparation**

MOLT-4 cells well cultured in IMDM for SILAC containing 20% dialyzed foetal bovine serum. Media were further supplemented with either unlabelled L-lysine (100 mg/l, K0) and L-arginine (84 mg/L, R0) or equimolar amounts of L-$^{13}C_6$-lysine (K6) and L-$^{13}C_6$-arginine (R6). L-proline (300 mg/L) was added to cell culture media avoid metabolic conversion of arginine to proline (272). For complete incorporation of labelled amino acids, cells were cultured for at least six cell doublings (308). The “heavy” cells (K6/R6) were irradiated by a dose of 1.5 Gy using a ^{60}Co gamma-ray source; the “light” cells (K0/R0) served as sham-irradiated controls. After irradiation, the flasks were placed into an incubator and the cells were harvested one hour after irradiation. Whole cell extracts were prepared using an ice-cold lysis buffer containing 137 mM NaCl, 10% glycerol, 1% n-octyl-β-glucopyranoside, 50 mM NaF, 20 mM Tris-HCl, (pH=8), and 1 mM Na_3VO_4, followed by centrifugation at 14 000 g for 30 min at 4 °C. 1 mg of extracted proteins (0.5 mg of “light” + 0.5 mg of “heavy” pooled together) were precipitated using acetone precipitation O/N (100 % acetone pre-cooled at -20 °C and added to the samples at 4:1 acetone: sample volume ratio), resolubilized in 8 M Urea/ 50 mM ABC, reduced with 10 mM DTT, alkylated with 20 mM IAA, and after dilution with 50 mM ABC subjected to trypsin digestion at an enzyme to protein ratio 1:50 at 37 °C overnight. Tryptic peptides were desalted using 3M Empore^{TM} C18-SD 7 mm/3 ml Extraction disk cartridges. For phosphopeptide enrichment, 1 mg of the desalted peptide sample was used. Enriched

phosphopeptides were desalted using 3M Empore^{TM} C18-SD 4 mm/1 ml Extraction disk cartridges.

3.2.4. Phosphopeptide enrichment protocols

3.2.4.1. NuTip® enrichment

10- to 200-µl TiO_2/ZrO_2 NuTip® (Glygen, Columbia, MD, USA) was washed with 100 µl of loading buffer (LB). Phosphopeptides were enriched by repetitive pipetting (20x) of 10 µl aliquots of sample dissolved in 100 µl of LB. The Tip was then washed twice with 200 µl of LB, three times with 200 µl of washing buffer 1 (WB 1) and three times with 200 µl of washing buffer 2 (WB 2). Phosphopeptides were then eluted five times with 10 µl aliquots of elution buffer (EB) by repetitive pipetting (20x) and the eluted fraction was then acidified with a mixture of 100% FA and 10% TFA (to final pH < 2).

3.2.4.2. TopTip® enrichment

10- to 200- µl TopTips® (Glygen, Columbia, MD, USA) packed with TiO_2, ZrO_2, or a mixture of both TiO_2 and ZrO_2 were tested for their phosphopeptide enrichment efficiency. The packed beads were washed with 200 µl of LB. The sample was dissolved in 200 µl of LB and loaded on the column two times. The washing procedure included two consecutive washes with 200 µl of LB, two washes with 200 µl of WB 1, and two washes with 200 µl of WB 2. Phosphopeptides were eluted with 200 µl of EB and the eluted fraction was then acidified with a mixture of 100% FA and 10% TFA (to final pH < 2).

3.2.4.3. Titanium dioxide enrichment using Titansphere® TiO_2 particles

Titansphere® TiO_2 particles (5 µm diameter; GL Sciences, Torrance, CA) were used for phosphopeptide enrichment using a "microtube approach". The sample was dissolved in 200 µl of LB and incubated with TiO_2 particles (peptide-to-TiO_2 ratio 1:8; mass/mass) on a shaker for 20 minutes. TiO_2 beads were then washed with 200 µl of LB, 200 µl of WB 1, and twice with 100 µl of WB 2. Phosphopeptides were eluted with 50 µl of EB and the eluted fraction was acidified with a mixture of 100% FA and 10% TFA (to final pH < 2).

3.2.5. Buffer conditions

Each of the chromatographic resins mentioned above: commercial tips NuTip packed with TiO_2/ZrO_2 (1:1), TopTips packed with TiO_2, TiO_2/ZrO_2 (1:1) or ZrO_2, and TiO_2 particles (Titansphere 5 μm) were employed for the enrichment of phosphopeptides under different buffer conditions following four published protocols with some minor modifications. LA, DHB, and Glu were used as the buffer additives to enhance the specifity of metal oxides towards phosphorylated peptides.

Every procedure for each peptide mixture, buffer condition, and phosphopeptide enrichment media was performed in 3 replicates.

3.2.5.1. Buffer conditions 1 – 5% TFA

Peptides were loaded onto commercial columns/mixed with TiO_2 particles in 80% acetonitrile and 5% TFA (LB). The columns/TiO_2 particles were then washed with 80% acetonitrile/ 1% TFA (WB 1) and then with 20% acetonitrile and 0.5% TFA. Peptides were eluted with NH_4OH pH 11 (EB).

3.2.5.2. Buffer conditions 2 – 1M LA

Peptides were loaded onto commercial columns/mixed with TiO_2 particles in 80% Acn/5% TFA/1 M LA (LB). The columns/TiO_2 particles were then washed with 80% Acn/ 1% TFA (WB 1) and then with 20% Acn/0.5% TFA (WB 2). Peptides were eluted with NH_4OH pH 11 (EB).

3.2.5.3. Buffer conditions 3 – 350 mg/ml DHB

Peptides were loaded onto commercial columns/mixed with TiO_2 particles in 65% Acn/2% TFA/350 mg/ml DHB (LB) according to Larsen's lab (222). The columns/TiO_2 particles were then washed with 65% Acn/ 2% TFA (WB 1) and then with 20% Acn/0.5% TFA (WB 2). Peptides were eluted with NH_4OH pH 11 (EB).

3.2.5.4. Buffer conditions 4 – 100 mM Glu

Peptides were loaded onto commercial columns/mixed with TiO_2 particles in 65% Acn/2% TFA/0.1 M glutamic acid (LB) according to Wu et al. (309).The columns/TiO_2 particles were then washed with 65% Acn/ 0.5% TFA (WB 1) and then with 65% Acn/0.1% TFA (WB 2). Peptides were eluted with NH_4OH pH 11 (EB).

3.2.6. **Purification and concentration of eluted peptides**

Eluted fractions were concentrated and desalted prior to MALDI analysis using custom made microcolumns prepared from Geloader tips packed with 3M EMPORE C18 disc and Poros Oligo R3 reversed phase material.

Acidified eluates from the columns/TiO_2 particles were loaded onto desalting columns. The columns were then washed twice with 50 µl of 0.1% TFA. Peptides were eluted with 10 µl of 60% Acn/ 0.1% TFA.

3.2.7. **Chromatography and mass spectrometry**

MALDI-TOF-MS/MS analysis was performed using an ABI 4800 mass spectrometer. Spectra were recorded in positive MS and MS/MS reflector mode. Acquired raw data files were processed using GPS Explorer TM Software vision *v3.6* connected to MASCOT server *v.2.1*. CHCA matrix (5 mg/ml) in 60% Acn/0.1% TFA or DHB matrix (5 mg/ml) in 30% Acn/0.1% TFA and 1% phosphoric acid were used as MALDI matrices. Phosphoric acid was used as a matrix additive to improve phosphopeptides mass resolution (310).

UV-VIS chromatography: Peptides were separated by reversed phase chromatography using Dionex Ultimate 3000. Peptides were loaded in solvent A (2% Acn, 0.1% TFA) onto a capillary column (C18 PepMap RSLC, 2 µm, 100 Å, 0.075 × 150 mm) followed by 115-min multi-step gradient to 95% solvent B (80% Acn, 0.1% TFA) and detected using Dionex Ultimate 3000 Variable Wavelength detector.

RPLC-ESI-MS/MS analysis of the complex samples (HeLa cells lysate, SILAC labelled irradiated MOLT-4 cells) was performed on Thermo Scientific Dionex Ultimate™ 3000 RSLCnano system coupled through Nanospray Flex ion source with Q Exactive mass spectrometer. TiO_2-enriched peptide sample was dissolved in 20 µl of 2% Acn/0.05% TFA and 3-8 µl according to estimated peptide sample concentration were injected into RSLCnano system. Peptides were loaded on capillary trap column (C18 PepMap100, 3 µm, 100 Å, 0.075 × 20 mm) by 2% Acn/0.05% TFA mobile phase at flow rate 5 µL/min for 5 min and then eluted and separated on capillary column (C18 PepMap RSLC, 2 µm, 100 Å, 0.075 × 150 mm). Elution was carried out by step linear gradient of mobile phase B (80% Acn/0.1% FA) over mobile phase A (0.1% FA); from 4% to 36% B in 19 min and from 36% to 55% B in 6 min at flow rate 300 nl/min. Temperature of the column was 40 °C and eluent was monitored at 215 nm during the separation. Spraying voltage was 1.7

kV and heated capillary temperature was 220 °C. The mass spectrometer was operated in the positive ion mode performing survey MS (range 300 to 1800 *m*/*z*) and data-dependent MS/MS scans performed on the six most intense precursors with dynamic exclusion window of 40 s. MS scans were acquired with 70,000 resolutions at 200 m/z from 1×10^6 accumulated charges (maximum fill time was 100 ms). The lock mass at *m*/*z* 445.12003 ($[(C_2H_6SiO)_6 + H]^+$) was used for internal calibration of mass spectra. Intensity threshold for triggering MS/MS was set at 1×10^5 for ions with $z \geq 2$ with a 3 Da isolation window. Precursor ions were accumulated with AGC of 1×10^5 (maximum fill time was 100 ms) and normalized collisional energy for HCD fragmentation was 27 units. MS/MS spectra were acquired with 17,500 resolution (at 200 *m*/*z*). Raw files were processed with MaxQuant *v1.3.0.5* using Andromeda as a search engine.

3.3. **Radiosensitization of MOLT-4 cells**

3.3.1. **Cell culture and cell culture conditions**

MOLT-4 cells were cultured in IMDM containing 20% foetal bovine serum, 2 mM glutamine, 100 UI/mL penicillin, and 0.1 mg/mL streptomycin at 37 °C under controlled 5% CO_2 and humidified atmosphere. The cultures were split every other day by dilution to a concentration of $2x10^5$ cells/ml. Cell counts were assessed by a haemocytometer, and cell membrane integrity was assessed by the Trypan Blue exclusion technique.

For the quantitative proteomic and phosphoproteomic experiments, MOLT-4 cells well cultured in IMDM for SILAC containing 20% dialyzed foetal bovine serum. Media were further supplemented with either unlabelled L-lysine (100 mg/l, K0) and L-arginine (84 mg/L, R0) or equimolar amounts of L-$^{13}C_6$-lysine (K6) and L-$^{13}C_6$-arginine (R6). L-proline (300 mg/L) was added to cell culture media avoid metabolic conversion of arginine to proline (272). For complete incorporation of labelled amino acids, cells were cultured for more than six cell doublings, usually 10 (308).

3.3.2. **Cell treatment (kinase inhibition and gamma-irradiation)**

A selective inhibitor of ATR kinase, 3-amino-6-(4-(methylsulfonyl)phenyl)-*N*-phenylpyrazine-2-carboxamide (VE-821), and a selective inhibitor of ATM kinase, 2-morpholin-4-yl-6-thianthrene-1-yl-pyran-4-one (KU55933), were dissolved in dimethyl sulfoxide (DMSO) to a concentration of 10 mM, and the aliquots were stored at −20 °C. Additional dilutions (1 mM, 2 mM, 5 mM, and inhibitor combinations as indicated) were also prepared in DMSO to maintain the same concentration of DMSO in all inhibitor-treated samples. In all experiments presented in this study, the inhibitors were added to cell culture 30 minutes prior to gamma irradiation. The inhibitors were washed out after one hour or 24 hours when indicated. Cells were irradiated using a ^{60}Co gamma-ray source with a dose rate of 0.5-0.45 Gy/min. Since MOLT-4 cells are relatively sensitive to gamma irradiation, the doses of irradiation were carefully chosen based on our previous publications (311–313) to only induce either cytostatic or sub-lethal damage.

3.3.3. Electrophoresis and western blotting

Cells were pre-treated by different concentrations of inhibitors or DMSO (control) and irradiated by an indicated dose of IR. One or six hours after irradiation, cells were washed with cold phosphate buffer saline (PBS), and whole cell extracts were prepared by lysis in 500 μL of lysis buffer per $1x10^7$ cells (137 mM NaCl; 10% glycerol; 50 mM NaF; 20 mM Tris-HCl, pH = 8; 1% n-octyl-β-glucopyranoside; 1 tablet of protease inhibitors Complete™ Mini/ 10 ml, 1:100 Phosphatase inhibitor cocktail 2 and 3). The lysate was clarified by centrifugation, and protein concentration was measured by a bicinchoninic acid protein assay. The lysates containing equal amount of protein (30 μg) were loaded onto a 12% SDS polyacrylamide gel. After electrophoresis, proteins were transferred to a polyvinylidene difluoride membrane and hybridized with an appropriate antibody: anti-Chk1 (1:500), anti-phospho-Chk1 (Ser345, 1:500), anti-Chk2 (1:250), anti-phospho-Chk2 (Thr68, 1: 250), anti-p70s6k (1:1000), anti-phospho p70s6k (Thr389; 1:1000) and beta actin (1: 20,000). After washing, the membranes were incubated with secondary peroxidase-conjugated antibody, and the signal was developed using a BM Chemiluminescence Western Blotting Kit.

3.3.4. Cell proliferation/viability WST-1 assay

Proliferation of MOLT-4 cells was evaluated by WST-1 (4-[3-(4-iodophenyl)-2-(4-nitrophenyl)-2H-5-tetrazolio]-1,3-benzene disulphonate) colorimetric assay (Roche Diagnostics, Mannheim, Germany). The assay is based on cleavage of WST-1 by mitochondrial dehydrogenases, and the absorbance of the cleavage product correlates with the number of viable cells. Prior to treatment, MOLT-4 cells were placed in 96-well microplates; the number of cells plated into each well were $3x10^4$, $1x10^4$, and $2.5x10^3$ for 24, 72, and 144 hours long experiments, respectively. After the addition of inhibitors and subsequent irradiation, the microplates were placed in an incubator and cultivated at 37 °C. Finally, WST-1 was added, and the plates were incubated for three hours at 37 °C. Absorbance of samples was then measured at 440 nm using a PARADIGM™ Detection Platform. Controls were normalized to 100 % for each assay, and all values were expressed as a percentage of the normalized controls.

3.3.5. Cell cycle analysis and apoptosis detection by flow cytometry

For cell cycle analysis, cells were collected 24 hours after irradiation by a dose of 3 Gy (± inhibitor pre-treatment), washed with ice-cold PBS, and fixed with ice-cold 70% ethanol. Prior to flow cytometry, cells were washed with ice-cold PBS, and DNA was stained using Vindelov's solution (10 mM Tris-HCl pH=7.6, 0.6 mg/ml NaCl, 0.01 mg/ml Ribonuclease A, 0.05 mg/ml PI).

For apoptosis detection, an Apoptest-FITC kit was used. The kit contains Annexin V, which binds to phosphatidylserine at the surface of apoptotic cells, and PI to detect cells with increased cell membrane permeability. Cells were pre-treated by the inhibitors and irradiated by a dose of 1 Gy. The proportion of apoptotic cells in each condition was measured 24 hours and 72 hours after IR according to the manufacturer's instructions.

Flow cytometric analysis was performed on a FACS analyser CyAn DakoCytomation. At least 20,000 cells were analysed per sample. Listmode data were analysed using Summit v4.3 software.

3.3.6. Sample preparation for quantitative proteomic and phosphoproteomic experiment

MOLT-4 cells well cultured in IMDM for stable SILAC containing 20 % of dialyzed foetal calf serum for at least six cell doublings as described above (308). Thirty minutes before irradiation, VE-821 was added to the "heavy" cells (K6/R6) at a concentration of 10 μM; the "light" cells (K0/R0) were mock treated with DMSO, whose final concentration in culture was lower than 0.1 %. Both groups were irradiated using a ^{60}Co gamma-ray source by a dose of 1.5 Gy. After irradiation, the flasks were placed into an incubator. Three biological replicates were analysed.

One hour after irradiation, the cells were washed with ice-cold PBS and lysed as was published (314) with minor modifications. Briefly, the cells were thoroughly resuspended in 2 ml ice-cold lysis buffer/1x10^7 cells (50 mM ammonium bicarbonate, 1% sodium deoxycholate, 1:100 Phosphatase inhibitor cocktail 2 and 3). The lysate was immediately placed into boiling water bath, and after 5 min incubation, the samples were cooled down to room temperature on ice. To cleave nucleic acids and decrease the viscosity of the lysate, bensonase nuclease (2.5 U/μl) and $MgCl_2$ (1.5 mM) were added to the

samples. The lysate was then clarified by centrifugation at 14,000 rpm, and protein concentration was measured by bicinchoninic acid assay. Sample volumes corresponding to 2 mg of "light" proteins and 2 mg of "heavy" proteins were pooled together to make a 1:1 protein sample.

The protein samples for phosphoproteomic analyses were diluted in lysis buffer and reduced with 10 mM DTT, alkylated with 20 mM IAA, and digested O/N with trypsin at an enzyme-to-substrate ratio of 1:60 (sequence grade modified trypsin). Sodium deoxycholate was then extracted by ethyl acetate as described earlier (315); tryptic peptides were desalted via 500 mg Supelco C18 SPE cartridges according to the manufacturer's instructions and dried using SpeedVac.

Sample preparation for the proteome analysis followed the protocol described above with minor modifications to adjust the volume and concentration of chemicals to a smaller sample amount (10+10 μg of the "heavy" and "light" samples).

3.3.7. Hydrophilic interaction liquid chromatography fractionation

Dried peptide samples were fractionated by HILIC according to a protocol that has been published previously (198) using the 4.6 × 25 cm TSKgel® Amide-80 HR 5 μm particle column with the TSKgel® Amide-80 HR 5 μm 4.6 × 1 cm guard column operated with Waters Separations Module 2695 at 0.5 mL/min. Briefly, 3.5 mg of evaporated samples were reconstituted in 80% B and loaded onto the HILIC column. Peptides were then separated by a gradient of A over B from 80% to 60% B in 40 min and from 60% to 0% B in 5 min. Across the gradient, 22 fractions were collected (2 × 2 and 20 × 1 mL) from each replicate. Mobile phase B consisted of 98% Acn/0.1% TFA; mobile phase A consisted of 2% Acn/0.1% TFA.

3.3.8. Phosphopeptide enrichment

Each HILIC fraction was enriched for phosphopeptides using titanium dioxide chromatography (222) using a protocol optimized in previous experiments. At first, each fraction was supplemented with TFA and glutamic acid to reach final concentrations of 2% TFA and 100 mM glutamic acid. Titanium dioxide particles (Titansphere® 5 μm particles) were suspended in loading solution (65% Acn, 2% TFA, 100 mM glutamic acid), and a volume of titanium dioxide suspension depending on an expected proportion of peptides

and phosphopeptides in a particular fraction (based on previous experiments) was added to each sample. Microparticles with bound phosphopeptides were washed with 200 µl of loading solution, 200 µl of washing solution 1 (65% Acn/0.5% TFA), 200 µl of washing solution 2 (65% Acn/ 0.1% TFA) and 100 µl of washing solution 2. Phosphopetides were eluted by 150 µl of elution solution (20% Acn/NH4OH, pH 11.5) in two sequential elutions. Late fractions were subjected to the second enrichment. Eluates from the first and second enrichment were pooled together, acidified with 100% formic acid, and placed in a SpeedVac until all crystals of ammonium formate were evaporated.

3.3.9. **Mass spectrometric analysis**

LC-MS/MS analyses were performed on Thermo Scientific Dionex Ultimate™ 3000 RSLCnano system (Thermo Scientific, Bremen, Germany) coupled through Nanospray Flex ion source with Q Exactive mass spectrometer (Thermo Scientific, Bremen, Germany). TiO_2-enriched HILIC fractions were dissolved in 18 µl of 2% Acn/0.05% TFA and 3-8 µl according to estimated peptide sample concentration were injected into RSLCnano system. Peptides were loaded on capillary trap column (C18 PepMap100, 3 µm, 100 Å, 0.075 × 20 mm) by 2% Acn/0.05% TFA mobile phase at flow rate 5 µL/min for 5 min and then eluted and separated on capillary column (C18 PepMap RSLC, 2 µm, 100 Å, 0.075 × 150 mm). Elution was performed by step linear gradient of mobile phase B (80% Acn/0.1% FA) over mobile phase A (0.1% FA) from 4% to 34% B in 48 min and from 34% to 55% B in 15 min at a flow rate 300 nl/min. Temperature of the column was 40 °C and eluent was monitored at 215 nm during the separation. Spraying voltage was 1.7 kV and heated capillary temperature was 250 °C. The mass spectrometer was operated in the positive ion mode performing survey MS (range 300 to 1800 *m*/*z*) and data-dependent MS/MS scans performed on the six most intense precursors with dynamic exclusion window of 40 s. MS scans were acquired with 70,000 resolutions at 200 m/z from 1×10^6 accumulated charges (maximum fill time was 100 ms). Intensity threshold for triggering MS/MS was set at 5 × 104 for ions with $z \geq 2$ with a 1.6 Da isolation window. Precursor ions were accumulated with AGC of 1 × 105 (maximum fill time was 100 ms) and normalized collisional energy for HCD fragmentation was 27 units. MS/MS spectra were acquired with 17,500 resolution (at 200 m/z).

3.3.10. **Mass spectrometry data processing and bioinformatic analysis**

3.3.10.1. Raw data processing

Raw data files acquired by LC-MS/MS were processed with MaxQuant *v1.5.2.8* (316). Peak lists were searched against the human SwissProt database (November 2015) using Andromeda search engine (317). Minimum peptide length was set to seven amino acids, and two missed cleavages were allowed. Carbamidomethylation of cysteine was set as a fixed modification while oxidation of methionine, protein N-terminal acetylation, and phosphorylation of serine, threonine, and tyrosine residues were used as variable modifications. Additionally, appropriate SILAC labels were selected (R6, K6), and the labelled amino acid filtering was disabled. Mass tolerances of 10 and 20 ppm were allowed for MS and MS^2 peaks, respectively. Only proteins, peptides, and phosphorylation sites with false discovery rate (FDR) lower than 0.01 were accepted. For modified peptides, a minimal score (40) and minimal delta score (6) were set as additional cut-offs. For protein quantification, only unmodified peptides, peptides oxidized at methionine residues, or acetylated at *N*-terminus were accepted; both razor and unique peptides were used for calculation of protein *H*/*L* ratios. The Re-quantify function was disabled whereas Match between runs was enabled during the search.

3.3.10.2. MaxQuant output data filtering and identification of significantly changed phosphorylation sites

Potential contaminants and hits from the reversed database were removed before further data processing, and data were further manually inspected to look for possible misquantifications caused by the labelling status (K6/R6) and disabled "Filter labelled amino acids" option in MaxQuant. Global rank test (GRT) was used to find differentially regulated phosphorylation sites. Only phosphorylation sites quantified in all three replicates were subjected to GRT, and FDR was estimated non-parametrically as described by Zhou et al. (318). The significance cut-off for differentially regulated sites was set to FDR < 0.005.

3.3.10.3. Gene ontology and signalling pathways over-representation analyses

Gene ontology (GO) and signalling pathways over-representation analyses were performed using ConsensusPathDB over-representation analysis web tool (319,320). For

the GO terms over-representation, proteins containing differentially regulated phosphorylation sites (both up- and down-) were tested against a custom background reference set comprising all phosphoproteins with at least one quantified phosphorylation site that was subjected to GRT (*i.e.* all phosphoproteins with at least one phosphorylation site quantified in all three biological replicates). Statistical significance of the over-representation analysis was estimated using hypergeometric testing with Benjamini-Hochberg FDR correction of calculated p-values, and the cut-off was set to FDR < 0.05. For the signalling pathways over-representation analysis, phosphoproteins with at least one regulated phosphorylation site were mapped to signalling pathways from three different databases: KEGG (321,322), REACTOME (323), and PID (324). Pathway-coverage was calculated for overrepresented pathways (FDR < 0.05, tested against a default background reference set comprising all Uniprot proteins included in at least one signalling pathway from a corresponding database).

3.3.10.4. Network analysis

Log_2 transformed SILAC H/L ratios of phosphorylation sites quantified in all three biological replicates were normalized (z-score calculation) and subjected to SubExtractor algorithm (325). Human protein-protein interactions with STRING score above 900 were used as the second input for the algorithm, and regulated subnetworks were extracted (FDR = 0.005, $\alpha = 0.2$, $\sigma = 4$). Extracted networks were visualized using Cytoscape *v3.2.1* (326).

3.3.10.5. Sequence motif analyses

To analyse and visualize sequence motifs surrounding phosphorylation sites identified and quantified in our study, we employed iceLogo tool (327) and motif-x algorithm (328). In both motif analyses, amino acid sequences (± 7 residues) surrounding either significantly up- or down-regulated phosphorylation sites were tested against a background reference set composed of sequences surrounding non-regulated phosphorylation sites detected in our study (as evaluated using GRT) that reached a minimal localization probability of 0.75 (*i.e.*, "class I phosphosites" (273)). Motif-x was employed to extract significantly enriched linear motifs. Search parameters were set to at least 10 occurrences of a motif, and the significance level to $p < 0.00003$ (which approximately corresponds to a *q*-value of 0.01 after Bonferroni correction for multiple hypothesis testing).

3.3.10.6. Identification of protein kinases responsible for the observed protein phosphorylations and evaluation of global changes in their activities

Class I phosphorylation sites quantified in all three biological replicates were annotated with previously known kinase-substrate relationships downloaded from the PhosphoSitePlus database (58). To increase the number of annotated phosphorylation sites, two kinase predictors were employed: NetworKIN 3 (329) and iGPS *v1.0* (330). Both predictors combine motif scoring with contextual information (*i.e.* protein-protein interaction scoring downloaded from the STRING database (331)). The kinase predictions were further filtered to reach NetworKIN score > 3 or "medium" significance threshold in iGPS (*i.e.* FDR of 6 % for S/T kinases and FDR of 9 % for Y kinases). The significance of global changes in kinase activities were evaluated using "1D annotation enrichment" tool available in Perseus software *v1.5.2.6* (332).

To further facilitate the interpretation of the results we also downloaded the "Regulatory sites" dataset from the PhosphoSitePlus database, which summarizes the current up-to-date knowledge about the known functions of specific phosphorylation sites. In text, these sites are referred as "regulatory" sites.

3.3.11. **Targeted metabolomic analysis**

3.3.11.1. Sample preparation

For the quantitative targeted metabolomic analysis, MOLT-4 cells were pre-treated either by VE-821 (10 μM) or DMSO (control groups) 30 minutes prior to IR (1.5 Gy). Six and twelve hours after irradiation, the cells were counted using a haemocytometer, and a cell suspension volume containing $2x10^6$ of cells was pipetted into five sample volumes of a pre-cooled (-40 °C) quenching solution (60% methanol, 0.85% ABC, pH 7.4) as described previously (333). The samples were gently mixed, and the cells were pelleted by centrifugation (1,000 g, 3 minutes). After the centrifugation, supernatant was removed, and the cells were resuspended in 150 μl of pre-cooled (-80 °C) methanol, transferred to a lyophilisation vial, and lyophilised. Three replicates were prepared for each condition. The lyophilisates were dissolved in 100 μl of 80% methanol and centrifuged (14,000 g for 10 min); a small volume of the sample (10 μl) was collected for quality control (QC) sample and the rest was transferred to vial and analysed.

QC sample was prepared by pooling equal volumes of cell extract sample. QC was analysed randomly throughout the run to provide a measurement not only of the system's stability and performance but also of the reproducibility of the sample preparation.

3.3.11.2. Instrumentation

The metabolite profiling of cell extracts and the QC samples performed by high-performance liquid chromatography tandem mass spectrometry enabled the analysis of 354 intermediary metabolites (acylcarnitines, amino acids, organic acids, saccharides, etc.).

For separation, an LC system UltiMate 3000 RS (Dionex, Sunnyvale, CA, USA) was used. The separation was performed with a LUNA NH2 column 3.0 µm, 2 x 100 mm, protected by a guard column, 4 x 2 mm ID, of the same material (Phenomenex, Torrance, USA) in normal aqueous phase mode. Mobile phase A consisted of 20 mM ammonium acetate at pH 9.75, and mobile phase B consisted of Acn. The gradient program was set as follows: 0-7 min: 95% → 10% B; 7-13 min: 10% B; 13-14 min: 10% → 95% B; 14-17 min: 95% B. The column was maintained at 35 °C, and the flow rate was 0.3 ml/min. Detection was performed using a Triple Quad 6500 tandem mass spectrometer (AB Sciex, Foster City, CA, USA) fitted with electrospray ionisation in both positive and negative mode. To enhance sensitivity, the targeted metabolites were scanned in scheduled multiple reaction monitoring mode with prolonged dwell times. Both quadrupoles were set at unit resolution. The parameters of the IonDriveTM Turbo V source and gases were as follows: curtain gas, 40 psi; collision gas, 8 psi; ion spray voltages, 5500 V/- 4500 V; both ion source gases, 40 psi and source temperature, 400 °C. Compound parameters such as the declustering potential, entrance potential, collision energy, and collision cell exit potential were previously optimized to standards. The instrument was controlled using the Analyst v1.6.2 software.

3.3.11.3. Data processing

The analytes were detected and identified according to the multiple reaction monitoring transitions and retention times in the MultiQuant *v3.0* software (AB Sciex, Foster City, CA, USA). The peak areas were extracted, and the corresponding peak areas were taken to create the final dataset.

3.3.11.4. Data treatment and statistical analysis

The data were treated and statistically processed in the R program language *v3.1.2* using basic statistical packages (e.g. Biobase, stats, graphics; (334)), the special packages XCMS (335–337) and robCompositions (338). The quality control-based robust local regression signal correction method was applied to the data (339). The coefficients of variation (CV) of the quality control samples were evaluated and features with a CV higher than 30% were excluded from the analysis. Zero values were imputed by two-thirds of the minimum metabolite value for the appropriate group of samples. The data were analysed as compositional using centred logratio transformation (340) and mean centring. The p-value for each metabolite was calculated by means of a t-test, and Bonferroni correction was applied. Finally, the data were evaluated by means of unsupervised (principal component analysis – PCA) and supervised (orthogonal partial least squares discriminant analysis – OPLS-DA) multivariate analysis. For clustering analysis, only ANOVA significant (permutation-based FDR < 0.05) metabolites were selected and subjected to hierarchical clustering using Euclidean distances.

4. Results

4.1. Optimization of metal oxide affinity enrichment of phosphopeptides from a standard tryptic peptide mixture

4.1.1. Summary of phosphopeptides detected in the optimization experiments

Commercially available α-casein that we used as the main phosphorylated component of our standard peptide mixtures is a mixture of two naturally occurring variants, the S1 variant (major component) and the S2 variant (minor component), and the preparations are usually contaminated with small amounts of β-casein. The S1 variant has nine known phosphorylation sites; the S2 variant has twelve known phosphorylation sites, and β-casein has five known phosphorylation sites. Asialofetuin, which we used as the second phosphorylated component of our mixture, has six known phosphorylation sites previously identified. Phosphopeptides originating from these proteins detected in our work are summarized in **table 1**. In summary, we detected 18 phosphopeptides originating from these phosphoproteins; eight of them were detected also in their oxidized form.

Table 1: *Overview of detected phosphopeptides from α-casein, β-casein, and asialofetuin*

Peptide sequence	Protein (Swiss-Prot)		No. of P-gr.	[M+H]+ (m/z)
TVDMESTEVFTK[1]	CAS2_BOVIN	153-164	1	1466.61
TVDMESTEVFTKK[1]	CAS2_BOVIN	153-165	1	1594.71
VPQLEIVPNSAEER	CAS1_BOVIN	121-134	1	1660.79
YLGEYLIVPNSAEER[2]	CAS1_BOVIN		1	1832.85
DIGSESTEDQAMEDIK[1]	CAS1_BOVIN	58-73	1	1847.73
DIGSESTEDQAMEDIK[1]	CAS1_BOVIN	58-73	2	1927.69
YKVPQLEIVPNSAEER	CAS1_BOVIN	119-134	1	1951.95
FQSEEQQQTEDELQDK	CASB_BOVIN	48-63	1	2061.83
FQSEEQQQTEDELQDKIHPF	CASB_BOVIN	48-67	1	2556.09
NTMEHVSSSEESIISQETYK[1]	CAS2_BOVIN	17-36	4	2618.9
VNELSKDIGSESTEDQAMEDIK[1]	CAS1_BOVIN	52-73	3	2678.02
QMEAESISSSEEIVPNSVEQK[1]	CAS1_BOVIN	74-94	5	2720.91
NTMEHVSSSEESIISQETYKQ	CAS2_BOVIN	17-37	4	2746.96
EKVNELSKDIGSESTEDQAMEDIK[1]	CAS1_BOVIN	50-73	3	2935.16
NANEEEYSIGSSSEESAEVATEEVK	CAS2_BOVIN	61-85	4	3008.03
NANEEEYSIGSSSEESAEVATEEVK	CAS2_BOVIN	61-85	5	3088
RELEELNVPGEIVESLSSSEESITR	CASB_BOVIN	16-40	4	3122.27
HTFSGVASVESSSGEAFHVGK	FETUA_BOVIN	313-333	1	2199.97
[1]- Peptides also detected in their oxidized forms [2]- Alternative splicing				

4.1.2. Comparison of enrichment efficiency of different metal oxide chromatographic resins

The evaluation of enrichment efficiency for phosphorylated peptides of different chromatographic resins under different buffer conditions was performed by comparing the maximal numbers of detected phosphopeptides and repeatability (*i.e.* repeated detection of the same phosphopeptides in three independent experiments).

Summarized results of the comparison are depicted in **figure 4** showing the results from the phospho-enrichment of mixture A and B. As shown in the figures, Titansphere® particles and NuTips® clearly outperformed the TopTips®. All three kinds of TopTips® tested in our experiments provided lower number of detected phosphopeptides than Titansphere® particles and NuTips® columns.

The addition of three different displacers of nonphosphorylated peptides improved the enrichment efficiency of TopTips®, but the obtained results were still not fully comparable with the NuTips® and Titansphere® enrichment. Whereas the maximal numbers of phosphopeptides detected after the phosphoenrichment from mixture A by NuTips® and Titansphere® particles ranged between 15 and 17 under the most phospho-efficient buffer conditions, TopTips® enrichment led to the detection of only 9 phosphopeptides under the best buffer/resin conditions. The same trend was observed in the enrichment of phosphopeptides from the mixture B. From the three TopTips® microcolumns tested, mixed TiO_2/ZrO_2 TopTips® provided the best enrichment results. The most phosphopeptides (17) were detected using NuTips® under the buffer conditions 4 (**figure 6A**).

Figure 5 shows the enrichment efficiency and repeatability for singly- and multiply- phosphorylated peptides. While the maximal numbers of mono-phosphorylated peptides did not differ substantially when comparing different resins, the only multiply phosphorylated peptide detected using TopTips® enrichment was a doubly-phosphorylated peptide 1927.69 from α-casein. Other multiply phosphorylated peptides were not detected. On the other hand, using NuTips® and Titansphere® particles, we detected several multiphosphorylated peptides (with up to 5 modifications; see **table 1**). Interestingly, 350 mg/ml DHB had a negative impact on the enrichment of monophosphorylated peptides in NuTips® and Titansphere® enrichment. Additionally, in the case of NuTips®, the addition of DHB caused a high level of noise in the low m/z region of MALDI-TOF spectra (**figure 6C**).

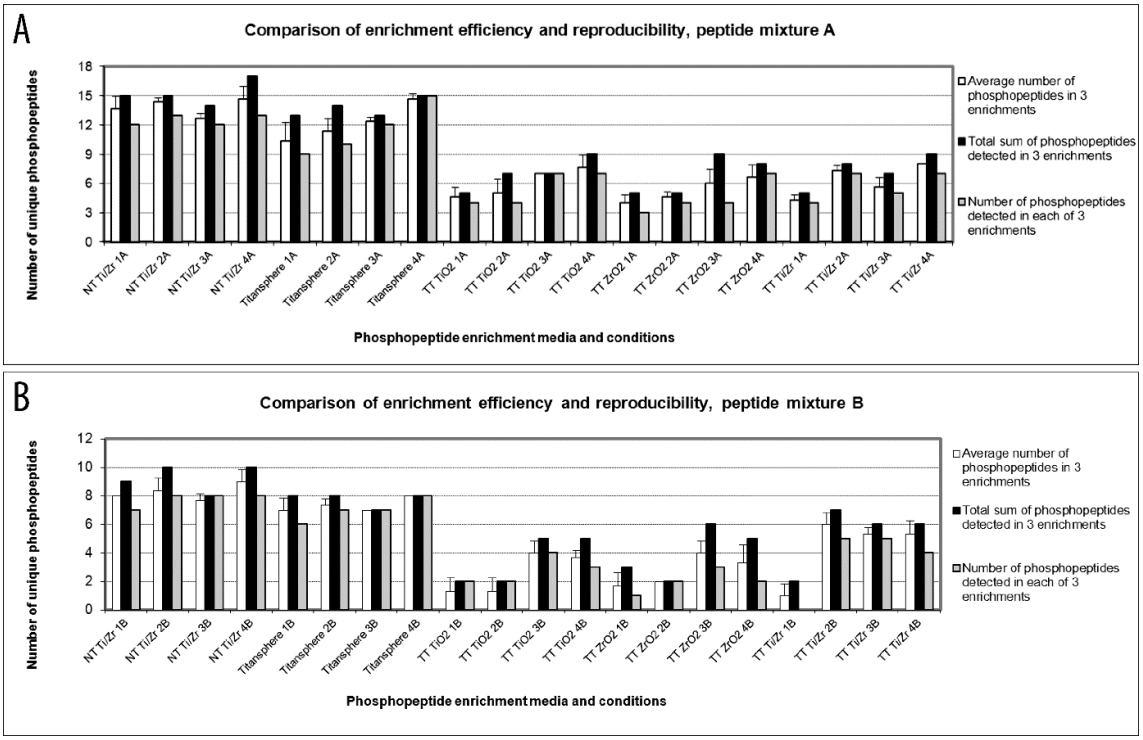

Figure 4: *Comparison of enrichment efficiency (average number of detected phosphopeptides with standard deviation and total sum of phosphopeptides obtained in 3 enrichments) and repeatability (number of phosphopeptides repeatedly detected in each of 3 enrichments) of phosphopeptide enrichment from peptide mixture A* ***(A)*** *and B* ***(B)*** *using different media and protocols. NT, NuTip; TT, TopTip; Ti, TiO2; Zr, ZrO2.*

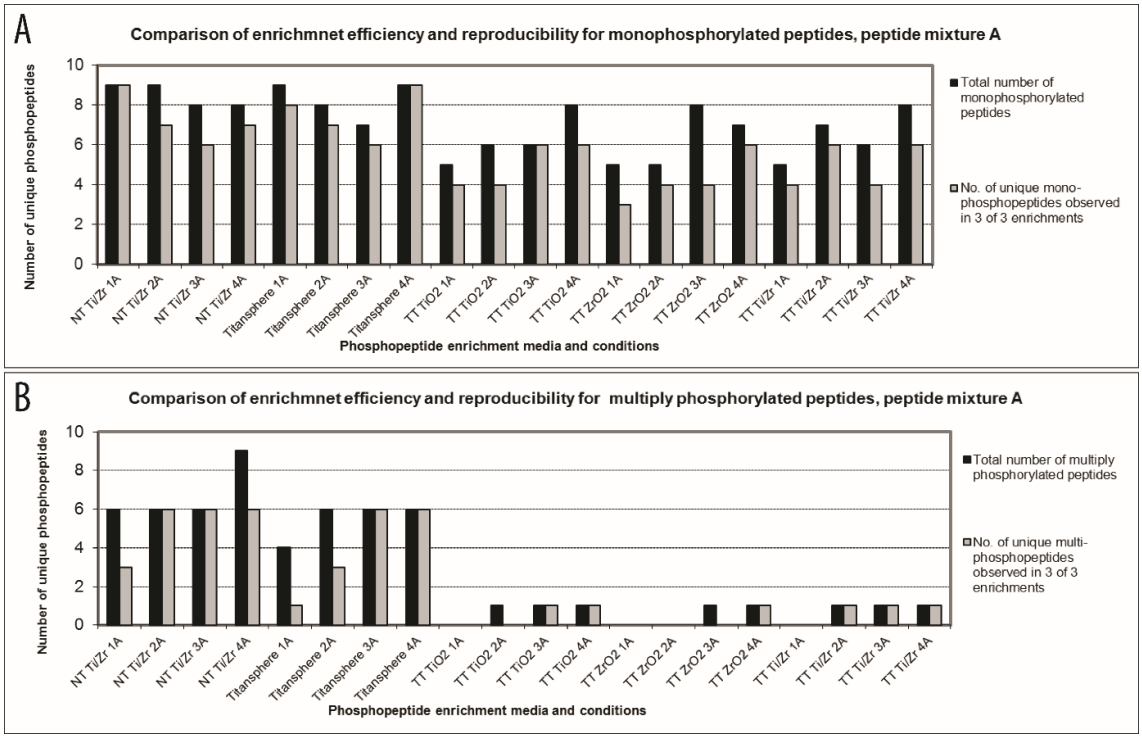

***Figure 5**: Comparison of efficiency (total sum of phosphopeptides obtained in 3 enrichments) and repeatability (number of phosphopeptides repeatedly detected in each of 3 enrichments) of mono-phosphorylated peptides **(A)** and multiply phosphorylated peptides **(B)** enrichment using different media and applied protocols (see Methods) on mixture A (1:1:5:5). NT, NuTip; TT, TopTip; Ti, TiO2; Zr, ZrO2.*

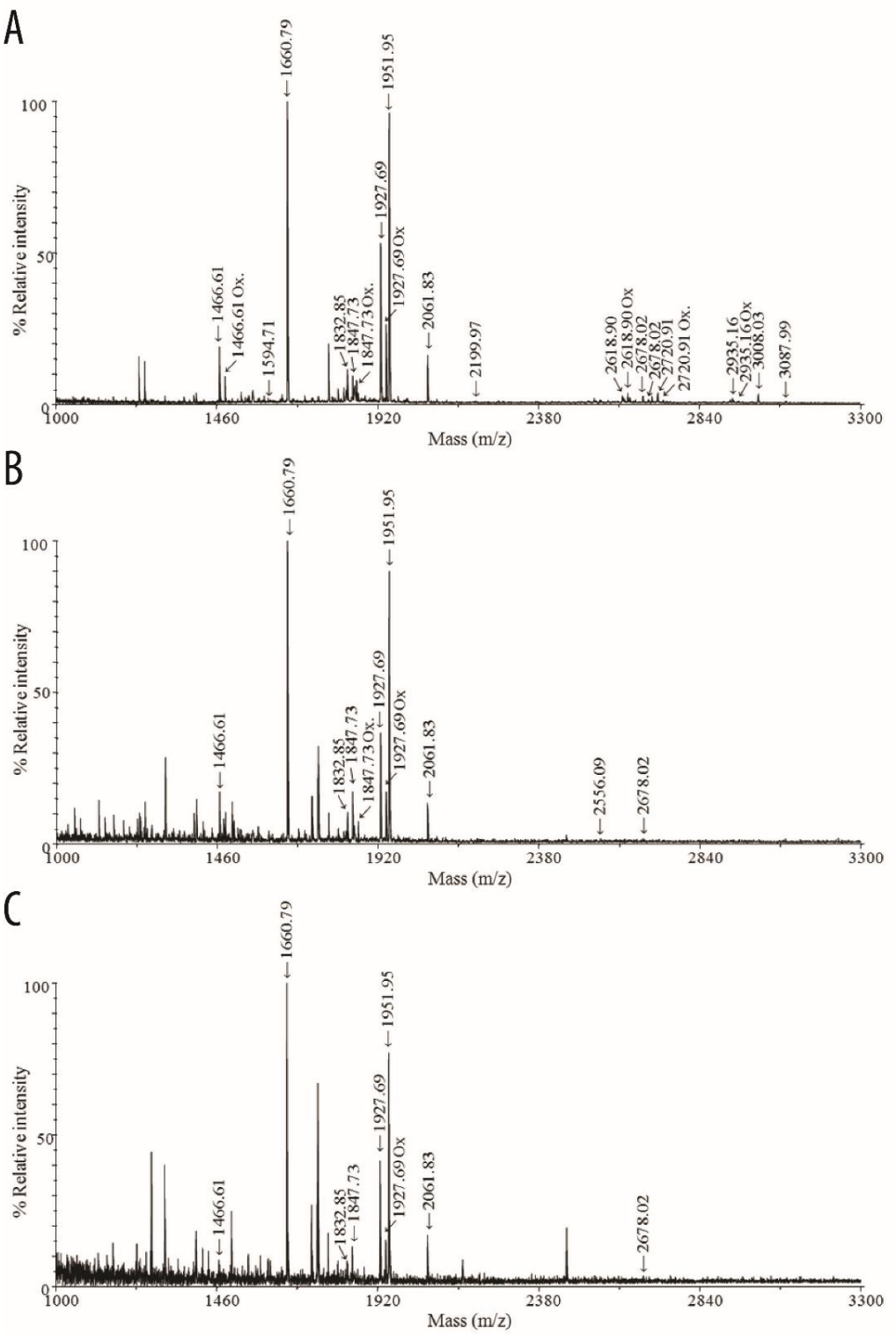

***Figure 6**: Representative MALDI-TOF MS spectra of peptides obtained by the enrichment of phosphopeptides from the peptide mixture A **(A)** and B **(B)** using NuTips® under buffer conditions 4 (using 65% Acn, 2% TFA and 0.1 M glutamic acid as loading buffer). **(C)** Representative MALDI-TOF MS spectra of peptides obtained by the enrichment of phosphopeptides from the peptide mixture B using NuTips® under buffer conditions 3 (using 65% Acn, 2% TFA and 350 mg/ml DHB as loading buffer). Phosphopeptides are marked with arrows*

4.1.3. Evaluation of binding selectivity for phosphorylated peptides under different buffer conditions

The binding selectivity for phosphorylated peptides was evaluated by comparing relative intensities of phosphorylated peptides with those of nonphosphorylated peptides in spectra recorded by MALDI-TOF mass spectrometry. The two most intensive nonphosphorylated peptides in the representative spectra shown in **figure 7** were **1749.66** (ECCHGDLLECADDR) and **2458.18** (DAIPENLPPLTADFAEDKDVCK) from BSA. These two peptides were the most intensive signals originating from nonphosphorylated peptides in most of the experiments; therefore, their presence in the spectra served as an indicator of enrichment selectivity of a particular resin under particular buffer conditions. As shown in the spectra, the intensity of these two unmodified peptides decreased in the following order: **5% TFA < 1 M LA < 0.1 M Glu < 350 mg/ml DHB**, and thus the phosphoenrichment was the most selective when DHB was added into the loading buffer. The spectra presented in **figure 7** were obtained by analysing the enriched fraction from the Titansphere® enrichment; however, the same trend was observed for all chromatographic materials tested. The binding selectivity of NuTips® was comparable to the selectivity of Titansphere® beads. On the other hand, the spectra resulting from TopTips® enrichment of mixture B usually contained high level of nonspecifically bound peptides even under the most efficient buffer conditions tested (**figure 8**).

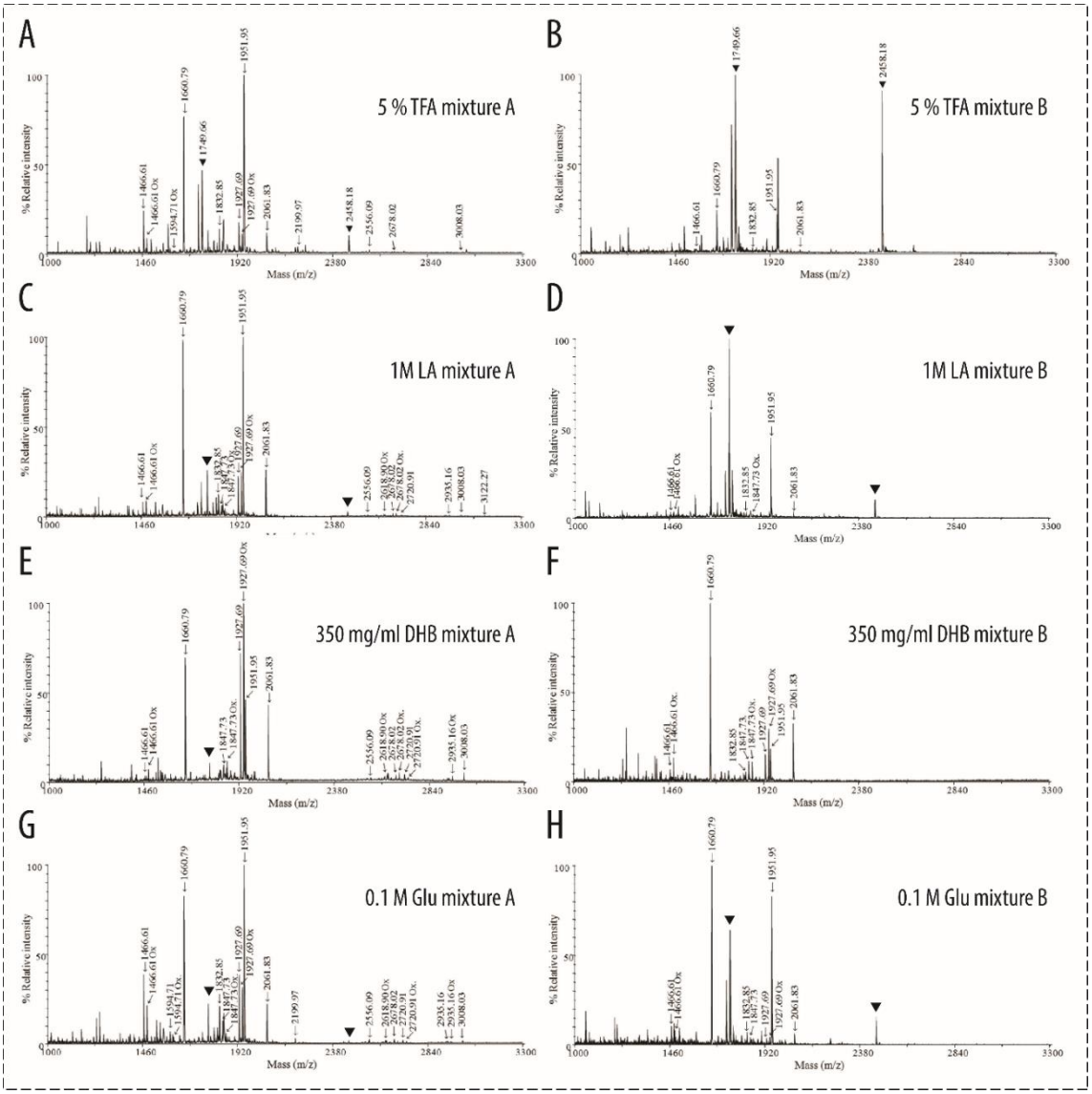

Figure 7: *Representative MALDI-TOF MS spectra of peptides obtained by the enrichment of phosphopeptides from both peptide mixtures using Titansphere® under indicated buffer conditions. Phosphopeptides are marked by arrows. The two most intensive non-phosphorylated peptides in the spectrum- m/z 1749.66 and m/z 2458.18 from BSA are indicated by black triangles.*

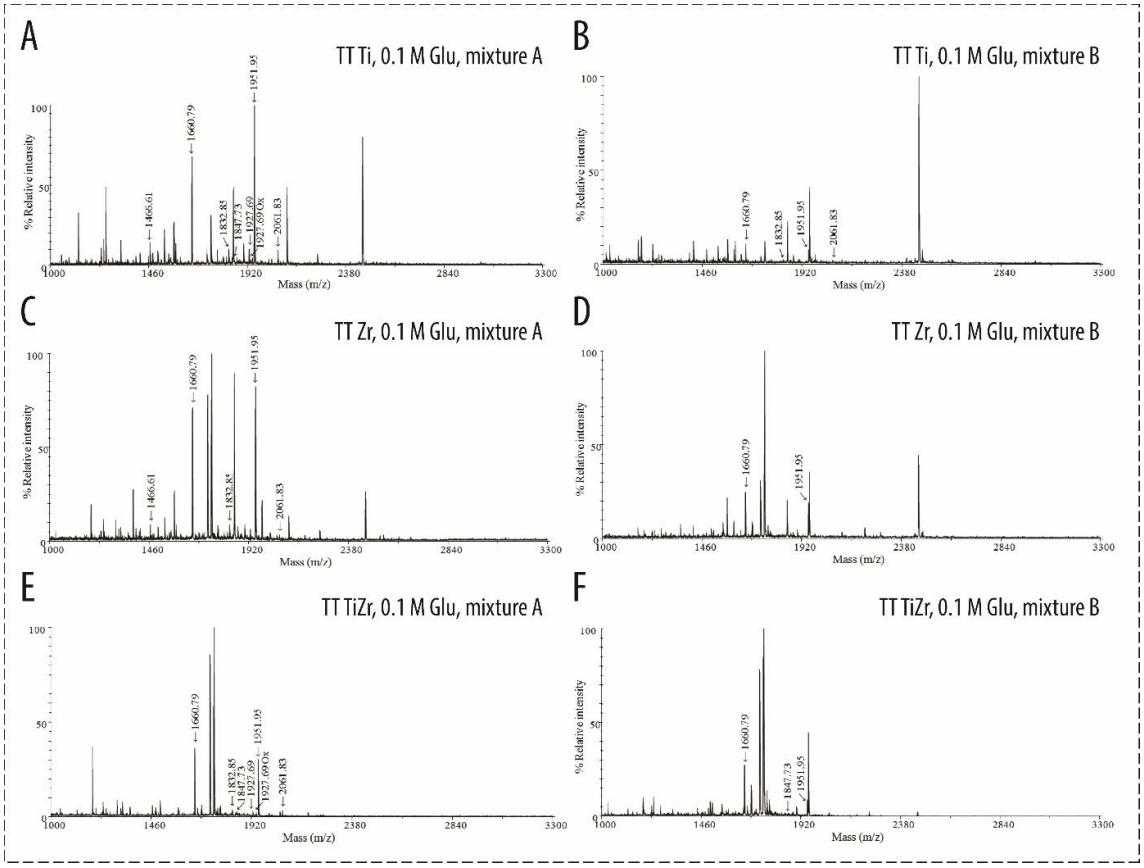

Figure 8: *Representative MALDI-TOF MS spectra of peptides obtained by the enrichment of phosphopeptides from both peptide mixtures using TopTips® under buffer conditions 4. Phosphopeptides are indicated by arrows. TT Ti – TopTips® TiO_2, TT Zr – TopTips® ZrO_2, TT TiZr – TopTips® TiO_2/ZrO_2*

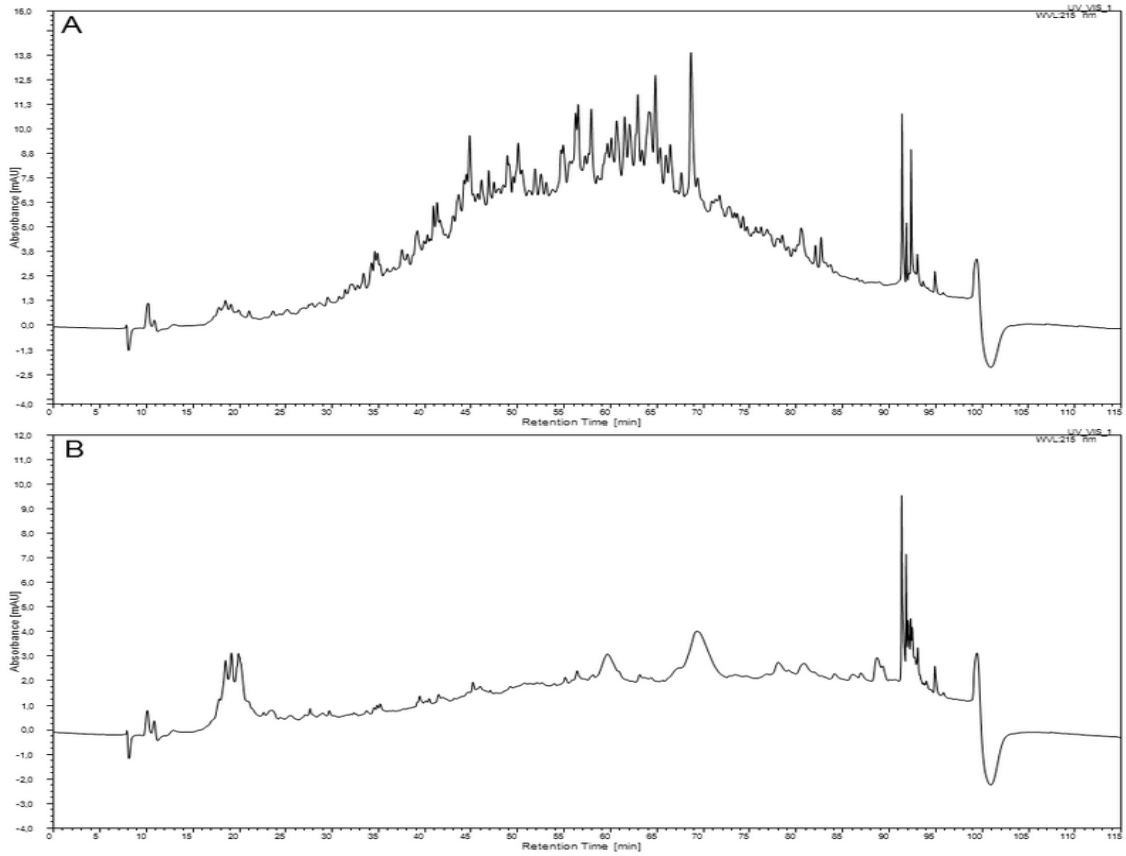

Figure 9: *Comparison of UV-VIS chromatograms obtained after application of Titansphere® (**panel A**) and NuTips® (**panel B**) along with glutamic acid protocol on the "real "- complex samples for enrichment of phosphopeptides from whole-cell lysate of HeLa cells. Peptides were separated by reversed phase chromatography using Dionex Ultimate 3000 (Thermo Scientific). Peptides were loaded in solvent A (2% Acn, 0.1% TFA) followed by 115-min multi-step gradient to 95% solvent B (80% Acn, 0.1% TFA) and detected using Dionex Ultimate 3000 Variable Wavelength detector (Thermo Scientific).*

4.1.4. Application of the two best performing protocols to a real sample analysis

The two best performing protocols were tested in a real complex sample analysis. The samples were prepared by digesting 1 mg of HeLa cells lysate using trypsin and enriched for phosphopeptides using either NuTips® or Titansphere® particles under *buffer conditions 4*.

The amount of material in the enriched fractions was estimated using UV-VIS chromatography (**figure 9**). We repeatedly observed that NuTips® were not an adequate enrichment media for such a high amount of a complex mixture since the amount of material in the eluates was extremely low in comparison to the fractions originating from Titansphere® enrichment. Finally, the eluate from Titansphere® particles was analysed using RPLC-ESI-MS/MS system, which yielded 898 phosphopeptides passing the 0.01 false discovery rate cut-off after processing the raw data with MaxQuant.

4.1.5. Application of the selected protocol to study phosphorylation response of irradiated MOLT-4 cells

A pilot quantitative (SILAC) phosphoproteomic study was performed to evaluate the performance of the chosen protocol (i.e. Titansphere® beads under *buffer conditions 4*) in the system of interest (i.e. irradiated MOLT-4 cells). The LC-MS/MS analysis of the enriched sample led to identification of 632 phosphorylation sites from 489 peptides originating from 335 phosphoproteins. 429 class I sites (localization probability > 0.75) were successfully quantified. Among them, 31 sites were upregulated and 32 were downregulated one hour after the irradiation by a dose of 1.5 Gy (1.5-fold change). More detailed overview and interpretation of the obtained data will be given in discussion section.

4.2. Radiosensitization of MOLT-4 cells by selective ATR and ATM inhibitors VE-821 and KU55933

4.2.1. Proliferation/ Viability assays

Two different proliferation assays were employed to assess the effect of specific inhibition of **ATM** and **ATR on** proliferation of MOLT-4 cells: WST-1 assay and viable cell counting using Trypan Blue exclusion technique.

4.2.1.1. Single-inhibitor treatment

A potent and specific inhibitor of ATM by KU55933 was well tolerated in concentrations up to 10 μM even when the inhibitor was present in the cell culture media for 7 days (**figure 10A-G**). Unexpectedly, 5 μM KU55933 significantly increased viability of MOLT-4 cells in both assays. On the other hand, inhibitor of ATR, VE-821, repeatedly inhibited the growth and viability of MOLT-4 cells in a dose dependent manner already at lower concentrations than KU55933 (**figure 10D-G**); a significant growth inhibition was achieved by application of 1 μM VE-821 when detected after six days of treatment using WST proliferation assay.

4.2.1.2. Inhibitor combinations and combinations with ionizing radiation

In WST-1 assays, the irradiation of MOLT-4 cells by a dose of 1 Gy led to growth inhibition which resulted in markedly decreased number of viable (metabolically active) cells 72 and 144 hours after irradiation (**figure 11A-C**). The addition of VE-821 in both 1 μM and 2 μM concentrations further significantly enhanced the antiproliferative effect of IR – the number of viable cells was below the limit of detection of the assay in the case of VE-821 2 μM and IR combination. Consistently with the single-inhibitor proliferation assays, lower concentrations of KU55933 (up to 5 μM) showed a positive effect on cellular proliferation, and moreover, they increased the number of viable cells in combination with irradiation. Notably, when applied in combination, KU55933 also diminished the antiproliferative effects of VE-821 72 hours after IR (**figure 11A**).

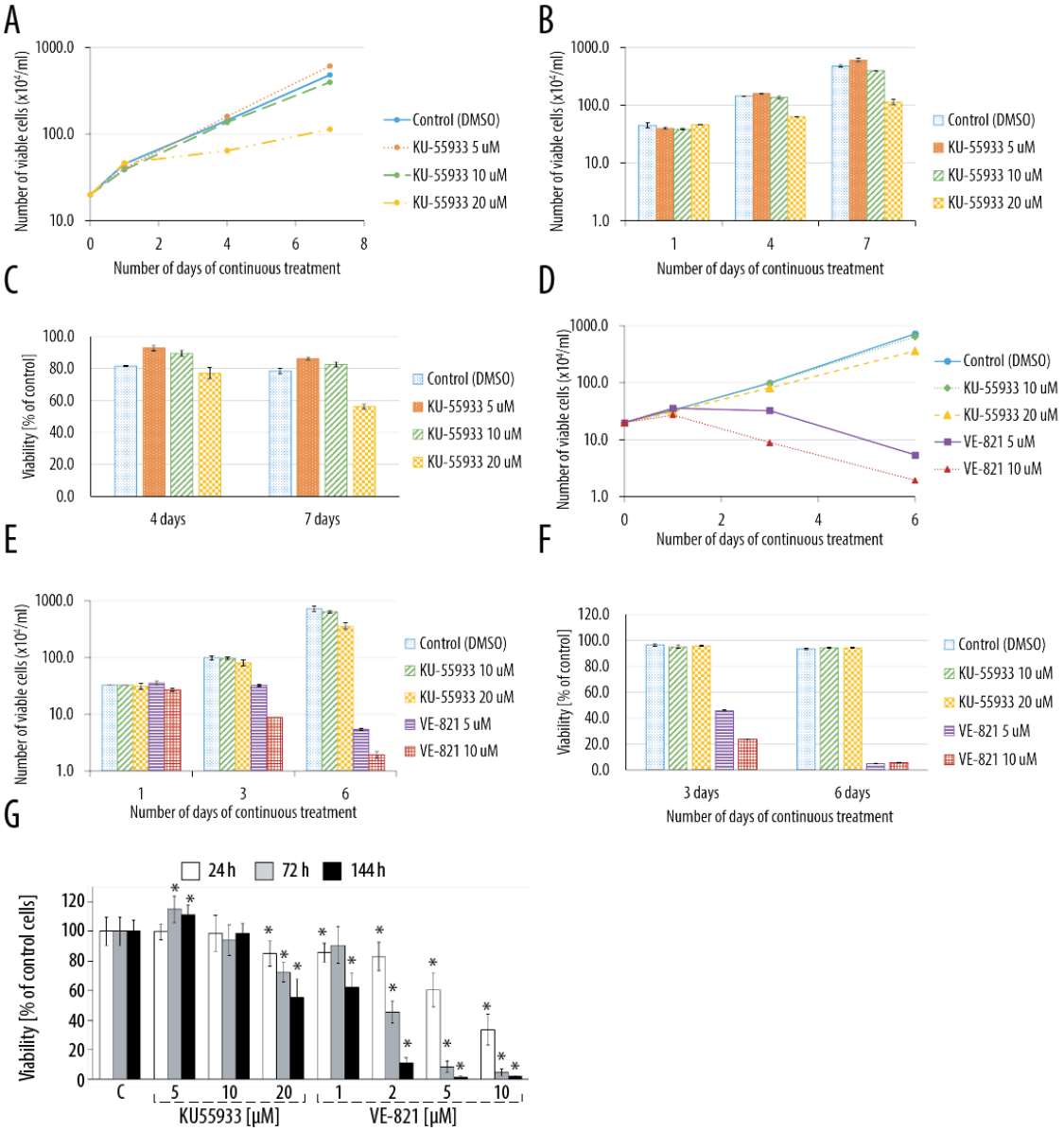

Figure 10: Characterization of VE-821 and KU55933 treatment effects on proliferation of MOLT-4 cells. *(**A, B, C**) Effects of different KU55933 concentrations. Number of viable cells and viability (defined as number of viable cells/total number of cells) were assessed by a haemocytometer using trypan blue exclusion technique 1, 4, and 7 days after the addition of the inhibitor with subsequent dilution to a concentration of $2x10^5$ cells/ml. Mean values ± SD from three measurements are presented. (**D, E, F**) Effects of different KU55933 and VE-821 concentrations. Number of viable cells and viability (defined as number of viable cells/total number of cells) were assessed by a haemocytometer using trypan blue exclusion technique 1, 3, and 6 days after the addition of the inhibitor with subsequent dilution to a concentration of $2x10^5$ cells/ml. Mean values ± SD from three measurements are presented. (**G**) Effect of different KU55933 and VE-821 concentrations. Viability was examined by WST-1 assay after 24, 72, and 144 hours of continuous inhibitor treatment. Data are expressed as percentage of viability of controls for each time interval. Mean values ± SD from at least five measurements are presented. *$p \leq 0.01$ vs. corresponding controls.*

Additionally, in a cell counting-based proliferation assay, VE-821 significantly sensitized cells to IR in 2 μM and 10 μM concentrations even when the inhibitor was present in cell culture media only transiently, for the first 24 hours of the treatment (**figure 11D**). In contrast to continuous treatment, VE-821 2 μM did not significantly affect the proliferation of sham-irradiated cells when washed out after 24 hours; however, it still increased the sensitivity of cells to ionizing radiation (1.5 Gy).

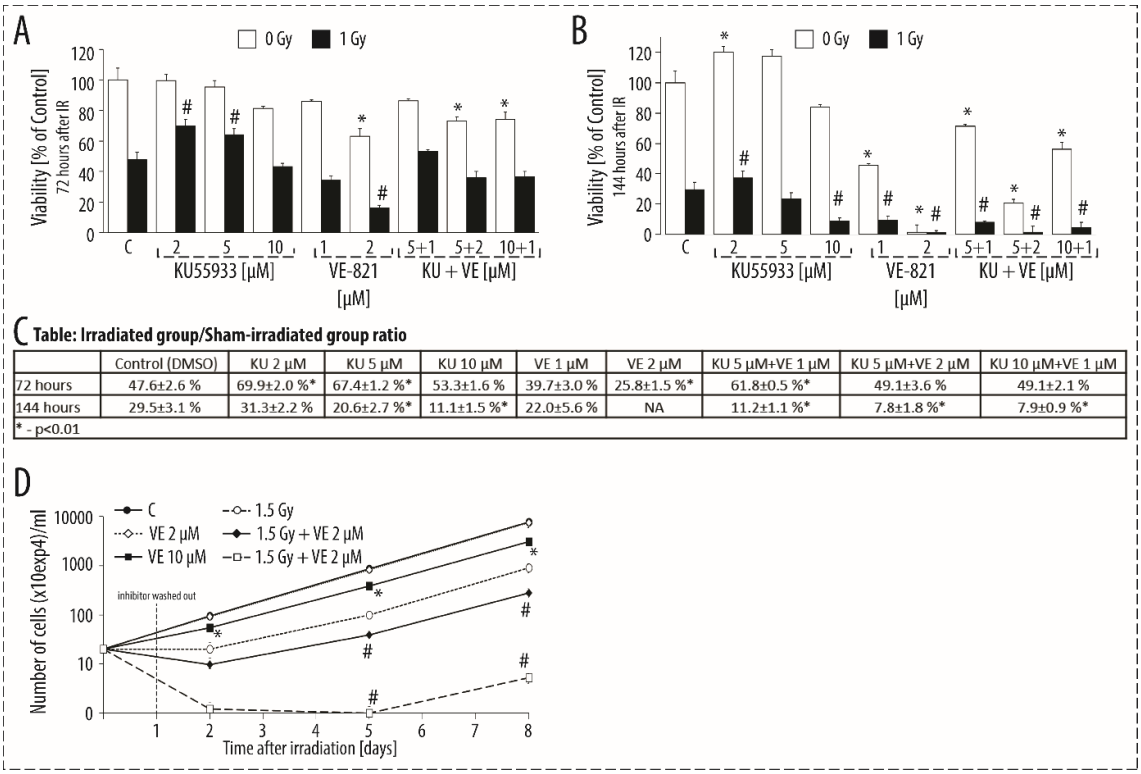

	Control (DMSO)	KU 2 μM	KU 5 μM	KU 10 μM	VE 1 μM	VE 2 μM	KU 5 μM+VE 1 μM	KU 5 μM+VE 2 μM	KU 10 μM+VE 1 μM
72 hours	47.6±2.6 %	69.9±2.0 %*	67.4±1.2 %*	53.3±1.6 %	39.7±3.0 %	25.8±1.5 %*	61.8±0.5 %*	49.1±3.6 %	49.1±2.1 %
144 hours	29.5±3.1 %	31.3±2.2 %	20.6±2.7 %*	11.1±1.5 %*	22.0±5.6 %	NA	11.2±1.1 %*	7.8±1.8 %*	7.9±0.9 %*
* - p<0.01									

Figure 11: Radio-sensitization of MOLT-4 cells using ATM and ATR inhibitors. *Cells were irradiated by the indicated dose. Viability (proportional to number of metabolically active cells) was examined by WST-1 assay after 72 hours* ***(A)*** *and 144 hours* ***(B)*** *of continuous inhibitor treatment.* ***(C)*** *Table shows an irradiated group/sham-irradiated group ratio for each treatment condition depicted in figures C and D.* ***(D)*** *VE-821/DMSO were washed out 24 hours after irradiation and the number of viable cells was assessed by a haemocytometer 2, 5, and 8 days after irradiation with subsequent dilution to a concentration of $2x10^5$ cells/ml. Mean values ± SD from five measurements are presented. In* ***(A-D)****,* ******* *indicates statistical significance ($p < 0.01$) of comparison to non-irradiated control;* ***#*** *indicates statistical significance ($p < 0.01$) of comparison to irradiated control group. P-values were calculated using two-sided t-test. In all experiments, the cells were pre-treated with inhibitors at indicated concentrations or DMSO in control groups (C) 30 minutes prior to IR.*

4.2.2. **Immunoblotting-based detection of ATM and ATR activation and inhibition**

To detect activation of both ATM and ATR kinases upon irradiation and their specific inhibition by VE-821 and KU55933 pre-treatment, Chk1 Ser 345 and Chk2 Thr 68 phosphorylation was assessed using immunoblotting one hour after 3 Gy of IR (**figure 12**). **Chk2 Thr 68** phosphorylation (marker of activated ATM) was not detected in sham-irradiated cells; however, it was strongly induced by irradiation. The treatment with KU55933 markedly decreased Chk2 phosphorylation in irradiated cells. **Chk1 Ser 345** phosphorylation (marker of activated ATR) was also detected in sham-irradiated cells, and upon irradiation, it was slightly upregulated. VE-821 abrogated this phosphorylation in a concentration dependent manner. Neither of both inhibitors influenced the expression level of Chk1 or Chk2 under given treatment conditions.

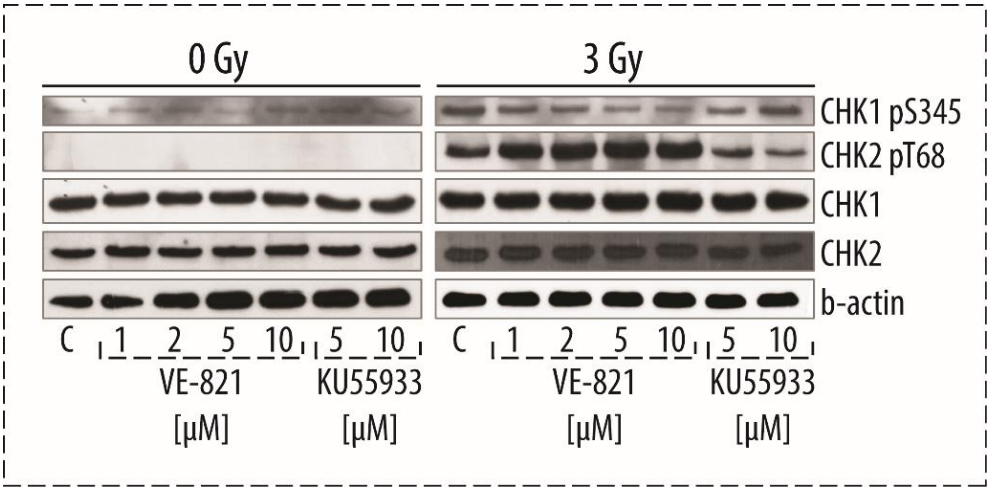

Figure 12: Effect of KU55933 and VE-821 on activation of ATM and ATR kinases by gamma-irradiation. *Cells were collected 1 hour after IR (3 Gy). Activation of both kinases and its suppression in the presence of inhibitors was monitored via the detection of their specific phosphorylations targets (Chk2 pT68 and Chk1 pS345, ATM and ATR respectively). The expression state of Chk1 and Chk2 was also evaluated. The representative blots from three independent experiments are shown. β-actin expression was analysed as a loading control.*

4.2.3. **DNA content analysis**

To investigate cell cycle effects of ATM and ATR inhibition, DNA content analysis was performed using propidium iodide (PI) staining and flow cytometric detection of PI fluorescence. The potential perturbation of the cell cycle by either one of the compounds or their combinations was examined 24 hours after irradiation (3 Gy).

As depicted in **Figure 13A** and **13B**, in sham-irradiated cells, none of the conditions induced significant cell cycle perturbation except for VE-821 10 μM, which caused a significant increase in number of G1 cells ($p < 0.01$). The irradiation by a dose of 3 Gy led to a significant G2/M arrest in MOLT-4 cells. The pre-incubation with VE-821 in both concentrations and its combinations with KU55933 disrupted the IR induced G2/M checkpoint. On the other hand, KU55933 further increased the accumulation of cells in G2/M.

4.2.4. **Apoptosis assay**

To assess the impact of different inhibitor concentrations on viability of MOLT-4 cells and IR induced cell death we applied flow-cytometric detection of nonviable cells using the Apoptest-FITC kit. The proportions of cells stained either by Annexin V (early apoptosis) or Annexin V and PI (late apoptosis and necrosis) were measured 24 and 72 hours after irradiation by a dose of 1 Gy. The cells were released into inhibitor-free media after 24 hours of treatment.

As shown in figure **13C** and **13E**, 10 μM VE-821 significantly affected viability of MOLT-4 cells 24 hours after the addition of the treatment and/or irradiation. The effect induced by 10 μM VE-821 was comparable to 1 Gy of IR; almost 40 % of PI positive cells were detected under both treatment conditions. When combined with IR, VE-821 in both concentrations significantly increased the IR-induced cell death. Viability was not significantly affected in any of the KU55933- and combination- treated groups.

72 hours after irradiation, further accumulation of nonviable cells was detected in VE-821 treated groups (2 and 10 μM, combination with 10 μM KU55933; **figure 13D**). Both inhibitors and their combinations increased IR-induced cell death. The most detrimental effect was observed when cells were treated by VE-821 10 μM and by the combination of both inhibitors (10 μM +10 μM). Application of these conditions led to more than 90% decrease in viability of MOLT-4 cells after 72 hours.

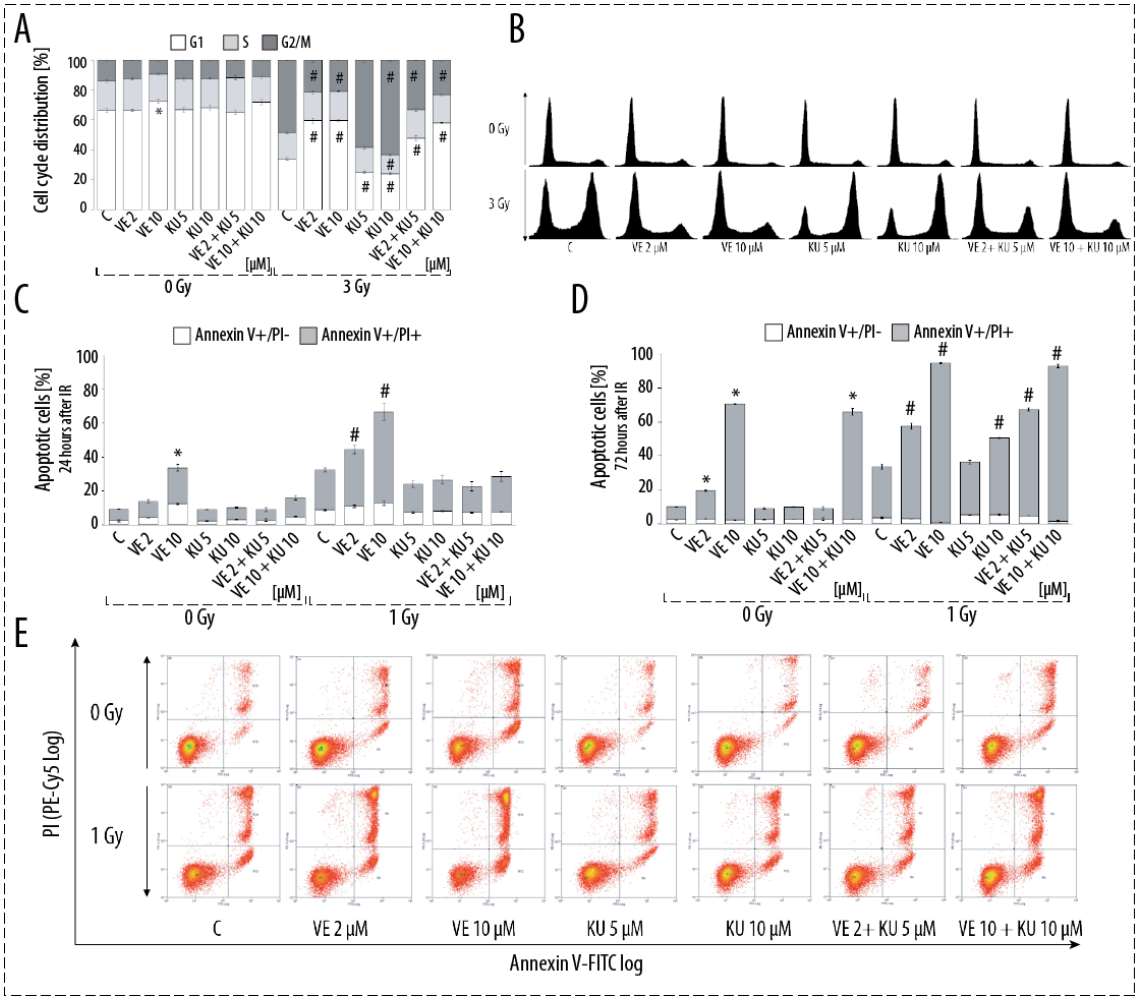

Figure 13: Flow cytometric analysis of MOLT-4 cells radiosensitization using VE-821 and KU55933*: (**A, B**) Cell cycle effects of ATM and ATR inhibition in irradiated MOLT-4 cells: Cell cycle perturbation was examined using propidium iodide staining of DNA detected by flow cytometry 24 hours after IR (3 Gy). (**A**) Data are expressed as relative proportion of viable cells in different phases of cell cycle. Mean values ± SD from three measurements are presented. (**B**) Representative histograms for each one of the conditions are shown. (**C, D, E**) Apoptosis induction in ATM and ATR inhibitors treated irradiated MOLT-4 cells: Cell death was detected by Annexin V/PI staining 24 (**C**) and 72 hours (**D**) after IR (1 Gy). Mean values ± SD from three measurements are presented. (E) Representative dot plots for each one of the conditions from the first measurement (24 hours after IR) are shown. Approximately 20 000 cells were analysed in each sample. In (**A, C, D**), * indicates statistical significance ($p < 0.01$) of comparison to non-irradiated control; # indicates statistical significance ($p < 0.01$) of comparison to irradiated control group. P-values were calculated using two-sided t-test. In all experiments, cells were pre-treated with inhibitors at indicated concentrations or DMSO in control groups (C) 30 minutes prior to IR.*

4.3. "Dual-omic" analysis of VE-821 treated MOLT-4 cells

To describe cellular mechanisms underlying the VE-821-mediated radiosensitization of MOLT-4 cells, we employed high-resolution MS to identify and quantify changes in **proteome, phosphoproteome**, and **metabolome** of irradiated VE-821-treated cells (**figure 14**). The metabolomic analysis was done in collaboration with Hana Janečková and David Friedecký from the Laboratory for Inherited Metabolic Disorders at the University Hospital Olomouc, who performed HPLC-MS/MS analysis of our samples and subsequent data processing including data normalization, statistical analysis, and KEGG pathways analysis.

4.3.1. Proteomic and phosphoproteomic analysis of VE-821 treated MOLT-4 cells

The quantification on both proteome and phosphoproteome levels was based on stable isotope labelling in cell culture ((270)). To specifically enrich for peptides modified by phosphorylation, desalted tryptic peptide samples were fractionated using hydrophilic interaction liquid chromatography followed by phosphopeptide enrichment using titanium dioxide chromatography (222), RPLC-MS/MS detection, and peptide identification and quantification using MaxQuant *v.1.5.2.8* (316) (**figure 14B**; **figure 14E** provides details on HILIC separation of phosphorylated peptides and enrichment efficacy over the fractions).

In summary, on a site false discovery rate level of 0.01, we identified 9285 phosphorylation sites from 3090 protein groups, among them 4504 were quantified in all three biological replicates (nearly 63 % of the data set). The phosphosite ratios correlated very strongly between the replicates (Pearson correlation coefficient was between 0.8 and 0.9, **figure 15C**). Only those sites quantified in all replicates were subjected to a non-parametric version of a global rank test ((318)) to identify sites with significantly up- or down- regulated phosphorylation consistently regulated in all three biological replicates. In GRT, we identified 623 regulated phosphorylation sites (455 phosphoproteins); most of them were upregulated (431).

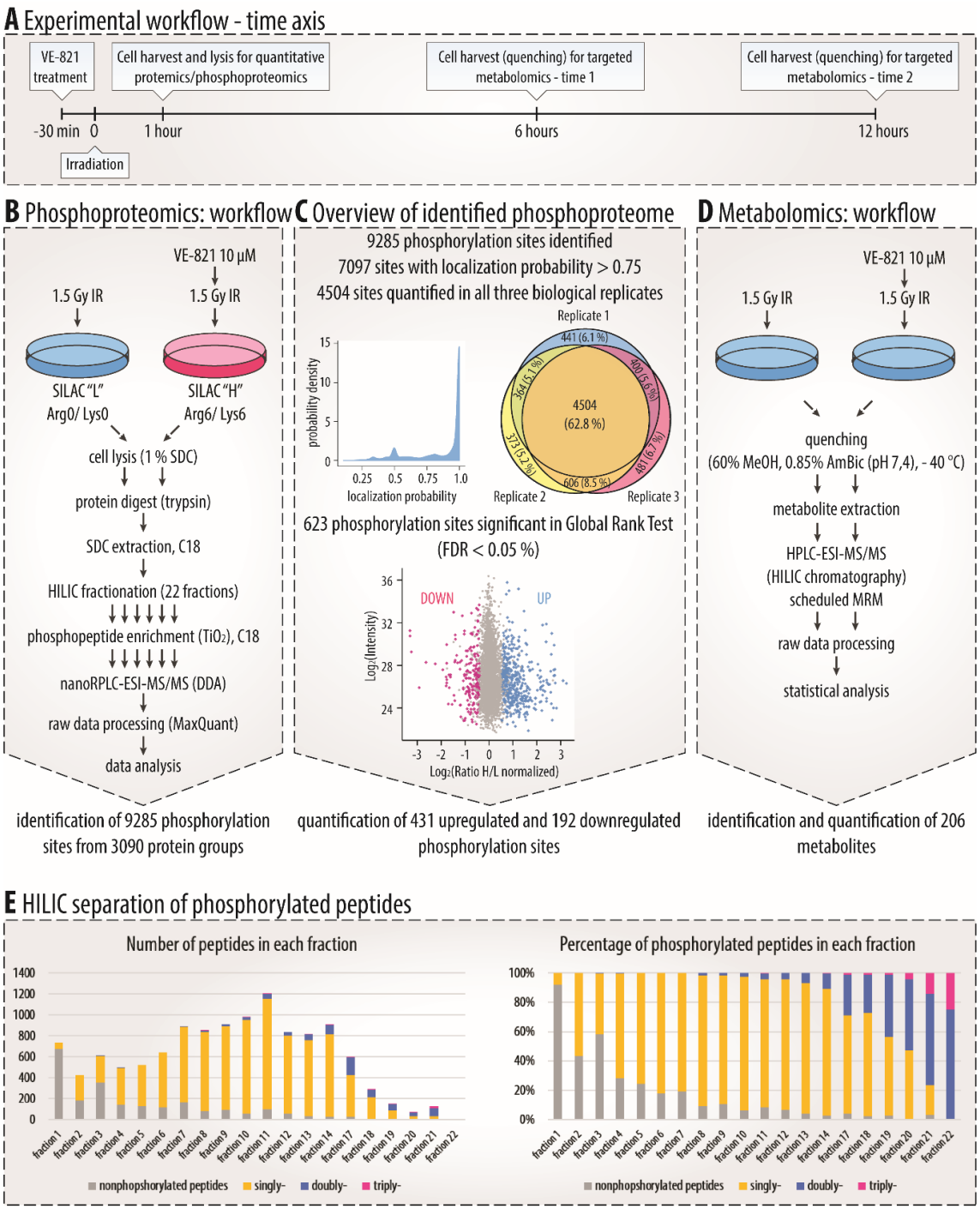

Figure 14: Identification and quantification of the VE-821-regulated phosphoproteome and metabolome in irradiated MOLT-4 cells using tandem mass spectrometry*: (**A**) Overview of time intervals used for both phosphoproteomic and metabolomic analyses of VE-821 perturbed cellular response to ionizing radiation (IR). (**B**) Overview of experimental design and workflow used for quantitative SILAC-based phosphoproteomics. (**C**) Summary of the identified and quantified phosphoproteome. (**D**) Overview of experimental design and workflow used for targeted metabolomics screening. (**E**) Distribution of phosphorylated peptides over the HILIC gradient. Numbers and percentage of non-, singly-, doubly-, and triply- phosphorylated peptides in each phosphoenriched HILIC fraction.*

The analysis of the whole proteome samples prepared using the same treatment and time interval resulted in quantification of the unmodified fraction of the proteome (phosphorylated peptides were not considered for proteome quantification). The analysis confirmed our expectations that there would be no significant changes of proteome one hour after irradiation combined with VE-821 treatment. As depicted in **figure 15A**, the distribution of normalized log_2 SILAC H/L ratios corresponding to quantification of unmodified proteins was very narrow, with most values distributed close to zero. Moreover, Pearson correlation between the replicates was weak (R 0.24 – 0.387; **figure 15B**), which is more likely caused by non-existing trends in an unperturbed system rather than by an irreproducibility of the analysis.

Pearson correlation between normalized log_2 SILAC H/L ratios of phosphopeptides and log_2 normalized SILAC H/L ratios of corresponding proteins was also calculated (the calculation was based on 2738 phosphorylation sites which represent almost 30 % of the data set), and the low correlation coefficient value (*R* was -0.013) further confirmed that the observed changes on the phosphoproteome level were not dependent on changes of the abundance of corresponding proteins (**figure 15A**).

The nature of further data analyses implementing multiple bioinformatic tools and databases search implies their presentation in the section Discussion.

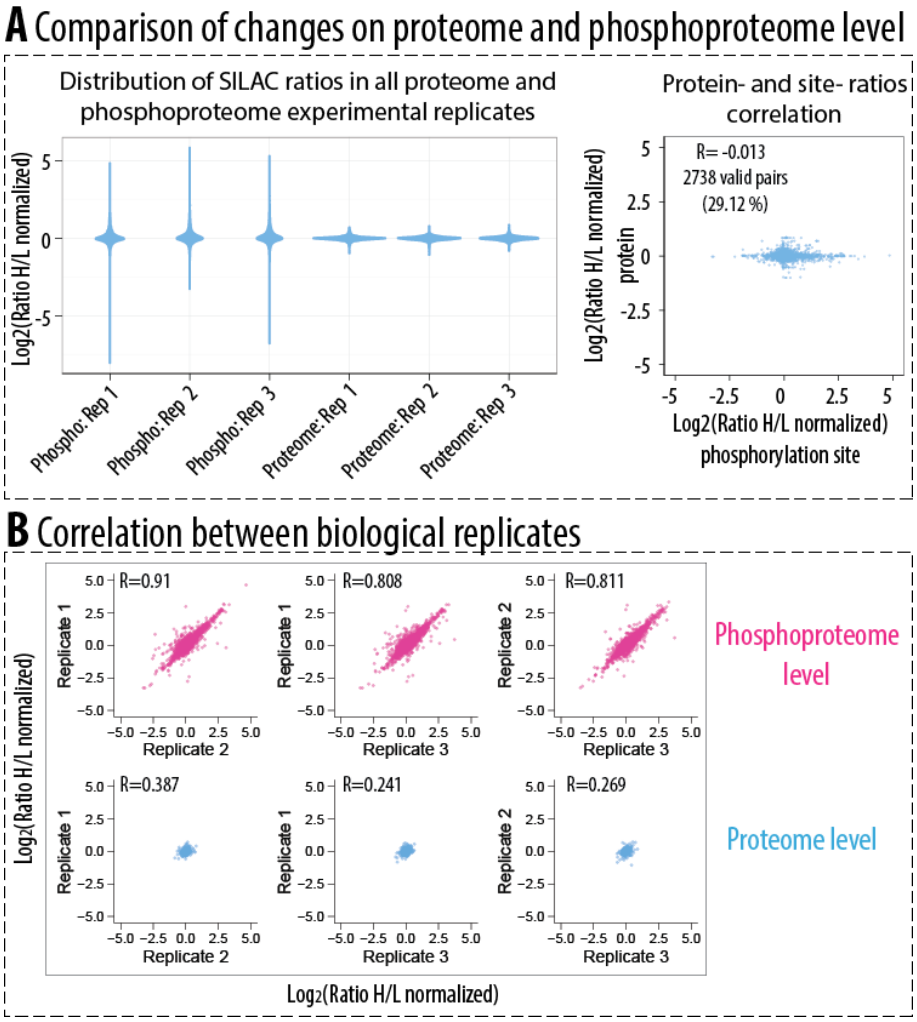

Figure 15: Comparison and correlation of changes on proteome and phosphoproteome level, and their quantitative reproducibility. *(**A**) Violin plots depict log_2 transformed SILAC H/L ratios distribution in all proteome and phosphoproteome biological replicates. (**B**) Pearson correlation between phosphosite and protein ratios. H/L ratios of 2738 phosphorylation sites (29 % percent of the identified phosphorylation sites) were plotted against H/L ratios of corresponding proteins and the Pearson correlation value (R) was calculated. (**C**) Pearson correlation (R) between biological replicates of both proteome and phosphoproteome experiment.*

4.3.2. Targeted metabolomic analysis of VE-821 treated MOLT-4 cells

Metabolite profiling was performed by a label-free targeted analysis of cellular extracts collected 6 and 12 hours after the treatment starting point (**figure 14A**). A method combining high-performance liquid chromatography using aminopropyl stationary phase and detection of the metabolites by Triple Quad 6500 tandem mass spectrometer enabled a quantitative analysis of 206 intermediary metabolites (**figure 14D**).

Hierarchical clustering (**figure 17A**) and multivariate analyses such as principal component analysis (PCA; **figure 16A**), PLS discriminant analysis (PLS-DA; **figure 16B**), and orthogonal PLS discriminant analysis (OPLS-DA; **figure 16C**) revealed that both treatment groups were clearly separated from each other based on the measured quantitative values for the metabolites. Based on sample localization in PCA and PLS-DA score plot (**figure 16A and 16B**), it is obvious that the inhibitor had a more significant impact on the group clustering than the incubation time. An overlap of QC samples in the PCA score plot showed the repeatability of the measurements (**figure 16A**).

Further clustering analysis of ANOVA significant metabolites (126 metabolites on 5% permutation-based FDR level) revealed three main clusters showing distinct behaviour across the four conditions measured (**figure 17**):

- **Upregulated** in VE-821 treated groups and showing an **increasing trend** between the time intervals in both groups (**figure 17B; cluster 1**): this group comprised metabolites that were **accumulated** over time in both groups; the **inhibitor potentiated the effect of IR**. **Lactate** is an example of a metabolite belonging to this cluster (**figure 17C**).
- **Upregulated** in VE-821 treated groups with **no significant trend** between the two time intervals (**figure 17B; cluster 2**): this group comprised metabolites, which were **altered** by VE-821 in irradiated MOLT-4 cells. **Glucose (and other hexoses)** is an example of a metabolite belonging to this cluster (**figure 17C**).
- **Downregulated** in VE-821 treated groups and showing a **decreasing trend** between the time intervals in both groups (**figure 17B; cluster 5**): this group comprises metabolites that were **depleted** over time in both groups; the **inhibitor potentiated the effect of IR**. **ATP** is an example of a compound belonging to this cluster (**figure 17C**).

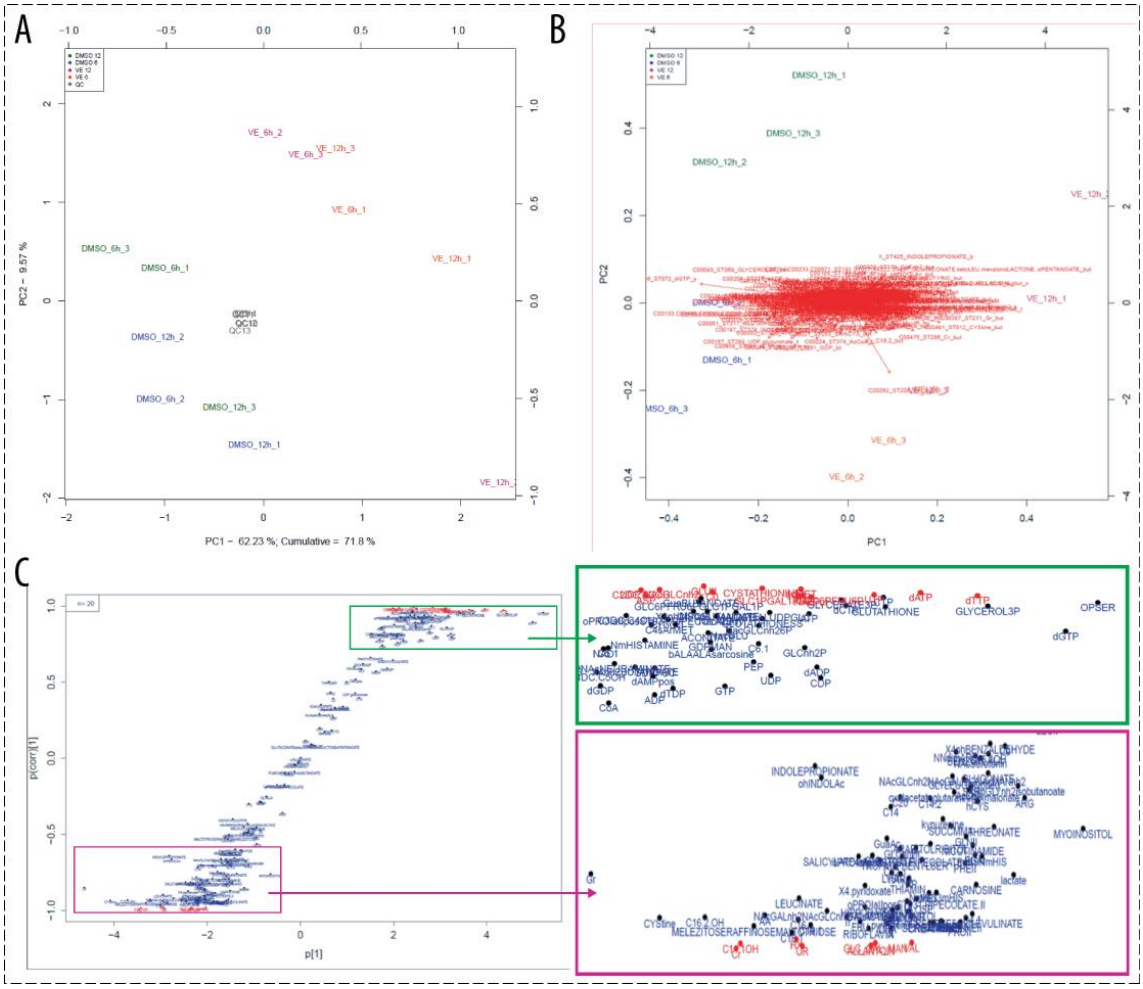

Figure 16: Targeted metabolomic analysis of VE-821 induced metabolome changes in irradiated MOLT-4 cells. *Statistical analysis of the results was performed using multivariate analyses such as PCA (A), PLS-DA (B), and OPLS-DA (C). DMSO – irradiated groups pre-treated with DMSO, VE – irradiated groups pre-treated with 10 μM VE-821*

Thus, there were two classes of changes observed in metabolome of irradiated cells after VE-821 treatment. First, changes that were observed in both treatment groups and showed the same, either decreasing or increasing, trend over time. In such cases, we assumed that the inhibitor caused potentiation of metabolism-altering effects of IR. Second, changes that showed no trend over time in irradiated control group. We interpreted these as alterations in metabolome of irradiated cells caused by VE-821.

The main significant changes in the metabolome of MOLT-4 cell line occurred in group of metabolites involved in **cellular antioxidant system**; intermediates of **glucose metabolism and citrate cycle**; **nucleosides, nucleotides, and deoxynucleotides**; **free amino acids**, **N-acetylated amino acids**, and **acylcarnitines**. The results will be further described and interpreted in the Discussion section in the context of other results obtained in this work.

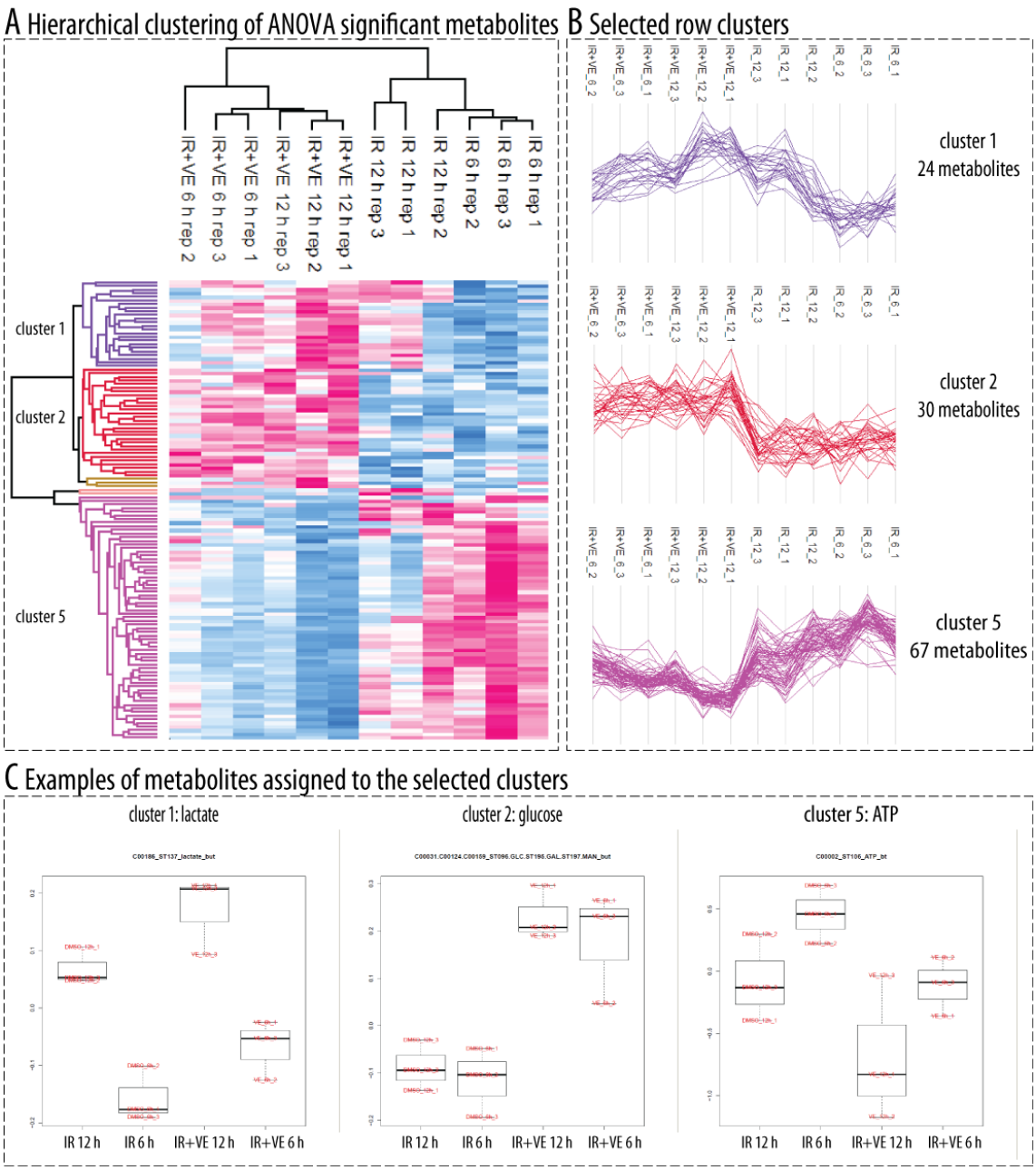

Figure 17: Hierarchical clustering of significantly changed metabolites: *ANOVA significant metabolites were clustered* ***(A)****, and three main row clusters of metabolites were identified* ***(B)****. Examples of metabolites for each cluster are given; distribution of quantitative values for a metabolite in each experiment is depicted using boxplots* ***(C)****.*

5. Discussion

5.1. Selection of the protocol for phosphopeptide enrichment from a standard and a complex biological sample

Since the discovery of the affinity of metal oxides for phosphorylated peptides (227), there have been many protocols for a selective phosphopeptide enrichment developed. Moreover, there are also many commercial products available that declare high selectivity towards phosphorylated peptides and applicability for the enrichment of phosphopeptides from complex biological matrices. However, these products are often not comparable and might differ in several parameters such as the metal oxide used, the amount of chromatographic material (in the case of pre-packed microcolumns), and the size and porosity of the chromatographic beads. All of these parameters can affect phosphopeptide binding capacity and selectivity.

To choose the most suitable protocol and chromatographic resin from the plethora of protocols and products commercially available, we first performed a series of optimization experiments. For these initial experiments, we used two mixtures of tryptic peptides originating from two phosphorylated (α-casein and asialofetuin) and nonphosphorylated proteins (BSA and myoglobin) in two different molar ratios (1:1:5:5 and 1:1:50:50), which simulated the relatively low abundance of phosphorylated proteins in a biological sample. To detect the peptides resulting from the enrichment step, we used MALDI-TOF MS analysis using an ABI 4800 mass spectrometer as it was the only mass spectrometer available in our lab in 2011 and 2012 when these initial optimization experiments were performed. To test the applicability of the chosen methods to enrich phosphopeptides from a complex mixture, we further performed a real complex sample enrichment (HeLa cells lysate) and detected the resulting peptides using an LC-MS/MS system. The final selected protocol was then used in a pilot quantitative SILAC-based phosphoproteomic study of irradiated MOLT-4 cells.

From the previously published protocols, we selected four different buffer conditions (detailed composition of the buffers can be found in the Methods part), which

mainly differed in the composition of the loading solution (or loading "buffer") including different acidic additives previously reported to enhance the phosphopeptide selectivity of the metal oxides. The first protocol involved only 5 % TFA to establish a low pH during the loading step, since in the initial MOAC studies it was shown that strongly acidic conditions were beneficial for the specificity of phosphopeptide enrichment (222). Three further protocols were based on addition of one of the previously reported efficient "nonphosphopeptide excluders" – 1 M lactic acid (223), 350 mg/ml DHB (222), or 0.1 M glutamic acid (186).

In the next step, we applied these buffer conditions in order to test 5 different commercially available chromatographic resins: **Titansphere®** 5 μm particles (GL Sciences, Torrance, CA, USA), which we used to enrich for phosphopeptides in a "microtube format"; **TopTips®** (TiO_2, TiO_2/ZrO_2 1:1, and ZrO_2; Glygen, Columbia, MD, USA), which are pre-filled micro-spin columns that can be used for phospho-enrichment in a "column format" using either centrifugal force or air pressure to ensure the flow of the loading and washing solvents through the beads; and **NuTips®** (TiO_2/ZrO_2 1:1) (Glygen, Columbia, MD, USA), which are pre-filled "pipette-tips" that can be used for phospho-enrichment via repetitive pipetting of a peptide solution through the bottom part of the tip containing embedded chromatographic resin. The undeniable advantage of using the Titansphere® beads in the microtube format or alternatively, in the form of in-house columns (which we also tested, but the data are not presented in this thesis), is the fact that their amount can be optimized for a specific application while the pre-packed tips are only available in two or three different sizes. The effect of a peptide-to-TiO_2 ratio has been investigated in several studies as an important parameter affecting the specifity of the enrichment (244,245). Based on our data (not shown) we decided to use a ratio of 1:8 for our optimization experiments.

5.1.1. Titansphere® particles and NuTips® provided markedly more efficient phosphopeptide enrichment than the TopTips®.

The evaluation of enrichment efficiency revealed that in our experiments, Titansphere® particles and NuTips® clearly outperformed the TopTips® in terms of the total and average numbers of phosphopeptides detectable by MALDI-TOF MS in the eluted fractions. The most apparent difference was observed when phosphopeptides

from mixture A were enriched; application of the best protocol for each of the chromatographic resins led to detection of 17 phosphopeptides by NuTips®, 15 phosphopeptides by Titansphere®, but only 9 phosphopeptides by TopTips®. In mixture B enrichment, NuTips® provided a total number of 10 phosphopeptides, Titansphere® led to the detection of 8 phosphopeptides, and TopTips® provided 7 phosphopeptides in total (**figure 4**).

Further analysis of the nature of peptides detected by different protocols showed that the main differences in numbers of phosphorylated sites detected between the two well performing products and TopTips® were caused by lower detectability of multiply-phosphorylated peptides while the enrichment efficiency for monophosphorylated peptides was comparable across the resins and buffer conditions (**figure 5**). Doubly- phosphorylated peptide 1927.69 $[M+H]^+$ from α-S1-casein was observed in most of the enrichments; however, multiply phosphorylated peptides were more challenging to detect. These peptides were typically observed as low intensity peptide ions in the higher m/z range of the MALDI-TOF MS spectra, and were only detected in the low complex mixture A using the most specific enrichment protocols.

TopTips® enrichment usually yielded a high number of nonspecifically bound non-phosphorylated peptides even under the most efficient buffer conditions tested, which might explain the low detectability of multiply phosphorylated peptides in the spectra as their ionization/signals were suppressed by the high amount of the nonphosphorylated peptides (**figure 8**).

5.1.2. 2,5-dihydroxybenzoic acid was the most potent non-phosphopeptide excluding additive.

As for one of the goals of this initial optimization study, we aimed to compare how binding specificity was modulated by buffer composition. The binding specifity was monitored by relative intensity of the most intensive non-phosphorylated peptides originating from BSA, **1749.66** $[M+H]^+$ (ECCHGDLLECADDR) and **2458.18** $[M+H]^+$ (DAIPENLPPLTADFAEDKDVCK), in recorded MALDI-TOF MS spectra. Both nonspecifically enriched peptides contained a relatively high number of acidic amino acids (as underscored in the sequences), which is in concordance with previously reported fact that especially nonphosphorylated peptides containing greater proportions of aspartic and glutamic acid bind nonspecifically to phosphopeptide enrichment resins (221).

In the first protocol used for phosphopeptide enrichment, *i.e.* ***buffer conditions 1***, the loading buffer consisted of 80% Acn that prevented hydrophobic interactions between peptides and a sorbent, and **5% TFA** to establish a low pH (typically < 2), which should minimize the binding of nonphosphorylated peptides by neutralizing negative charges of potentially dissociated acidic amino acids. However, as indicated in the recorded MALDI-TOF MS spectra, 5% TFA was not strong enough to prevent the nonspecific binding of acidic BSA peptides resulting in relatively highly intensive signals of the nonphosphorylated peptides (**figure 7A and 7B**).

To improve the specifity of the enrichment by preventing nonspecific binding of peptides containing greater proportions of acidic amino acids, three different "nonphosphopeptides excluders" reported previously in literature were employed. In the second protocol, *i.e.* ***buffer conditions 2***, the loading solution included **1 M lactic acid (LA)**, which was evaluated to be the most efficient additive for phosphopeptide enrichment from a panel of hydroxy acids tested in a previous study (223). The level of nonspecific binding was notably decreased compared to the first protocol (**figure 7C**). However, LA as an excluder was still not very efficient for more complex peptide mixture B (**figure 7D**). The improved efficacy for excluding nonphosphorylated peptides allowed detection of more multiply phosphorylated peptides but with a poor reproducibility. Therefore, in our study, 1 M LA did not seem efficient enough to prevent unspecific binding of non-phosphorylated peptides. We also tested a higher concentration of LA than it was originally recommended (*i.e.* 2 M), however the increase in LA concentration did not lead to any significant improvement in the performance of the second protocol (data not shown).

The third enrichment protocol, *i.e.* ***buffer conditions* 3**, included the addition of glutamic acid (Glu) in the sample loading buffer as an effective nonphosphorylated peptides-excluding agent (**figure 7G and 7H**). Glu has been reported previously as an efficient loading buffer additive (186); its potency for enhancing specifity of MOAC is caused by its competition with Glu residues of peptides. In our setting, the addition of **0.1 M Glu** was more effective than the addition of LA, and it led to improved efficiency and reproducibility of the enrichment, but it was still surpassed by the effect of DHB.

In 2005, Larsen and his co-workers investigated the effect of different aromatic carboxylic acids and aliphatic carboxylic acids added into loading buffer for phosphopeptide enrichment. DHB and other substituted aromatic carboxylic acids (salicylic acid, phthalic acid) showed the best efficacy in inhibition of adsorption

of nonphosphorylated peptides (222). DHB was also found to be the most potent additive in another study (224). In the fourth protocol, ***buffer conditions 4***, **DHB** was added to the loading buffer in a concentration of **350 mg/ml** (close to a saturated solution) for complex mixtures of peptides according to the recommendation in Larsen's protocol. We observed that DHB was the most potent excluder for nonphosphorylated peptides when added during phosphopeptide enrichment using Titansphere® particles and TopTips® since the relative intensities of nonphosphorylated peptides were very low (**figure 7E and 7F**). Additionally, multiply phosphorylated peptides were more clearly detected than in other MALDI-TOF MS spectra obtained by different phosphopeptide enrichment protocols probably because of lowered ion suppression, which is normally affecting the signals of multiply phosphorylated peptides during MALDI-TOF MS. On the other hand, monophosphorylated peptides were slightly less reproducibly enriched when DHB was used, which might indicate that weaker bound monophosphorylated peptides could be also displaced from metal oxide surface by this potent "excluder" (**figure 5A**).

Thus, the non-phosphopeptide excluding efficiency of the additives increased in the following order: **5% TFA < 1 M LA < 0.1 M Glu < 350 mg/ml DHB**.

5.1.3. The addition of glutamic acid into the loading buffer provided the best phospho-enrichment efficiency.

Even though DHB was shown to provide the highest non-phosphopeptide exclusion efficiency among the additives tested, it was actually 0.1 M Glu that enabled the detection of the most phosphorylated peptides. Although the signals of multiply phosphorylated peptides were not as clear as in the case of the DHB protocol, glutamic acid MOAC chromatography seemed to have the highest enrichment efficiency within the four protocols tested. The addition of glutamic acid led to detection of 17 and 15 phosphopeptides in total in NuTip® and Titansphere® enrichment, respectively, which were the highest numbers of detected phosphopeptides in our optimization study. Additionally, the protocol that included Titansphere® particles and glutamic acid reached the best repeatability among all the protocols tested with 15 phosphopeptides repeatedly detected in all three independent enrichments.

The lower yields of phosphopeptides detected in DHB enriched eluates were mostly caused by aforementioned lower recovery of monophosphorylated peptides in the presence of 350 mg/ml DHB. In addition to the negative effect on the detection of mono-

phosphorylated peptides, we also observed a high level of noise in the low m/z region of MALDI-TOF MS spectra recorded from the samples enriched using NuTips® and DHB as an additive. This observation has been already reported in a previous study that also evaluated the performance of NuTips® for phosphopeptide enrichment (341). We are aware of the fact that this issue could have been further addressed by testing lower concentrations of DHB; however, such investigation was far beyond our interests.

Moreover, it has been reported previously (223) that DHB added to loading buffer decreased the number of nonspecifically bound nonphosphorylated peptides but also the number of identified phosphopeptides because it caused problems in the RPLC-ESI-MS/MS system used in the study. Therefore, it might be risky to use DHB in cases when the samples are supposed to be injected into an LC-MS/MS system. On the contrary, Glu is a compound that does not have such a strong affinity for hydrophobic reversed phase, and thus its use in such system is more feasible. Therefore, we selected the glutamic acid including protocol for further studies.

5.1.4. **Titansphere® particles outperformed NuTips® in the real sample analysis.**

We further tested the two best performing protocols in an analysis of a real complex sample. The real peptide samples were prepared by digesting 500 µg of HeLa cells lysate using trypsin, and the samples were enriched for phosphopeptides using either NuTips® or Titansphere® particles and the Glu containing protocol (*i.e. buffer conditions 4*). Enriched fractions resulting from these enrichments were analysed using an RPLC-ESI-MS/MS system.

Surprisingly, we repeatedly observed that NuTips® were not an adequate enrichment media for such a high amount of a complex mixture since the amount of material in the eluates was extremely low in comparison to the fractions obtained by Titansphere® enrichment. According to the description provided by the manufacturer, ZrO_2/TiO_2 NuTips® 10-200 µl have a binding capacity of 2.5 µg which in our opinion should be sufficient for the enrichment of phosphopeptides from 500 µg of unfractionated whole cell lysate. We also tried to use multiple tips for sequential enrichment of the same sample (i.e. the flow-throughs were re-loaded onto the column), but this modification did not bring any improvement observable in the UV-VIS chromatography spectra (data not shown). However, the results were rather disappointing with only several peaks detected

in UV-VIS chromatography. NuTip® might have an excellent selectivity and outperform Titansphere® in the analysis of low complex samples, but in the analysis of a highly complex mixture of peptides, the amount of the beads embedded into the tips is probably not sufficient to robustly enrich phosphorylated peptides.

On the contrary, Titansphere® particles, which can be easily adjusted for any sample volume and amount of starting material, yielded 898 phosphopeptides passing the 0.01 false discovery rate cut-off. Thus, in our hands, Titansphere®, proved as the most efficient media for analysis of a highly complex real sample.

5.1.5. Application of the optimized protocol to study phosphorylation response of irradiated MOLT-4 cells led to identification of more than 600 hundred phosphorylation sites.

To further evaluate the performance of the chosen protocol for phosphopeptide enrichment in the system of interest, i.e. irradiated leukemic cells, we performed a pilot study investigating the phosphorylation response in MOLT-4 cells that were irradiated by a dose of 1.5 Gy chosen on the basis of our previous work (342). In the presented experiment, the quantification of phosphorylation changes between the irradiated and control cells was achieved using SILAC labelling. After mixing the samples 1:1, tryptic digestion of the protein mixture and phosphopeptide enrichment using the Titansphere® particles at a peptide-to-TiO_2 ratio 1:8 under *buffer conditions 4* (100 mM glutamic acid as an additive), and a LC-MS/MS analysis of the resulting fraction, we identified 632 phosphorylation sites from 489 peptides originating from 335 phosphoproteins (summary of the results is given in **figure 18**).

Among the identified sites, 476 were classified as class I phosphosites (based on the localization confidence defined by localization probability calculated by MaxQuant; **figure 18A**). The total number of successfully quantified class I sites was 429; the relative distribution of phosphorylated S, T, and Y were similar to values reported in previous studies (**figure 18B;** (201,273)). Applying the previously reported 1.5 and 0.5 heavy/light ratio cut-offs (normalized SILAC H/L ratios without any log transformation; (343)), we assessed that 31 sites were upregulated and 32 were downregulated one hour after the irradiation (**figure 18C**). As shown in **figure 18D and 18E**, when analysing this first data

set we were able to find statistically over-represented signalling pathways (**figure 18D)** and kinases that were up- and downregulated in response to IR (**figure 18E**).

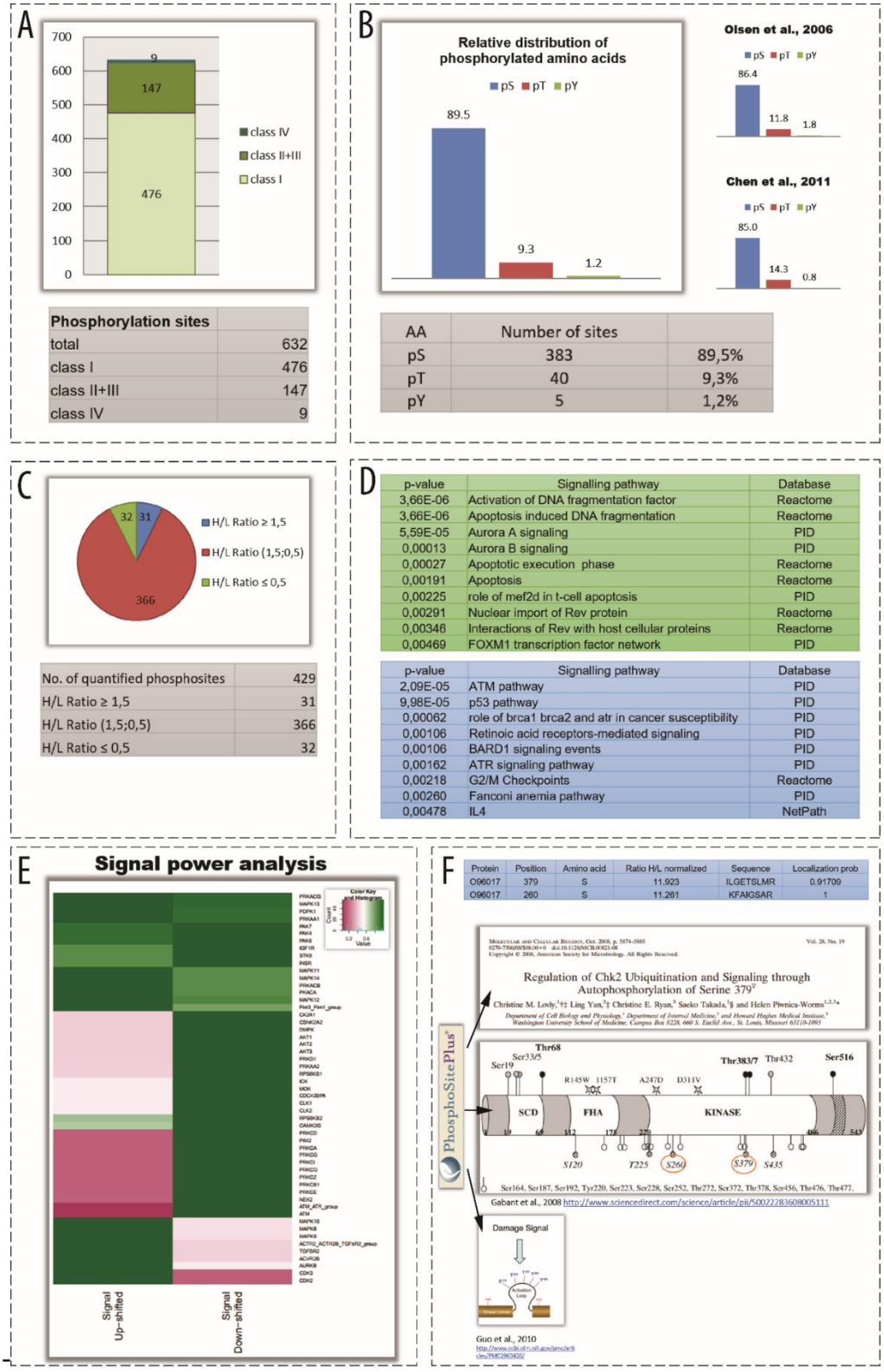

Phosphorylation sites	
total	632
class I	476
class II+III	147
class IV	9

AA	Number of sites	
pS	383	89,5%
pT	40	9,3%
pY	5	1,2%

No. of quantified phosphosites	429
H/L Ratio ≥ 1,5	31
H/L Ratio (1,5;0,5)	366
H/L Ratio ≤ 0,5	32

p-value	Signalling pathway	Database
3,66E-06	Activation of DNA fragmentation factor	Reactome
3,66E-06	Apoptosis induced DNA fragmentation	Reactome
5,59E-05	Aurora A signaling	PID
0,00013	Aurora B signaling	PID
0,00027	Apoptotic execution phase	Reactome
0,00191	Apoptosis	Reactome
0,00225	role of mef2d in t-cell apoptosis	PID
0,00291	Nuclear import of Rev protein	Reactome
0,00346	Interactions of Rev with host cellular proteins	Reactome
0,00469	FOXM1 transcription factor network	PID

p-value	Signalling pathway	Database
2,09E-05	ATM pathway	PID
9,98E-05	p53 pathway	PID
0,00062	role of brca1 brca2 and atr in cancer susceptibility	PID
0,00106	Retinoic acid receptors-mediated signaling	PID
0,00106	BARD1 signaling events	PID
0,00162	ATR signaling pathway	PID
0,00218	G2/M Checkpoints	Reactome
0,00260	Fanconi anemia pathway	PID
0,00478	IL4	NetPath

Protein	Position	Amino acid	Ratio H/L normalized	Sequence	Localization prob
O96017	379	S	11.923	ILGETSLMR	0.91709
O96017	260	S	11.261	KFAIGSAR	1

Figure 18: Summary of the results obtained in the pilot study of irradiated MOLT-4 cells: (A) *Classification of the phosphorylation sites based on their localization probability.* ***(B)*** *The relative distribution of pS, pT, and pY in the quantified class I sites*

subset. ***(C)*** *Pie chart depicting proportion of up- and down-regulated phosphorylation sites in the quantified class I sites subset.* ***(D)*** *Signalling pathways overrepresentation analysis. Up- (green) or down- (blue) regulated sites were annotated by the pathways membership using ConsensusPathDB and statistically evaluated (hypergeometric testing, default background).* ***(E)*** *Kinase activity analysis. Kinases phosphorylating the 429 quantified class I sites were predicted using Networkin 2.0; statistical analysis and visualization was conducted using PhosphoSiteAnalyzer; colour code indicates statistical significance of a finding – low p-values are depicted with dark purple.* ***(F)*** *Chk2 Ser 379 and Ser 260 were found in the upregulated dataset. Using PhosphoSitePlus database, we confirmed the biological relevance of these phosphorylation events in the context of irradiation.*

As for the over-represented signalling pathways, most of them were pathways involved in DDR – for instance activation of ATM- and p53 signalling pathways, cell death by apoptosis, and activation of cell cycle checkpoints. In the kinase activity analysis, we found ATM_ATR group significant among the upregulated kinases and CDKs among the downregulated kinases, which is in concordance with the well-known roles of ATM/Chk2 and ATR/Chk1 in regulation of cell cycle checkpoints in response to genotoxic stress.

Two examples of significantly upregulated phosphorylation sites are given in **figure 18F**. Two strongly upregulated (11-fold) phosphorylation sites were observed in Chk2 after IR. Data mining using the most comprehensive phosphorylation database PhosphoSitePlus (58) revealed that these two phosphorylation sites were localized in the kinase activation loop of Chk2 (344,345), and Ser 379 phosphorylation has been previously shown to be IR-triggered (346).

As these results were fully in concordance with known facts about the IR-triggered cellular response, we could conclude that our workflow was capable of identification and quantification of phosphorylation changes in irradiated leukemic cells. It also proved that it enabled further analysis of the acquired data using bioinformatic tools to describe biological significance of the measured changes.

5.2. **Radiosensitization of MOLT-4 cells by selective ATR and ATM inhibitors, VE-821 and KU55933**

To investigate the radiosensitizing potential of ATR inhibitor, VE-821, and compare it to the effects of ATM inhibitor, KU55933, the MOLT-4 cell line was chosen. MOLT-4 is a T-cell acute lymphoblastic leukaemia (T-ALL) cell line. The effects of IR and other DNA damage inducing agents in this cell line have been extensively studied, especially at our department and the collaborating Department of Radiobiology at the Faculty of Military Health Sciences (347–350,342,351–357). In these studies, it has been shown that MOLT-4 cells are relatively radiosensitive cells with D_0 value (dose reducing survival to 37 %) of 0.87 Gy, and the cells express wild-type p53 and possess a functional ATM/p53 pathway, which is triggered in a dose-dependent manner (342,347,353). After irradiation, the cells have been shown to die by both pre- and post-mitotic apoptosis (348,358). Notably, it has been suggested that MOLT-4 cells could have some defect in DNA repair pathways promoting their radiosensitivity (a possible defect in Nbs1 phosphorylation have been discussed previously (351)). The cells have been also already used to study radiosensitizing effects of several kinase inhibitors such as caffeine (low potent ATM/ATR inhibitor; (354,359)), U0126 (MEK1/2 inhibitor; (359), and DNA-PK inhibitors NU7026 and NU7441 (355,357) in leukemic cell lines, where MOLT-4 cells were chosen to represent a p53 wt model cell line.

To get an overview of MOLT-4 cell line genetic background, we extracted MOLT-4 relevant data from the COSMIC (Catalogue of somatic mutations in cancer) database, which is the most comprehensive database of somatic mutations in human cancer (360). The database search revealed 1476 entries; among them, 56 were mutations in census genes (*i.e.* genes known to be involved in cancer). Importantly, MOLT-4 cells suffer from mutations of signal transduction pathways which are known to be frequently mutated in T-ALL leukaemia such as **NOTCH1**, **IL7R-JAK-STAT**, **RAS-MEK-ERK**, and **(PTEN)-PI3K-AKT** pathways (reviewed in (361)). The only census gene that was detected with homozygous deletion was the Phosphatase and tensin homolog *PTEN*, which is a tumour suppressor gene commonly mutated in a wide range of cancers (362). It acts as an important negative regulator of the PI3K-AKT-mTOR pathway, which is responsible for regulation of cellular metabolism, proliferation and survival. Therefore, the inactivation of PTEN triggers overactivation of the pathway and uncontrolled cellular proliferation,

ultimately leading to cancer (reviewed in (363). Furthermore, MOLT-4 cells suffer from multiple heterozygous mutations in several DDR genes such as *ATM*, *BRCA1*, *FANCA*, and *TP53*. Together, these data indicated that the PI3K-AKT pathway might be dysregulated, and the DNA repair capacity might be impaired in MOLT-4 cells.

5.2.1. **Both VE-821 and KU55933 treatment abrogated the radiation-induced phosphorylation of corresponding checkpoint kinases.**

To confirm the inhibitory effect of VE-821 and KU55933 on ATR and ATM kinases, respectively, we assessed phosphorylation of two downstream effector kinases: **Checkpoint kinase-1 (Chk1)** Ser 345 and **Checkpoint kinase-2 (Chk2)** Thr 68. As expected, both phosphorylation sites were upregulated upon irradiation (3 Gy, one hour after irradiation). Chk2 phosphorylation, which is a marker of DNA DSBs-activated ATM, was markedly decreased with increasing concentration of KU55933. Accordingly, the status of Chk1 Ser 345 phosphorylation site, which is a widely-accepted marker of ATR activation, was proportionally inhibited by increasing concentration of VE-821. Therefore, we confirmed that in our cell line model the pre-incubation with VE-821 and KU55933 specifically inhibited ATR and ATM kinase, respectively, without any off-target effect towards the other kinase. Such observation was not surprising, as the IC50(ATR) of KU55933 was assessed to be 100 μM (364), and the Ki(ATM) of VE-821 is 16 μM (IC50 has not been assessed; (11)). Additionally, the selectivity of VE-821 towards ATR has been confirmed in previous studies (11,134).

5.2.2. **KU55933 treatment was not toxic for sham-irradiated cells and enhanced the IR induced growth inhibition and cell death of MOLT-4 cells.**

KU55933 was the first potent and selective ATM inhibitor with IC50 of 13 nM (364). As well as its more recent analogues, it has been shown to sensitize cells to IR and DSB-inducing drugs without sensitizing cells derived from A-T patients (364–366). Radiosensitization using KU55933 and its derivatives is not specifically targeting cancer cells; however, ATM inhibition alone has been shown to be nontoxic for normal tissues outside the radiation field (366). The p53-dependency was investigated, but the results are too contradictory to make any conclusion (365,366). In the presented data, KU55933 was

well tolerated by the p53-wt expressing MOLT-4 cells in concentrations up to 10 μM; to induce a significant perturbation of cell growth, it was necessary to apply at least 20 μM KU55933. Interestingly, 5 μM KU55933 significantly increased the number of viable metabolically active cells six days after the start of the treatment in two independent proliferation assays (**figure 10**) without affecting the number of nonviable cells and the cell cycle (**figure 13**) confirming that KU55933 was not toxic for sham-irradiated MOLT-4 cells in concentrations up to 10 μM.

Since MOLT-4 cells express a wild-type p53 and possess a functional ATM/p53 pathway (342,347,353), and cellular response to DNA DSBs is to a great extent ATM/p53 pathway dependent, we expected that ATM inhibition would sensitize MOLT-4 cells to IR. In concordance with our expectation, 10 μM KU55933 caused a significant decrease in MOLT-4 cells proliferation when combined with IR and detected 6 days after irradiation (**figure 11**) and increased the IR-induced cell death 3 days after irradiation (**figure 13**). KU55933 showed no effect on the G2/M cell cycle arrest triggered by IR, which was in concordance with the known fact that the intra-S and G2/M DNA damage checkpoints are mainly directed by the ATR/Chk1 pathway (reviewed in(110).

5.2.3. VE-821 is a more potent inhibitor of MOLT-4 cells growth than KU55933 in both single treatment and combination with irradiation.

While ATM mainly responds to severe DNA lesions, ATR is an indispensable regulator of cellular proliferation as it responds to stress that cells undergo during normal replication of DNA as well as replicative stress caused by exposure to genotoxic agents. It has been shown to be essential for viability; homozygous mutation of ATR caused peri-implantation embryonic lethality in mice (85,86). However, transient inhibition of ATR by VE-821 has been proven to cause mere reversible growth arrest in normal cells, which was abrogated when the inhibitor was removed from the cultivation media (11). Importantly, the newest highly potent and specific ATR inhibitors have been shown to directly eradicate or sensitize cancer cells to a variety of genotoxic agents without affecting normal, non-tumour, cells (8,11,12,138,139). The sensitivity of cancer cells to ATR inhibitors has been already explained by several cancer-specific defects such as loss of functional ATM/p53 pathway (8–12) and elevated levels of replication stress induced by increased oncogenic signalling (1–7).

In the presented study, VE-821 significantly inhibited proliferation of p53-wt MOLT-4 cells already at 1 μM concentration although such concentration caused only a partial ATR inhibition when detected as a Chk1 Ser 345 phosphorylation using western blotting (**figure 12**). This effect was further accented in correlation with increasing inhibitor concentration (**figure 10**). Thus, in MOLT-4 cells, continuous inhibition of ATR by VE-821 has a significantly stronger effect on proliferation than the inhibition of ATM.

In combination with IR, VE-821 significantly abated the number of viable cells in both irradiated groups already 72 hours after irradiation. As both concentrations used in our experiments directly affected the proliferation of sham-irradiated cells, we further calculated a ratio between irradiated and sham-irradiated group for each inhibitor treated condition to resolve if the combination of irradiation and the inhibitor has a more profound effect on proliferation than the inhibitor itself (**figure 11**). Whereas the irradiation caused nearly 50 % decrease of control cells viability after 72 hours of treatment, the irradiation of pre-treated cells (2 μM VE-821) led to almost 75 % loss of viability in comparison to inhibitor treated cells, suggesting an additive effect of VE-821 and IR combination. Additionally, we also observed that VE-821 in 2 μM and 10 μM concentrations modulated the proliferation of irradiated MOLT-4 cells when the inhibitor was present in cell culture media only transiently, for the first 24 hours of the treatment, and then it was washed out (**figure 11D**). In contrast to continuous treatment, 2 μM VE-821 did not significantly affect the proliferation of sham-irradiated cells when washed out after 24 hours; however, it still enhanced the antiproliferative effects of IR. Taken together, these data showed that VE-821 strongly affected proliferation of p53-wt MOLT-4 cells, and in combination with IR, the proliferation was influenced even when the inhibitor was present only transiently.

5.2.4. Both KU55933 and VE-821 increased the ionizing radiation-induced cell death in MOLT-4 cells.

As mentioned above, KU55933 did not induce any significant changes in viability of both sham-irradiated cells and irradiated cells after 24 hours (**figure 13**); however, VE-821 affected the viability of the cells significantly. Strikingly, the combination of both inhibitors diminished this detrimental effect of VE-821. This is consistent with the results of proliferation experiments, in which we observed similar trend. When applying three different inhibitor combinations, we observed that KU55933 suppressed the VE-821 induced decrease in MOLT-4 cells proliferation in both irradiated and sham-irradiated

groups. However, in contrast with WST-1 assay, which does not distinguish between the changes of viable cells numbers caused by cell cycle effects, changes in metabolic activity, or cell death inducing effects of a tested compound, these results indicated that in our short-term incubation experiments, KU55933 prevented VE-821 induced cell death. Similar observations were reported in a study investigating the effect of caffeine, a low potent and unspecific ATM inhibitor, on mitoxantrone induced cell death in MOLT-4 cells. Incubation with caffeine temporarily protected the cells by delaying the onset of cell death, most likely by the inhibition of p53-dependent apoptosis (359).

Three days after irradiation, in the VE-821 treated groups, the percentage of cells with compromised viability further decreased despite the absence of the inhibitor in cultivation media (**figure 13**). On the contrary, we did not notice the "protective" effect of KU55933 that we observed 24 hours after irradiation when the inhibitor was not present. Such finding further confirms that ATM inhibition only delayed the onset of cell death. Importantly, both inhibitors and their combinations increased sensitivity of MOLT-4 cells to IR. The most detrimental effect was observed when cells were treated by 10 μM VE-821 and by the combination of both inhibitors (10 μM +10 μM). Application of these conditions led to more than 90% decrease in viability of MOLT-4 cells 72 hours after irradiation. In conclusion, both inhibitors led to increased cell death when combined with IR in an appropriate experimental design (i.e. appropriate dose and incubation time) and thus radiosensitized MOLT-4 cells.

5.2.5. VE-821, but not KU55933 disrupted ionizing radiation-induced G2/M arrest in MOLT-4 cells.

As one of the proposed mechanism of radiosensitization using ATR inhibitors is the disruption of the G2/M checkpoint in G1 checkpoint-deficient cells (11), we investigated modulation of the cell cycle by ATR and ATM inhibition (**figure 13**). None of the conditions we applied affected the cell cycle in sham-irradiated cells except for 10 μM VE-821 and its combination with KU55933, which repeatedly caused a significant increase in number of cells in G1. In concordance with our previous results (367), irradiation by the dose of 3 Gy led to a significant G2/M arrest in viable MOLT-4 cells 24 hours after irradiation. The pre-incubation with VE-821 and with the inhibitor combinations led to a significant disruption of G2/M checkpoint in the viable fraction of cells. On the other hand, the inhibition of ATM by KU55933 further increased the proportion of cells in G2/M

together with corresponding significant decrease in the number of cells in G1. The abrogation of the G2/M checkpoint by VE-821 10 μM was also achieved when a lower dose of irradiation was applied (1.5 Gy; data not shown). As it has been reported previously, caffeine disrupted mitoxantrone induced G2/M arrest in MOLT-4 cells(359) . After examining the effects of specific ATM and ATR inhibition, we suggest that the G2/M block disruption was rather caused by "non-specific" ATR-inhibiting effects of caffeine, which was originally proposed as an ATM inhibitor; however, it has been shown that it also inhibits ATR, although with a lower potency (IC50(ATM): 0.2 mM; IC50(ATR): 1.1 mM). Altogether, these results confirmed that ATR is the main kinase controlling the G2/M- cell cycle checkpoints after irradiation in MOLT-4 cells.

5.3. Phosphoproteomic analysis of VE-821 treated MOLT-4 cells

5.3.1. Selection of the experimental design for phosphoproteomic and metabolomic inhibitor studies

As described in the previous chapter, both VE-821 and KU55933 increased MOLT-4 cells sensitivity to IR. However, there were several reasons why we selected to preferentially use ATR inhibition by10 μM VE-821 for further experiments:

1) ATM/p53 pathway is the key mechanism in cellular response to IR-induced DSBs, and therefore, its inhibition was assumed to cause radiosensitization in wt-p53 expressing cell line. On the contrary, ATR is mostly known to respond to "milder" types of stress and it is not dominant in response to IR. Even though it has been already described to sensitize cells towards IR, the mechanism is not deeply understood, and it is mostly described as S- and G2/M checkpoints dysregulation in ATM/p53 deficient or higher levels of replication stress-suffering cells. In our opinion this explanation was too simplistic and needed further investigation.
2) As described in the Introduction section (chapter 1.3.1), ATR inhibitors offer a great promise in oncology. Two of the most recent potent and selective ATR inhibitors are currently being tested in phase I clinical trials. Better understanding of the mechanism of action might be beneficial for future use of the drugs in clinics. For instance, if a novel pathway affected by the inhibitor treatment is identified, such knowledge can help to predict potential synthetic lethality in tumours with specific genetic background and therefore, increase the range of tumours which might be treated using the inhibitors of ATR.
3) Moreover, we detected two distinct phenotypes caused by VE-821: the first was observed after 2 μM VE-821 treatment and was mostly characterized by enhancing of the IR-induced cell viability and growth inhibition – disrupting the IR-triggered G2/M checkpoint and increasing the IR-induced cell death. In experiments with shorter incubation times (i.e. 24 hours) and inhibitor-only treatment, this concentration was not proven to significantly affect viability of MOLT-4 cells. Moreover, 2 μM VE-821 itself did not cause any significant

perturbation of the cell cycle. The second phenotype was induced by 10 μM VE-821 and characterized by marked proliferation inhibition and decreased viability of MOLT-4 cells in both single inhibitor treatment and its combination with IR, which led to more than a 90 % decrease of viability in 3 days. This inhibitor concentration also affected the cell cycle of treated cells inducing a slight, but significant, accumulation of cells in the G1 phase. Hence, using the combination of two high-throughput -omic techniques we aimed to provide a deep insight into underlying molecular mechanisms of the potent antiproliferative activity of 10 μM VE-821 in MOLT-4 cells.

5.3.2. Phosphoproteomic analysis of VE-821-modulated cellular response to ionizing radiation identified and quantified thousands of phosphorylation sites.

To describe cellular mechanisms underlying the VE-821-mediated radiosensitization of MOLT-4 cells, we employed high-resolution MS to identify and quantify changes in proteome, phosphoproteome, and metabolome of irradiated VE-821-treated cells (**figure 14**). The quantification on both proteomic levels was based on SILAC (270)). To specifically enrich for peptides modified by phosphorylation, desalted tryptic peptide samples were fractionated using HILIC followed by phosphopeptide enrichment using titanium dioxide chromatography (222), RPLC-MS/MS detection, and peptide identification and quantification using MaxQuant *v.1.5.2.8* (316). Using this approach, we identified 9285 phosphorylation sites from 3090 protein groups at a site FDR level of 0.01, among them 4504 were quantified in all three biological replicates (nearly 63 % of the data set). In GRT, we identified 623 regulated phosphorylation sites (455 phosphoproteins); among them the majority were upregulated (431). As discussed previously (133), the higher number of phosphorylation sites upregulated than downregulated in response to a kinase inhibitor treatment was probably caused by the length of the treatment (one hour), which was chosen to rather identify signalling pathways rewired by ATR inhibition in irradiated cells than phosphorylations that are directly dependent on ATR kinase activity in response to IR.

In the analysis of the whole proteome samples prepared using the same treatment and time interval we detected no significant changes on the proteomic level (**figure 15**). Taken together, we showed that VE-821 co-treatment significantly affected the

phosphorylation response in cells treated with IR, and that the observed changes were not induced by the changes on the proteome level – since the proteome remained unperturbed.

5.3.3. Gene ontology enrichment analysis of regulated phosphoproteins provided a general description of VE-821 modulated phosphoproteome.

To functionally classify phosphoproteins identified and quantified in our study and statistically evaluate enriched categories, we performed a functional annotation and over-representation analysis using ConsensusPathDB over-representation analysis web tool (319,320). By this tool, proteins were annotated using GO terms level 4 and the over-representation was evaluated using hypergeometric testing.

At first, we analysed all phosphoproteins identified in our study against a default background reference set to characterize the phosphoproteome detectable using our experimental design. While the over-representation of nuclear and cytosolic proteins and under-representation of membrane proteins was probably caused by sample preparation and better detectability of soluble proteins, over-representation of GO terms related to cell cycle (especially mitosis), DNA repair and replication, and gene expression confirmed the essential role of phosphorylation in regulation of these processes (data not shown).

Then, a list of 455 phosphoproteins containing VE-821-regulated sites was tested against a custom background reference set derived from our data comprising all phosphoproteins with at least one phosphorylation site quantified in all three biological replicates. In this analysis, we identified over-represented biological processes (BP), cellular compartments (CC), and molecular functions (MF). As shown in **figure 19A**, regulated phosphoproteins were over-represented in nucleus, specifically in chromosomes, mitotic spindle, and replication fork and involved in chromatin organization, DNA repair and metabolism, cell cycle, and regulation of transcription factors.

5.3.4. Signalling pathways annotation and over-representation analysis revealed several pathways possibly dysregulated by VE-821 treatment.

Using the ConsensusPathDB tool, we also mapped regulated phosphoproteins to signalling pathways from three different pathways databases: KEGG (321,322), REACTOME (323), and PID (324) and pathway coverage was calculated for each pathway

(**figure 19B**). The list of pathways containing proteins with VE-821-regulated phosphorylation sites, and thus pathways potentially modulated by VE-821 treatment contained pathways involved in **DNA repair**, **replication**, and **telomeres synthesis** (e.g. "DNA replication", "Fanconi anaemia pathway", "BARD1 signalling events", "ATM/ATR pathway", "DNA double strand breaks response", "DNA strand elongation", and "Extension of telomeres"), **apoptosis** (e.g. "Caspase Cascade in Apoptosis or "Apoptotic execution phase"), **regulation of mitosis** ("Aurora A/B and signalling", "PLK1 signalling events", "Mitotic metaphase and anaphase", and "Kinesins"), **transcription factors regulation** ("ATF-2 transcription factor network", "Activation of AP-1 family of transcription factors", and "Regulation of cytoplasmic and nuclear SMAD2/3 signalling"), **chromatin regulation via histones modification** ("Signalling events mediated by HDAC class I"), but also pathways primarily related to **cellular metabolism** ("AMPK signalling pathway" and "mTOR signalling).

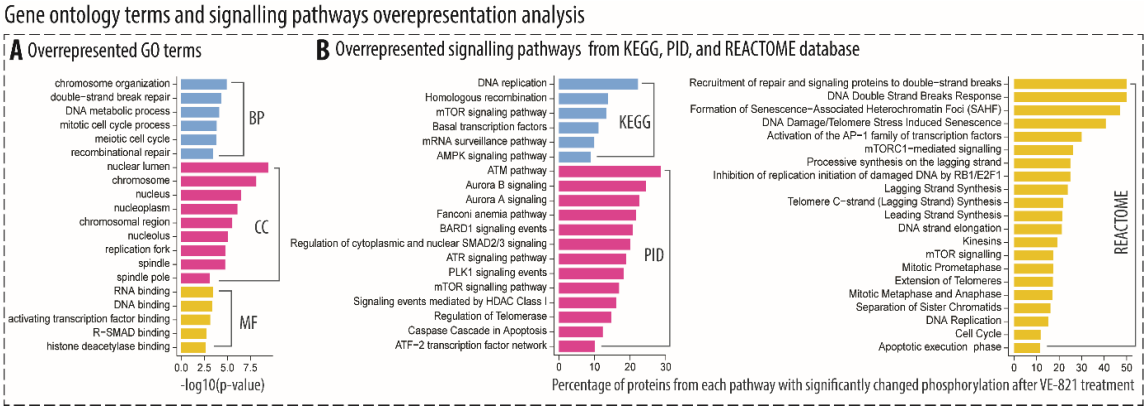

Figure 19: Selected results from Gene Ontology level 4 terms and signalling pathways overrepresentation analysis*. Functional annotation of proteins with phosphorylation sites significantly affected by VE-821 treatment and over-representation analysis were done using ConsensusPathDB overrepresentation-analysis online tool. (**A**) Overrepresented GO terms (FDR < 0.05, all proteins quantified in our study were used as a statistical background). (**B**) Regulated phosphoproteins were mapped to signalling pathways from 3 different databases (KEGG, REACTOME, and PID) and pathway-coverage was calculated for overrepresented pathways (FDR < 0.05, all proteins comprised in detected pathways were used as a statistical background).*

5.3.5. Network analysis revealed the complexity of cellular response and multiple functionally related clusters affected by VE-821.

Using the SubExtractor algorithm (325), we extracted multiple subnetworks of interconnected nodes with the most prominent changes in phosphorylation after VE-821

treatment. The largest subnetwork is depicted in **figure 20.** For each group of interconnected nodes, we further performed functional annotation enrichment analysis to better understand its functions. To simplify the interpretation, the clusters were divided into two groups.

The first one can be concisely described as a **multi-level stress induced regulation of gene expression**: regulation of RNA biogenesis, its modification and stability, and translation. Namely, SubExtractor extracted a cluster that contains chromatin modifying enzymes (mostly histone acetylation and methylation) and thus contributes to regulation of gene expression. Furthermore, transcription initiation and elongation complexes were also extracted. The largest module centred around **Protein mago nashi homolog (MAGOH)** comprises many proteins from the mRNA splicing machinery. And finally, VE-821 treatment also affected phosphorylation of ribosomal proteins suggesting that it might also alter protein synthesis. The ribosomal cluster is further tightly linked to a cluster that mostly contains members of the mTOR pathway indicating that this pathway might be dysregulated by VE-821 treatment, and consequently, result in affected cell growth and proliferation.

The second group is mostly related to already known functions of ATR; it contains clusters corresponding to **DNA damage response** including both DNA damage repair proteins and proteins involved in stress-induced cell cycle regulation. As shown in **figure 20** we detected a densely interconnected cluster composed of members of minichromosome maintenance complex (MCMs), origin recognition complex subunits (ORCs), and DNA polymerases; this cluster also includes several known ATR-interacting proteins and corresponds to the regulation of origin firing and S-phase progression by ATR in response to stress. Further hubs in the extracted network comprised four cell cycle regulating kinases – **cyclin dependent kinase 1 (CDK1)**, **cyclin dependent kinase 1 (CDK2)**, **Serine/threonine kinase PLK1 (PLK1)**, and **Aurora kinase A (AURKA)** - and their regulated substrates extracted as their interactors. These kinases refer to the disruption of IR induced DNA damage cell cycle checkpoints and dysregulation of mitosis and cell division by VE-821 treatment as detected by the DNA content analysis. Unexpectedly, the algorithm also extracted a small cluster containing enzymes from the *de novo* pyrimidine synthesis metabolic pathway connected to the DNA repair cluster suggesting that metabolism of nucleotides might be also affected by ATR inhibition.

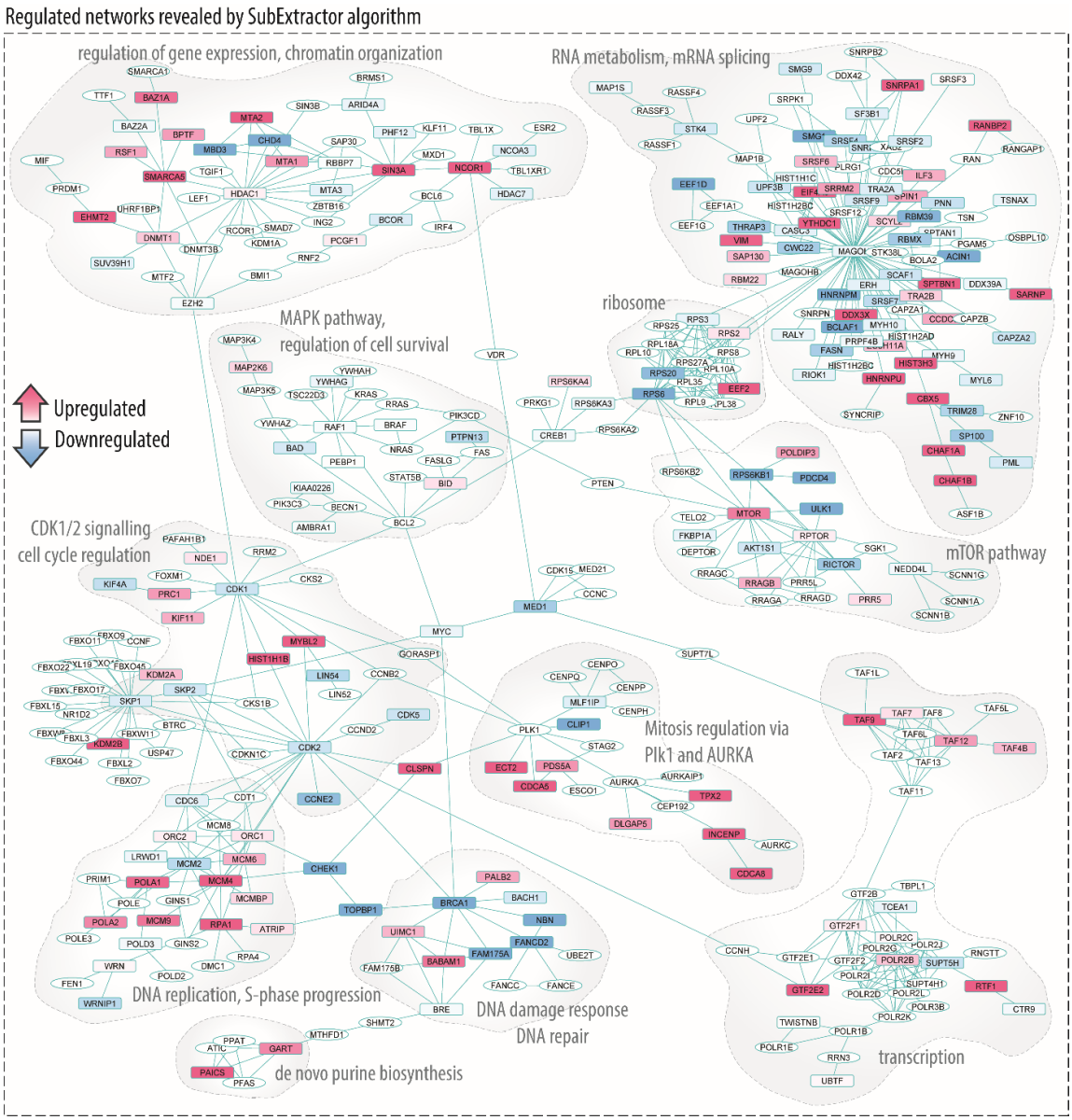

Figure 20: Protein network extracted using SubExtractor algorithm and visualized in Cytoscape. *Protein-protein interactions with STRING score above 900 were used as an input for the algorithm and regulated subnetworks were extracted (FDR < 0.005). Proteins in rectangles were identified and quantified in our study; proteins in ellipses were added to the network by the algorithm. Proteins with downregulated phosphorylation are depicted in blue; proteins with upregulated phosphorylations are depicted in pink. The colour intensity corresponds to the degree of regulation (combined z-score).*

The complexity of the extracted network containing multiple cellular mechanism pointed out the multi-layered nature of cellular response to stress affected by VE-821 treatment. Moreover, we identified multiple protein kinases in the centres of extracted modules indicating a possible dysregulation of these kinases by the treatment. This was not unexpected; inhibition of one protein kinase in a cell naturally leads to dysregulation of its dependent downstream cellular signalling mediated by other protein kinases. To investigate

kinome dysregulation induced by VE-821 treatment, we performed sequence motif analysis and kinase activity analysis together with statistical evaluation of the possible changes, and the results of these analyses are presented below.

5.3.6. **Sequence motifs analysis identified global trends in VE-821 induced phosphorylation changes.**

To characterize the detected phosphorylation sites, we first calculated the distribution of phosphorylated serines (pS), threonines (pT), and tyrosines (pY) identified and quantified in all three biological replicates. As depicted in **figure 21A**, the distribution was very similar to values reported previously, in studies employing comparable phospho-enrichment strategies and sample analysis (*i.e.* 87.6 % of pS, 11.8 % of pT, 0.6 % of pY). Interestingly, when we calculated the same distribution ratio for sites that were significantly regulated after VE-821 treatment, we found that pT were over-represented in the regulated data set (19.3 % of all regulated sites, enrichment factor of 1.65, FDR of $9.97x10^{-10}$ calculated using Fisher exact test). We observed the same trend in our previous data (133), and the over-representation of pT has been also reported in another study investigating genistein induced phosphorylation changes in breast cancer cell line, which mostly affected cell cycle regulation and DDR (294). Since in the sequence logos of CDK1 and CDK2 generated using their known substrates (PhosphoSitePlus database) it is apparent that pT is overrepresented in comparison to the regular distribution of pT usually detected in phosphoproteomes (**figure 22A**), we assume that in our case, the over-representation of pTs might be caused by a high number of regulated sites phosphorylated by these kinases - they were predicted to phosphorylate between 27 – 37 % of the regulated dataset, and about 40 % of these sites are phosphorylated threonines (**figure 22B**).

Next, we analysed and visualized sequence motifs using iceLogo tool (327) and motif-x algorithm (328). When analysing all class I sites identified in our study with SwissProt average amino acid frequencies as a background reference set, we found a significant bias of our data towards proline-directed motifs (**figure 21B**). Furthermore, basic and acidic amino acids (R, K, and E) were slightly overrepresented, and hydrophobic amino acids were slightly underrepresented (L). The slight bias towards the hydrophilic residues and underrepresentation of hydrophobic ones might be caused by chromatographic methods used for peptide fractionation, phosphopeptide enrichment, and LC-MS/MS analysis, together with the aforementioned high proportion of CDK1 and

CDK2 substrates in our data, which both contain basic amino acids in their sequence motifs (**figure 22**). In the upregulated dataset, proline-directed motifs followed by basic amino acids were significantly over-represented, which corresponds well to the known sequence logo of CDK 1 and 2 (**figure 22A**). On the other hand, from the sequences surrounding downregulated sites, SQ motif was extracted using motif-x providing a confirmation of the downregulation of DNA repair kinases-mediated phosphorylation as this motif is typical for PI3K-related kinases ATM, ATR, and DNA-PK (**figure 1**).

Taken together, sequence motifs analyses identified global trends in VE-821 induced phosphoproteome changes with dominant representation of upregulated CDKs and downregulated PIKKs.

Figure 21: Sequence motif and kinase activity analyses: (A) Pie charts *depict proportions of STY phosphorylations in the whole class I (localization probability > 0.75) dataset and in the regulated fraction.* ***(B) Sequence motif analysis*** *was performed using IceLogo and motif-x. Amino acid sequences of differentially up- or down- regulated phosphorylation sites were analysed against a statistical background comprising all class I sites quantified in our study. Depicted motifs were found enriched at indicated significance levels. In IceLogo analysis, amino acids that were more frequently observed in the proximity of a regulated phosphorylation site are indicated over the middle line, whereas the amino acids with lower frequency are indicated below the line; phosphorylated amino acid is located at position 0* ***(C) Kinase activity analysis.*** *Phosphorylation sites were annotated with their known kinases using PhosphoSitePlus database if available. iGPS v1.0 and Networkin 3 were used to predict kinases for all class I sites, and the predictions were filtered as*

indicated. ***Venn diagram*** *shows the overlap between phosphorylation sites annotated by each method and applying desired filtering criteria.* ***Boxplots*** *depict SILAC H/L ratios distribution of phosphorylation sites assigned to each kinase/group. The distribution, median, and/or outlier-shifts to positive values indicate a possible upregulation of kinase activity; trends toward negative ratio values show a possible downregulation of kinase activity. Statistical analysis was performed using 1D enrichment analysis in Perseus (v 1.5.2.6), and the test FDR value for each kinase/group was used to rank the boxplots in ascending order. The higher color intensity corresponds to the lower 1D enrichment FDR value and vice versa.*

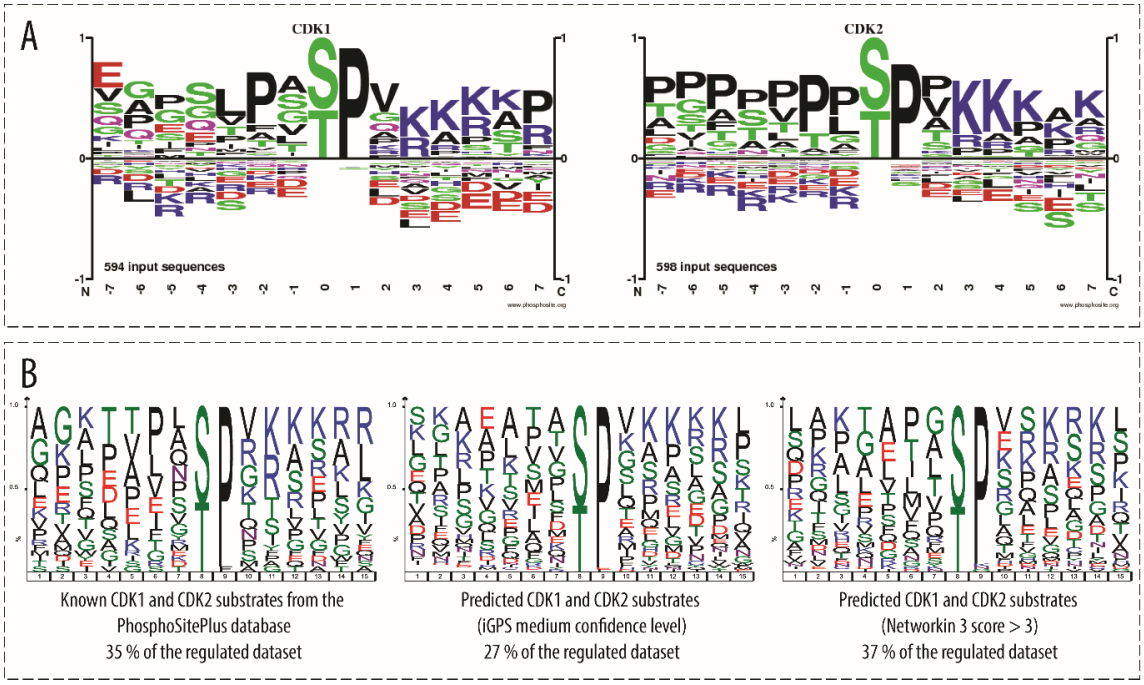

Figure 22: Characterization of sequences phosphorylated by CDK1 and CDK2. (A) *Sequence logos for CDK1 and CDK2 were downloaded from the PhosphoSitePlus database.* ***(B)*** *Sequence logos were generated in IceLogo for sequences that were either known CDK1/2 substrates or predicted by iGPS or Networkin 3, and the percentage of these sequences in the regulated dataset was calculated.*

5.3.7. **Kinase activity analysis confirmed the downregulation of PIKKs substrates after VE-821 treatment.**

5.3.7.1. VE-821 specifically inhibited ATR kinase and did not affect the IR-triggered ATM signalling.

In addition to SQ/TQ motifs enriched among downregulated sites in both sequence motif analyses, 1D enrichment analysis of known and predicted kinase motifs repeatedly indicated that the SILAC H/L ratio distribution of the ATM/ATR group substrates shows a significant declining trend (**figure 21C**). From these ratio shifts, the activity of ATM/ATR group might be inferred as downregulated. Even though both kinases share the same phosphorylation motif, both prediction algorithms clearly favour ATM over ATR. This bias is probably introduced by a better annotation of ATM substrates and protein-protein interactions in the databases.

Nevertheless, using an antibody against Chk2 Thr 68 phosphorylation, which is a widely-used marker of ATM kinase activation in response to ATM activating stress, we showed that 10 μM VE-821 did not inhibit ATM signalling in our experiments (**figure 12**). Furthermore, we found additional pieces of evidence of unaffected ATM signalling in our phosphoproteomic data: ATM Ser 2996 autophosphorylation site, which has been previously shown to be rapidly induced by IR (43), was not affected by the treatment. Similarly, two IR-induced autophosphorylation sites of a downstream ATM target Chk2, Ser 260 and Ser 379 (344,345), were also not significantly changed.

On the contrary, known ATR targets located within the Chk1 regulatory domain were observed to be downregulated upon VE-821 treatment: Ser 345 phosphorylation was detected by western blotting (**figure 12**), and Ser 317 phosphorylation was quantified in our phosphoproteomic experiment. An important marker of Chk1 activity, the autophosphorylation site Ser 296, was not detected in our study. Chk1 itself was evaluated as significantly downregulated in the 1D enrichment analysis of the known substrates, providing further evidence of downregulated ATR/Ckh1 pathway. Considering the high selectivity of VE-821 towards ATR kinase (IC50 (ATR): 26 nM, Ki (ATR): 13 nM, Ki (DNA-PK): 2.2 μM, Ki (ATM): 16 μM), we can assume that significant changes within SQ/TQ phosphorylations motifs assigned to ATM_ATR group can be explained by specifically inhibited ATR kinase activity.

DNA-PK, which is also known to share the glutamine directed phosphorylation motif (**figure 1**), was evaluated to be significantly downregulated using the iGPS predictions. However, we did not find any known site of DNA-PK that would be downregulated in our study (the only known DNA-PK phosphorylation site was Ser 430 on Vimentin, which was unchanged). Moreover, 10 μM VE-821 was proven to leave DNA-PK signalling unaffected in a cell-based assay (11), and thence, we assume that the DNA-PK inhibition is rather unlikely.

In all three experimental replicates, we identified and quantified 21 downregulated SQ/TQ class I phosphorylation sites; among them eleven were known substrates of ATM/ATR kinases or predicted by iGPS or Networkin 3. Most of the downregulated sites were located on proteins with confirmed roles in DDR; however, potential functions of some of them have not been elucidated yet.

5.3.7.2. VE-821 treatment altered phosphorylation of MRN and BRCA1-BRCT/Abraxas complexes and several other proteins with known role in DNA damage response.

On the list of regulated ATM/ATR targets, we found two VE-821 responsive phosphorylation sites on **MRN complex**, the major sensor of DNA DSBs and ATM kinase activator, which has been also shown to be required for ATR activation after IR (368). **Double-strand break repair protein MRE11A (MRE11)** Ser 678 is a known ATM substrate essential for homology directed repair (369); Ser 397 phosphorylation of **Nibrin (NBS1)** has been previously detected, but the phosphorylation of this site does not have any known function. Furthermore, phosphorylation of **BRCA1-BRCT/Abraxas complex** was also shown to be altered by ATR inhibition; we detected two downregulated phosphorylation sites on **Breast cancer type 1 susceptibility protein (BRCA1)** - Ser 1239 and Ser 1524 - the latter one has been shown to be important for cellular response to DSBs (370) and phosphorylated by either ATM or ATR depending on the source of the stress (371). In addition to BRCA1, **BRCA1-A complex subunit Abraxas (FAM17A)** Thr 365 was also found to be dephosphorylated after ATR inhibition – this phosphorylation of FAM17A does not have any known function; however, phosphorylation has been shown to be essential for Abraxas regulation very recently (372).

Another instances of VE-821-regulated phosphorylations, and thus potential ATR targets, are Ser 319 of an important member of **Fanconi Anaemia pathway Fanconi anaemia group D2 protein (FANCD2)** and Ser 368 of **E3 ubiquitin-protein ligase**

RAD18 (RAD18), an important E3 ubiquitin ligase responsible for monoubiquitination of **Proliferating cell nuclear antigen (PCNA)** in response to stress (373). Moreover, we also found a markedly downregulated SQ site in **RAD51-associated protein 1 (RAD51AP1)** (Ser 120), which has been detected and validated in another very recent phosphoproteomic study using ATR inhibitors in combination with replication stress induced by hydroxyurea (135).

5.3.8. **Dysregulation of cyclin-dependent kinases and aurora kinases was responsible for the disruption of G2/M checkpoint and faster progression through mitosis.**

In the DNA content analysis, we showed that VE-821 disrupted IR-induced G2/M arrest in MOLT-4 cells. Cells treated with ATR inhibitor were not able to activate the G2/M checkpoint, which in turn led to faster progression into mitosis with unrepaired IR-induced DNA damage. Such progression has been shown to cause mitotic catastrophe and apoptotic cell death in haematological malignant cell lines (134,313,374). Using phosphoproteomics, we aimed to elucidate, which kinases were dysregulated by ATR inhibition and thus may contribute to the G2/M checkpoint disruption. As depicted in **figure 21C**, the combination of kinase annotation and 1D enrichment analysis revealed a possible upregulation of G2/M checkpoint controlling **CDK1** kinase, mitotic kinases **Aurora A** and **B**, and kinases from the NEK family, particularly **Serine/threonine protein kinase NEK2 (NEK2)** kinase.

5.3.8.1. VE-821 caused CDK1 upregulation and increased phosphorylation of many known CDK1 targets involved in G2/M transition and mitosis in irradiated MOLT-4 cells.

Sequence motif analysis showed overrepresentation of phosphorylated amino acids followed by proline and basic amino acids – a well-known motif of cyclin dependent kinases. And indeed, the kinase activity analysis confirmed a significant upregulation of cyclin dependent kinases, predominantly CDK1 (or CDC2), with a median ratio only slightly deviated to positive values, but many outliers strongly upregulated after VE-821 pre-treatment (**figure 21C**). Many of these outliers were classified as so-called "regulatory" sites (*i.e.* sites with previously discovered and experimentally validated effects on the modified protein) with a known function in mitosis, or their function has not been

elucidated yet, but the corresponding phosphoproteins have been shown to have important roles in the onset of mitosis and mitotic progression. Examples of the most interesting CDK1-phosphorylated sites and their functions are given.

Seven phosphorylation sites were detected on **Stathmin (STMN1)**; three of them were upregulated in our study (Ser 16, Ser 25, and Ser 63). There are multiple kinases known or predicted to phosphorylate the upregulated sites; CDK1 dysregulation might be responsible for elevated Ser 25 phosphorylation. These STMN1 sites have been shown to be phosphorylated in a cell cycle specific manner and essential for G2/M transition and proper spindle formation (375). Nevertheless, increased Ser 16 and Ser 63 phosphorylation have been also observed after apoptosis induction (376). **Protein regulator of cytokinesis 1 (PRC1)** is a key regulator of cytokinesis shown to be phosphorylated by CDK1 in early mitosis. Increased phosphorylation of a "regulatory" Thr 481 site was detected, previously described to regulate PRC1 interaction with another mitotic kinase, Polo-like kinase 1 (PLK1) (377). Thr 926 phosphorylation of **Kinesin-like protein KIF11 (KIF11)** is a mitosis-specific phosphorylation conducted by CDK1 which regulates KIF11 interaction with mitotic spindle and thus regulates mitosis (378). Another example of an elevated mitosis-specific phosphorylation detected in our study is Ser 1213 phosphorylation of **DNA topoisomerase 2-alpha (TOP2A).** Ser 1213 has been shown to be phosphorylated by proline-directed kinases (CDK1 or ERKs) inducing the localization of TOP2A to mitotic chromosomes (379). **Sororin (CDCA5)** is CDK1-phosphorylated in mitosis (Ser 75 and Ser 79), and this modification causes its release from chromatin while affecting sister chromatid cohesion (380).

Protein phosphorylation of N-terminal domain of **Nucleolin (NCL)** has been shown to be essential for normal proliferation (381); Thr 121 detected in our study has been already detected as a substrate of CDK1 in high-throughput phosphoproteomic screen for CDK1 substrates (382). **Nuclear ubiquitous casein and cyclin-dependent kinase substrate 1 (NUCKS1)** - Ser 181 phosphorylation – is another example of a CDK1 substrate identified in a high-throughput experiment (382). Furthermore, Bensimon et al. showed that phosphorylation of NUCKS1 Ser 181 after neocarzinostatin (NCS) treatment was ATM-dependent (42), and it has been shown recently that NUCKS1 plays a role in homology directed repair of damaged DNA (383). **Lamina-associated polypeptide 2, isoform alpha (TMPO)** has been shown to be phosphorylated in a mitosis-specific manner

and might be important for post-mitotic nuclear assembly (384). However, Ser 424 upregulated in our study does not have any known function.

Components of nuclear lamina are known to be hyper-phosphorylated to induce reversible disintegration of nuclear envelope. We detected four upregulated phosphorylation sites of nuclear lamins: **Lamin-B1 (LMNB1;** Ser 23, Thr 20, and Thr 5) and **Lamin-B2 (LMNB2;** Ser 37) induced by VE-821 pre-treatment of irradiated cells.

Additionally, unscheduled CDK1 activity in G1 phase has been shown to trigger apoptosis in X-irradiated MOLT-4 cells (385). In our data, VE-821 significantly affected viability of MOLT-4 cells itself and in combination with IR and increased the number of early- and late- apoptotic cells. It is possible that in addition to G2/M checkpoint disruption and induction of post-mitotic cell death, the dysregulation of CDK1 by ATR inhibition contributes to the increased rate of apoptosis in MOLT-4 cells.

5.3.8.2. VE-821 upregulated Aurora A and B kinases further contributing to dysregulation of mitosis.

Kinases from the Aurora kinases family - Aurora kinases A and B - are master regulators of mitosis progression and onset of cytokinesis, whose activities require tight spatial and temporal regulation, and their dysregulation might cause errors in mitosis, faster progression through abscission checkpoint, and affect postmitotic genome surveillance. In our analysis, we found that the activities of these two kinases might be upregulated by VE-821 treatment (**figure 21C**). As in the case of CDKs, examples of the most interesting phosphorylation sites are given.

Targeting protein for Xklp2 (TPX2) is a spindle assembly factor, whose activity is tightly interconnected with Aurora kinase A activity. TPX2 contributes to Aurora A activation (386), and the other hand, Aurora A has been shown to phosphorylate TPX2 on Ser 121 and Ser 125 to regulate mitotic spindle length and control microtubule flux (387). In addition to these two known "regulatory" sites we detected three more upregulated phosphorylation sites on this protein that were predicted to be possible substrates of Aurora A (Ser 486, Thr 369, and Ser 738).

Kinesin-like protein KIF2C (KIF2C) Ser 115 has been shown to be phosphorylated by Aurora B previously, and this phosphorylation regulates KIF2C interaction with centromeres and kinetochores and its microtubule depolymerisation activity. Thus, it regulates the turnover of microtubules at the kinetochore and chromosome segregation during mitosis (388). Another known Aurora B substrate found upregulated

in our study was **Chromobox protein homolog 5 (CBX5)** that has been previously shown to be hyper-phosphorylated during mitosis (389).

Notably, we found hyper-phosphorylation of **Antigen KI-67 (MKI67)** (from 22 sites detected, 12 upregulated in GRT), with most of the sites predicted to be substrates of Aurora A, CDK1, or NEK kinases by Networkin 3. MKI67 is a protein essential for normal cellular proliferation (390) and has been shown to interact with known mitotic proteins (391).

Taken together, our data indicate that ATR inhibition induced dysregulation of the main mitotic kinases. The results are in concordance with previous data, which were obtained using similar treatment in a different leukemic cell line HL-60 (133), in which dysregulation of CDK1, PLK1, and NEK2 was observed. Data mining in published studies confirmed that many of the substrates assigned to each one of these mitotic kinases have already been described as the essential players in cell cycle and mitosis control. Moreover, we found multiple regulated phosphorylation sites on these proteins, which might be worth functional validation in further studies.

5.3.9. Downregulated mTOR and its downstream p70s6k kinase indicate possible impact of VE-821 on cellular growth and metabolism.

5.3.9.1. The key regulator of cellular metabolism, Serine/threonine protein kinase mTOR, was inhibited by 10 μM VE-821 treatment, possibly contributing to the growth inhibition.

To our surprise, in the 1D enrichment analysis of kinases assigned to their substrates based on known kinase-substrate relationships, we found a significant downregulation of the **Serine/threonine protein kinase mTOR (mTOR).** The protein kinase **mTOR** is the principle regulator of cellular metabolism promoting anabolic processes and inhibiting catabolic processes such as autophagy. It integrates signals from different upstream pathways triggered by a wide variety of signals including nutrients, hormones, growth factors, and also cellular stresses to regulate cell growth, metabolism, cell survival, protein synthesis, and transcription (reviewed in (31)). In total, we found seven known direct mTOR targets downregulated in our study and several other proteins included in "mTOR signalling pathway" from KEGG pathway database (depicted in **figure 23A** and summarized in **figure 23B**).

Four of the mTOR-phosphorylated proteins are involved in transcription and translation regulation and thus contribute to regulation of cell growth and proliferation. **Eukaryotic translation initiation factor 4E-binding protein 1 (EIF4EBP1)** Ser 65 is a known "regulatory" site targeted by mTOR or MAPK-driven pathways. Together with phosphorylation of Thr 70, Ser 65 phosphorylation affects translation initiation – when hypo-phosphorylated, EIF4EBP1 strongly binds to EIF4E, an essential member of the translation initiation EIF4 complex (392). Furthermore, we found four downregulated phosphorylation sites on **Protein PAT1 homolog 1 (PATL1;** Ser 179 and Ser 184) and **La-related protein 1 (LARP1;** Ser 766 and Ser 774); both proteins have been described as downstream mTOR targets involved in regulating mRNA stability and degradation (393,394). Both of them were also identified as rapamycin sensitive phosphorylation sites in a high throughput phosphoproteomic screen for potential mTOR substrates (395). Moreover, we also detected downregulation of an mTOR mediated phosphorylation of **Repressor of RNA polymerase III transcription MAF1 homolog (MAF1)** a previously described regulator of transcription; Ser 75 phosphorylation has been described as a "regulatory" protein modification decreasing RNA polymerase III (Pol III) transcription repressing ability of MAF1 (396).

In addition to proteins involved in translation regulation, we also identified significantly changed phosphorylation of two phosphoproteins linked to autophagy, an evolutionarily conserved process that enables degradation and recycling of proteins or whole organelles to maintain cellular homeostasis under both normal and stress conditions (reviewed in (397)). **Death-associated protein 1 (DAP1)** is a suppressor of autophagy in growing cells that is functionally silenced through mTOR dependent phosphorylations on Ser 3 (downregulated in our study) and Ser 51. Inactivation of mTOR has been shown to rapidly reduce phosphorylation of these sites and activation of the repressor function of DAP1 (398). **Serine/threonine-protein kinase ULK1 (ULK1)** is a protein kinase that plays a key role inducing autophagy in response to starvation. Under normal growth condition, ULK1 is phosphorylated and negatively regulated by mTOR. Serine 450, detected in our study and predicted to be a substrate of mTOR by the iGPS prediction algorithm, has been shown to be dephosphorylated upon starvation (399). Unfortunately, we did not detect the Ser 638/758 that have been further validated as functional phosphorylation sites inhibiting autophagy induction by ULK1 under normal cell growth conditions (399).

A Significantly changed phosphorylation sites in mTOR signalling pathway (KEGG)

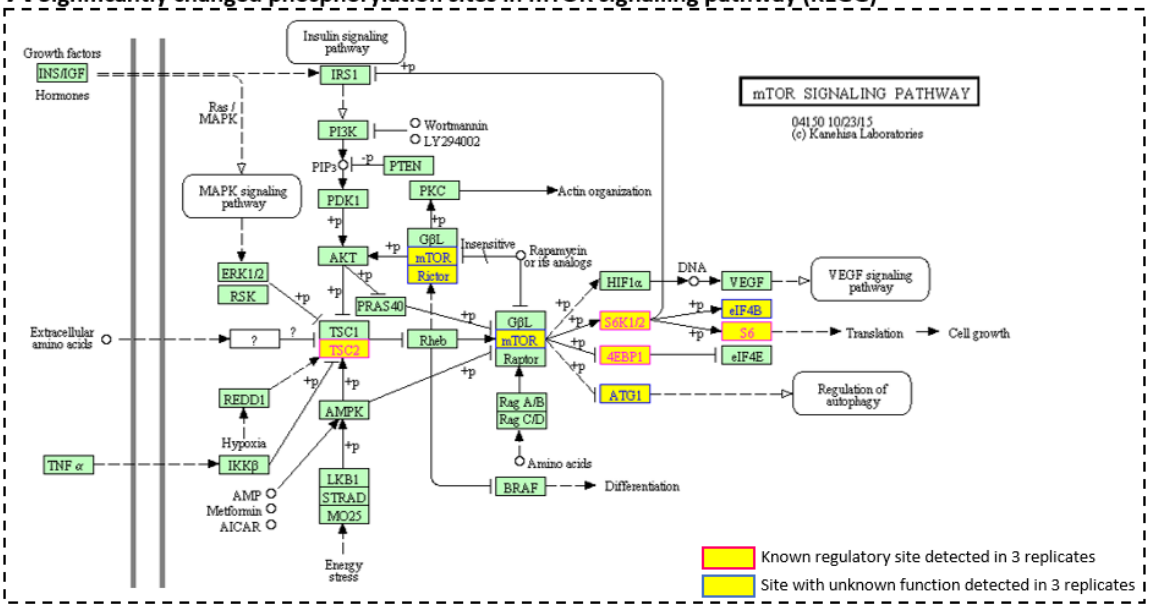

B Summary of phosphorylation sites in mTOR pathway and mTOR substrates detected in our study

AA	Pos.	Gene name	Protein name	regulated	Regulatory site	Known kinase
S	3	DAP	Death-associated protein 1	DOWN	YES	NaN, but mTOR dependent
S	359	EIF4B	Eukaryotic translation initiation factor 4B	DOWN		NaN
S	65	EIF4EBP1; 4EBP1	Eukaryotic translation initiation factor 4E-binding protein 1	DOWN	YES	mTOR
S	65	EIF4EBP1; 4EBP1	Eukaryotic translation initiation factor 4E-binding protein 1	DOWN	YES	DYRK2; ERK1; ERK2; mTOR
S	766	LARP1	La-related protein 1	DOWN		mTOR
S	774	LARP1	La-related protein 1	DOWN		mTOR
S	75	MAF1	Repressor of RNA polymerase III transcription MAF1 homolog	DOWN	YES	mTOR
S	1261	MTOR	Serine/threonine-protein kinase mTOR	UP		NaN
S	179	PATL1	Protein PAT1 homolog 1	DOWN		mTOR
S	184	PATL1	Protein PAT1 homolog 1	DOWN		mTOR
S	1177	RICTOR	Rapamycin-insensitive companion of mTOR	DOWN		NaN
S	236	RPS6; S6	40S ribosomal protein S6	DOWN	YES	p70S6K; p90RSK; PKCD; RSK2
S	240	RPS6; S6	40S ribosomal protein S6	DOWN		p70S6K
S	235	RPS6; S6	40S ribosomal protein S6	DOWN	YES	p70S6K; p90RSK; PKCD; RSK2
S	427	RPS6KB1; S6K	Ribosomal protein S6 kinase beta-1	DOWN	YES	NaN
T	1462	TSC2	Tuberin	UP	YES	Akt1
S	450	ULK1; ATG1	Serine/threonine-protein kinase ULK1	DOWN		NaN

C Effect of irradiation and VE-821 treatment on mTOR activity

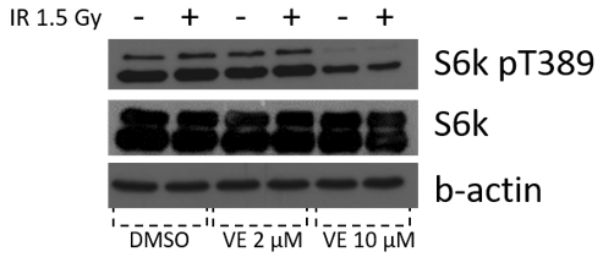

Figure 23: Significant changes in mTOR signalling pathway. *Proteins with significantly changed phosphorylation sites were mapped onto KEGG signalling pathways* ***(A)***. *Summary of all phosphorylation sites comprised in "mTOR signalling pathway" pathway in KEGG database and phosphorylation sites that are known mTOR substrates or known to be mTOR-dependent* ***(B)***. *Immunoblotting analysis of mTOR activity* ***(C)***. *Cells were collected 2 hour after IR (1.5 Gy). Activity of mTOR was monitored via the detection of its target pT389 of p70S6K (S6K, RPS6KB1). The expression state of p70S6K was also evaluated. β-actin expression was analysed as a loading control.*

To further validate and investigate the VE-821-mediated mTOR inhibition predicted from our SILAC data, we performed a confirmation experiment using an antibody detection of a regulatory **Ribosomal protein S6 kinase beta-1 (p70s6K)** Thr 389 phosphorylation site that is commonly used to examine the activity of mTOR in molecular biology studies. As shown in **figure 23C**, while irradiation by a dose of 1.5 Gy did not affect p70S6K phosphorylation, mTOR-dependent p70S6K phosphorylation was almost diminished after 10 μM VE-821 treatment in both irradiated and sham-irradiated cells. On the other hand, 2 μM VE-821 did not have any significant effect on Thr 389 phosphorylation site.

The mTOR inhibition by 10 μM VE-821 and not 2 μM treatment might correlate with the results of our proliferation and DNA analysis experiments and explain the difference we observed between the 2 μM and 10 μM VE-821 treated groups. While both concentrations of the inhibitor radiosensitized MOLT-4 cells, 10 μM had much stronger inhibitory effect on the number of viable (metabolically active) sham-irradiated cells (**figures 10** and **11**). Likewise, while both concentrations caused the disruption of the IR-induced G2/M arrest, it was only the higher concentration, which caused a significant accumulation in G1 phase in sham-irradiated cells (**figure 13**). These conclusions are supported by the fact that mTOR inhibition triggers G1 metabolic checkpoint and inhibits cell growth and proliferation (reviewed in (400). The mTOR inhibition by 10 μM VE-821 might also explain the high sensitivity of MOLT-4 cell line to VE-821 treatment. It has been shown that *PTEN*-deficient tumours were more likely to be sensitive to mTOR inhibition (401,402), and as it was mentioned above, MOLT-4 cells suffer from homozygous deletion of *PTEN*.

5.3.9.2. P70S6K, an important downstream effector of mTOR, was inhibited by 10 μM VE-821 treatment and likely contributed to translation inhibition.

In addition to the downregulation of mTOR, we also observed a significant downregulation of the **p70S6K** (or RPS6KB1) in all kinase activity analyses (**figure 21C**). P70S6K is an important kinase that acts downstream of mTOR to promote protein synthesis and cellular proliferation (403,404). In addition to the western blotting detection of changes in Ser 379 phosphorylation (**figure 23C**) induced by VE-821 treatment, we also detected another downregulated mTOR dependent "regulatory" phosphorylation site (Ser 427) in our phosphoproteomic data. From the known p70s6k substrates, we detected three strongly downregulated phosphorylation sites on **40S ribosomal protein S6 (RPS6)** – Ser

235, Ser 236, and Ser 240. These phosphorylation sites are phosphorylated by ribosomal kinases to initiate translation (405), and thus the inhibition of their phosphorylation causes inhibition of protein synthesis. Moreover, iGPS and Networkin 3 predicted two more members of the translation machinery to be downregulated substrates of RSKs - **Eukaryotic translation initiation factor 3 subunit A (EIF3A)** Ser 584 and **Eukaryotic translation initiation factor 4B (EIF4B)** Ser 119, providing further evidence for translation inhibition caused by inhibitor treatment.

5.3.9.3. The downregulation of dihydroorotase phosphorylation, a substrate of p70S6K, showed a possible link to nucleotide synthesis alteration induced by VE-821 treatment.

Surprisingly, on the known/predicted p70S6K substrates list detected in our study, we did not find phosphoproteins involved solely in protein synthesis. **Dihydroorotase (CAD)** is an enzyme required for the first steps of *de novo* pyrimidine synthesis. Phosphorylation on Ser 1859 by p70S6K downstream of mTOR stimulates dihydroorotase activity of CAD to induce pyrimidine synthesis (406). Ser 1859 was detected to be downregulated in our study, suggesting that VE-821 treatment might also hamper synthesis of nucleotides, which are necessary for both cellular proliferation and DNA repair after DNA damage induction.

Based on this striking possibility of nucleotide synthesis dysregulation induced by VE-821 treatment, we further examined our data to search for regulated phosphorylation sites located on enzymes included in nucleotide synthesis pathways. In all three replicates, we identified two additional regulated phosphorylation sites on proteins from the *de novo* purine synthesizing pathway: **Phosphoribosylglycinamide formyltransferase (GART)** Tyr 348 and **Phosphoribosylaminoimidazole carboxylase (PAICS)** Ser 27; the latter one has been identified as a potential substrate of CDKs in two high-throughput phosphoproteomic screenings (407,408); however, none of these enzymes has been proven to be regulated by phosphorylation, and thus we can only speculate whether these two phosphorylation events might have some effect on *de novo* purine synthesis or not.

5.4. Metabolomic analysis of VE-821 treated MOLT-4 cells

In the phosphoproteomic analysis of VE-821 treated irradiated cells, changes in the mTOR activity were detected via kinases activity analysis and further confirmed by western blotting. As mTOR is the principal regulator of cellular metabolism (reviewed in (31)), this finding raised an intriguing question – whether the inhibitor treatment modulates cellular metabolism after irradiation. We further examined our data and found several metabolic enzymes containing phosphorylation sites affected by VE-821.

The metabolic responses of different cell lines to various doses of IR have been investigated in several studies (409–411). Briefly, these studies showed that IR triggered production of free oxygen radicals by radiolysis of water induced changes in glutathione levels, disturbed energetic metabolism resulting in a rapid decrease of cellular ATP levels, and increased levels of free amino acids, choline, and lipids, which are produced by degradation of damaged proteins and membranes. However, to our knowledge, no study has been published yet investigating the modulation of this response by small molecular kinase inhibitor of any of the PIKKs family. Therefore, we performed a metabolomic analysis of irradiated MOLT-4 cells, whose response to IR was modulated by ATR (and mTOR) inhibition by 10 μM VE-821.

Hierarchical clustering of the measured metabolomic data revealed two main patterns of behaviour induced by VE-821. In the first case, the metabolites showed significant either decreasing or increasing trend between the two time intervals (six and twelve hours after IR), and this trend was further potentiated by the addition of the inhibitor. In the second case, the metabolites showed no significant trend over time in irradiated groups and the inhibitor significantly altered the response of MOLT-4 cells to IR (**figure 17**). The main significant changes in the metabolome of MOLT-4 cell line occurred in a group of metabolites involved in cellular antioxidant system, intermediates of glucose metabolism and citrate cycle, nucleosides, nucleotides, deoxynucleotides, free amino acids, and acylcarnitines.

5.4.1. Exposure to VE-821 potentiated changes in cellular antioxidant defence, degradation of proteins and membranes, and damage to mitochondria induced by IR.

When cells are exposed to IR, cellular structures can be damaged by ionization directly by deposition of energy, but also indirectly by water radiolysis and stimulation of nitric oxide synthases and NADPH oxidases, which leads to generation of highly reactive oxygen and nitrogen species (ROS/RNS) secondarily attacking nucleic acids and other biomolecules such as proteins and lipids contained in membranes (reviewed in (412)). Reduced glutathione (GSH) is an important cellular antioxidant, and the reduced/oxidized glutathione ratio (GSH/GSSG) is a sensitive biomarker of oxidative stress (413). It has been reported previously that radiation induced a significant decrease in cellular glutathione levels (409,410). In our study, we observed a decrease in GSH over incubation time and this decrease was amplified by inhibitor exposure (**figure 24A**). However, GSSG was also depleted as well as important precursors of GSH biosynthesis (glutamate and glycine, **figure 25A**). Therefore, we assume that the overall decrease of GSH/GSSH pair was caused by increased turnover of GSH and missing precursors at the same time. Additionally, we observed increased levels of allantoin and decreased levels of taurine. Allantoin can be formed in the presence of ROS by non-enzymatic reactions, and similarly to GSH, it can be used as a marker of oxidative stress (414). Taurine in an intermediate in metabolism of methionine and an anti-oxidant, and its decrease might indicate its elevated consumption in VE-821 treated cells as a part of preventive mechanisms counter-acting oxidative stress. Taken together, our data provide indirect evidence that the cellular response to oxidative stress induced by IR might have been affected by the pre-incubation with the inhibitor.

In addition to the changes in cellular redox system, direct effects on proteins and membranes were also observed. Increased levels of several amino acids (phenylalanine, proline, tryptophan, tyrosine, valine, isoleucine, and methionine) indicate increased turnover of proteins which were damaged by ROS/RNS exposure (**figure 25**). Elevated levels of docosahexaenoic acid and choline provided evidence for the increased membrane degradation induced by the inhibitor treatment (**figure 24B**). IR induces autophagy by inhibition of mTOR (415) probably via a pathway involving ATM and AMPK (416). VE-821 10 μM, but not 2 μM inhibited mTOR in both sham-irradiated and irradiated MOLT-4 cells (**figure 23C)**, and we also detected several significantly changed

phosphorylations in autophagy-regulating proteins. Thus, we can hypothesize that the treatment might have induced degradation of damaged structures (potentially via autophagy), resulting in increased accumulation of degradation products in cells.

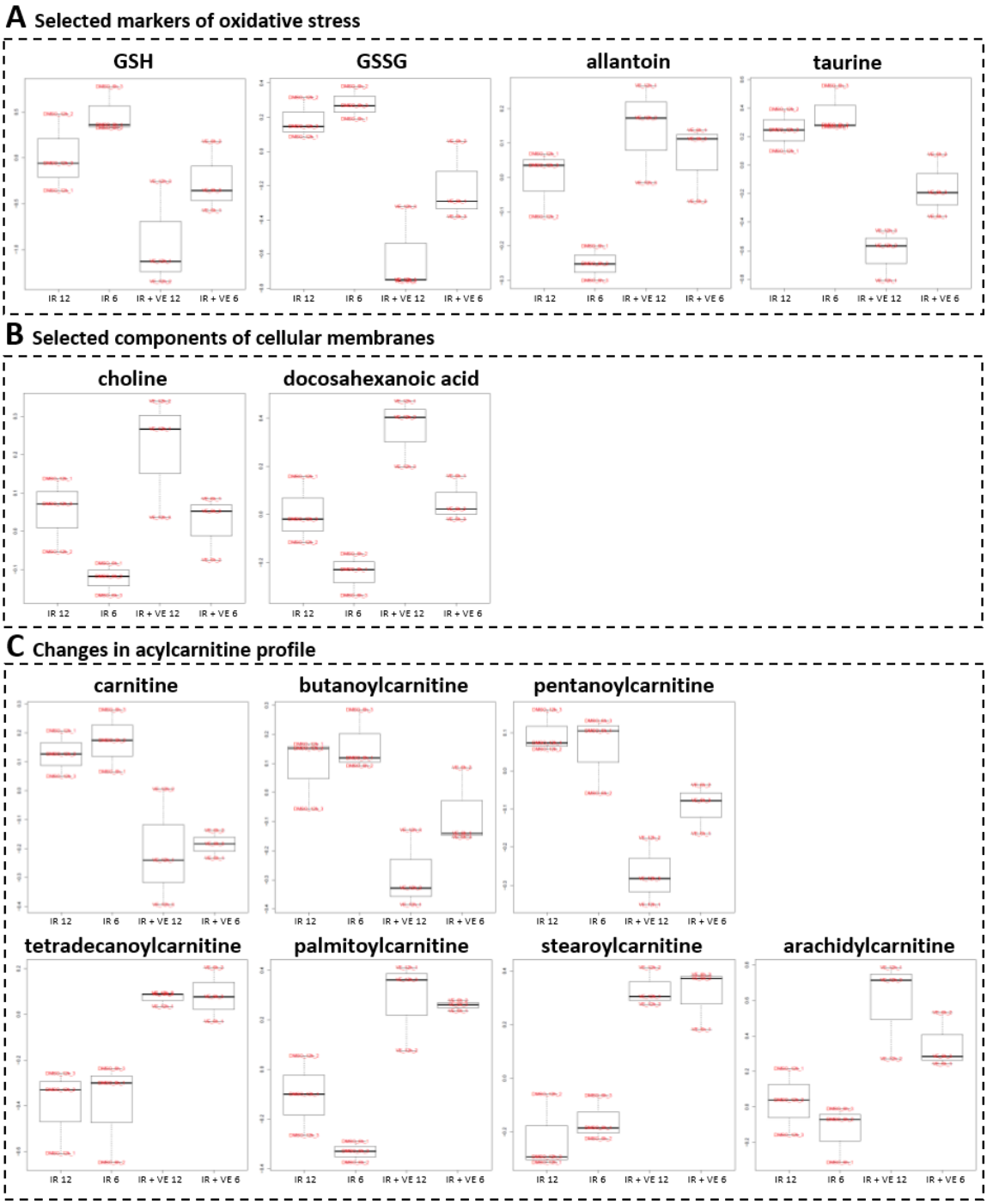

Figure 24: VE-821 induced changes in cellular response to oxidative stress (A), degradation of membranes (B), and acylcarnitine profile (C). *GSH – glutathione, GSSG – glutathione disulphide (oxidised glutathione), IR – irradiated cells pre-treated with DMSO, VE – irradiated cells pre-treated with 10 μM VE-821*

We further observed prominent changes in the acylcarnitine profile (**figure 24C**), which might indicate mitochondrial disturbances induced by VE-821. Increased levels

of long-chain acylcarnitines (tetradecanoyl-, palmitoyl-, and stearoyl- carnitine) and decreased levels of free carnitine, isovaleryl-/ methyl- butyrylcarnitine, and malonyl-/ 3-hydroxy- butyrylcarnitine were observed. Acylcarnitine changes have been already observed in a study investigating metabolic effects of low dose (20 mGy) X-irradiation (411) and in a targeted lipidomic study investigating changes in livers of irradiated mice (417). Moreover, it has been shown that L-carnitine acts as a free-radical scavenger protecting irradiated mice from oxidative damage in response to IR (418). Our observation of the lipid changes in mitochondrial membrane might be explained by lipid peroxidation induced by increased ROS generation in VE-821 treated cells, which was evidenced above as decreased GSH and altered allantoin and taurine levels.

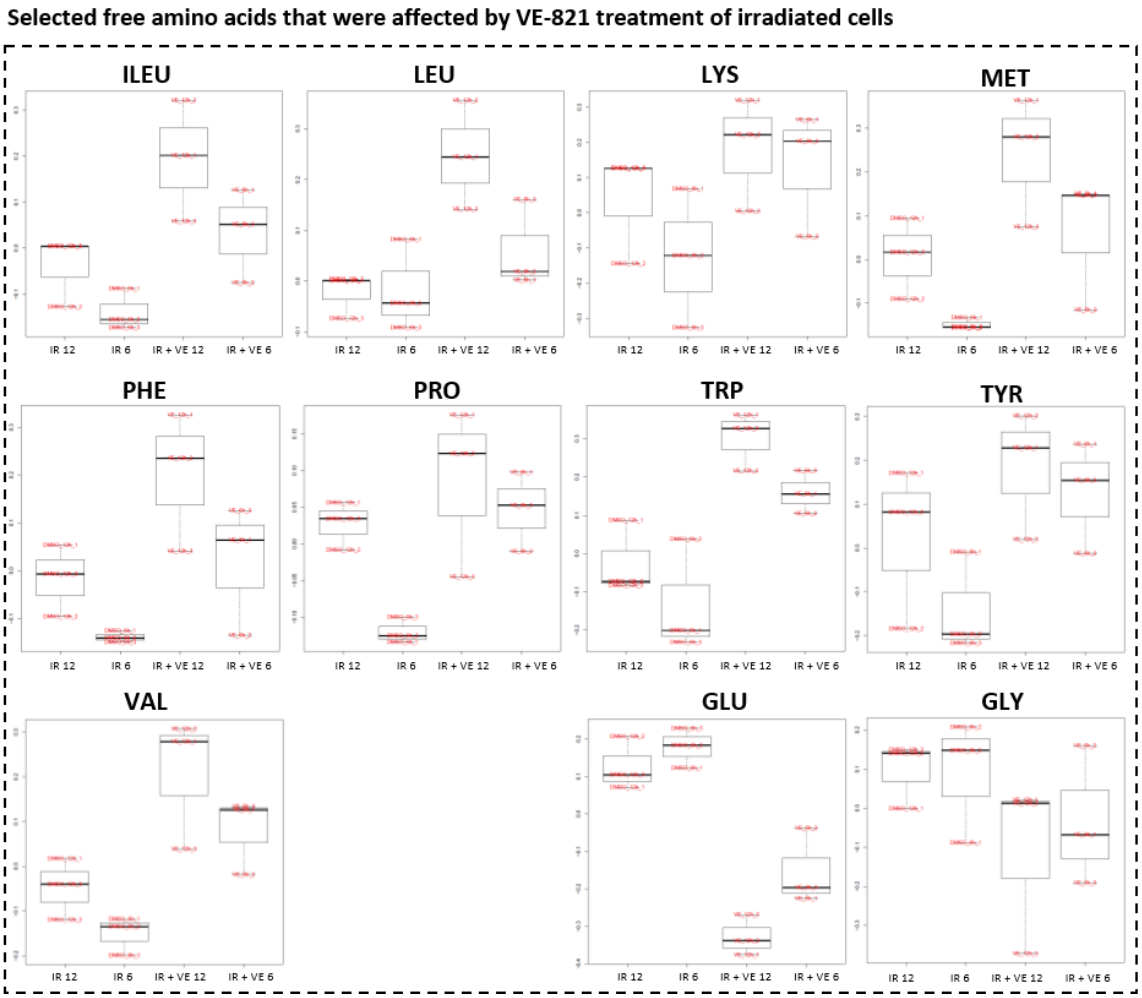

Figure 25: Changes in free amino acids levels in irradiated and VE-821 treated cells*. IR – irradiated cells pre-treated with DMSO, VE – irradiated cells pre-treated with 10 μM VE-821*

5.4.2. **VE-821 potentiated the energy metabolism disruption induced by IR.**

IR has been shown to disturb energetic metabolism demonstrated by a rapid decrease of cellular ATP levels in irradiated cells (409,419) and serum ATP levels in irradiated mice (420). In our study, we found decreased levels of nucleoside triphosphates (NTPs; ATP, GTP, CTP, and UTP), diphosphates (NDPs; ADP and UDP), and their derivatives (UDP-hexoses, GDP-hexoses, and UDP-N-acetylglucosamine) and on the contrary, increased levels of ribonucleosides (adenosine, guanosine, and pseudouridine) and bases (uracil). The overview of changes in purine and pyrimidine metabolism induced by VE-821 is given in **figures 26** and **27**.

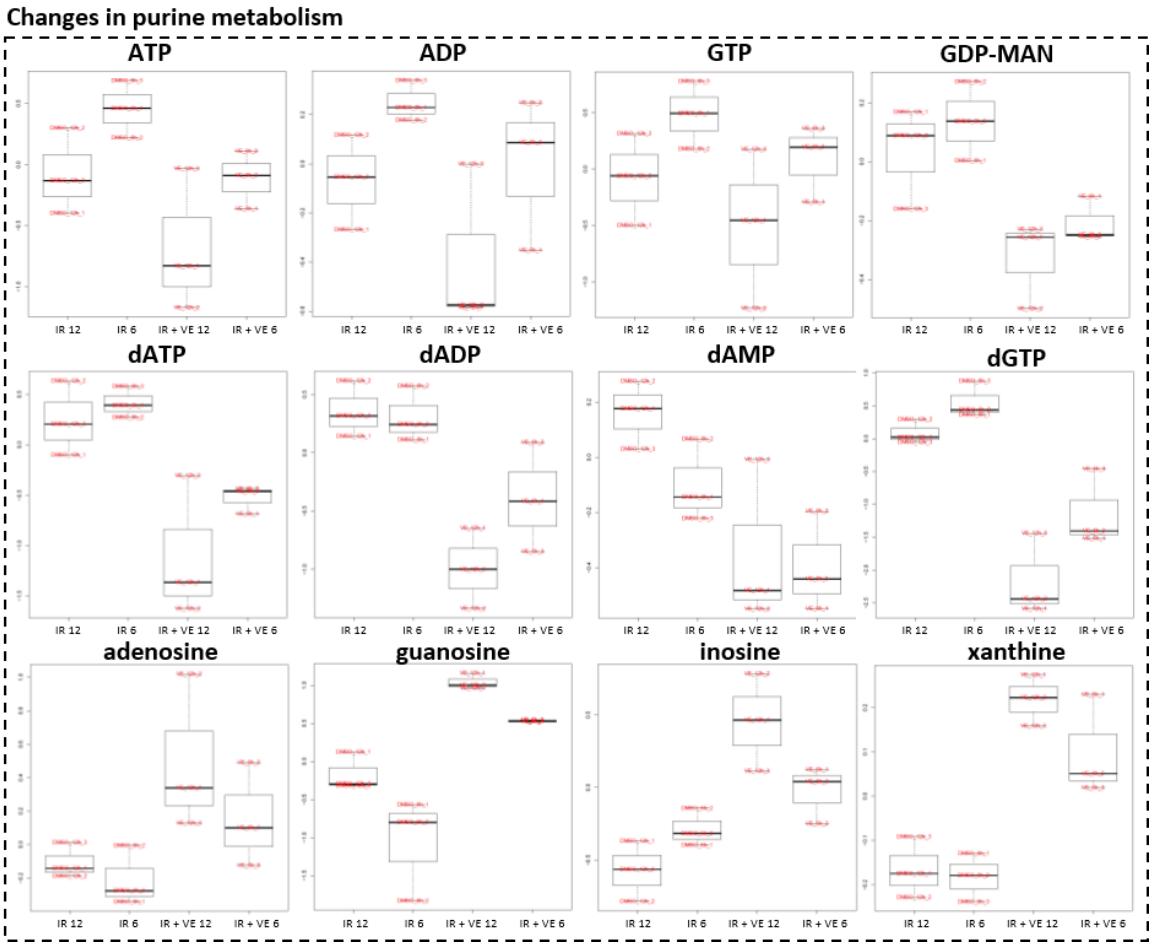

Figure 26: Changes in purine metabolism induced by VE-821 in irradiated cells. *IR – irradiated cells pre-treated with DMSO, VE – irradiated cells pre-treated with 10 μM VE-821. MAN - mannose*

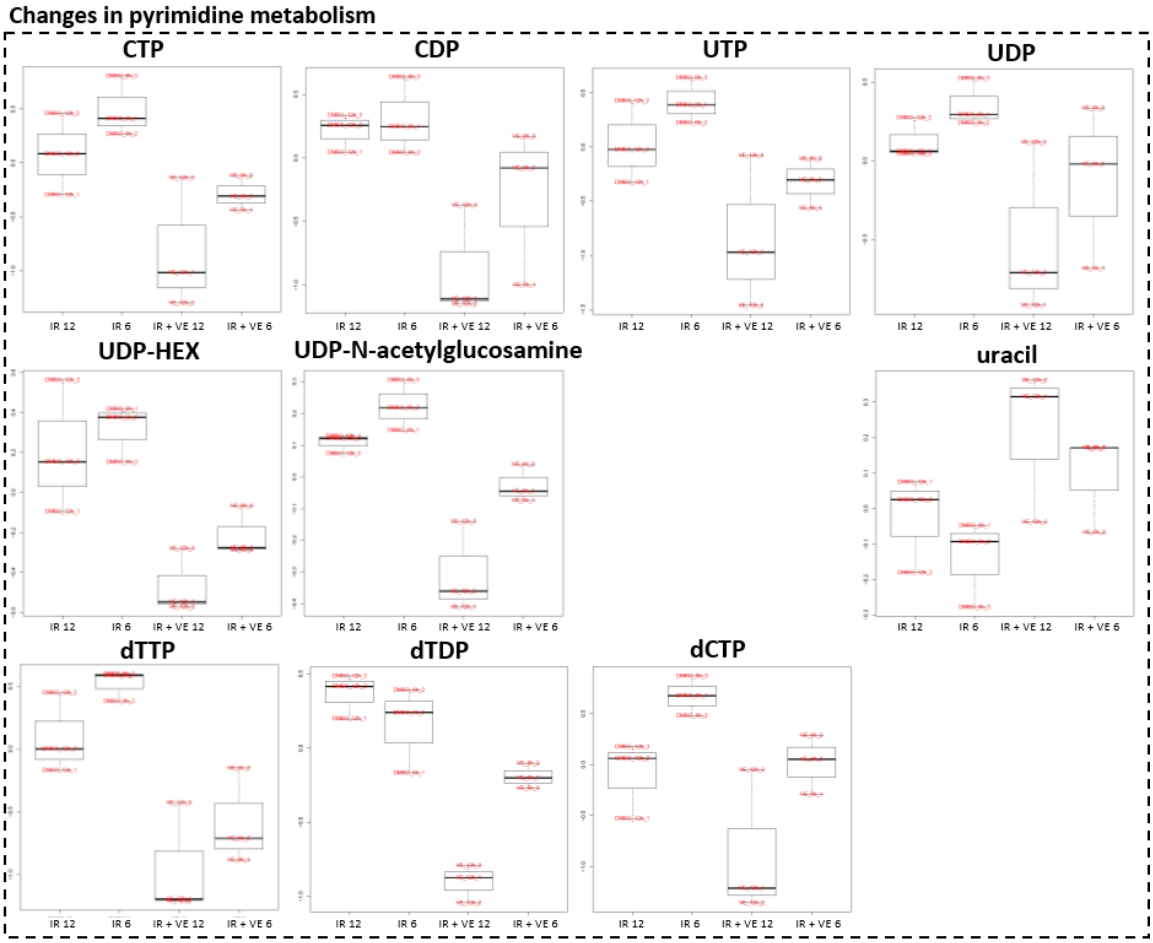

Figure 27: Changes in metabolism of pyrimidine induced by VE-821 in irradiated MOLT-4 cells. *IR – irradiated cells pre-treated with DMSO, VE – irradiated cells pre-treated with 10 μM VE-821. HEX - hexose*

Decreased levels of high-energetic phosphorylated compounds might indicate disruption in energy metabolism induced by exposure to IR. Importantly, VE-821 amplified the energy depletion caused by IR. It is not clear from our data, whether the observed time-dependent decrease is due to increased utilization of NTPs needed as a "molecular fuel" for cellular signalling, reparation processes, and programmed cell death following DNA damage induction by IR or by their decreased synthesis in damaged mitochondria.

Significant changes were also found in **glycolysis** (**figure 28**). Increased glucose and decreased intermediates of glycolysis (glucose 6-phosphate, 3-phosphoglycerate, and phosphoenolpyruvate) could probably reflect inhibition of hexokinase - the first step of glycolysis. The aforementioned insufficiency of ATP for an initial deposit energy into the first reaction could be the reason. On the other hand, decreased intermediates of glycolysis can be interpreted as preferential utilization of glycolysis. This hypothesis

could be supported by pronounced time-dependent increase of lactate in irradiated control and VE-821-treated cells. We also detected an activating phosphorylation on **phosphofructokinase 1 (PFKL)** Ser 775 in two experimental replicates of our phosphoproteomic analysis**,** which has been previously shown to be responsive to insulin treatment and activating glycolysis (421), suggesting that the metabolic flux through glycolysis might be increased one hour after irradiation. However, further metabolomic and phosphoproteomic experiments covering multiple time points would be necessary to fully understand the temporal regulation of glycolysis upon IR and VE-821 treatment. We also observed significant modulation of **citric acid cycle** metabolites (**figure 28**). Markedly lower levels of aconitate, malate, and citrate/isocitrate were found in VE-821 treated cells; moreover, citrate/isocitrate showed a time-dependent decrease in control irradiated-only cells. On the contrary, succinate and fumarate were slightly increased in VE-821 treated cells. We assume that these intermediates could have been replenished by anaplerotic reaction from the amino acids obtained by protein degradation.

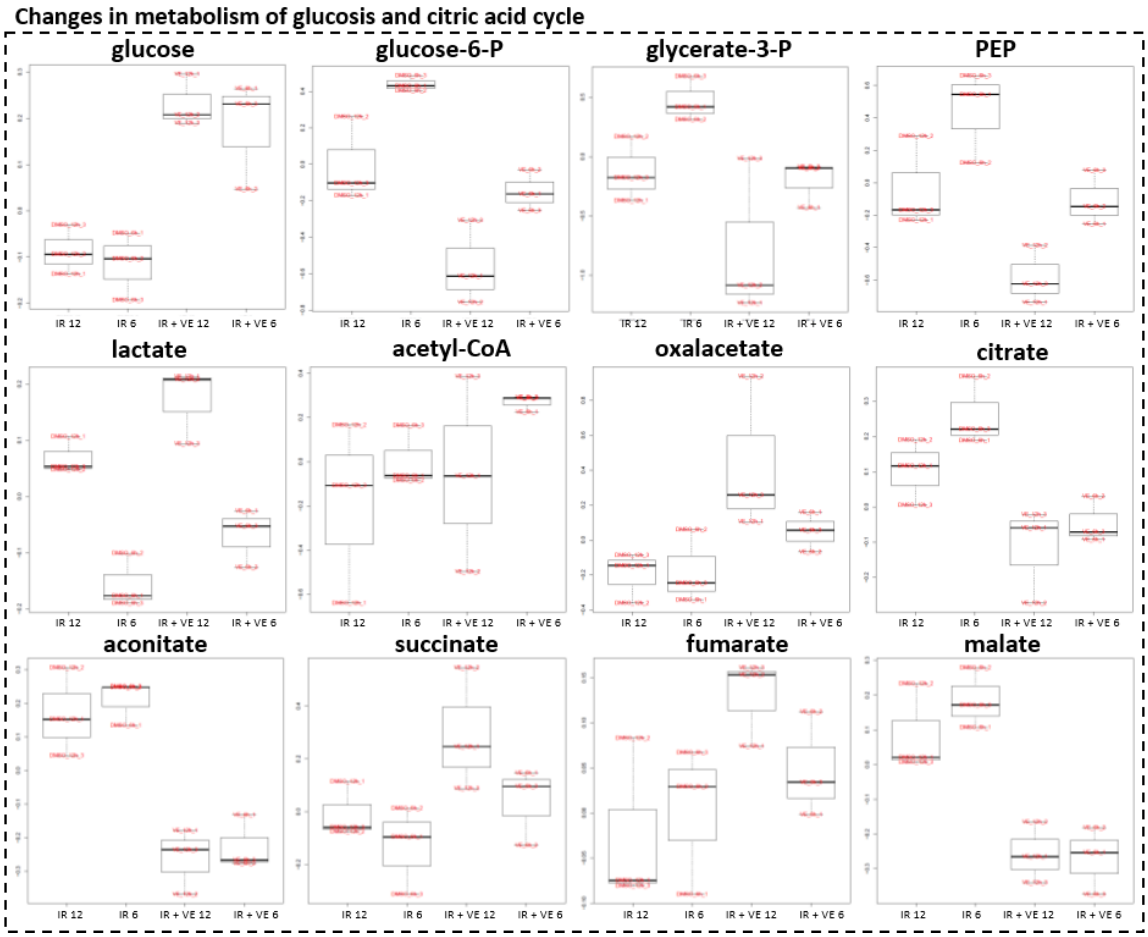

Figure 28: Selected metabolites included in metabolism of glucose and citric acid cycle. *IR – irradiated cells pre-treated with DMSO, VE – irradiated cells pre-treated with 10 μM VE-821. PEP - phosphoenolpyruvate*

5.4.3. VE-821 affected deoxynucleotide pools in irradiated cells.

Decreased levels of deoxynucleoside diphosphates (dNDPs; dADP and dTDP) and triphosphates (dNTPs; dATP, dGTP, and dTTP) were found in VE-821 treated irradiated cells. dCTP was also decreased due to VE-821; moreover, time-dependent reduction was observed in irradiated control cells. We also found several purine and pyrimidine bases and ribosides (xanthine, inosine, cytidine, uridine, and thymidine) elevated in VE-821 treated cells; nucleoside monophosphates (AMP and GMP) were slightly reduced (**figure 26** and **27**).

Deoxyribonucleotides arise either via *de novo* pathways, which involve step-by-step assembly of purine and pyrimidine rings and formation of deoxyribonucleosides diphosphates from their corresponding ribonucleosides diphosphates precursors, or by salvage pathways involving reutilization of nucleosides and nucleobases produced

by nucleic acid degradation (reviewed in (422)). Thus, in principle, the deoxynucleotide levels might have decreased either by downregulation of their *de novo* synthesis or due to their degradation and downregulation of the salvage pathways. Importantly, dNTPs damaged by IR and oxidised due to increased levels of ROS in irradiated cells are degraded by hydrolysis, largely contributing to dNTPs depletion upon irradiation.

As discussed above, in our study, we observed a time-dependent decrease in NDPs and NTPs, i.e. the precursors of dNDPs and dNTPs in *de novo* pathways, which was further amplified by the inhibitor, supporting the idea that the decrease in dNTPs might have been induced by insufficiency of the precursors for their *de novo* synthesis. Furthermore, we also detected a significantly decreased stimulating phosphorylation on **CAD** Ser 1859, an important regulator of *de novo* pyrimidine synthesis, and two phosphorylations on two enzymes involved in *de novo* purine biosynthesis (**GART** and **PAICS**) with unknown functions. The salvage pathways could have been also affected by the inhibitor treatment; this idea is supported by a recent study showing that activity of **deoxycytidine kinase** (**dCK**) is ATR-dependent after stress induction (423). dCK catalyses the first and rate limiting step of the deoxyribonucleotide salvage pathway (424), and as a consequence of its broad substrate specificity (which comprises deoxycytidine, deoxyadenosine, and deoxyguanosine), it is the main enzyme in the salvage of deoxyribonucleotides (reviewed in (425)). Beyaert et al. investigated the dCK activity dependency on ATM and ATR after different stress inducing stimuli. VE-821 significantly reduced upregulation of dCK induced by various genotoxic agents. Importantly, after irradiation, dCK activity was dependent on ATR only in ATM-deficient cells (423). However, it is necessary to note that the authors examined short time intervals after irradiation (two hours), when ATM signalling is predominant. It is possible that after longer incubation with the inhibitor, VE-821 might inhibit dCK even in irradiated cells with functional ATM pathway – since the basal activity of dCK has been shown to be significantly downregulated by ATR silencing (423). Thus, it is apparent that several mechanisms could contribute to dNTPs depletion upon IR in VE-821 treated cells. Further validation experiments would be necessary to reveal the exact mechanism.

6. Summary of the most important findings

- From the plethora of protocols for selective enrichment of phosphopeptides published so far, we selected four, which were applied for phospho-enrichment using different chromatographic resins with subsequent detection of enriched phosphopeptides by MALDI-TOF MS. After the first tests, where we evaluated the selectivity for phosphopeptides and enrichment efficiency from low complex samples composed of standard phosphorylated and non-phosphorylated peptides, **Titansphere®** particles and **NuTips®** were selected for further testing using more complex samples. Protocol including **200 mM glutamic acid** as a selectivity-enhancing additive was selected as the most beneficial.
- Using HeLa cell line lysate as the more complex sample, **Titansphere®** particles were shown to be more efficient and advantageous than the **NuTips®,** and hence they were selected for further studies investigating the phosphorylation response of MOLT-4 cells to the combination of IR and DDR inhibitor treatment.
- We showed that MOLT-4 cells were **radiosensitized** by both high potent inhibitors of ATM and ATR, **KU55933** and **VE-821**, respectively. While the effect of KU55933 was shown to be mostly radiosensitizing without affecting the proliferation and viability of sham-irradiated cells, treatment with VE-821 induced two distinct phenotypes depending on the dose.
- Treatment with **2 μM VE-821** caused mostly radiosensitization and disruption of the G2/M arrest without affecting the viability of sham-irradiated cells. On the other hand, **10 μM VE-821** treatment was characterized by marked proliferation inhibition (with slight, but significant G1 arrest) and decreased viability of MOLT-4 cells in both single inhibitor treatment and its combination with IR.
- Phosphoproteomic analysis revealed the complexity of the cellular response to IR modulated by 10 μM VE-821 treatment. In this analysis, we detected **9285 phosphorylation sites from 3090 protein groups**. By applying GRT, we identified 623 differentially regulated phosphorylation sites; most of them were upregulated (431). Using bioinformatic tools available, we aimed to describe

comprehensively, which protein kinases and signalling pathways might be affected by the inhibitor treatment upon irradiation.

- Gene ontology terms over-representation analysis revealed that proteins with regulated phosphorylation sites were significantly over-represented in **nucleus**, specifically in **chromosomes**, **mitotic spindle**, and **replication fork**; involved in **chromatin organization**, **DNA repair** and **metabolism**, **cell cycle**, and **regulation of transcription factors**.
- Signalling pathways over-representation analysis identified pathways involved in DNA repair, replication, telomeres synthesis, apoptosis, regulation of mitosis, transcription factors regulation, and chromatin regulation via histones modification, but also pathways primarily related to cellular metabolism.
- Based on kinase activity inference, we detected a **decreased activity of ATR**, which was in concordance with our expectations and antibody-based detection of ATR activity using western blotting and thus provided an important **confirmation of the validity of our data**. Among the known and predicted ATR substrates detected in our study, several DDR proteins were detected with significantly downregulated phosphorylation sites, such as members of the **MRN complex**, **BRCA1-BRCT/Abraxas complex**, and members of the **Fanconi anaemia pathway**.
- The activity of several mitotic kinases was modulated by VE-821 treatment, which was in concordance with previous knowledge of the dominant role of ATR/Chk1 pathway in triggering the S- and G2/M phase checkpoints. In addition to **CDKs** upregulated in the response to VE-821 treatment, we found known or predicted substrates of **Aurora A**, **Aurora B**, and **NEK** kinases with upregulated phosphorylation. We found multiple regulated phosphorylation sites on known "mitotic proteins" such as **CBX5**, **CDCA5**, **KIF2C**, **KIF11**, **PRC1**, **STMN1**, **TOP2A**, and **TPX2**. Thus, the inhibitor treatment might affect both **progression through G2/M checkpoint** and **mitosis**.
- After irradiation, 10 μM VE-821 was shown to inhibit the main regulator of cellular metabolism - **mTOR**, together with its downstream effectors **P70S6K** and **CAD**. Their inhibition was inferred from downregulation of several of their phosphorylation targets: **CAD**, **EIF3A**, **EIF4B**, **EIF4EBP1**, **LARP1**, **MAF1**, **PATL1**, and **RPS6**. This fact might contribute to the phenotype observed

in proliferation and viability assays and indicate that the inhibitor might cause p**rotein and nucleotide synthesis inhibition**. Moreover, a possible link to **autophagy modulation** has been found suggested by phosphorylation changes on **DAP1** and **ULK1**.

- In western blotting analysis, the addition of sham-irradiated controls and treatment with 2 μM VE-821 showed that the inhibition of mTOR occurred also in sham-irradiated cells, and the lower concentration of the inhibitor did not induce any mTOR inhibition detectable by western blotting. Therefore, we assume that the **mTOR inhibition was most likely induced by an off-target of the inhibitor**. This finding is of the utmost importance as in several studies VE-821 has been used in 10 μM concentration, and possible contribution of mTOR inhibition to the observed phenotype has not been considered.
- Importantly, we provide **the first metabolomic profile of cells treated with a PIKKs family kinase inhibitor**. To our knowledge, no such study has been published yet providing an insight into metabolic pathways modulated by ATR inhibitor in response to DNA damage. In our targeted metabolomic analysis, **206 intermediary metabolites were quantified**, and two trends were observed – first, 10 μM VE-821 potentiated the effects of IR and second, 10 μM VE-821 modulated the metabolism of irradiated cells.
- VE-821 potentiated the metabolic disruption induced by IR affecting the levels of **NDPs**, **NTPs** and intermediates of **glycolysis** (glucose 6-phosphate, 3-phosphoglycerate, phosphoenolpyruvate), and **lactate**. IR induced oxidative stress might be increased upon the addition of VE-821 as demonstrated by changed **GSH** and **allantoin** levels. VE-821 also induced changes in **citric acid cycle intermediates**.
- VE-821 induced decrease in **dNDPs** and **dNTPs** levels. As we did not observe any time-dependent decrease in irradiated cells, we assumed that the changes were probably not caused entirely by the insufficiency of NDPs and NTPs in their *de novo* synthesis. Lately, the enzymatic activity of dCK, which is the main regulator of nucleotide salvage pathways, has been proven to be dependent upon ATR after DNA damaging stress. Therefore, the **downregulation of salvage pathways** by ATR inhibition might be the main cause of the decrease of dNTPs necessary for repair of damaged DNA.

7. Conclusion

DNA damage induction by either radio- or chemo- therapy has been the most widely used approach in oncology exploiting one of the hallmarks of cancer: genomic instability. However, such treatment is very unspecific and often accompanied by collateral damage to healthy tissues. In recent years, much effort has been focused on discovery and development of tumour specific treatment, which would only specifically target cancer cells and not affect the normal tissues. A promising concept that has been developed recently is to take advantage of the tumour specific abnormalities in DDR, and target the DDR kinases from the PIKKs family - ATM, ATR, and DNA-PK.

In the presented doctoral thesis, we aimed to elucidate molecular mechanisms underlying radiosensitization of MOLT-4 cell line (T-ALL) by PIKKs inhibitors. To do so, we tested two highly potent inhibitors of two kinases from the PIKKs family - ATR and ATM, VE-821 and KU55933, respectively for their effects on proliferation, viability, and cell cycle of sham-irradiated and irradiated MOLT-4 cells. In these initial tests, both inhibitors proved to radiosensitize MOLT-4 cells and furthermore, 10 μM VE-821 was shown to act as a strong antiproliferative agent in sham-irradiated MOLT-4 cells.

To further describe cellular mechanisms underlying the VE-821-mediated radiosensitization of MOLT-4 cells, we employed high-resolution MS to identify and quantify changes in **proteome, phosphoproteome**, and **metabolome** of irradiated VE-821-treated cells. As the detection and quantification of phosphorylated peptides in complex biological samples is challenging due to their low stoichiometry, first of all we optimized protocol for the enrichment of phosphorylated peptides from their mixture with their nonphosphorylated counterparts. Several commercially available chromatographic materials and published protocols were selected and tested using MALDI-TOF MS detection of phosphorylated peptides enriched from standard tryptic peptides mixtures. The most successful protocols were further evaluated using complex samples, such as HeLa cells lysate and SILAC-labelled MOLT-4 cells lysate. Based on the optimization part, a protocol including the **Titansphere® particles** and loading buffer containing **200 mM glutamic acid** as a specificity and efficiency enhancer was compiled for further experiments.

The optimized protocol was then successfully applied to study VE-821-dependent changes in irradiated MOLT-4 cells. In concordance with our expectations, VE-821 **did**

not cause any significant changes on the proteome level. However, we detected **623 differentially regulated phosphorylation sites**; most of them (431) were upregulated in response to the inhibitor treatment. Using bioinformatic tools, we described, which protein kinases and signalling pathways might be affected by the inhibitor treatment upon irradiation. These analyses revealed changes in **DDR related pathways and kinases**, but also pathways and kinases involved in **maintaining cellular metabolism**. Notably, we found a **downregulation of mTOR**, the main regulator of cellular metabolism, which was also confirmed by western blotting. Although there are multiple signalling pathways connecting IR-induced DDR and mTOR regulation that might be potentially regulated by ATR inhibition, we assumed that in our case the downregulation was most likely caused by an **off-target effect of VE-821 at 10 μM concentration**. We further concluded that mTOR inhibition could be one of the factors contributing to the phenotype we observed after treating MOLT-4 cells with 10 μM VE-821, which was different from a lower, mTOR non-inhibitory, concentration.

To our best knowledge, no study has been published yet investigating the modulation of cellular metabolism by small molecular kinase inhibitor of any of the PIKKs family kinases. Therefore, we performed a targeted metabolomic analysis of irradiated MOLT-4 cells, whose response to IR was modulated by 10 μM VE-821. In this analysis, **206 intermediary metabolites were quantified**. Subsequent data analysis showed that VE-821 potentiated the **metabolic disruption** induced by IR and increased the IR induced **oxidative stress**. Our data also indicated that in response to IR, **recovery of dNTPs** might be affected by VE-821 possibly hampering the DNA repair by dNTPs insufficiency.

Thus, in this thesis we described a complex scenario of cellular events that might be dependent on ATR or triggered by ATR inhibition in irradiated MOLT-4 cells. This thesis raised several research questions.

- Which of the mitotic kinases are regulated by ATR, in which phase of mitosis, and how? Is it only the G2/M checkpoint dysregulated by VE-821 treatment in irradiated cells?
- How exactly does VE-821 regulate the mTOR activity? Is it only the off-target effect, or are there also any other pathways contributing to mTOR regulation affected? Several upstream kinases are involved in mTOR regulation in response to stress, such as AMPK, PI3K/Akt, or p38 MAPK. Is there any link between these kinases and ATR? Does VE-821 induce autophagy, and is it a result of the

inhibited mTOR? Is the sensitivity of MOLT-4 cells to the mTOR-inhibiting dose of VE-821 caused by *PTEN* deficiency?

- What is the reason for VE-821-mediated potentiation of metabolic disruption induced by IR and increase of oxidative stress? Is it just increased mitochondrial stress?
- Is ATR necessary for dNTPs salvage pathways in irradiated cells? Does ATR inhibition affect their *de novo* synthesis, and is phosphorylation involved in regulation of these metabolic pathways?

Unfortunately, addressing these questions is beyond the extent of this doctoral thesis. However, data presented in this work might serve as a resource for follow-up studies and provide a platform for future work with other (more potent or specific) inhibitors.

Taken together, we conclude that using ATR inhibitors to radiosensitize cancer cell seems to be an effective anti-tumour strategy. Nevertheless, even using a highly specific inhibitor might lead to a complex response and similar MS-based studies are suitable to reveal additional information on off-target effects and provide insights into other possibly non-reported regulatory mechanisms.

8. References

1. Ferrao PT, Bukczynska EP, Johnstone RW, McArthur GA. Efficacy of CHK inhibitors as single agents in MYC-driven lymphoma cells. Oncogene. 2012 Mar 29;31(13):1661–72.
2. Gilad O, Nabet BY, Ragland RL, Schoppy DW, Smith KD, Durham AC, et al. Combining ATR suppression with oncogenic Ras synergistically increases genomic instability, causing synthetic lethality or tumorigenesis in a dosage-dependent manner. Cancer Res. 2010 Dec 1;70(23):9693–702.
3. Höglund A, Nilsson LM, Muralidharan SV, Hasvold LA, Merta P, Rudelius M, et al. Therapeutic Implications for the Induced Levels of Chk1 in Myc-Expressing Cancer Cells. Clin Cancer Res. 2011 Nov 15;17(22):7067–79.
4. Murga M, Campaner S, Lopez-Contreras AJ, Toledo LI, Soria R, Montaña MF, et al. Exploiting oncogene-induced replicative stress for the selective killing of Myc-driven tumors. Nat Struct Mol Biol. 2011 Dec;18(12):1331–5.
5. Schoppy DW, Ragland RL, Gilad O, Shastri N, Peters AA, Murga M, et al. Oncogenic stress sensitizes murine cancers to hypomorphic suppression of ATR. J Clin Invest. 2012 Jan;122(1):241–52.
6. Toledo LI, Murga M, Zur R, Soria R, Rodriguez A, Martinez S, et al. A cell-based screen identifies ATR inhibitors with synthetic lethal properties for cancer-associated mutations. Nat Struct Mol Biol. 2011 Jun;18(6):721–7.
7. Toledo LI, Murga M, Fernandez-Capetillo O. Targeting ATR and Chk1 kinases for cancer treatment: a new model for new (and old) drugs. Mol Oncol. 2011 Aug;5(4):368–73.
8. Fokas E, Prevo R, Pollard JR, Reaper PM, Charlton PA, Cornelissen B, et al. Targeting ATR in vivo using the novel inhibitor VE-822 results in selective sensitization of pancreatic tumors to radiation. Cell Death Dis. 2012;3:e441.
9. Fokas E, Prevo R, Hammond EM, Brunner TB, McKenna WG, Muschel RJ. Targeting ATR in DNA damage response and cancer therapeutics. Cancer Treat Rev. 2014 Feb;40(1):109–17.
10. Peasland A, Wang L-Z, Rowling E, Kyle S, Chen T, Hopkins A, et al. Identification and evaluation of a potent novel ATR inhibitor, NU6027, in breast and ovarian cancer cell lines. Br J Cancer. 2011 Jul 26;105(3):372–81.
11. Reaper PM, Griffiths MR, Long JM, Charrier J, Maccormick S, Charlton PA, et al. Selective killing of ATM- or p53-deficient cancer cells through inhibition of ATR. Nature Chemical Biology. 2011 Jul;7(7):428–30.
12. Vendetti FP, Lau A, Schamus S, Conrads TP, O'Connor MJ, Bakkenist CJ. The orally active and bioavailable ATR kinase inhibitor AZD6738 potentiates the anti-tumor effects of cisplatin to resolve ATM-deficient non-small cell lung cancer in vivo. Oncotarget. 2015 Oct 27;
13. Cohen P. The origins of protein phosphorylation. Nat Cell Biol. 2002 May;4(5):E127-130.
14. Newman RH, Zhang J, Zhu H. Toward a systems-level view of dynamic phosphorylation networks. Front Genet. 2014;5:263.
15. Blume-Jensen P, Hunter T. Oncogenic kinase signalling. Nature. 2001 May 17;411(6835):355–65.
16. Harsha HC, Pandey A. Phosphoproteomics in cancer. Mol Oncol. 2010 Dec;4(6):482–95.
17. Azzam EI, Jay-Gerin J-P, Pain D. Ionizing radiation-induced metabolic oxidative stress and prolonged cell injury. Cancer Lett. 2012 Dec 31;327(0):48–60.
18. Řezáčová M, Vávrová J. Molekulární mechanismy účinku ionizujícího záření. Hradec Králové: Nucleus HK; 2011.
19. Prasad KN. Handbook of Radiobiology. CRC Press; 1995. 356 p.
20. Resnick MA, Martin P. The repair of double-strand breaks in the nuclear DNA of Saccharomyces cerevisiae and its genetic control. Molec Gen Genet. 1976 Jan 1;143(2):119–29.
21. Tichý A, Durišová K, Novotná E, Zárybnická L, Vávrová J, Pejchal J, et al. Phosphatidylinositol-3-kinase related kinases (PIKKS) in radiotion-induced DNA damage. Mil Med Sci Lett. 2012 Dec;81(4):177–87.
22. Keith CT, Schreiber SL. PIK-related kinases: DNA repair, recombination, and cell cycle checkpoints. Science. 1995 Oct 6;270(5233):50–1.
23. Bosotti R, Isacchi A, Sonnhammer ELL. FAT: a novel domain in PIK-related kinases. Trends in Biochemical Sciences. 2000 May 1;25(5):225–7.
24. Fernandes N, Sun Y, Chen S, Paul P, Shaw RJ, Cantley LC, et al. DNA Damage-induced Association of ATM with Its Target Proteins Requires a Protein Interaction Domain in the N Terminus of ATM. J Biol Chem. 2005 Apr 15;280(15):15158–64.

25. Kim ST, Lim DS, Canman CE, Kastan MB. Substrate specificities and identification of putative substrates of ATM kinase family members. J Biol Chem. 1999 Dec 31;274(53):37538–43.
26. Burma S, Chen BP, Murphy M, Kurimasa A, Chen DJ. ATM Phosphorylates Histone H2AX in Response to DNA Double-strand Breaks. J Biol Chem. 2001 Nov 9;276(45):42462–7.
27. Stiff T, O'Driscoll M, Rief N, Iwabuchi K, Löbrich M, Jeggo PA. ATM and DNA-PK Function Redundantly to Phosphorylate H2AX after Exposure to Ionizing Radiation. Cancer Res. 2004 Apr 1;64(7):2390–6.
28. Ward IM, Chen J. Histone H2AX is phosphorylated in an ATR-dependent manner in response to replicational stress. J Biol Chem [Internet]. 2001 Oct 22 [cited 2015 Dec 19]; Available from: http://www.jbc.org/content/early/2001/10/22/jbc.C100569200
29. Matsuoka S, Ballif BA, Smogorzewska A, McDonald ER, Hurov KE, Luo J, et al. ATM and ATR Substrate Analysis Reveals Extensive Protein Networks Responsive to DNA Damage. Science. 2007 May 25;316(5828):1160–6.
30. Novotná E, Tichý A, Pejchal J, Lukášová E, Šalovská B, Vávrová J. DNA-dependent protein kinase and its inhibition in support of radiotherapy. International Journal of Radiation Biology. 2013 Jun 1;89(6):416–23.
31. Shimobayashi M, Hall MN. Making new contacts: the mTOR network in metabolism and signalling crosstalk. Nat Rev Mol Cell Biol. 2014 Mar;15(3):155–62.
32. Hasty P, Sharp ZD, Curiel TJ, Campisi J. mTORC1 and p53. Cell Cycle. 2013 Jan 1;12(1):20–5.
33. Sanli T, Steinberg GR, Singh G, Tsakiridis T. AMP-activated protein kinase (AMPK) beyond metabolism. Cancer Biol Ther. 2014 Feb 1;15(2):156–69.
34. Chen H, Ma Z, Vanderwaal RP, Feng Z, Gonzalez-Suarez I, Wang S, et al. The mTOR inhibitor rapamycin suppresses DNA double-strand break repair. Radiat Res. 2011 Feb;175(2):214–24.
35. Schiewer MJ, Den R, Hoang DT, Augello MA, Lawrence YR, Dicker AP, et al. mTOR is a selective effector of the radiation therapy response in androgen receptor-positive prostate cancer. Endocr Relat Cancer. 2012 Feb;19(1):1–12.
36. Herceg Z, Hulla W, Gell D, Cuenin C, Lleonart M, Jackson S, et al. Disruption of Trrap causes early embryonic lethality and defects in cell cycle progression. Nat Genet. 2001 Oct;29(2):206–11.
37. Yamashita A, Kashima I, Ohno S. The role of SMG-1 in nonsense-mediated mRNA decay. Biochim Biophys Acta. 2005 Dec 30;1754(1–2):305–15.
38. Shiloh Y, Ziv Y. The ATM protein kinase: regulating the cellular response to genotoxic stress, and more. Nat Rev Mol Cell Biol. 2013 Apr;14(4):197–210.
39. Savitsky K, Bar-Shira A, Gilad S, Rotman G, Ziv Y, Vanagaite L, et al. A single ataxia telangiectasia gene with a product similar to PI-3 kinase. Science. 1995 Jun 23;268(5218):1749–53.
40. Lavin MF, Shiloh Y. The genetic defect in ataxia-telangiectasia. Annu Rev Immunol. 1997;15:177–202.
41. Bakkenist CJ, Kastan MB. DNA damage activates ATM through intermolecular autophosphorylation and dimer dissociation. Nature. 2003 Jan 30;421(6922):499–506.
42. Bensimon A, Schmidt A, Ziv Y, Elkon R, Wang S-Y, Chen DJ, et al. ATM-dependent and -independent dynamics of the nuclear phosphoproteome after DNA damage. Sci Signal. 2010;3(151):rs3.
43. Kozlov SV, Graham ME, Jakob B, Tobias F, Kijas AW, Tanuji M, et al. Autophosphorylation and ATM activation: additional sites add to the complexity. J Biol Chem. 2011 Mar 18;286(11):9107–19.
44. Kozlov SV, Graham ME, Peng C, Chen P, Robinson PJ, Lavin MF. Involvement of novel autophosphorylation sites in ATM activation. EMBO J. 2006 Aug 9;25(15):3504–14.
45. Sun Y, Jiang X, Chen S, Fernandes N, Price BD. A role for the Tip60 histone acetyltransferase in the acetylation and activation of ATM. Proc Natl Acad Sci USA. 2005 Sep 13;102(37):13182–7.
46. Sun Y, Xu Y, Roy K, Price BD. DNA damage-induced acetylation of lysine 3016 of ATM activates ATM kinase activity. Mol Cell Biol. 2007 Dec;27(24):8502–9.
47. Bhatti S, Kozlov S, Farooqi AA, Naqi A, Lavin M, Khanna KK. ATM protein kinase: the linchpin of cellular defenses to stress. Cellular And Molecular Life Sciences: CMLS. 2011 Sep;68(18):2977–3006.
48. Stewart GS, Maser RS, Stankovic T, Bressan DA, Kaplan MI, Jaspers NG, et al. The DNA double-strand break repair gene hMRE11 is mutated in individuals with an ataxia-telangiectasia-like disorder. Cell. 1999 Dec 10;99(6):577–87.
49. Carney JP, Maser RS, Olivares H, Davis EM, Le Beau M, Yates JR 3rd, et al. The hMre11/hRad50 protein complex and Nijmegen breakage syndrome: linkage of double-strand break repair to the cellular DNA damage response. Cell. 1998 May 1;93(3):477–86.
50. Waltes R, Kalb R, Gatei M, Kijas AW, Stumm M, Sobeck A, et al. Human RAD50 deficiency in a Nijmegen breakage syndrome-like disorder. Am J Hum Genet. 2009 May;84(5):605–16.

51. Williams RS, Williams JS, Tainer JA. Mre11-Rad50-Nbs1 is a keystone complex connecting DNA repair machinery, double-strand break signaling, and the chromatin template. Biochem Cell Biol. 2007 Aug;85(4):509–20.
52. Stracker TH, Petrini JHJ. The MRE11 complex: starting from the ends. Nat Rev Mol Cell Biol. 2011 Feb;12(2):90–103.
53. Stucki M, Clapperton JA, Mohammad D, Yaffe MB, Smerdon SJ, Jackson SP. MDC1 Directly Binds Phosphorylated Histone H2AX to Regulate Cellular Responses to DNA Double-Strand Breaks. Cell. 2005 Dec 29;123(7):1213–26.
54. Polo SE, Jackson SP. Dynamics of DNA damage response proteins at DNA breaks: a focus on protein modifications. Genes Dev. 2011 Mar 1;25(5):409–33.
55. Choi S, Srivas R, Fu KY, Hood BL, Dost B, Gibson GA, et al. Quantitative proteomics reveal ATM kinase-dependent exchange in DNA damage response complexes. J Proteome Res. 2012 Oct 5;11(10):4983–91.
56. Marzano V, Santini S, Rossi C, Zucchelli M, D'Alessandro A, Marchetti C, et al. Proteomic profiling of ATM kinase proficient and deficient cell lines upon blockage of proteasome activity. Journal of Proteomics. 2012 Aug 3;75(15):4632–46.
57. Mu J-J, Wang Y, Luo H, Leng M, Zhang J, Yang T, et al. A proteomic analysis of ataxia telangiectasia-mutated (ATM)/ATM-Rad3-related (ATR) substrates identifies the ubiquitin-proteasome system as a regulator for DNA damage checkpoints. J Biol Chem. 2007 Jun 15;282(24):17330–4.
58. Hornbeck PV, Kornhauser JM, Tkachev S, Zhang B, Skrzypek E, Murray B, et al. PhosphoSitePlus: a comprehensive resource for investigating the structure and function of experimentally determined post-translational modifications in man and mouse. Nucleic Acids Res. 2012 Jan;40(Database issue):D261–70.
59. Lavin MF, Gueven N. The complexity of p53 stabilization and activation. Cell Death Differ. 2006 Apr 7;13(6):941–50.
60. Kastan MB, Zhan Q, El-Deiry WS, Carrier F, Jacks T, Walsh WV, et al. A mammalian cell cycle checkpoint pathway utilizing p53 and GADD45 is defective in ataxia-telangiectasia. Cell. 1992 Nov 13;71(4):587–97.
61. Chehab NH, Malikzay A, Appel M, Halazonetis TD. Chk2/hCds1 functions as a DNA damage checkpoint in G(1) by stabilizing p53. Genes Dev. 2000 Feb 1;14(3):278–88.
62. Chehab NH, Malikzay A, Stavridi ES, Halazonetis TD. Phosphorylation of Ser-20 mediates stabilization of human p53 in response to DNA damage. Proc Natl Acad Sci USA. 1999 Nov 23;96(24):13777–82.
63. Matsuoka S, Huang M, Elledge SJ. Linkage of ATM to Cell Cycle Regulation by the Chk2 Protein Kinase. Science. 1998 Dec 4;282(5395):1893–7.
64. Haupt Y, Maya R, Kazaz A, Oren M. Mdm2 promotes the rapid degradation of p53. Nature. 1997 May 15;387(6630):296–9.
65. Marine J-C, Lozano G. Mdm2-mediated ubiquitylation: p53 and beyond. Cell Death Differ. 2010 Jan;17(1):93–102.
66. Khosravi R, Maya R, Gottlieb T, Oren M, Shiloh Y, Shkedy D. Rapid ATM-dependent phosphorylation of MDM2 precedes p53 accumulation in response to DNA damage. PNAS. 1999 Dec 21;96(26):14973–7.
67. Maya R, Balass M, Kim ST, Shkedy D, Leal JF, Shifman O, et al. ATM-dependent phosphorylation of Mdm2 on serine 395: role in p53 activation by DNA damage. Genes Dev. 2001 May 1;15(9):1067–77.
68. Xiong Y, Hannon GJ, Zhang H, Casso D, Kobayashi R, Beach D. p21 is a universal inhibitor of cyclin kinases. Nature. 1993 Dec 16;366(6456):701–4.
69. Wade Harper J, Adami GR, Wei N, Keyomarsi K, Elledge SJ. The p21 Cdk-interacting protein Cip1 is a potent inhibitor of G1 cyclin-dependent kinases. Cell. 1993 Nov 19;75(4):805–16.
70. Mirzayans R, Andrais B, Scott A, Murray D. New insights into p53 signaling and cancer cell response to DNA damage: implications for cancer therapy. J Biomed Biotechnol. 2012;2012:170325.
71. Pietrzak M, Puzianowska-Kuznicka M. p53-dependent repression of the human MCL-1 gene encoding an anti-apoptotic member of the BCL-2 family: the role of Sp1 and of basic transcription factor binding sites in the MCL-1 promoter. Biological Chemistry. 2008;389(4):383–393.
72. Hadian K, Krappmann D. Signals from the nucleus: activation of NF-kappaB by cytosolic ATM in the DNA damage response. Sci Signal. 2011;4(156):pe2.
73. Smith J, Tho LM, Xu N, Gillespie DA. The ATM-Chk2 and ATR-Chk1 pathways in DNA damage signaling and cancer. Adv Cancer Res. 2010;108:73–112.
74. Chen BPC, Uematsu N, Kobayashi J, Lerenthal Y, Krempler A, Yajima H, et al. Ataxia telangiectasia mutated (ATM) is essential for DNA-PKcs phosphorylations at the Thr-2609 cluster upon DNA double strand break. J Biol Chem. 2007 Mar 2;282(9):6582–7.

75. Xu N, Lao Y, Zhang Y, Gillespie DA. Akt: a double-edged sword in cell proliferation and genome stability. J Oncol. 2012;2012:951724.
76. Beucher A, Birraux J, Tchouandong L, Barton O, Shibata A, Conrad S, et al. ATM and Artemis promote homologous recombination of radiation-induced DNA double-strand breaks in G2. EMBO J. 2009 Nov 4;28(21):3413–27.
77. Li S, Ting NS, Zheng L, Chen PL, Ziv Y, Shiloh Y, et al. Functional link of BRCA1 and ataxia telangiectasia gene product in DNA damage response. Nature. 2000 Jul 13;406(6792):210–5.
78. Gatei M, Young D, Cerosaletti KM, Desai-Mehta A, Spring K, Kozlov S, et al. ATM-dependent phosphorylation of nibrin in response to radiation exposure. Nat Genet. 2000 May;25(1):115–9.
79. Lim D-S, Kim S-T, Xu B, Maser RS, Lin J, Petrini JHJ, et al. ATM phosphorylates p95/nbs1 in an S-phase checkpoint pathway. Nature. 2000 Apr 6;404(6778):613–7.
80. Di Virgilio M, Ying CY, Gautier J. PIKK-dependent phosphorylation of Mre11 induces MRN complex inactivation by disassembly from chromatin. DNA Repair. 2009 Nov 2;8(11):1311–20.
81. Gatei M, Jakob B, Chen P, Kijas AW, Becherel OJ, Gueven N, et al. ATM Protein-dependent Phosphorylation of Rad50 Protein Regulates DNA Repair and Cell Cycle Control. J Biol Chem. 2011 Sep 9;286(36):31542–56.
82. Falck J, Mailand N, Syljuåsen RG, Bartek J, Lukas J. The ATM–Chk2–Cdc25A checkpoint pathway guards against radioresistant DNA synthesis. Nature. 2001 Apr 12;410(6830):842–7.
83. Lukas J, Lukas C, Bartek J. Mammalian cell cycle checkpoints: signalling pathways and their organization in space and time. DNA Repair. 2004 Aug;3(8–9):997–1007.
84. Cimprich KA, Cortez D. ATR: an essential regulator of genome integrity. Nature Reviews Molecular Cell Biology. 2008 Aug;9(8):616–27.
85. Brown EJ, Baltimore D. ATR disruption leads to chromosomal fragmentation and early embryonic lethality. Genes Dev. 2000 Feb 15;14(4):397–402.
86. Takai H, Tominaga K, Motoyama N, Minamishima YA, Nagahama H, Tsukiyama T, et al. Aberrant cell cycle checkpoint function and early embryonic death in Chk1−/− mice. Genes Dev. 2000 Jun 15;14(12):1439–47.
87. O'Driscoll M, Ruiz-Perez VL, Woods CG, Jeggo PA, Goodship JA. A splicing mutation affecting expression of ataxia–telangiectasia and Rad3–related protein (ATR) results in Seckel syndrome. Nat Genet. 2003 Apr;33(4):497–501.
88. Cortez D, Guntuku S, Qin J, Elledge SJ. ATR and ATRIP: partners in checkpoint signaling. Science. 2001 Nov 23;294(5547):1713–6.
89. Fanning E, Klimovich V, Nager AR. A dynamic model for replication protein A (RPA) function in DNA processing pathways. Nucleic Acids Res. 2006;34(15):4126–37.
90. Ellison V, Stillman B. Biochemical Characterization of DNA Damage Checkpoint Complexes: Clamp Loader and Clamp Complexes with Specificity for 5′ Recessed DNA. PLoS Biol. 2003 Nov 17;1(2):e33.
91. Zou L, Cortez D, Elledge SJ. Regulation of ATR substrate selection by Rad17-dependent loading of Rad9 complexes onto chromatin. Genes Dev. 2002 Jan 15;16(2):198–208.
92. Delacroix S, Wagner JM, Kobayashi M, Yamamoto K, Karnitz LM. The Rad9–Hus1–Rad1 (9–1–1) clamp activates checkpoint signaling via TopBP1. Genes Dev. 2007 Jun 15;21(12):1472–7.
93. Kumagai A, Lee J, Yoo HY, Dunphy WG. TopBP1 Activates the ATR-ATRIP Complex. Cell. 2006 Mar 10;124(5):943–55.
94. Mordes DA, Glick GG, Zhao R, Cortez D. TopBP1 activates ATR through ATRIP and a PIKK regulatory domain. Genes Dev. 2008 Jun 1;22(11):1478–89.
95. Liu S, Shiotani B, Lahiri M, Maréchal A, Tse A, Leung CCY, et al. ATR Autophosphorylation as a Molecular Switch for Checkpoint Activation. Mol Cell. 2011 Jul 22;43(2):192–202.
96. Hall AB, Newsome D, Wang Y, Boucher DM, Eustace B, Gu Y, et al. Potentiation of tumor responses to DNA damaging therapy by the selective ATR inhibitor VX-970. Oncotarget. 2014 Jul 30;5(14):5674–85.
97. Huntoon CJ, Flatten KS, Wahner Hendrickson AE, Huehls AM, Sutor SL, Kaufmann SH, et al. ATR inhibition broadly sensitizes ovarian cancer cells to chemotherapy independent of BRCA status. Cancer Res. 2013 Jun 15;73(12):3683–91.
98. Wang X, Zou L, Lu T, Bao S, Hurov KE, Hittelman WN, et al. Rad17 Phosphorylation Is Required for Claspin Recruitment and Chk1 Activation in Response to Replication Stress. Molecular Cell. 2006 Aug 4;23(3):331–41.
99. Kumagai A, Kim S-M, Dunphy WG. Claspin and the Activated Form of ATR-ATRIP Collaborate in the Activation of Chk1. J Biol Chem. 2004 Nov 26;279(48):49599–608.
100. Walker M, Black EJ, Oehler V, Gillespie DA, Scott MT. Chk1 C-terminal regulatory phosphorylation mediates checkpoint activation by de-repression of Chk1 catalytic activity. Oncogene. 2009 May 4;28(24):2314–23.

101. Wilsker D, Petermann E, Helleday T, Bunz F. Essential function of Chk1 can be uncoupled from DNA damage checkpoint and replication control. PNAS. 2008 Dec 30;105(52):20752–7.
102. Sørensen CS, Syljuåsen RG, Falck J, Schroeder T, Rönnstrand L, Khanna KK, et al. Chk1 regulates the S phase checkpoint by coupling the physiological turnover and ionizing radiation-induced accelerated proteolysis of Cdc25A. Cancer Cell. 2003 Mar;3(3):247–58.
103. Dai Y, Grant S. New Insights into Checkpoint Kinase 1 in the DNA Damage Response Signaling Network. Clin Cancer Res. 2010 Jan 15;16(2):376–83.
104. Pearl LH, Schierz AC, Ward SE, Al-Lazikani B, Pearl FMG. Therapeutic opportunities within the DNA damage response. Nat Rev Cancer. 2015 Mar;15(3):166–80.
105. Lucchesi JC. Synthetic Lethality and Semi-Lethality Among Functionally Related Mutants of Drosophila Melanogaster. Genetics. 1968 May 1;59(1):37–44.
106. Bryant HE, Schultz N, Thomas HD, Parker KM, Flower D, Lopez E, et al. Specific killing of BRCA2-deficient tumours with inhibitors of poly(ADP-ribose) polymerase. Nature. 2005 Apr 14;434(7035):913–7.
107. Farmer H, McCabe N, Lord CJ, Tutt ANJ, Johnson DA, Richardson TB, et al. Targeting the DNA repair defect in BRCA mutant cells as a therapeutic strategy. Nature. 2005 Apr 14;434(7035):917–21.
108. Sabharwal SS, Schumacker PT. Mitochondrial ROS in cancer: initiators, amplifiers or an Achilles' heel? Nat Rev Cancer. 2014 Nov;14(11):709–21.
109. O'Connor MJ. Targeting the DNA Damage Response in Cancer. Molecular Cell. 2015 Nov 19;60(4):547–60.
110. Chen T, Stephens PA, Middleton FK, Curtin NJ. Targeting the S and G2 checkpoint to treat cancer. Drug Discovery Today. 2012 Mar;17(5–6):194–202.
111. Kandoth C, McLellan MD, Vandin F, Ye K, Niu B, Lu C, et al. Mutational landscape and significance across 12 major cancer types. Nature. 2013 Oct 17;502(7471):333–9.
112. Macheret M, Halazonetis TD. DNA Replication Stress as a Hallmark of Cancer. Annual Review of Pathology: Mechanisms of Disease. 2015;10(1):425–48.
113. Durisova K, Salovska B, Pejchal J, Tichy A. Chemical inhibition of DNA repair kinases as a promising tool in oncology. Biomed Pap Med Fac Univ Palacky Olomouc Czech Repub. 2015 Oct 21;
114. Blasina A, Price BD, Turenne GA, McGowan CH. Caffeine inhibits the checkpoint kinase ATM. Current Biology. 1999 Oct 7;9(19):1135–8.
115. Sarkaria JN, Busby EC, Tibbetts RS, Roos P, Taya Y, Karnitz LM, et al. Inhibition of ATM and ATR Kinase Activities by the Radiosensitizing Agent, Caffeine. Cancer Res. 1999 Sep 1;59(17):4375–82.
116. Nishida H, Tatewaki N, Nakajima Y, Magara T, Ko KM, Hamamori Y, et al. Inhibition of ATR protein kinase activity by schisandrin B in DNA damage response. Nucleic Acids Res. 2009 Sep;37(17):5678–89.
117. Tatewaki N, Nishida H, Yoshida M, Ando H, Kondo S, Sakamaki T, et al. Differential Effect of Schisandrin B Stereoisomers on ATR-Mediated DNA Damage Checkpoint Signaling. Journal of Pharmacological Sciences. 2013;122(2):138–48.
118. Harrison LRE, Ottley CJ, Pearson DG, Roche C, Wedge SR, Dolan ME, et al. The kinase inhibitor O6-cyclohexylmethylguanine (NU2058) potentiates the cytotoxicity of cisplatin by mechanisms that are independent of its effect upon CDK2. Biochemical Pharmacology. 2009 May 15;77(10):1586–92.
119. Sultana R, Abdel-Fatah T, Perry C, Moseley P, Albarakti N, Mohan V, et al. Ataxia Telangiectasia Mutated and Rad3 Related (ATR) Protein Kinase Inhibition Is Synthetically Lethal in XRCC1 Deficient Ovarian Cancer Cells. PLoS ONE. 2013 Feb 25;8(2):e57098.
120. Link W, Oyarzabal J, Serelde BG, Albarran MI, Rabal O, Cebriá A, et al. Chemical Interrogation of FOXO3a Nuclear Translocation Identifies Potent and Selective Inhibitors of Phosphoinositide 3-Kinases. J Biol Chem. 2009 Oct 9;284(41):28392–400.
121. Maira S-M, Stauffer F, Brueggen J, Furet P, Schnell C, Fritsch C, et al. Identification and characterization of NVP-BEZ235, a new orally available dual phosphatidylinositol 3-kinase/mammalian target of rapamycin inhibitor with potent in vivo antitumor activity. Mol Cancer Ther. 2008 Jul 1;7(7):1851–63.
122. Konstantinidou G, Bey EA, Rabellino A, Schuster K, Maira MS, Gazdar AF, et al. Dual PI3K/mTOR blockade is an effective radiosensitizing strategy for the treatment of non-small cell lung cancer harboring K-RAS mutations. Cancer Res. 2009 Oct 1;69(19):7644–52.
123. Gamper AM, Rofougaran R, Watkins SC, Greenberger JS, Beumer JH, Bakkenist CJ. ATR kinase activation in G1 phase facilitates the repair of ionizing radiation-induced DNA damage. Nucl Acids Res. 2013 Dec 1;41(22):10334–44.
124. Teng P, Bateman NW, Darcy KM, Hamilton CA, Maxwell GL, Bakkenist CJ, et al. Pharmacologic inhibition of ATR and ATM offers clinically important distinctions to enhancing platinum or radiation response in ovarian, endometrial, and cervical cancer cells. Gynecol Oncol. 2015 Mar;136(3):554–61.

125. Charrier J-D, Durrant SJ, Golec JMC, Kay DP, Knegtel RMA, MacCormick S, et al. Discovery of potent and selective inhibitors of ataxia telangiectasia mutated and Rad3 related (ATR) protein kinase as potential anticancer agents. J Med Chem. 2011 Apr 14;54(7):2320–30.
126. Pires IM, Olcina MM, Anbalagan S, Pollard JR, Reaper PM, Charlton PA, et al. Targeting radiation-resistant hypoxic tumour cells through ATR inhibition. Br J Cancer. 2012 Jul 10;107(2):291–9.
127. Wouters BG, Brown JM. Cells at intermediate oxygen levels can be more important than the "hypoxic fraction" in determining tumor response to fractionated radiotherapy. Radiat Res. 1997 May;147(5):541–50.
128. Prevo R, Fokas E, Reaper PM, Charlton PA, Pollard JR, McKenna WG, et al. The novel ATR inhibitor VE-821 increases sensitivity of pancreatic cancer cells to radiation and chemotherapy. Cancer Biol Ther. 2012 Sep;13(11):1072–81.
129. Alsubhi N, Middleton F, Abdel-Fatah TMA, Stephens P, Doherty R, Arora A, et al. Chk1 phosphorylated at serine345 is a predictor of early local recurrence and radio-resistance in breast cancer. Molecular Oncology. 2016 Feb;10(2):213–23.
130. Jossé R, Martin SE, Guha R, Ormanoglu P, Pfister TD, Reaper PM, et al. ATR inhibitors VE-821 and VX-970 sensitize cancer cells to topoisomerase i inhibitors by disabling DNA replication initiation and fork elongation responses. Cancer Res. 2014 Dec 1;74(23):6968–79.
131. Krajewska M, Fehrmann RSN, Schoonen PM, Labib S, de Vries EGE, Franke L, et al. ATR inhibition preferentially targets homologous recombination-deficient tumor cells. Oncogene. 2015 Jun;34(26):3474–81.
132. Middleton FK, Patterson MJ, Elstob CJ, Fordham S, Herriott A, Wade MA, et al. Common cancer-associated imbalances in the DNA damage response confer sensitivity to single agent ATR inhibition. Oncotarget. 2015 Oct 15;6(32):32396–409.
133. Salovská B, Fabrik I, Durišová K, Link M, Vávrová J, Rezáčová M, et al. Radiosensitization of Human Leukemic HL-60 Cells by ATR Kinase Inhibitor (VE-821): Phosphoproteomic Analysis. Int J Mol Sci. 2014;15(7):12007–26.
134. Vávrová J, Zárybnická L, Lukášová E, Řezáčová M, Novotná E, Sinkorová Z, et al. Inhibition of ATR kinase with the selective inhibitor VE-821 results in radiosensitization of cells of promyelocytic leukaemia (HL-60). Radiat Environ Biophys. 2013 Nov;52(4):471–9.
135. Wagner SA, Oehler H, Voigt A, Dalic D, Freiwald A, Serve H, et al. ATR inhibition rewires cellular signaling networks induced by replication stress. Proteomics. 2016 Feb 1;16(3):402–16.
136. Hall AB, Newsome D, Wang Y, Boucher DM, Eustace B, Gu Y, et al. Potentiation of tumor responses to DNA damaging therapy by the selective ATR inhibitor VX-970. Oncotarget. 2014 Aug 4;5(14):5674–85.
137. Foote KM, Blades K, Cronin A, Fillery S, Guichard SS, Hassall L, et al. Discovery of 4-{4-[(3R)-3-Methylmorpholin-4-yl]-6-[1-(methylsulfonyl)cyclopropyl]pyrimidin-2-yl}-1H-indole (AZ20): A Potent and Selective Inhibitor of ATR Protein Kinase with Monotherapy in Vivo Antitumor Activity. J Med Chem. 2013 Mar 14;56(5):2125–38.
138. Kwok M, Davies N, Agathanggelou A, Smith E, Oldreive C, Petermann E, et al. ATR inhibition induces synthetic lethality and overcomes chemoresistance in TP53 or ATM defective chronic lymphocytic leukemia cells. Blood. 2015 Jan 1;blood-2015-05-644872.
139. Kwok M, Davies N, Agathanggelou A, Smith E, Petermann E, Yates E, et al. Synthetic lethality in chronic lymphocytic leukaemia with DNA damage response defects by targeting the ATR pathway. The Lancet. 2015 Feb 26;385, Supplement 1:S58.
140. Reinders J, Sickmann A. State-of-the-art in phosphoproteomics. Proteomics. 2005 Nov;5(16):4052–61.
141. Sharma K, D'Souza RCJ, Tyanova S, Schaab C, Wiśniewski JR, Cox J, et al. Ultradeep Human Phosphoproteome Reveals a Distinct Regulatory Nature of Tyr and Ser/Thr-Based Signaling. Cell Reports. 2014 Sep 11;8(5):1583–94.
142. Zhang H, Zha X, Tan Y, Hornbeck PV, Mastrangelo AJ, Alessi DR, et al. Phosphoprotein analysis using antibodies broadly reactive against phosphorylated motifs. J Biol Chem. 2002 Oct 18;277(42):39379–87.
143. Knezevic I, Bachem S, Sickmann A, Meyer HE, Stülke J, Hengstenberg W. Regulation of the glucose-specific phosphotransferase system (PTS) of Staphylococcus carnosus by the antiterminator protein GlcT. Microbiology (Reading, Engl). 2000 Sep;146 (Pt 9):2333–42.
144. Weigt C, Korte H, Pogge R, Vonstrandmann R, Hengstenberg W, Meyer H. Identification of Phosphocysteine by Electrospray Mass-Spectrometry Combined with Edman Degradation. J Chromatogr A. 1995 Sep 29;712(1):141–7.
145. Sanders D, Gillececastro B, Stock A, Burlingame A, Koshland D. Identification of the Site of Phosphorylation of the Chemotaxis Response Regulator Protein, Chey. J Biol Chem. 1989 Dec 25;264(36):21770–8.

146. Sickmann A, Meyer HE. Phosphoamino acid analysis. Proteomics. 2001 Feb;1(2):200–6.
147. Matthews H. Protein-Kinases and Phosphatases That Act on Histidine, Lysine, or Arginine Residues in Eukaryotic Proteins - a Possible Regulator of the Mitogen-Activated Protein-Kinase Cascade. Pharmacol Ther. 1995;67(3):323–50.
148. Hultquist DE. The preparation and characterization of phosphorylated derivatives of histidine. Biochim Biophys Acta. 1968 Feb 12;153(2):329–40.
149. Hunter T, Sefton BM. Transforming gene product of Rous sarcoma virus phosphorylates tyrosine. Proc Natl Acad Sci USA. 1980 Mar;77(3):1311–5.
150. Manning G, Whyte DB, Martinez R, Hunter T, Sudarsanam S. The protein kinase complement of the human genome. Science. 2002 Dec 6;298(5600):1912–34.
151. Blagoev B, Ong S-E, Kratchmarova I, Mann M. Temporal analysis of phosphotyrosine-dependent signaling networks by quantitative proteomics. Nat Biotechnol. 2004 Sep;22(9):1139–45.
152. Rush J, Moritz A, Lee KA, Guo A, Goss VL, Spek EJ, et al. Immunoaffinity profiling of tyrosine phosphorylation in cancer cells. Nat Biotech. 2005 Jan;23(1):94–101.
153. Schumacher JA, Crockett DK, Elenitoba-Johnson KSJ, Lim MS. Evaluation of Enrichment Techniques for Mass Spectrometry. J Mol Diagn. 2007 Apr;9(2):169–77.
154. van der Mijn JC, Labots M, Piersma SR, Pham TV, Knol JC, Broxterman HJ, et al. Evaluation of different phospho-tyrosine antibodies for label-free phosphoproteomics. Journal of Proteomics. 2015 Sep 8;127, Part B:259–63.
155. Grønborg M, Kristiansen TZ, Stensballe A, Andersen JS, Ohara O, Mann M, et al. A Mass Spectrometry-based Proteomic Approach for Identification of Serine/Threonine-phosphorylated Proteins by Enrichment with Phospho-specific Antibodies Identification of a Novel Protein, Frigg, as a Protein Kinase A Substrate. Mol Cell Proteomics. 2002 Jul 1;1(7):517–27.
156. Zhang H, Zha X, Tan Y, Hornbeck PV, Mastrangelo AJ, Alessi DR, et al. Phosphoprotein Analysis Using Antibodies Broadly Reactive against Phosphorylated Motifs. J Biol Chem. 2002 Oct 18;277(42):39379–87.
157. Pink M, Verma N, Polato F, Bonn GK, Baba HA, Rettenmeier AW, et al. Precipitation by lanthanum ions: A straightforward approach to isolating phosphoproteins. Journal of Proteomics. 2011 Dec 21;75(2):375–83.
158. Verma N, Bäuerlein C, Pink M, Rettenmeier AW, Schmitz-Spanke S. Proteome and phosphoproteome of primary cultured pig urothelial cells. Electrophoresis. 2011 Dec;32(24):3600–11.
159. Holland C, Schmid M, Zimny-Arndt U, Rohloff J, Stein R, Jungblut PR, et al. Quantitative phosphoproteomics reveals link between Helicobacter pylori infection and RNA splicing modulation in host cells. Proteomics. 2011 Jul 1;11(14):2798–811.
160. Nilsson CL, Dillon R, Devakumar A, Shi SD-H, Greig M, Rogers JC, et al. Quantitative Phosphoproteomic Analysis of the STAT3/IL-6/HIF1α Signaling Network: An Initial Study in GSC11 Glioblastoma Stem Cells. J Proteome Res. 2010 Jan 4;9(1):430–43.
161. Brehmer D, Godl K, Zech B, Wissing J, Daub H. Proteome-wide Identification of Cellular Targets Affected by Bisindolylmaleimide-type Protein Kinase C Inhibitors. Mol Cell Proteomics. 2004 May 1;3(5):490–500.
162. Edbauer D, Cheng D, Batterton MN, Wang C-F, Duong DM, Yaffe MB, et al. Identification and Characterization of Neuronal Mitogen-activated Protein Kinase Substrates Using a Specific Phosphomotif Antibody. Mol Cell Proteomics. 2009 Apr 1;8(4):681–95.
163. Goshe MB, Conrads TP, Panisko EA, Angell NH, Veenstra TD, Smith RD. Phosphoprotein isotope-coded affinity tag approach for isolating and quantitating phosphopeptides in proteome-wide analyses. Anal Chem. 2001 Jun 1;73(11):2578–86.
164. Goshe MB, Veenstra TD, Panisko EA, Conrads TP, Angell NH, Smith RD. Phosphoprotein isotope-coded affinity tags: application to the enrichment and identification of low-abundance phosphoproteins. Anal Chem. 2002 Feb 1;74(3):607–16.
165. Oda Y, Nagasu T, Chait BT. Enrichment analysis of phosphorylated proteins as a tool for probing the phosphoproteome. Nat Biotechnol. 2001 Apr;19(4):379–82.
166. Poot AJ, Ruijter E, Nuijens T, Dirksen EHC, Heck AJR, Slijper M, et al. Selective enrichment of Ser-/Thr-phosphorylated peptides in the presence of Ser-/Thr-glycosylated peptides. Proteomics. 2006 Dec;6(24):6394–9.
167. Steen H, Mann M. A new derivatization strategy for the analysis of phosphopeptides by precursor ion scanning in positive ion mode. J Am Soc Mass Spectrom. 2002 Aug;13(8):996–1003.
168. Arrigoni G, Resjö S, Levander F, Nilsson R, Degerman E, Quadroni M, et al. Chemical derivatization of phosphoserine and phosphothreonine containing peptides to increase sensitivity for MALDI-based analysis and for selectivity of MS/MS analysis. Proteomics. 2006 Feb;6(3):757–66.

169. Thaler F, Valsasina B, Baldi R, Xie J, Stewart A, Isacchi A, et al. A new approach to phosphoserine and phosphothreonine analysis in peptides and proteins: chemical modification, enrichment via solid-phase reversible binding, and analysis by mass spectrometry. Anal Bioanal Chem. 2003 Jun;376(3):366–73.
170. Zhou H, Watts JD, Aebersold R. A systematic approach to the analysis of protein phosphorylation. Nat Biotechnol. 2001 Apr;19(4):375–8.
171. Tao WA, Wollscheid B, O'Brien R, Eng JK, Li X, Bodenmiller B, et al. Quantitative phosphoproteome analysis using a dendrimer conjugation chemistry and tandem mass spectrometry. Nat Methods. 2005 Aug;2(8):591–8.
172. Lansdell TA, Tepe JJ. Isolation of phosphopeptides using solid phase enrichment. Tetrahedron Letters. 2004 Jan;45(1):91–3.
173. Grimsrud PA, Swaney DL, Wenger CD, Beauchene NA, Coon JJ. Phosphoproteomics for the masses. ACS Chem Biol. 2010 Jan 15;5(1):105–19.
174. Washburn MP, Wolters D, Yates JR. Large-scale analysis of the yeast proteome by multidimensional protein identification technology. Nat Biotechnol. 2001 Mar;19(3):242–7.
175. Wolters DA, Washburn MP, Yates JR. An automated multidimensional protein identification technology for shotgun proteomics. Anal Chem. 2001 Dec 1;73(23):5683–90.
176. Beausoleil SA, Jedrychowski M, Schwartz D, Elias JE, Villén J, Li J, et al. Large-scale characterization of HeLa cell nuclear phosphoproteins. Proc Natl Acad Sci U S A. 2004 Aug 17;101(33):12130–5.
177. Gruhler A, Olsen JV, Mohammed S, Mortensen P, Faergeman NJ, Mann M, et al. Quantitative phosphoproteomics applied to the yeast pheromone signaling pathway. Mol Cell Proteomics. 2005 Mar;4(3):310–27.
178. Stone MD, Chen X, McGowan T, Bandhakavi S, Cheng B, Rhodus NL, et al. Large-Scale Phosphoproteomics Analysis of Whole Saliva Reveals a Distinct Phosphorylation Pattern. J Proteome Res. 2011 Apr 1;10(4):1728–36.
179. Swaney DL, Wenger CD, Thomson JA, Coon JJ. Human embryonic stem cell phosphoproteome revealed by electron transfer dissociation tandem mass spectrometry. Proc Natl Acad Sci USA. 2009 Jan 27;106(4):995–1000.
180. Villén J, Beausoleil SA, Gerber SA, Gygi SP. Large-scale phosphorylation analysis of mouse liver. Proc Natl Acad Sci USA. 2007 Jan 30;104(5):1488–93.
181. Zhou H, Low TY, Hennrich ML, van der Toorn H, Schwend T, Zou H, et al. Enhancing the identification of phosphopeptides from putative basophilic kinase substrates using Ti (IV) based IMAC enrichment. Mol Cell Proteomics. 2011 Oct;10(10):M110.006452.
182. Benschop JJ, Mohammed S, O'Flaherty M, Heck AJR, Slijper M, Menke FLH. Quantitative phosphoproteomics of early elicitor signaling in Arabidopsis. Mol Cell Proteomics. 2007 Jul;6(7):1198–214.
183. Lee H-J, Na K, Kwon M-S, Kim H, Kim KS, Paik Y-K. Quantitative analysis of phosphopeptides in search of the disease biomarker from the hepatocellular carcinoma specimen. Proteomics. 2009 Jun;9(12):3395–408.
184. Lemeer S, Jopling C, Gouw J, Mohammed S, Heck AJR, Slijper M, et al. Comparative Phosphoproteomics of Zebrafish Fyn/Yes Morpholino Knockdown Embryos. Mol Cell Proteomics. 2008 Nov 1;7(11):2176–87.
185. Lemeer S, Pinkse MWH, Mohammed S, van Breukelen B, den Hertog J, Slijper M, et al. Online automated in vivo zebrafish phosphoproteomics: from large-scale analysis down to a single embryo. J Proteome Res. 2008 Apr;7(4):1555–64.
186. Wu J, Shakey Q, Liu W, Schuller A, Follettie MT. Global profiling of phosphopeptides by titania affinity enrichment. J Proteome Res. 2007 Dec;6(12):4684–9.
187. Gauci S, Helbig AO, Slijper M, Krijgsveld J, Heck AJR, Mohammed S. Lys-N and trypsin cover complementary parts of the phosphoproteome in a refined SCX-based approach. Anal Chem. 2009 Jun 1;81(11):4493–501.
188. Taouatas N, Altelaar AFM, Drugan MM, Helbig AO, Mohammed S, Heck AJR. Strong cation exchange-based fractionation of Lys-N-generated peptides facilitates the targeted analysis of post-translational modifications. Mol Cell Proteomics. 2009 Jan;8(1):190–200.
189. Han G, Ye M, Zou H. Development of phosphopeptide enrichment techniques for phosphoproteome analysis. Analyst. 2008 Sep;133(9):1128–38.
190. Nühse TS, Stensballe A, Jensen ON, Peck SC. Large-scale analysis of in vivo phosphorylated membrane proteins by immobilized metal ion affinity chromatography and mass spectrometry. Mol Cell Proteomics. 2003 Nov;2(11):1234–43.
191. Dai J, Jin W-H, Sheng Q-H, Shieh C-H, Wu J-R, Zeng R. Protein phosphorylation and expression profiling by Yin-yang multidimensional liquid chromatography (Yin-yang MDLC) mass spectrometry. J Proteome Res. 2007 Jan;6(1):250–62.

192. Wu Y-B, Dai J, Yang X-L, Li S-J, Zhao S-L, Sheng Q-H, et al. Concurrent quantification of proteome and phosphoproteome to reveal system-wide association of protein phosphorylation and gene expression. Mol Cell Proteomics. 2009 Dec;8(12):2809–26.
193. Dai J, Wang L-S, Wu Y-B, Sheng Q-H, Wu J-R, Shieh C-H, et al. Fully automatic separation and identification of phosphopeptides by continuous pH-gradient anion exchange online coupled with reversed-phase liquid chromatography mass spectrometry. J Proteome Res. 2009 Jan;8(1):133–41.
194. Nie S, Dai J, Ning Z-B, Cao X-J, Sheng Q-H, Zeng R. Comprehensive Profiling of Phosphopeptides Based on Anion Exchange Followed by Flow-Through Enrichment with Titanium Dioxide (AFET). J Proteome Res. 2010 Sep 3;9(9):4585–94.
195. Alpert AJ. Hydrophilic-interaction chromatography for the separation of peptides, nucleic acids and other polar compounds. J Chromatogr. 1990 Jan 19;499:177–96.
196. Hemström P, Irgum K. Hydrophilic interaction chromatography. J Sep Sci. 2006 Aug;29(12):1784–821.
197. Gilar M, Olivova P, Daly AE, Gebler JC. Orthogonality of separation in two-dimensional liquid chromatography. Anal Chem. 2005 Oct 1;77(19):6426–34.
198. McNulty DE, Annan RS. Hydrophilic interaction chromatography reduces the complexity of the phosphoproteome and improves global phosphopeptide isolation and detection. Mol Cell Proteomics. 2008 May;7(5):971–80.
199. Albuquerque CP, Smolka MB, Payne SH, Bafna V, Eng J, Zhou H. A Multidimensional Chromatography Technology for In-depth Phosphoproteome Analysis. Mol Cell Proteomics. 2008 Jul;7(7):1389–96.
200. Alpert AJ. Electrostatic repulsion hydrophilic interaction chromatography for isocratic separation of charged solutes and selective isolation of phosphopeptides. Anal Chem. 2008 Jan 1;80(1):62–76.
201. Chen X, Wu D, Zhao Y, Wong BHC, Guo L. Increasing phosphoproteome coverage and identification of phosphorylation motifs through combination of different HPLC fractionation methods. J Chromatogr B Analyt Technol Biomed Life Sci. 2011 Jan 1;879(1):25–34.
202. Chien K-Y, Liu H-C, Goshe MB. Development and application of a phosphoproteomic method using electrostatic repulsion-hydrophilic interaction chromatography (ERLIC), IMAC, and LC-MS/MS analysis to study Marek's Disease Virus infection. J Proteome Res. 2011 Sep 2;10(9):4041–53.
203. Porath J, Carlsson J, Olsson I, Belfrage G. Metal chelate affinity chromatography, a new approach to protein fractionation. Nature. 1975 Dec 18;258(5536):598–9.
204. Andersson L, Porath J. Isolation of phosphoproteins by immobilized metal (Fe3+) affinity chromatography. Anal Biochem. 1986 Apr;154(1):250–4.
205. Qi D, Mao Y, Lu J, Deng C, Zhang X. Phosphate-functionalized magnetic microspheres for immobilization of Zr4+ ions for selective enrichment of the phosphopeptides. Journal of Chromatography A. 2010 Apr;1217(16):2606–17.
206. Xue Y, Wei J, Han H, Zhao L, Cao D, Wang J, et al. Application of open tubular capillary columns coated with zirconium phosphonate for enrichment of phosphopeptides. J Chromatogr B Analyt Technol Biomed Life Sci. 2009 Mar 15;877(8–9):757–64.
207. Zhang L, Wang H, Liang Z, Yang K, Zhang L, Zhang Y. Facile preparation of monolithic immobilized metal affinity chromatography capillary columns for selective enrichment of phosphopeptides. J Sep Sci. 2011 Aug;34(16–17):2122–30.
208. Thingholm TE, Jensen ON, Larsen MR. Analytical strategies for phosphoproteomics. Proteomics. 2009 Mar;9(6):1451–68.
209. Ficarro SB, McCleland ML, Stukenberg PT, Burke DJ, Ross MM, Shabanowitz J, et al. Phosphoproteome analysis by mass spectrometry and its application to Saccharomyces cerevisiae. Nat Biotechnol. 2002 Mar;20(3):301–5.
210. Thingholm TE, Jensen ON, Robinson PJ, Larsen MR. SIMAC (sequential elution from IMAC), a phosphoproteomics strategy for the rapid separation of monophosphorylated from multiply phosphorylated peptides. Mol Cell Proteomics. 2008 Apr;7(4):661–71.
211. Carrascal M, Ovelleiro D, Casas V, Gay M, Abian J. Phosphorylation analysis of primary human T lymphocytes using sequential IMAC and titanium oxide enrichment. J Proteome Res. 2008 Dec;7(12):5167–76.
212. Wilson-Grady JT, Villén J, Gygi SP. Phosphoproteome analysis of fission yeast. J Proteome Res. 2008 Mar;7(3):1088–97.
213. Zhou H, Ye M, Dong J, Han G, Jiang X, Wu R, et al. Specific Phosphopeptide Enrichment with Immobilized Titanium Ion Affinity Chromatography Adsorbent for Phosphoproteome Analysis. J Proteome Res. 2008 Sep 5;7(9):3957–67.
214. Zhou H, Ye M, Dong J, Corradini E, Cristobal A, Heck AJR, et al. Robust phosphoproteome enrichment using monodisperse microsphere–based immobilized titanium (IV) ion affinity chromatography. Nat Protocols. 2013 Mar;8(3):461–80.

215. Matheron L, van den Toorn H, Heck AJR, Mohammed S. Characterization of Biases in Phosphopeptide Enrichment by Ti4+-Immobilized Metal Affinity Chromatography and TiO2 Using a Massive Synthetic Library and Human Cell Digests. Anal Chem. 2014 Aug 19;86(16):8312–20.
216. de Graaf EL, Giansanti P, Altelaar AFM, Heck AJR. Single-step Enrichment by Ti4+-IMAC and Label-free Quantitation Enables In-depth Monitoring of Phosphorylation Dynamics with High Reproducibility and Temporal Resolution. Mol Cell Proteomics. 2014 Sep;13(9):2426–34.
217. de Graaf EL, Kaplon J, Mohammed S, Vereijken LAM, Duarte DP, Redondo Gallego L, et al. Signal Transduction Reaction Monitoring Deciphers Site-Specific PI3K-mTOR/MAPK Pathway Dynamics in Oncogene-Induced Senescence. J Proteome Res. 2015 Jul 2;14(7):2906–14.
218. Ikeguchi Y, Nakamura H. Determination of Organic Phosphates by Column-Switching High Performance Anion-Exchange Chromatography Using On-Line Preconcentration on Titania. Analytical Sciences. 1997;13(3):479–83.
219. Matsuda H, Nakamura H, Nakajima T. New ceramic titania: Selective adsorbent for organic phosphates. Analytical Sciences. 1990;6(6):911–2.
220. Tani K, Suzuki Y. Investigation of the ion-exchange behaviour of titania: Application as a packing material for ion chromatography. Chromatographia. 1997 Dec;46(11–12):623–7.
221. Klemm C, Otto S, Wolf C, Haseloff RF, Beyermann M, Krause E. Evaluation of the titanium dioxide approach for MS analysis of phosphopeptides. J Mass Spectrom. 2006 Dec;41(12):1623–32.
222. Larsen MR, Thingholm TE, Jensen ON, Roepstorff P, Jørgensen TJD. Highly selective enrichment of phosphorylated peptides from peptide mixtures using titanium dioxide microcolumns. Mol Cell Proteomics. 2005 Jul;4(7):873–86.
223. Sugiyama N, Masuda T, Shinoda K, Nakamura A, Tomita M, Ishihama Y. Phosphopeptide Enrichment by Aliphatic Hydroxy Acid-modified Metal Oxide Chromatography for Nano-LC-MS/MS in Proteomics Applications. Mol Cell Proteomics. 2007 Jun 1;6(6):1103–9.
224. Yu L-R, Zhu Z, Chan KC, Issaq HJ, Dimitrov DS, Veenstra TD. Improved titanium dioxide enrichment of phosphopeptides from HeLa cells and high confident phosphopeptide identification by cross-validation of MS/MS and MS/MS/MS spectra. J Proteome Res. 2007 Nov;6(11):4150–62.
225. Park S-S, Maudsley S. Discontinuous pH gradient-mediated separation of TiO2-enriched phosphopeptides. Anal Biochem. 2011 Feb 1;409(1):81–8.
226. Simon ES, Young M, Chan A, Bao Z-Q, Andrews PC. Improved enrichment strategies for phosphorylated peptides on titanium dioxide using methyl esterification and pH gradient elution. Anal Biochem. 2008 Jun 15;377(2):234–42.
227. Pinkse MWH, Uitto PM, Hilhorst MJ, Ooms B, Heck AJR. Selective Isolation at the Femtomole Level of Phosphopeptides from Proteolytic Digests Using 2D-NanoLC-ESI-MS/MS and Titanium Oxide Precolumns. Anal Chem. 2004 Jul 1;76(14):3935–43.
228. Cantin GT, Shock TR, Park SK, Madhani HD, Yates JR. Optimizing TiO2-based phosphopeptide enrichment for automated multidimensional liquid chromatography coupled to tandem mass spectrometry. Anal Chem. 2007 Jun 15;79(12):4666–73.
229. Wolschin F, Weckwerth W. Combining metal oxide affinity chromatography (MOAC) and selective mass spectrometry for robust identification of in vivo protein phosphorylation sites. Plant Methods. 2005 Nov 1;1:9.
230. Li Y, Lin H, Deng C, Yang P, Zhang X. Highly selective and rapid enrichment of phosphorylated peptides using gallium oxide-coated magnetic microspheres for MALDI-TOF-MS and nano-LC-ESI-MS/MS/MS analysis. Proteomics. 2008 Jan;8(2):238–49.
231. Ficarro SB, Parikh JR, Blank NC, Marto JA. Niobium(V) oxide (Nb2O5): application to phosphoproteomics. Anal Chem. 2008 Jun 15;80(12):4606–13.
232. Leitner A, Sturm M, Smått J-H, Järn M, Lindén M, Mechtler K, et al. Optimizing the performance of tin dioxide microspheres for phosphopeptide enrichment. Anal Chim Acta. 2009 Apr 6;638(1):51–7.
233. Leitner A, Sturm M, Hudecz O, Mazanek M, Smått J-H, Lindén M, et al. Probing the phosphoproteome of HeLa cells using nanocast metal oxide microspheres for phosphopeptide enrichment. Anal Chem. 2010 Apr 1;82(7):2726–33.
234. Rivera JG, Choi YS, Vujcic S, Wood TD, Colón LA. Enrichment/isolation of phosphorylated peptides on hafnium oxide prior to mass spectrometric analysis. Analyst. 2008 Dec 15;134(1):31–3.
235. Qi D, Lu J, Deng C, Zhang X. Development of core–shell structure Fe3O4@Ta2O5 microspheres for selective enrichment of phosphopeptides for mass spectrometry analysis. Journal of Chromatography A. 2009 Jul;1216(29):5533–9.
236. Kweon HK, Håkansson K. Selective zirconium dioxide-based enrichment of phosphorylated peptides for mass spectrometric analysis. Anal Chem. 2006 Mar 15;78(6):1743–9.
237. Jensen SS, Larsen MR. Evaluation of the impact of some experimental procedures on different phosphopeptide enrichment techniques. Rapid Commun Mass Spectrom. 2007;21(22):3635–45.

238. Yu Y-Q, Fournier J, Gilar M, Gebler JC. Phosphopeptide enrichment using microscale titanium dioxide solid phase extraction. J Sep Sci. 2009 Apr;32(8):1189–99.
239. Dobson KD, McQuillan AJ. In situ infrared spectroscopic analysis of the adsorption of aromatic carboxylic acids to TiO2, ZrO2, Al2O3, and Ta2O5 from aqueous solutions. Spectrochim Acta A Mol Biomol Spectrosc. 2000 Feb 15;56(3):557–65.
240. Aryal UK, Ross ARS. Enrichment and analysis of phosphopeptides under different experimental conditions using titanium dioxide affinity chromatography and mass spectrometry. Rapid Commun Mass Spectrom. 2010 Jan;24(2):219–31.
241. Tanl K, Sumizawa T, Watanabe M, Tachibana M, Koizumi H, Kiba T. Evaluation of titania as an ion-exchanger and as a ligand-exchanger in HPLC. Chromatographia. 2002 Jan;55(1–2):33–7.
242. Mazanek M, Mituloviae G, Herzog F, Stingl C, Hutchins JRA, Peters J-M, et al. Titanium dioxide as a chemo-affinity solid phase in offline phosphopeptide chromatography prior to HPLC-MS/MS analysis. Nat Protoc. 2007;2(5):1059–69.
243. Mazanek M, Roitinger E, Hudecz O, Hutchins JRA, Hegemann B, Mitulović G, et al. A new acid mix enhances phosphopeptide enrichment on titanium- and zirconium dioxide for mapping of phosphorylation sites on protein complexes. J Chromatogr B Analyt Technol Biomed Life Sci. 2010 Feb 15;878(5–6):515–24.
244. Li Q, Ning Z, Tang J, Nie S, Zeng R. Effect of peptide-to-TiO2 beads ratio on phosphopeptide enrichment selectivity. J Proteome Res. 2009 Nov;8(11):5375–81.
245. Montoya A, Beltran L, Casado P, Rodríguez-Prados J-C, Cutillas PR. Characterization of a TiO_2 enrichment method for label-free quantitative phosphoproteomics. Methods. 2011 Aug;54(4):370–8.
246. Liang S-S, Makamba H, Huang S-Y, Chen S-H. Nano-titanium dioxide composites for the enrichment of phosphopeptides. J Chromatogr A. 2006 May 26;1116(1–2):38–45.
247. Lin B, Li T, Zhao Y, Huang F-K, Guo L, Feng Y-Q. Preparation of a TiO2 nanoparticle-deposited capillary column by liquid phase deposition and its application in phosphopeptide analysis. J Chromatogr A. 2008 May 23;1192(1):95–102.
248. Lu Z, Duan J, He L, Hu Y, Yin Y. Mesoporous TiO2 Nanocrystal Clusters for Selective Enrichment of Phosphopeptides. Anal Chem. 2010 Sep 1;82(17):7249–58.
249. Krásný L, Pompach P, Strohalm M, Obsilova V, Strnadová M, Novák P, et al. In-situ enrichment of phosphopeptides on MALDI plates modified by ambient ion landing. J Mass Spectrom. 2012 Oct;47(10):1294–302.
250. Qiao L, Roussel C, Wan J, Yang P, Girault HH, Liu B. Specific on-plate enrichment of phosphorylated peptides for direct MALDI-TOF MS analysis. J Proteome Res. 2007 Dec;6(12):4763–9.
251. Krásný L, Pompach P, Strnadová M, Hynek R, Vališ K, Havlíček V, et al. High-throughput workflow for identification of phosphorylated peptides by LC-MALDI-TOF/TOF-MS coupled to in situ enrichment on MALDI plates functionalized by ion landing. J Mass Spectrom. 2015 Jun;50(6):802–11.
252. Lo C-Y, Chen W-Y, Chen C-T, Chen Y-C. Rapid enrichment of phosphopeptides from tryptic digests of proteins using iron oxide nanocomposites of magnetic particles coated with zirconia as the concentrating probes. J Proteome Res. 2007 Feb;6(2):887–93.
253. Li Y, Leng T, Lin H, Deng C, Xu X, Yao N, et al. Preparation of Fe3O4@ZrO2 core-shell microspheres as affinity probes for selective enrichment and direct determination of phosphopeptides using matrix-assisted laser desorption ionization mass spectrometry. J Proteome Res. 2007 Nov;6(11):4498–510.
254. Nelson CA, Szczech JR, Dooley CJ, Xu Q, Lawrence MJ, Zhu H, et al. Effective Enrichment and Mass Spectrometry Analysis of Phosphopeptides Using Mesoporous Metal Oxide Nanomaterials. Anal Chem. 2010 Sep 1;82(17):7193–201.
255. Wan H, Yan J, Yu L, Zhang X, Xue X, Li X, et al. Zirconia layer coated mesoporous silica microspheres used for highly specific phosphopeptide enrichment. Talanta. 2010 Oct 15;82(5):1701–7.
256. Craig AG, Hoeger CA, Miller CL, Goedken T, Rivier JE, Fischer WH. Monitoring protein kinase and phosphatase reactions with matrix-assisted laser desorption/ionization mass spectrometry and capillary zone electrophoresis: comparison of the detection efficiency of peptide-phosphopeptide mixtures. Biol Mass Spectrom. 1994 Aug;23(8):519–28.
257. Liao PC, Leykam J, Andrews PC, Gage DA, Allison J. An approach to locate phosphorylation sites in a phosphoprotein: mass mapping by combining specific enzymatic degradation with matrix-assisted laser desorption/ionization mass spectrometry. Anal Biochem. 1994 May 15;219(1):9–20.
258. Steen H, Jebanathirajah JA, Rush J, Morrice N, Kirschner MW. Phosphorylation analysis by mass spectrometry: myths, facts, and the consequences for qualitative and quantitative measurements. Mol Cell Proteomics. 2006 Jan;5(1):172–81.
259. Olsen JV, Macek B, Lange O, Makarov A, Horning S, Mann M. Higher-energy C-trap dissociation for peptide modification analysis. Nat Meth. 2007 Sep;4(9):709–12.

260. Zubarev RA, Horn DM, Fridriksson EK, Kelleher NL, Kruger NA, Lewis MA, et al. Electron capture dissociation for structural characterization of multiply charged protein cations. Anal Chem. 2000 Feb 1;72(3):563–73.
261. Syka JEP, Coon JJ, Schroeder MJ, Shabanowitz J, Hunt DF. Peptide and protein sequence analysis by electron transfer dissociation mass spectrometry. Proc Natl Acad Sci U S A. 2004 Jun 29;101(26):9528–33.
262. Tichy A, Salovska B, Rehulka P, Klimentova J, Vavrova J, Stulik J, et al. Phosphoproteomics: searching for a needle in a haystack. J Proteomics. 2011 Nov 18;74(12):2786–97.
263. Webb-Robertson B-JM, Wiberg HK, Matzke MM, Brown JN, Wang J, McDermott JE, et al. Review, Evaluation, and Discussion of the Challenges of Missing Value Imputation for Mass Spectrometry-Based Label-Free Global Proteomics. J Proteome Res. 2015 May 1;14(5):1993–2001.
264. Cox J, Hein MY, Luber CA, Paron I, Nagaraj N, Mann M. Accurate Proteome-wide Label-free Quantification by Delayed Normalization and Maximal Peptide Ratio Extraction, Termed MaxLFQ. Mol Cell Proteomics. 2014 Sep 1;13(9):2513–26.
265. Schilling B, Rardin MJ, MacLean BX, Zawadzka AM, Frewen BE, Cusack MP, et al. Platform-independent and Label-free Quantitation of Proteomic Data Using MS1 Extracted Ion Chromatograms in Skyline APPLICATION TO PROTEIN ACETYLATION AND PHOSPHORYLATION. Mol Cell Proteomics. 2012 May 1;11(5):202–14.
266. Huttlin EL, Jedrychowski MP, Elias JE, Goswami T, Rad R, Beausoleil SA, et al. A Tissue-Specific Atlas of Mouse Protein Phosphorylation and Expression. Cell. 2010 Dec 23;143(7):1174–89.
267. Humphrey SJ, Azimifar SB, Mann M. High-throughput phosphoproteomics reveals in vivo insulin signaling dynamics. Nat Biotech. 2015 Sep;33(9):990–5.
268. Giansanti P, Aye TT, van den Toorn H, Peng M, van Breukelen B, Heck AJR. An Augmented Multiple-Protease-Based Human Phosphopeptide Atlas. Cell Reports. 2015 Jun 23;11(11):1834–43.
269. Ong S-E, Blagoev B, Kratchmarova I, Kristensen DB, Steen H, Pandey A, et al. Stable Isotope Labeling by Amino Acids in Cell Culture, SILAC, as a Simple and Accurate Approach to Expression Proteomics. Mol Cell Proteomics. 2002 May 1;1(5):376–86.
270. Ong S, Mann M. A practical recipe for stable isotope labeling by amino acids in cell culture (SILAC). Nature Protocols. 2006 Dec;1(6):2650–60.
271. Fabrik I, Link M, Härtlova A, Dankova V, Rehulka P, Stulik J. Application of SILAC Labeling to Primary Bone Marrow-Derived Dendritic Cells Reveals Extensive GM-CSF-Dependent Arginine Metabolism. J Proteome Res. 2014 Feb 7;13(2):752–62.
272. Bendall SC, Hughes C, Stewart MH, Doble B, Bhatia M, Lajoie GA. Prevention of Amino Acid Conversion in SILAC Experiments with Embryonic Stem Cells. Mol Cell Proteomics. 2008 Sep;7(9):1587–97.
273. Olsen JV, Blagoev B, Gnad F, Macek B, Kumar C, Mortensen P, et al. Global, In Vivo, and Site-Specific Phosphorylation Dynamics in Signaling Networks. Cell. 2006 Nov 3;127(3):635–48.
274. Lam YW, Lamond AI, Mann M, Andersen JS. Analysis of Nucleolar Protein Dynamics Reveals the Nuclear Degradation of Ribosomal Proteins. Current Biology. 2007 May 1;17(9):749–60.
275. Geiger T, Wisniewski JR, Cox J, Zanivan S, Kruger M, Ishihama Y, et al. Use of stable isotope labeling by amino acids in cell culture as a spike-in standard in quantitative proteomics. Nat Protocols. 2011 Jan;6(2):147–57.
276. Geiger T, Cox J, Ostasiewicz P, Wisniewski JR, Mann M. Super-SILAC mix for quantitative proteomics of human tumor tissue. Nat Meth. 2010 May;7(5):383–5.
277. Krüger M, Moser M, Ussar S, Thievessen I, Luber CA, Forner F, et al. SILAC Mouse for Quantitative Proteomics Uncovers Kindlin-3 as an Essential Factor for Red Blood Cell Function. Cell. 2008 Jul 25;134(2):353–64.
278. Zanivan S, Krueger M, Mann M. In Vivo Quantitative Proteomics: The SILAC Mouse. In: Shimaoka M, editor. Integrin and Cell Adhesion Molecules [Internet]. Humana Press; 2012 [cited 2016 Jun 17]. p. 435–50. (Methods in Molecular Biology). Available from: http://dx.doi.org/10.1007/978-1-61779-166-6_25
279. Monetti M, Nagaraj N, Sharma K, Mann M. Large-scale phosphosite quantification in tissues by a spike-in SILAC method. Nat Meth. 2011 Aug;8(8):655–8.
280. Schweppe DK, Rigas JR, Gerber SA. Quantitative phosphoproteomic profiling of human non-small cell lung cancer tumors. Journal of Proteomics. 2013 Oct 8;91:286–96.
281. Zanivan S, Meves A, Behrendt K, Schoof EM, Neilson LJ, Cox J, et al. In Vivo SILAC-Based Proteomics Reveals Phosphoproteome Changes during Mouse Skin Carcinogenesis. Cell Reports. 2013 Feb 21;3(2):552–66.
282. Ting L, Rad R, Gygi SP, Haas W. MS3 eliminates ratio distortion in isobaric multiplexed quantitative proteomics. Nat Meth. 2011 Nov;8(11):937–40.

283. Wenger CD, Lee MV, Hebert AS, McAlister GC, Phanstiel DH, Westphall MS, et al. Gas-phase purification enables accurate, multiplexed proteome quantification with isobaric tagging. Nat Meth. 2011 Nov;8(11):933–5.
284. Thompson A, Schäfer J, Kuhn K, Kienle S, Schwarz J, Schmidt G, et al. Tandem Mass Tags: A Novel Quantification Strategy for Comparative Analysis of Complex Protein Mixtures by MS/MS. Anal Chem. 2003 Apr 1;75(8):1895–904.
285. Ross PL, Huang YN, Marchese JN, Williamson B, Parker K, Hattan S, et al. Multiplexed Protein Quantitation in Saccharomyces cerevisiae Using Amine-reactive Isobaric Tagging Reagents. Mol Cell Proteomics. 2004 Dec 1;3(12):1154–69.
286. Wiese S, Reidegeld KA, Meyer HE, Warscheid B. Protein labeling by iTRAQ: A new tool for quantitative mass spectrometry in proteome research. Proteomics. 2007 Feb 1;7(3):340–50.
287. Zhang Y, Wolf-Yadlin A, Ross PL, Pappin DJ, Rush J, Lauffenburger DA, et al. Time-resolved Mass Spectrometry of Tyrosine Phosphorylation Sites in the Epidermal Growth Factor Receptor Signaling Network Reveals Dynamic Modules. Mol Cell Proteomics. 2005 Sep 1;4(9):1240–50.
288. Boja ES, Phillips D, French SA, Harris RA, Balaban RS. Quantitative Mitochondrial Phosphoproteomics Using iTRAQ on an LTQ-Orbitrap with High Energy Collision Dissociation. J Proteome Res. 2009 Oct 2;8(10):4665–75.
289. Wu J, Warren P, Shakey Q, Sousa E, Hill A, Ryan TE, et al. Integrating titania enrichment, iTRAQ labeling, and Orbitrap CID-HCD for global identification and quantitative analysis of phosphopeptides. Proteomics. 2010 Jun 1;10(11):2224–34.
290. Glibert P, Meert P, Van Steendam K, Martens L, Deforce D, Dhaenens M. Phospho-iTRAQ data article: Assessing isobaric labels for the large-scale study of phosphopeptide stoichiometry. Data Brief. 2015 May 6;4:60–5.
291. Glibert P, Meert P, Van Steendam K, Van Nieuwerburgh F, De Coninck D, Martens L, et al. Phospho-iTRAQ: Assessing Isobaric Labels for the Large-Scale Study Of Phosphopeptide Stoichiometry. J Proteome Res. 2015 Feb 6;14(2):839–49.
292. Curran TG, Zhang Y, Ma DJ, Sarkaria JN, White FM. MARQUIS: A multiplex method for absolute quantification of peptides and posttranslational modifications. Nat Commun. 2015 Jan 12;6:5924.
293. Jia W, Andaya A, Leary JA. Novel Mass Spectrometric Method for Phosphorylation Quantification Using Cerium Oxide Nanoparticles and Tandem Mass Tags. Anal Chem. 2012 Mar 6;84(5):2466–73.
294. FANG Y, ZHANG Q, WANG X, YANG X, WANG X, HUANG Z, et al. Quantitative phosphoproteomics reveals genistein as a modulator of cell cycle and DNA damage response pathways in triple-negative breast cancer cells. Int J Oncol. 2016 Jan 11;48(3):1016–28.
295. Nirujogi RS, Wright JD, Manda SS, Zhong J, Na CH, Meyerhoff J, et al. Phosphoproteomic analysis reveals compensatory effects in the piriform cortex of VX nerve agent exposed rats. Proteomics. 2015 Jan 1;15(2–3):487–99.
296. Paulo JA, Gaun A, Gygi SP. Global Analysis of Protein Expression and Phosphorylation Levels in Nicotine-Treated Pancreatic Stellate Cells. J Proteome Res. 2015 Oct 2;14(10):4246–56.
297. DeSouza LV, Taylor AM, Li W, Minkoff MS, Romaschin AD, Colgan TJ, et al. Multiple Reaction Monitoring of mTRAQ-Labeled Peptides Enables Absolute Quantification of Endogenous Levels of a Potential Cancer Marker in Cancerous and Normal Endometrial Tissues. J Proteome Res. 2008 Aug 1;7(8):3525–34.
298. Mertins P, Udeshi ND, Clauser KR, Mani DR, Patel J, Ong S, et al. iTRAQ Labeling is Superior to mTRAQ for Quantitative Global Proteomics and Phosphoproteomics. Mol Cell Proteomics. 2012 Jun 1;11(6):M111.014423.
299. Oppermann FS, Klammer M, Bobe C, Cox J, Schaab C, Tebbe A, et al. Comparison of SILAC and mTRAQ Quantification for Phosphoproteomics on a Quadrupole Orbitrap Mass Spectrometer. J Proteome Res. 2013 Sep 6;12(9):4089–100.
300. Boersema PJ, Aye TT, van Veen TAB, Heck AJR, Mohammed S. Triplex protein quantification based on stable isotope labeling by peptide dimethylation applied to cell and tissue lysates. Proteomics. 2008 Nov 1;8(22):4624–32.
301. Boersema PJ, Raijmakers R, Lemeer S, Mohammed S, Heck AJR. Multiplex peptide stable isotope dimethyl labeling for quantitative proteomics. Nat Protocols. 2009 Mar;4(4):484–94.
302. Hsu J-L, Huang S-Y, Chow N-H, Chen S-H. Stable-Isotope Dimethyl Labeling for Quantitative Proteomics. Anal Chem. 2003 Dec 1;75(24):6843–52.
303. Huang S-Y, Tsai M-L, Wu C-J, Hsu J-L, Ho S-H, Chen S-H. Quantitation of protein phosphorylation in pregnant rat uteri using stable isotope dimethyl labeling coupled with IMAC. Proteomics. 2006 Mar 1;6(6):1722–34.
304. Boersema PJ, Foong LY, Ding VMY, Lemeer S, Breukelen B van, Philp R, et al. In-depth Qualitative and Quantitative Profiling of Tyrosine Phosphorylation Using a Combination of Phosphopeptide

Immunoaffinity Purification and Stable Isotope Dimethyl Labeling. Mol Cell Proteomics. 2010 Jan 1;9(1):84–99.
305. Engholm-Keller K, Birck P, Størling J, Pociot F, Mandrup-Poulsen T, Larsen MR. TiSH — a robust and sensitive global phosphoproteomics strategy employing a combination of TiO2, SIMAC, and HILIC. Journal of Proteomics. 2012 Oct 22;75(18):5749–61.
306. Wilson-Grady JT, Haas W, Gygi SP. Quantitative comparison of the fasted and re-fed mouse liver phosphoproteomes using lower pH reductive dimethylation. Methods. 2013 Jun 15;61(3):277–86.
307. Tsai C-F, Wang Y-T, Yen H-Y, Tsou C-C, Ku W-C, Lin P-Y, et al. Large-scale determination of absolute phosphorylation stoichiometries in human cells by motif-targeting quantitative proteomics. Nat Commun. 2015 Mar 27;6:6622.
308. Ong S-E, Mann M. Identifying and quantifying sites of protein methylation by heavy methyl SILAC. Curr Protoc Protein Sci. 2006 Dec;Chapter 14:Unit 14.9.
309. Wu J, Shakey Q, Liu W, Schuller A, Follettie MT. Global Profiling of Phosphopeptides by Titania Affinity Enrichment. J Proteome Res. 2007 Dec 1;6(12):4684–9.
310. Kjellström S, Jensen ON. Phosphoric Acid as a Matrix Additive for MALDI MS Analysis of Phosphopeptides and Phosphoproteins. Anal Chem. 2004 Sep 1;76(17):5109–17.
311. Tichý A, Záškodová D, Pejchal J, ŘezáČová M, Österreicher J, Vávrová J, et al. Gamma irradiation of human leukaemic cells HL-60 and MOLT-4 induces decrease in Mcl-1 and Bid, release of cytochrome c, and activation of caspase-8 and caspase-9. Int J Radiat Biol. 2008 Jan 1;84(6):523–30.
312. Tichý A, Záskodová D, Zoelzer F, Vávrová J, Sinkorová Z, Pejchal J, et al. Gamma-radiation-induced phosphorylation of p53 on serine 15 is dose-dependent in MOLT-4 leukaemia cells. Folia Biol (Praha). 2009;55(2):41–4.
313. Vávrová J, Rezácová M, Vokurková D, Psutka J. Cell cycle alteration, apoptosis and response of leukemic cell lines to gamma radiation with high- and low-dose rate. Physiol Res. 2004;53(3):335–42.
314. Rogers LD, Fang Y, Foster LJ. An integrated global strategy for cell lysis, fractionation, enrichment and mass spectrometric analysis of phosphorylated peptides. Mol BioSyst. 2010 May 10;6(5):822–9.
315. Yeung Y-G, Stanley ER. Rapid Detergent Removal From Peptide Samples With Ethyl Acetate For Mass Spectrometry Analysis. Curr Protoc Protein Sci. 2010 Feb;CHAPTER:Unit-16.12.
316. Cox J, Mann M. MaxQuant enables high peptide identification rates, individualized p.p.b.-range mass accuracies and proteome-wide protein quantification. Nature Biotechnology. 2008 Dec;26(12):1367–72.
317. Cox J, Neuhauser N, Michalski A, Scheltema RA, Olsen JV, Mann M. Andromeda: a peptide search engine integrated into the MaxQuant environment. J Proteome Res. 2011 Apr 1;10(4):1794–805.
318. Zhou Y, Cras-Méneur C, Ohsugi M, Stormo GD, Permutt MA. A global approach to identify differentially expressed genes in cDNA (two-color) microarray experiments. Bioinformatics. 2007 Aug 15;23(16):2073–9.
319. Kamburov A, Wierling C, Lehrach H, Herwig R. ConsensusPathDB—a database for integrating human functional interaction networks. Nucl Acids Res. 2009 Jan 1;37(suppl 1):D623–8.
320. Kamburov A, Pentchev K, Galicka H, Wierling C, Lehrach H, Herwig R. ConsensusPathDB: toward a more complete picture of cell biology. Nucl Acids Res. 2011 Jan 1;39(suppl 1):D712–7.
321. Kanehisa M, Sato Y, Kawashima M, Furumichi M, Tanabe M. KEGG as a reference resource for gene and protein annotation. Nucleic Acids Res. 2016 Jan 4;44(D1):D457-462.
322. Kanehisa M, Goto S. KEGG: kyoto encyclopedia of genes and genomes. Nucleic Acids Res. 2000 Jan 1;28(1):27–30.
323. Croft D. Building models using Reactome pathways as templates. Methods Mol Biol. 2013;1021:273–83.
324. Schaefer CF, Anthony K, Krupa S, Buchoff J, Day M, Hannay T, et al. PID: the Pathway Interaction Database. Nucleic Acids Res. 2009 Jan;37(Database issue):D674-679.
325. Klammer M, Godl K, Tebbe A, Schaab C. Identifying differentially regulated subnetworks from phosphoproteomic data. BMC Bioinformatics. 2010 Jun 28;11(1):351.
326. Shannon P, Markiel A, Ozier O, Baliga NS, Wang JT, Ramage D, et al. Cytoscape: A Software Environment for Integrated Models of Biomolecular Interaction Networks. Genome Res. 2003 Nov;13(11):2498–504.
327. Colaert N, Helsens K, Martens L, Vandekerckhove J, Gevaert K. Improved visualization of protein consensus sequences by iceLogo. Nat Methods. 2009 Nov;6(11):786–7.
328. Chou MF, Schwartz D. Biological sequence motif discovery using motif-x. Curr Protoc Bioinformatics. 2011 Sep;Chapter 13:Unit 13.15-24.
329. Horn H, Schoof EM, Kim J, Robin X, Miller ML, Diella F, et al. KinomeXplorer: an integrated platform for kinome biology studies. Nat Meth. 2014 Jun;11(6):603–4.

330. Song C, Ye M, Liu Z, Cheng H, Jiang X, Han G, et al. Systematic analysis of protein phosphorylation networks from phosphoproteomic data. Mol Cell Proteomics. 2012 Jul 13;mcp.M111.012625.
331. Franceschini A, Szklarczyk D, Frankild S, Kuhn M, Simonovic M, Roth A, et al. STRING v9.1: protein-protein interaction networks, with increased coverage and integration. Nucleic Acids Res. 2013 Jan;41(Database issue):D808-815.
332. Cox J, Mann M. 1D and 2D annotation enrichment: a statistical method integrating quantitative proteomics with complementary high-throughput data. BMC Bioinformatics. 2012;13 Suppl 16:S12.
333. Sellick CA, Hansen R, Stephens GM, Goodacre R, Dickson AJ. Metabolite extraction from suspension-cultured mammalian cells for global metabolite profiling. Nat Protocols. 2011 Jul;6(8):1241–9.
334. Huber W, Carey VJ, Gentleman R, Anders S, Carlson M, Carvalho BS, et al. Orchestrating high-throughput genomic analysis with Bioconductor. Nat Meth. 2015 Feb;12(2):115–21.
335. Benton HP, Want EJ, Ebbels TMD. Correction of mass calibration gaps in liquid chromatography–mass spectrometry metabolomics data. Bioinformatics. 2010 Oct 1;26(19):2488–9.
336. Smith CA, Want EJ, O'Maille G, Abagyan R, Siuzdak G. XCMS: Processing Mass Spectrometry Data for Metabolite Profiling Using Nonlinear Peak Alignment, Matching, and Identification. Anal Chem. 2006 Feb 1;78(3):779–87.
337. Tautenhahn R, Böttcher C, Neumann S. Highly sensitive feature detection for high resolution LC/MS. BMC Bioinformatics. 2008;9:504.
338. Templ M, Hron K, Filzmoser P. robCompositions: Robust Estimation for Compositional Data [Internet]. 2016 [cited 2016 Dec 17]. Available from: https://cran.r-project.org/web/packages/robCompositions/index.html
339. Dunn WB, Broadhurst D, Begley P, Zelena E, Francis-McIntyre S, Anderson N, et al. Procedures for large-scale metabolic profiling of serum and plasma using gas chromatography and liquid chromatography coupled to mass spectrometry. Nature Protocols. 2011 Jun 1;6(7):1060–83.
340. Aitchinson J. The Statistical Analysis of Compositional Data. Monographs on Statistics and Applied Probability. London (UK): Chapman & Hall Ltd.; 1986. 416 p.
341. Gates MB, Tomer KB, Deterding LJ. Comparison of Metal and Metal Oxide Media for Phosphopeptide Enrichment Prior to Mass Spectrometric Analyses. J Am Soc Mass Spectrom. 2010 Oct;21(10):1649–59.
342. Tichý A, Záskodová D, Rezácová M, Vávrová J, Vokurková D, Pejchal J, et al. Gamma-radiation-induced ATM-dependent signalling in human T-lymphocyte leukemic cells, MOLT-4. Acta Biochim Pol. 2007;54(2):281–7.
343. Blagoev B, Ong S-E, Kratchmarova I, Mann M. Temporal analysis of phosphotyrosine-dependent signaling networks by quantitative proteomics. Nat Biotech. 2004 Sep;22(9):1139–45.
344. Gabant G, Lorphelin A, Nozerand N, Marchetti C, Bellanger L, Dedieu A, et al. Autophosphorylated Residues Involved in the Regulation of Human Chk2 In Vitro. Journal of Molecular Biology. 2008 Jul 11;380(3):489–503.
345. Guo X, Ward MD, Tiedebohl JB, Oden YM, Nyalwidhe JO, Semmes OJ. Interdependent Phosphorylation within the Kinase Domain T-loop Regulates CHK2 Activity. J Biol Chem. 2010 Oct 22;285(43):33348–57.
346. Lovly CM, Yan L, Ryan CE, Takada S, Piwnica-Worms H. Regulation of Chk2 Ubiquitination and Signaling through Autophosphorylation of Serine 379. Mol Cell Biol. 2008 Oct;28(19):5874–85.
347. Szkanderová S, Vávrová J, Rézacová M, Vokurková D, Pavlová S, Smardová J, et al. Gamma irradiation results in phosphorylation of p53 at serine-392 in human T-lymphocyte leukaemia cell line MOLT-4. Folia Biol (Praha). 2003;49(5):191–6.
348. Vávrová J, Rezácová M, Vokurková D, Psutka J. Cell cycle alteration, apoptosis and response of leukemic cell lines to gamma radiation with high- and low-dose rate. Physiol Res. 2004;53(3):335–42.
349. Szkanderová S, Vávrová J, Hernychová L, Neubauerová V, Lenco J, Stulík J. Proteome alterations in gamma-irradiated human T-lymphocyte leukemia cells. Radiat Res. 2005 Mar;163(3):307–15.
350. Záskodová D, Rezácová M, Vávrová J, Vokurková D, Tichy A. Effect of valproic acid, a histone deacetylase inhibitor, on cell death and molecular changes caused by low-dose irradiation. Ann N Y Acad Sci. 2006 Dec;1091:385–98.
351. Rezácová M, Tichý A, Vávrová J, Vokurková D, Lukásová E. Is defect in phosphorylation of Nbs1 responsible for high radiosensitivity of T-lymphocyte leukemia cells MOLT-4? Leuk Res. 2008 Aug;32(8):1259–67.
352. Tichý A, Záskodová D, Pejchal J, Rezácová M, Osterreicher J, Vávrová J, et al. Gamma irradiation of human leukaemic cells HL-60 and MOLT-4 induces decrease in Mcl-1 and Bid, release of cytochrome c, and activation of caspase-8 and caspase-9. Int J Radiat Biol. 2008 Jun;84(6):523–30.

353. Tichý A, Záskodová D, Zoelzer F, Vávrová J, Sinkorová Z, Pejchal J, et al. Gamma-radiation-induced phosphorylation of p53 on serine 15 is dose-dependent in MOLT-4 leukaemia cells. Folia Biol (Praha). 2009;55(2):41–4.
354. Tichý A, Muthná D, Vávrová J, Pejchal J, Šinkorová Z, Zárybnická L, et al. Caffeine-suppressed ATM pathway leads to decreased p53 phosphorylation and increased programmed cell death in gamma-irradiated leukaemic molt-4 cells. Journal of Applied Biomedicine. 2011;9(1):49–56.
355. Tichý A, Novotná E, Durisová K, Salovská B, Sedlaríková R, Pejchal J, et al. Radio-sensitization of human leukaemic molt-4 cells by DNA-dependent protein kinase inhibitor, NU7026. Acta Medica (Hradec Kralove). 2012;55(2):66–73.
356. Muthna D, Vavrova J, Lukasova E, Tichy A, Knizek J, Kohlerova R, et al. Valproic acid decreases the reparation capacity of irradiated MOLT-4 cells. Mol Biol (Mosk). 2012 Feb;46(1):122–8.
357. Tichy A, Durisova K, Salovska B, Pejchal J, Zarybnicka L, Vavrova J, et al. Radio-sensitization of human leukaemic MOLT-4 cells by DNA-dependent protein kinase inhibitor, NU7441. Radiat Environ Biophys. 2013 Oct 8;53(1):83–92.
358. Shinohara K, Nakano H. Interphase death and reproductive death in X-irradiated MOLT-4 cells. Radiat Res. 1993 Aug;135(2):197–205.
359. Seifrtová M, Havelek R, Chmelařová M, Cmielová J, Muthná D, Stoklasová A, et al. The effect of ATM and ERK1/2 inhibition on mitoxantrone-induced cell death of leukaemic cells. Folia Biol (Praha). 2011;57(2):74–81.
360. Forbes SA, Beare D, Gunasekaran P, Leung K, Bindal N, Boutselakis H, et al. COSMIC: exploring the world's knowledge of somatic mutations in human cancer. Nucl Acids Res. 2015 Jan 28;43(D1):D805–11.
361. Mendes RD, Canté-Barrett K, Pieters R, Meijerink JPP. The relevance of PTEN-AKT in relation to NOTCH1-directed treatment strategies in T-cell acute lymphoblastic leukemia. Haematologica. 2016 Sep;101(9):1010–7.
362. Li J, Yen C, Liaw D, Podsypanina K, Bose S, Wang SI, et al. PTEN, a putative protein tyrosine phosphatase gene mutated in human brain, breast, and prostate cancer. Science. 1997 Mar 28;275(5308):1943–7.
363. Vogelstein B, Kinzler KW. Cancer genes and the pathways they control. Nat Med. 2004 Aug;10(8):789–99.
364. Hickson I, Zhao Y, Richardson CJ, Green SJ, Martin NMB, Orr AI, et al. Identification and Characterization of a Novel and Specific Inhibitor of the Ataxia-Telangiectasia Mutated Kinase ATM. Cancer Res. 2004 Dec 15;64(24):9152–9.
365. Batey MA, Zhao Y, Kyle S, Richardson C, Slade A, Martin NMB, et al. Preclinical evaluation of a novel ATM inhibitor, KU59403, in vitro and in vivo in p53 functional and dysfunctional models of human cancer. Mol Cancer Ther. 2013 Jun;12(6):959–67.
366. Golding SE, Rosenberg E, Valerie N, Hussaini I, Frigerio M, Cockcroft XF, et al. Improved ATM kinase inhibitor KU-60019 radiosensitizes glioma cells, compromises insulin, AKT and ERK prosurvival signaling, and inhibits migration and invasion. Mol Cancer Ther. 2009 Oct;8(10):2894–902.
367. Tichý A, Novotná E, Durisová K, Salovská B, Sedlaríková R, Pejchal J, et al. Radio-sensitization of human leukaemic molt-4 cells by DNA-dependent protein kinase inhibitor, NU7026. Acta Medica (Hradec Kralove). 2012;55(2):66–73.
368. He J, Shi LZ, Truong LN, Lu C-S, Razavian N, Li Y, et al. Rad50 Zinc Hook Is Important for the Mre11 Complex to Bind Chromosomal DNA Double-stranded Breaks and Initiate Various DNA Damage Responses. J Biol Chem. 2012 Sep 14;287(38):31747–56.
369. Kijas AW, Lim YC, Bolderson E, Cerosaletti K, Gatei M, Jakob B, et al. ATM-dependent phosphorylation of MRE11 controls extent of resection during homology directed repair by signalling through Exonuclease 1. Nucl Acids Res. 2015 Sep 30;43(17):8352–67.
370. Cortez D, Wang Y, Qin J, Elledge SJ. Requirement of ATM-Dependent Phosphorylation of Brca1 in the DNA Damage Response to Double-Strand Breaks. Science. 1999 Nov 5;286(5442):1162–6.
371. Gatei M, Zhou B-B, Hobson K, Scott S, Young D, Khanna KK. Ataxia Telangiectasia Mutated (ATM) Kinase and ATM and Rad3 Related Kinase Mediate Phosphorylation of Brca1 at Distinct and Overlapping Sites IN VIVO ASSESSMENT USING PHOSPHO-SPECIFIC ANTIBODIES. J Biol Chem. 2001 May 18;276(20):17276–80.
372. Wu Q, Paul A, Su D, Mehmood S, Foo TK, Ochi T, et al. Structure of BRCA1-BRCT/Abraxas Complex Reveals Phosphorylation-Dependent BRCT Dimerization at DNA Damage Sites. Molecular Cell. 2016 Feb 4;61(3):434–48.
373. Hoege C, Pfander B, Moldovan G-L, Pyrowolakis G, Jentsch S. RAD6-dependent DNA repair is linked to modification of PCNA by ubiquitin and SUMO. Nature. 2002 Sep 12;419(6903):135–41.

374. Mareková M, Vávrová J, Vokurková D. Monitoring of premitotic and postmitotic apoptosis in gamma-irradiated HL-60 cells by the mitochondrial membrane protein-specific monoclonal antibody APO2.7. Gen Physiol Biophys. 2003 Jun;22(2):191–200.
375. Larsson N, Marklund U, Gradin HM, Brattsand G, Gullberg M. Control of microtubule dynamics by oncoprotein 18: dissection of the regulatory role of multisite phosphorylation during mitosis. Mol Cell Biol. 1997 Sep;17(9):5530–9.
376. Vancompernolle K, Boonefaes T, Mann M, Fiers W, Grooten J. Tumor Necrosis Factor-induced Microtubule Stabilization Mediated by Hyperphosphorylated Oncoprotein 18 Promotes Cell Death. J Biol Chem. 2000 Oct 27;275(43):33876–82.
377. Abe Y, Takeuchi T, Kagawa-Miki L, Ueda N, Shigemoto K, Yasukawa M, et al. A Mitotic Kinase TOPK Enhances Cdk1/cyclin B1-dependent Phosphorylation of PRC1 and Promotes Cytokinesis. Journal of Molecular Biology. 2007 Jul 6;370(2):231–45.
378. Slangy A, Lane HA, d'Hérin P, Harper M, Kress M, Niggt EA. Phosphorylation by p34cdc2 regulates spindle association of human Eg5, a kinesin-related motor essential for bipolar spindle formation in vivo. Cell. 1995 Dec 29;83(7):1159–69.
379. Ishida R, Takashima R, Koujin T, Shibata M, Nozaki N, Seto M, et al. Mitotic Specific Phosphorylation of Serine-1212 in Human DNA Topoisomerase IIα. Cell Structure and Function. 2001;26(4):215–26.
380. Dreier MR, Bekier ME, Taylor WR. Regulation of sororin by Cdk1-mediated phosphorylation. J Cell Sci. 2011 Sep 1;124(17):2976–87.
381. Xiao S, Caglar E, Maldonado P, Das D, Nadeem Z, Chi A, et al. Induced Expression of Nucleolin Phosphorylation-Deficient Mutant Confers Dominant-Negative Effect on Cell Proliferation. PLoS One [Internet]. 2014 Oct 14 [cited 2016 Mar 4];9(10). Available from: http://www.ncbi.nlm.nih.gov/pmc/articles/PMC4196967/
382. Blethrow JD, Glavy JS, Morgan DO, Shokat KM. Covalent capture of kinase-specific phosphopeptides reveals Cdk1-cyclin B substrates. Proc Natl Acad Sci U S A. 2008 Feb 5;105(5):1442–7.
383. Parplys AC, Zhao W, Sharma N, Groesser T, Liang F, Maranon DG, et al. NUCKS1 is a novel RAD51AP1 paralog important for homologous recombination and genome stability. Nucleic Acids Res. 2015 Nov 16;43(20):9817–34.
384. Dechat T, Gotzmann J, Stockinger A, Harris CA, Talle MA, Siekierka JJ, et al. Detergent-salt resistance of LAP2alpha in interphase nuclei and phosphorylation-dependent association with chromosomes early in nuclear assembly implies functions in nuclear structure dynamics. EMBO J. 1998 Aug 17;17(16):4887–902.
385. Wu J, Feng Y, Xie D, Li X, Xiao W, Tao D, et al. Unscheduled CDK1 activity in G1 phase of the cell cycle triggers apoptosis in X-irradiated lymphocytic leukemia cells. Cell Mol Life Sci. 2006 Nov;63(21):2538–45.
386. Bird AW, Hyman AA. Building a spindle of the correct length in human cells requires the interaction between TPX2 and Aurora A. J Cell Biol. 2008 Jul 28;182(2):289–300.
387. Fu J, Bian M, Xin G, Deng Z, Luo J, Guo X, et al. TPX2 phosphorylation maintains metaphase spindle length by regulating microtubule flux. J Cell Biol. 2015 Aug 3;210(3):373–83.
388. Andrews PD, Ovechkina Y, Morrice N, Wagenbach M, Duncan K, Wordeman L, et al. Aurora B Regulates MCAK at the Mitotic Centromere. Developmental Cell. 2004 Feb;6(2):253–68.
389. Minc E, Allory Y, Worman HJ, Courvalin JC, Buendia B. Localization and phosphorylation of HP1 proteins during the cell cycle in mammalian cells. Chromosoma. 1999 Aug;108(4):220–34.
390. Schlütter C, Duchrow M, Wohlenberg C, Becker M, Key G, Flad H, et al. The cell proliferation-associated antigen of antibody Ki-67: a very large, ubiquitous nuclear protein with numerous repeated elements, representing a new kind of cell cycle-maintaining proteins. J Cell Biol. 1993 Nov 1;123(3):513–22.
391. Sueishi M, Takagi M, Yoneda Y. The Forkhead-associated Domain of Ki-67 Antigen Interacts with the Novel Kinesin-like Protein Hklp2. J Biol Chem. 2000 Sep 15;275(37):28888–92.
392. Lekmine F, Sassano A, Uddin S, Smith J, Majchrzak B, Brachmann SM, et al. Interferon-γ engages the p70 S6 kinase to regulate phosphorylation of the 40S S6 ribosomal protein. Experimental Cell Research. 2004 Apr 15;295(1):173–82.
393. Ozgur S, Chekulaeva M, Stoecklin G. Human Pat1b Connects Deadenylation with mRNA Decapping and Controls the Assembly of Processing Bodies. Mol Cell Biol. 2010 Sep;30(17):4308–23.
394. Tcherkezian J, Cargnello M, Romeo Y, Huttlin EL, Lavoie G, Gygi SP, et al. Proteomic analysis of cap-dependent translation identifies LARP1 as a key regulator of 5′TOP mRNA translation. Genes Dev. 2014 Feb 15;28(4):357–71.
395. Hsu PP, Kang SA, Rameseder J, Zhang Y, Ottina KA, Lim D, et al. The mTOR-regulated phosphoproteome reveals a mechanism of mTORC1-mediated inhibition of growth factor signaling. Science. 2011 Jun 10;332(6035):1317–22.

396. Shor B, Wu J, Shakey Q, Toral-Barza L, Shi C, Follettie M, et al. Requirement of the mTOR Kinase for the Regulation of Maf1 Phosphorylation and Control of RNA Polymerase III-dependent Transcription in Cancer Cells. J Biol Chem. 2010 May 14;285(20):15380–92.
397. Ondrej M, Cechakova L, Durisova K, Pejchal J, Tichy A. To live or let die: Unclear task of autophagy in the radiosensitization battle. Radiotherapy and Oncology [Internet]. 2016 [cited 2016 Jun 2]; Available from: http://www.sciencedirect.com/science/article/pii/S016781401600116X
398. Koren I, Reem E, Kimchi A. DAP1, a Novel Substrate of mTOR, Negatively Regulates Autophagy. Current Biology. 2010 Jun 22;20(12):1093–8.
399. Shang L, Chen S, Du F, Li S, Zhao L, Wang X. Nutrient starvation elicits an acute autophagic response mediated by Ulk1 dephosphorylation and its subsequent dissociation from AMPK. Proc Natl Acad Sci U S A. 2011 Mar 22;108(12):4788–93.
400. Fingar DC, Blenis J. Target of rapamycin (TOR): an integrator of nutrient and growth factor signals and coordinator of cell growth and cell cycle progression. Oncogene. 2004 Apr 19;23(18):3151–71.
401. Dillon LM, Miller TW. Therapeutic targeting of cancers with loss of PTEN function. Current drug targets. 2014 Jan;15(1):65.
402. Meric-Bernstam F, Akcakanat A, Chen H, Do K-A, Sangai T, Adkins F, et al. PIK3CA/PTEN Mutations and Akt Activation As Markers of Sensitivity to Allosteric mTOR Inhibitors. Clin Cancer Res. 2012 Mar 15;18(6):1777–89.
403. Fingar DC, Richardson CJ, Tee AR, Cheatham L, Tsou C, Blenis J. mTOR Controls Cell Cycle Progression through Its Cell Growth Effectors S6K1 and 4E-BP1/Eukaryotic Translation Initiation Factor 4E. Molecular and Cellular Biology. 2004 Jan;24(1):200.
404. Holz MK, Ballif BA, Gygi SP, Blenis J. mTOR and S6K1 Mediate Assembly of the Translation Preinitiation Complex through Dynamic Protein Interchange and Ordered Phosphorylation Events. Cell. 2005 Nov 18;123(4):569–80.
405. Roux PP, Shahbazian D, Vu H, Holz MK, Cohen MS, Taunton J, et al. RAS/ERK Signaling Promotes Site-specific Ribosomal Protein S6 Phosphorylation via RSK and Stimulates Cap-dependent Translation. J Biol Chem. 2007 May 11;282(19):14056–64.
406. Ben-Sahra I, Howell JJ, Asara JM, Manning BD. Stimulation of de Novo Pyrimidine Synthesis by Growth Signaling Through mTOR and S6K1. Science. 2013 Mar 15;339(6125):1323–8.
407. Blethrow JD, Glavy JS, Morgan DO, Shokat KM. Covalent capture of kinase-specific phosphopeptides reveals Cdk1-cyclin B substrates. Proc Natl Acad Sci U S A. 2008 Feb 5;105(5):1442–7.
408. Chi Y, Welcker M, Hizli AA, Posakony JJ, Aebersold R, Clurman BE. Identification of CDK2 substrates in human cell lysates. Genome Biol. 2008;9(10):R149.
409. Kwon Y-K, Ha IJ, Bae H-W, Jang WG, Yun HJ, Kim SR, et al. Dose-Dependent Metabolic Alterations in Human Cells Exposed to Gamma Irradiation. PLoS One [Internet]. 2014 Nov 24 [cited 2016 Jan 13];9(11). Available from: http://www.ncbi.nlm.nih.gov/pmc/articles/PMC4242643/
410. Patterson AD, Li H, Eichler GS, Krausz KW, Weinstein JN, Fornace AJ, et al. UPLC-ESI-TOFMS-Based Metabolomics and Gene Expression Dynamics Inspector Self-Organizing Metabolomic Maps as Tools for Understanding the Cellular Response to Ionizing Radiation. Anal Chem. 2008 Feb 1;80(3):665–74.
411. Tsuyama N, Mizuno H, Katafuchi A, Abe Y, Kurosu Y, Yoshida M, et al. Identification of low-dose responsive metabolites in X-irradiated human B lymphoblastoid cells and fibroblasts. J Radiat Res. 2015 Jan;56(1):46–58.
412. Azzam EI, Jay-Gerin J-P, Pain D. Ionizing radiation-induced metabolic oxidative stress and prolonged cell injury. Cancer Lett. 2012 Dec 31;327(0):48–60.
413. Lee R, Britz-McKibbin P. Differential rates of glutathione oxidation for assessment of cellular redox status and antioxidant capacity by capillary electrophoresis-mass spectrometry: an elusive biomarker of oxidative stress. Anal Chem. 2009 Aug 15;81(16):7047–56.
414. Yardim-Akaydin S, Sepici A, Özkan Y, Torun M, Şimşek B, Sepici V. Oxidation of Uric Acid in Rheumatoid Arthritis: Is Allantoin a Marker of Oxidative Stress? Free Radical Research. 2004 Jun 1;38(6):623–8.
415. Paglin S, Lee N-Y, Nakar C, Fitzgerald M, Plotkin J, Deuel B, et al. Rapamycin-Sensitive Pathway Regulates Mitochondrial Membrane Potential, Autophagy, and Survival in Irradiated MCF-7 Cells. Cancer Res. 2005 Dec 1;65(23):11061–70.
416. Park JM, Tougeron D, Huang S, Okamoto K, Sinicrope FA. Beclin 1 and UVRAG confer protection from radiation-induced DNA damage and maintain centrosome stability in colorectal cancer cells. PLoS ONE. 2014;9(6):e100819.
417. Cheema AK, Pathak R, Zandkarimi F, Kaur P, Alkhalil L, Singh R, et al. Liver Metabolomics Reveals Increased Oxidative Stress and Fibrogenic Potential in Gfrp Transgenic Mice in Response to Ionizing Radiation. J Proteome Res. 2014 Jun 6;13(6):3065–74.

418. Dokmeci D, Akpolat M, Aydogdu N, Uzal C, Doganay L, Turan FN. The Protective Effect of L-carnitine on Ionizing Radiation-induced Free Oxygen Radicals. Scandinavian Journal of Laboratory Animal Sciences. 2006;33(2):75–83.
419. Goodwin PM, Lewis PJ, Davies MI, Skidmore CJ, Shall S. The effect of gamma radiation and neocarzinostatin on NAD and ATP levels in mouse leukaemia cells. Biochim Biophys Acta. 1978 Nov 1;543(4):576–82.
420. Khan AR, Rana P, Devi MM, Chaturvedi S, Javed S, Tripathi RP, et al. Nuclear magnetic resonance spectroscopy-based metabonomic investigation of biochemical effects in serum of γ-irradiated mice. Int J Radiat Biol. 2011 Jan;87(1):91–7.
421. Yugi K, Kubota H, Toyoshima Y, Noguchi R, Kawata K, Komori Y, et al. Reconstruction of Insulin Signal Flow from Phosphoproteome and Metabolome Data. Cell Reports. 2014 Aug 21;8(4):1171–83.
422. Mathews CK. Deoxyribonucleotide metabolism, mutagenesis and cancer. Nat Rev Cancer. 2015 Sep;15(9):528–39.
423. Beyaert M, Starczewska E, Van Den Neste E, Bontemps F. A crucial role for ATR in the regulation of deoxycytidine kinase activity. Biochem Pharmacol. 2016 Jan 15;100:40–50.
424. Arnér ES, Eriksson S. Mammalian deoxyribonucleoside kinases. Pharmacol Ther. 1995;67(2):155–86.
425. Staub M, Eriksson S. The Role of Deoxycytidine Kinase in DNA Synthesis and Nucleoside Analog Activation. In: Peters GJ, editor. Deoxynucleoside Analogs In Cancer Therapy [Internet]. Humana Press; 2006 [cited 2016 Dec 4]. p. 29–52. (Cancer Drug Discovery and Development). Available from: http://link.springer.com/chapter/10.1007/978-1-59745-148-2_2

9. Appendices

9.1. Appendix 1

Tichy A, **Salovska B**, Rehulka P, Klimentova J, Vavrova J, Stulik J, Hernychova L. Phosphoproteomics: Searching for a needle in a haystack. Journal of Proteomics. 2011 Nov 18;74(12):2786–97. **IF = 4.878**

9.2. **Appendix 2**

Salovska B, Tichy A, Rezacova M, Vavrova J, Novotna E. Enrichment strategies for phosphoproteomics: state-of-the-art. Reviews in Analytical Chemistry. 2012 Mar;31(1):29–41. **IF = 0.436**

9.3. **Appendix 3**

Salovska B, Tichy A, Fabrik I, Rezacova M, Vavrova J. Comparison of Resins for Metal Oxide Affinity Chromatography with Mass Spectrometry Detection for the Determination of Phosphopeptides. Analytical Letters. 2013 Jul 3;46(10):1505–24. **IF = 0.982**

9.4. **Appendix 4**

Šalovská B, Fabrik I, Ďurišová K, Link M, Vávrová J, Řezáčová M, Tichý A. Radiosensitization of human leukemic HL-60 cells by ATR kinase inhibitor (VE-821): phosphoproteomic analysis. Int J Mol Sci. 2014;15(7):12007–26. **IF = 2.862**